



HAL
open science

Trouble du spectre de l'alcoolisation fœtale : vers des marqueurs neuroanatomiques en imagerie

Justine Fraize

► **To cite this version:**

Justine Fraize. Trouble du spectre de l'alcoolisation fœtale : vers des marqueurs neuroanatomiques en imagerie. Médecine humaine et pathologie. Université Paris Cité, 2023. Français. NNT : 2023UNIP7011 . tel-04373675

HAL Id: tel-04373675

<https://theses.hal.science/tel-04373675>

Submitted on 5 Jan 2024

HAL is a multi-disciplinary open access archive for the deposit and dissemination of scientific research documents, whether they are published or not. The documents may come from teaching and research institutions in France or abroad, or from public or private research centers.

L'archive ouverte pluridisciplinaire **HAL**, est destinée au dépôt et à la diffusion de documents scientifiques de niveau recherche, publiés ou non, émanant des établissements d'enseignement et de recherche français ou étrangers, des laboratoires publics ou privés.

Université Paris Cité

École doctorale Cerveau, Cognition, Comportement (158)

Laboratoire NeuroDiderot, équipe InDEV, Inserm

UNIACT, NeuroSpin, CEA

Trouble du spectre de l'alcoolisation foétale : vers des marqueurs neuroanatomiques en imagerie

Par Justine FRAIZE

Thèse de doctorat de Neurosciences

Dirigée par Lucie HERTZ-PANNIER

Présentée et soutenue publiquement le 4 octobre 2023

Devant un jury composé de :

Lucie HERTZ-PANNIER	DR, Université Paris Cité	Directrice de thèse
Olivier COULON	DR, Université Aix-Marseille	Rapporteur
Marie SCHAER	DR, Université de Genève	Rapporteur
Sylvie NGUYEN	PU-PH, Université de Lille	Présidente du jury
Stéphanie VALENCE	MD, PhD, Sorbonne Université	Examinatrice
Bérénice DORAY	PU-PH, Université de la Réunion	Examinatrice
David GERMANAUD	MD, PhD, Université Paris Cité	Co-encadrant

Trouble du spectre de l'alcoolisation fœtale : vers des marqueurs neuroanatomiques en imagerie

RÉSUMÉ

Les troubles neurodéveloppementaux liés à l'alcool sont une cause majeure de handicap cognitif et comportemental mal reconnue en France, en partie à cause du manque de spécificité du diagnostic clinique des troubles du spectre de l'alcoolisation fœtale (TSAF) en l'absence de l'ensemble des éléments malformatifs du syndrome d'alcoolisation fœtale (SAF). Par ailleurs, le phénotype clinique et le niveau d'exposition à l'alcool expliquent mal le pronostic. Le déficit de croissance cérébrale est quasi constant dans les TSAF, parfois associé à des atteintes cérébrales focales, encourageant à rechercher des marqueurs neuroanatomiques de la maladie. Les récentes études de neuroanatomie en l'imagerie par résonance magnétique (IRM) assistée par ordinateur ont étendu le champ des atteintes cérébrales associées aux TSAF, mais beaucoup de ces résultats restent discutés et aucun marqueur n'a pour l'heure émergé qui soit utile au diagnostic des formes non spécifiques de TSAF (TSAF-NS) ou au pronostic fonctionnel en général. Notre but était d'identifier des marqueurs neuroanatomiques, caractérisables à l'échelle individuelle et intégrables à la démarche clinique actuelle.

Ainsi, nous avons organisé une base de données sur des sujets ayant un TSAF à partir d'un large recrutement clinique monocentrique de patients extensivement phénotypés sur le plan clinique et cognitif, et imagés (IRM T1 et de diffusion). Cette série a été comparée à plus d'une centaine de sujets contrôles au développement typique. Les marqueurs morphométriques ont été recherchés sur la séquence pondérée T1, avec des mesures manuelles simples puis par morphométrie informatisée (segmentation automatique, identification et mesure de régions ou structures cérébrales). Nous avons étudié le cervelet et ses sous-parties lobaires ainsi que le corps calleux et chacun de ces segments. Un effort particulier a été fourni pour générer et utiliser des outils de segmentation anatomique complémentaires originaux pour une validation croisée des résultats, afin de limiter les biais méthodologiques. De plus, l'analyse de la variance de taille doit intégrer que l'homothétie (zoom) n'est pas la règle entre les cerveaux de tailles différentes au développement pourtant typique, en particulier dans des études comparatives portant sur les TSAF où les cerveaux sont en moyenne « trop petits ». Nous avons modélisé les phénomènes d'allométrie (changement des proportions avec la taille) sur la base d'une loi de puissance. Dans l'optique de la translation à la démarche clinique, nous avons identifié des candidats marqueurs chez les sujets avec un SAF et grâce à des combinaisons et des outils d'apprentissage automatisé, d'étudier leur intérêt diagnostique chez les sujets TSAF-NS.

Nous avons trouvé un gradient antéro-inféro-postérieur d'atteinte intracérébelleuse. Par des mesures manuelles du corps calleux, nous avons retrouvé un sur-rétrécissement isthmique confirmé par des mesures automatisées. Cette méthode automatisée a permis de révéler que l'atteinte isthmique s'associe à un amincissement du splénium et un raccourcissement de la longueur du corps calleux indépendamment de la réduction de taille du cerveau. Dans un sous-groupe, nous avons confirmé cette atteinte calleuse postérieure en analyse surfacique. Nos résultats suggèrent que l'atteinte spléniale est indépendante de la surface corticale qu'elle connecte, alors que l'atteinte péri-isthmique, plus marquée, pourrait être associée à une atteinte de l'extension corticale homologue.

Nous avons montré qu'il était possible de caractériser une signature neuroanatomique des SAF et de la retrouver en partie chez les TSAF-NS y compris à l'échelle individuelle, ce qui pourrait aider à renforcer la certitude diagnostique et potentiellement à prédire le pronostic fonctionnel. À côté de l'intérêt clinique dans la prise en charge des TSAF, ce travail pourrait éclairer la compréhension de la toxicité développementale de l'alcool en révélant la sensibilité ou la relative préservation de certaines structures neuroanatomiques.

MOTS-CLÉS

Trouble du spectre de l'alcoolisation fœtale ; Syndrome d'alcoolisation fœtale ; Microcéphalie ; Imagerie par résonance magnétique ; Morphométrie cérébrale ; Cervelet ; Corps calleux ; *Scaling* ; Allométrie ; Analyse normative

Fetal alcohol spectrum disorder: towards neuroanatomical markers in imaging

ABSTRACT

Alcohol-related neurodevelopmental disorders are a major cause of cognitive and behavioral disability in France but are poorly recognized, partly due to the lack of specificity in the clinical diagnosis of fetal alcohol spectrum disorders (FASD) in the absence of all clinical features of the fetal alcohol syndrome (FAS). Furthermore, clinical phenotype and level of alcohol exposure do not explain prognosis. Cerebral growth deficiency is a near-constant feature of FASD, sometimes associated with focal brain damage, encouraging the search for neuroanatomical markers of the FASD. Recent neuroanatomical studies in computer-assisted magnetic resonance imaging (MRI) have broadened the scope of brain damage associated with FASD, but many of these findings remain debated and no marker has yet emerged that is useful for the diagnosis of non-specific forms of FASD (NS-FASD) or for functional prognosis. Our aim was to identify neuroanatomical markers that could be characterized at the individual level and integrated into the current clinical approach.

Thus, we organized a database of subjects with FASD from a large monocentric clinical recruitment of patients extensively clinically and cognitively described and imaged (T1 and diffusion MRI). This series was compared with over a hundred typically developing control subjects. Morphometric markers were sought on the T1-weighted sequence, using simple manual measurements, followed by computerized morphometry (automatic segmentation, identification and measurement of brain regions or structures). We studied the cerebellum and its lobar sub-parts, as well as the corpus callosum and each of its segments. A special effort was made to generate and use original complementary anatomical segmentation tools for cross-validation of results, in order to limit methodological biases. In addition, the analysis of size variance must take into account the fact that homotheticity (zooming) is not the rule between brains of different sizes with typical development, particularly in comparative studies of FASD where brains are on average "too small". We have modeled the allometry (change in proportions with size) using a power law. To translate to the clinical approach, we identified candidate markers in subjects with FAS and, using combinations and automated learning tools, to study their diagnostic value in the NS-FASD population.

We found an anterior-inferior-posterior gradient of intracerebellar damage. Manual measurements of the corpus callosum revealed isthmic over-narrowing, confirmed by automated measurements. This automated method revealed that isthmic damage is associated with thinning of the splenium and shortening of the length of the corpus callosum, independently of the reduction in brain size. In a subgroup, we confirmed this posterior callosal damage by surface analysis. Our results suggest that splenial damage is independent

of the cortical surface it connects, whereas the more marked peri-isthmic damage may be associated with damage to homologous cortical extension.

We have shown that it is possible to characterize a neuroanatomical signature of FAS and to find it in part in NS-FASD, including at the individual level, which could help to strengthen diagnostic certainty and potentially predict functional prognosis. In addition to its clinical value in FASD, this work could shed light on the understanding of developmental alcohol toxicity by revealing the sensitivity or relative preservation of certain neuroanatomical structures.

KEYWORDS

Fetal alcohol spectrum disorder; Fetal alcohol syndrome; Microcephaly; Magnetic resonance imaging; Brain morphometry; Cerebellum; Corpus callosum; Scaling; Allometry; Normative analysis

REMERCIEMENTS

Je tiens tout d'abord à exprimer ma profonde gratitude à David Germanaud et Lucie Hertz-Pannier pour leur supervision, leur accompagnement et la confiance qu'ils m'ont accordée tout au long de ce travail scientifique, ainsi que pour les responsabilités qu'ils m'ont confiées. Mes remerciements vont également à la Professeure Marie Schaer et à Monsieur Olivier Coulon, qui, en tant que rapporteurs, ont consacré leur temps et leurs efforts du jury pour évaluer mon travail. J'adresse mes sincères remerciements à la Professeure Sylvie Nguyen The Tich, à la Professeure Bérénice Doray et au Docteur Stéphanie Valence d'avoir accepté de faire partie du jury de la thèse.

Je souhaite exprimer ma reconnaissance au Professeur Vincent Desportes et à Monsieur Jean-François Mangin pour avoir suivi attentivement l'évolution de mon travail et pour m'avoir prodigué de précieux conseils en tant que membres du comité de suivi de thèse. J'adresse mes remerciements sincères à Monsieur Julien Lefèvre, avec qui j'ai eu le plaisir de collaborer sur le plan scientifique. Mes remerciements vont également au Docteur Catherine Chiron, ainsi qu'à Mesdames Jessica Dubois et Marion Noulhiane, pour leur accueil chaleureux au sein de l'équipe InDEV et pour leurs conseils empreints de sagesse.

Je souhaite également exprimer ma reconnaissance à Eliot Kerdreux avec qui j'ai eu le plaisir de travailler dans la bienveillance et le calme. J'ai également une pensée amicale pour les anciens membres de l'équipe 'Alcool' : Gabrielle Convert, Florent Sylvestre-Marconville. Mes remerciements vont à Pauline Garzón, qui a posé les premiers jalons de ce travail sur la cohorte et qui a veillé à sa transmission minutieuse. Je tiens à remercier Yann Leprince pour son expertise et son temps précieux, malgré ses nombreuses sollicitations, ainsi que Clara Fischer et Dhaif Bekha pour leur aide. Mes remerciements vont également aux membres de l'équipe InDEV, aux doctorantes et aux stagiaires, post-doctorants, qui ont contribué à créer une atmosphère de travail détendue.

J'exprime ma gratitude à l'équipe de radiologie de l'Hôpital Robert-Debré, la Professeure Marianne Alison, Monique Elmaleh-Bergès et Alexandra Ntorkou, ainsi qu'aux manipulateurs en radiologie, pour avoir permis le bon déroulement des acquisitions cliniques. Mes remerciements vont à l'équipe de neurologie pédiatrique qui a pris en charge les patients, les médecins, notamment la Professeure Odile Boespflug-Tanguy, les neuropsychologues et les soignants du service de l'Hôpital Robert-Debré. Je remercie également le service de pédopsychiatrie de l'enfant, notamment pour avoir fourni les données des sujets contrôles.

Je remercie les enfants et adolescents inclus dans cette étude ainsi leurs familles et les associations des patients, dont '*Vivre avec le SAF*' pour leur soutien à la recherche.

J'adresse mes remerciements à l'Agence Nationale de la Recherche pour avoir financé la réalisation de mon travail. Je tiens également à remercier NeuroSpin et l'École Doctorale ED3C en tant qu'institution de m'avoir offert un cadre propice à l'apprentissage et à la recherche.

Enfin, je souhaite exprimer ma gratitude aux médecins qui m'ont accueilli durant mon temps consacré à la clinique, dans des conditions toujours arrangeantes, les Docteurs Amandine Aurore à l'IEM de Bondy, Barbara Dusourd à l'Hôpital d'Orsay, et France Gacoin au CAMSP de Saint Denis.

TABLE DES MATIÈRES

RÉSUMÉ	2
MOTS-CLÉS	3
ABSTRACT	4
KEYWORDS.....	5
REMERCIEMENTS	6
TABLE DES MATIÈRES.....	7
CHAPITRE 1 : INTRODUCTION.....	10
RECONNAISSANCE DES CONSÉQUENCES DE L'EXPOSITION PRÉNATALE À L'ALCOOL	10
<i>Historique nosographique</i>	10
<i>Conséquences neurodéveloppementales</i>	12
<i>Données épidémiologiques</i>	13
<i>Étude de l'effet tératogène dans les modèles animaux</i>	14
APPORT DE LA NEUROIMAGERIE DES TSAF	15
<i>Retour sur trente ans d'étude de la morphologie cérébrale en imagerie</i>	15
<i>Limites de l'impact de la neuroimagerie dans le raisonnement diagnostique et la pratique clinique</i>	17
ENJEUX MÉTHODOLOGIQUES.....	18
<i>Analyse normative, définir une norme et prendre en compte la variance inter-individuelle</i>	18
<i>Analyse de l'effet de taille du cerveau</i>	18
HYPOTHÈSES, OBJECTIFS ET PLAN DE TRAVAIL	20
CHAPITRE 2 : CADRE MÉTHODOLOGIQUE	22
PARTICIPANTS.....	22
<i>Préambule</i>	22
<i>Population TSAF et critères d'inclusion</i>	22
<i>Population des contrôles</i>	28
<i>Aspects éthiques</i>	28
APPLICATION DES ENJEUX MÉTHODOLOGIQUES PRINCIPAUX	29
<i>Modélisation de l'effet de taille</i>	29
<i>Modèle normatif</i>	30
<i>Prise en compte des covariables</i>	30
CHAPITRE 3 : ÉTUDE EN RADIOLOGIE CLINIQUE DE L'ATTEINTE DU VERMIS ET DU CORPS CALLEUX	32
INTRODUCTION	32
COMBINER LES CARACTÉRISTIQUES NEUROANATOMIQUES POUR ÉTAYER LE DIAGNOSTIC DE TROUBLE DU SPECTRE DE L'ALCOOLISATION FŒTALE	32
RÉSUMÉ	33
RÉSUMÉ GRAPHIQUE	34
MATÉRIELS SUPPLÉMENTAIRES	47
COMPLÉMENTS DE DISCUSSION	53

CHAPITRE 4 : ÉTUDE EN IMAGERIE COMPUTATIONNELLE DE L'ATTEINTE DU CERVELET	55
INTRODUCTION	55
AMÉLIORATION DU DIAGNOSTIC DES TROUBLES DU SPECTRE DE L'ALCOOLISATION FŒTALE GRÂCE À UN CLASSIFICATEUR BASÉ SUR LE GRADIENT INTRACÉRÉBELLEUX DU SOUS-DIMENSIONNEMENT VOLUMÉTRIQUE .	55
RÉSUMÉ	56
RÉSUMÉ GRAPHIQUE	57
MATÉRIELS SUPPLÉMENTAIRES	74
COMPLÉMENT DE DISCUSSION	76
CHAPITRE 5 : ÉTUDE EN IMAGERIE COMPUTATIONNELLE DE L'ATTEINTE DU CORPS CALLEUX	77
INTRODUCTION COMMUNE	77
CARTOGRAPHIE DE LA RÉDUCTION DE LA SURFACE DU CORPS CALLEUX DANS LES TROUBLES DU SPECTRE DE L'ALCOOLISATION FŒTALE À L'AIDE DES SILLONS ET D'UNE PARCELLISATION BASÉE SUR LA CONNECTIVITÉ	77
RÉSUMÉ	78
RÉSUMÉ GRAPHIQUE	79
PROFILAGE SPECTRAL DE L'ÉPAISSEUR DU CORPS CALLEUX DANS LES TROUBLES DU SPECTRE DE L'ALCOOLISATION FŒTALE.....	94
RÉSUMÉ	94
RÉSUMÉ GRAPHIQUE	95
MATÉRIELS SUPPLÉMENTAIRES	124
COMPLÉMENTS DE DISCUSSION	126
<i>Résultats concordants</i>	126
<i>Cohérence des analyses normatives</i>	126
<i>Objectifs complémentaires</i>	127
CHAPITRE 6 : DISCUSSION GÉNÉRALE	129
RÉSUMÉS DES PRINCIPAUX RÉSULTATS.....	129
QUÊTE DE MARQUEURS NEUROANATOMIQUES DANS LES TSAF	130
<i>Spectre d'atteinte de l'exposition prénatale à l'alcool</i>	130
<i>Complexité de la signature</i>	132
APPROCHES MÉTHODOLOGIQUES AU SERVICE D'UNE QUESTION CLINIQUE	132
PARTICULARITÉ DE LA SÉRIE CLINIQUE.....	134
QUESTION DE LA SPÉCIFICITÉ ET VALEUR PRÉDICTIVE	137
<i>Preuve de la spécificité</i>	137
<i>Vers des marqueurs prédictifs</i>	138
QUESTIONNEMENTS EN SUSPENS	139
PERSPECTIVES ET CONCLUSION	140
<i>Autres marqueurs diagnostiques envisageables</i>	140
<i>Translation clinique</i>	140
CONTRIBUTIONS SCIENTIFIQUES NON INCLUSES DANS LA THÈSE.....	142

QUESTIONNER L'HÉTÉROGÉNÉITÉ COGNITIVE ET LE FONCTIONNEMENT INTELLECTUEL DANS LES TROUBLES DU SPECTRE DE L'ALCOOLISATION FŒTALE À PARTIR DE L'ÉCHELLE D'INTELLIGENCE DE WECHSLER POUR LES ENFANTS	142
<i>Résumé</i>	142
PERTURBATION DU VECTEUR DE FIEDLER : INTÉRÊT POUR LES MESURES DE GRAPHES ET L'ANALYSE DE FORME	143
<i>Résumé</i>	143
COMMUNICATIONS ET PROMOTIONS SCIENTIFIQUES	144
COMMUNICATIONS ORALES EN CONGRÈS	144
COMMUNICATIONS POSTER EN CONGRÈS	144
ORGANISATION ET ANIMATION D'UN CONGRÈS SCIENTIFIQUE FRANÇAIS 2021 & 2022	145
BIBLIOGRAPHIE	146
ANNEXE	167
OUTIL D'INTERPRÉTATION DES MESURES RADIOLOGIQUES UTILISABLE EN CLINIQUE	167

CHAPITRE 1

INTRODUCTION

RECONNAISSANCE DES CONSÉQUENCES DE L'EXPOSITION PRÉNATALE À L'ALCOOL

HISTORIQUE NOSOGRAPHIQUE

Le premier article décrivant les effets délétères de l'exposition prénatale à l'alcool a été publié en 1968 par un pédiatre français, Paul Lemoine. Le suivi prospectif de 127 d'enfants nés de parents considérés comme 'alcooliques' lui a permis de faire l'inventaire des anomalies cliniques, de la morphologie de la face et de croissance ainsi qu'une d'une série d'atteintes cognitives et comportementales (Lemoine et al., 1968). Il a fait alors le lien étiologique entre les anomalies observées et l'alcoolisme maternel et a émis des réserves pour les cas où seul l'éthylisme paternel était rapporté. Toutefois, ces travaux publiés en français, sont restés largement méconnus et ce n'est qu'avec les publications dans des revues prestigieuses de Jones, Smith et de leurs collègues en 1973, que les conséquences néfastes de l'exposition prénatale à l'alcool ont attiré l'attention (Jones and Smith, 1973; Jones et al., 1973). Tout comme Lemoine, ils ont décrit le retard de croissance, les déficits cognitifs et la dysmorphie faciale. Enfin, ils ont introduit le terme de syndrome d'alcoolisation fœtale (SAF) pour décrire cette embryofœtopathie alcoolique.

En 1978, Clarren et Smith (Clarren and Smith, 1978) ont rapporté que l'exposition à l'alcool pouvait entraîner un spectre de conséquences développementales plus large, sans que les caractéristiques faciales soient présentes. Ils ont alors introduit la notion « d'effets présumés de l'alcool sur le fœtus » (*suspected fetal alcohol effects*)¹ pour décrire l'expression partielle ou incomplète du SAF. De nombreuses nomenclatures diagnostiques se sont ensuite succédé pour aider les cliniciens à reconnaître l'ensemble de ces conséquences. En 1980, Rosett sous l'égide du *Fetal Alcohol Study Group* de la Société de Recherche sur l'Alcoolisme américaine (Rosett, 1980) a proposé des critères spécifiques et structurés du diagnostic de SAF comprenant un retard de croissance prénatal et postnatal, une atteinte neurologique, incluant l'atteinte neurodéveloppementale, associés à une dysmorphie faciale caractéristique.

Pour autant en 1989, Sokol et Clarren ont déploré l'usage ambigu et le détournement du terme *possible/suspected fetal alcohol effects* (Sokol and Clarren, 1989). En effet, ces auteurs regrettaient que ce terme, qui avait introduit la notion utile dans le suivi prospectif de « risque

¹ Les termes de la nomenclature anglaise sont systématiquement rapportés pour pouvoir se référer à la littérature. Une traduction française est alors proposée entre guillemets.

développemental après exposition », ait pu être employé pour parler des anomalies congénitales jugées moins sévères que le SAF, ou pour suggérer une relation supposée avec l'alcool insuffisamment documentée. Ils ont alors plaidé pour l'introduction d'un diagnostic positif, bien que probabiliste, qui « impliquait l'attribution d'un résultat observé anatomique ou fonctionnel, à l'impact de l'alcool sur la progéniture », qu'ils ont nommé « anomalie congénitale liée à l'alcool » (*alcohol related birth defect*). L'adhésion de la communauté n'a pas été immédiate et l'*Institute of Medicine* américain a convoqué, en 1994, un comité dont Sokol et Clarren faisaient partie, pour établir un rapport complet des connaissances scientifiques d'alors sur les conséquences de l'exposition prénatale à l'alcool. Le document final de plus de deux cents pages, reprenait les données épidémiologiques de la consommation d'alcool chez la femme enceinte, la prévalence du SAF, des vignettes cliniques pour illustrer les tableaux des patients, et finalement produisait des recommandations d'usage diagnostique. La catégorie diagnostique de SAF a été divisée en deux, en reconnaissant l'existence de formes partielles du SAF, où certaines des caractéristiques du SAF sont présentes, mais pas toutes, et l'exposition est confirmée. La seconde grande catégorie diagnostique, nommée *alcohol related effects* ou « effets relatifs à l'alcool », regroupait deux sous-catégories qui ne sont pas mutuellement exclusives : « les anomalies congénitales liées à l'alcool » (*alcohol related birth defect*) quand une ou plusieurs anomalies congénitales étaient retrouvées en contexte d'exposition confirmée et les « troubles neurodéveloppementaux liés à l'alcool » (*alcohol related neurodevelopmental disorder*) quand des troubles neurodéveloppementaux étaient retrouvés en contexte d'exposition confirmée (Stratton et al., 1996). Ces appellations et catégories sont encore utilisées et constituent le socle des recommandations de l'*Institute of Medicine* encore à l'usage à l'heure actuelle, après des mises à jour successives (Hoyme et al., 2005, 2016).

Pour tenter d'opérationnaliser et objectiver les critères diagnostiques Astley et Clarren (Astley and Clarren, 2000) ont élaboré un système diagnostique reposant sur les quatre caractéristiques du SAF : le déficit de croissance, la dysmorphie faciale, le dysfonctionnement du système nerveux central et l'exposition prénatale à l'alcool, dont l'intensité et/ou la certitude sont cotées de un à quatre. Les 256 combinaisons à quatre chiffres, ainsi obtenues sont réparties en 22 catégories dont les noms sont construits de manière séquentielle, à partir de quatre termes : « signes physiques sentinelles » (*sentinel physical findings*), « troubles neurocomportementaux » (*neurobehavioural disorder*), « encéphalopathie statique » (*static encephalopathy*), « état d'exposition à l'alcool » (*alcohol exposure status*), associés ou non à la confirmation de l'exposition à l'alcool. Au-delà de ce système complexe et fastidieux à utiliser, c'est bien l'étendue des conséquences néfastes que les auteurs mettent en lumière (Astley, 2004). Dans les suites, le terme diagnostique de « trouble du spectre de l'alcoolisation fœtale » (TSAF) (*fetal alcohol spectrum disorder, FASD*) a été introduit et officialisé. La *National Organization on Fetal Alcohol Syndrome* avait alors réuni les *National Institutes of Health*, le *Centers for Disease Control and Prevention* (CDC), et les *Substance Abuse and Mental Health Services Administration* américains ainsi que d'autres experts du domaine, afin d'élaborer une définition consensuelle des TSAF.

Concomitamment, le réseau canadien du *Canada Fetal Alcohol Spectrum Disorder Research Network* a proposé des recommandations diagnostiques (Chudley et al., 2005; Cook et al., 2016; Chudley, 2018). À partir de 2016, une tendance inverse aux propositions américaines a ramené à seulement deux, les catégories diagnostiques : les « TSAF avec les caractéristiques faciales sentinelles » (*FASD with sentinel facial features*) où l'exposition prénatale à l'alcool peut être confirmée ou rester inconnue et les « TSAF sans les caractéristiques faciales sentinelles » (*FASD without sentinel facial features*) où l'exposition doit être confirmée. Ces recommandations ont introduit également la notion de diagnostic dynamique et de facteur de risque développemental, en mettant à part la catégorie de patients « à risque de troubles neurodéveloppementaux et de TSAF, associés à l'exposition prénatale à l'alcool » (*at risk for neurodevelopmental disorder and FASD, associated with prenatal alcohol exposure*).

CONSÉQUENCES NEURODÉVELOPPEMENTALES

L'*American Psychiatric Association* a inclus dans la version de 2013 de son « Manuel diagnostique et statistique des troubles mentaux » (*diagnostic and statistical manual of mental disorders, DSM-5*), le terme de « trouble neurocomportemental associé à l'exposition prénatale à l'alcool » (*neurobehavioral disorder associated with prenatal alcohol exposure*), alors même que la tendance de cette version était de mieux distinguer les diagnostics de troubles du neurodéveloppement des maladies causales (Battle, 2013). L'accent est alors mis sur les conséquences neurocognitives, développementales et psychiatriques de l'exposition, reléguant au second plan les caractéristiques physiques. Kable et al., en 2016 a dessiné précisément les contours des troubles du neurodéveloppementaux de ces patients (Kable et al., 2016) en synthétisant la littérature des trente dernières années (Connor et al., 2006; Kodituwakku, 2009; Mattson et al., 2011).

Le phénotype cognitif et comportemental des TSAF couvre l'ensemble du spectre des troubles du neurodéveloppement, même s'il n'a pas toujours été décrit dans ce cadre nosographique et sans pouvoir établir un profil complètement spécifique (Kodituwakku, 2009; Mattson et al., 2011; Kable et al., 2016). Cependant, certains domaines fonctionnels sont plus fréquemment affectés, se regroupant dans un profil cognitif évocateur, avec par ordre décroissant de fréquence, le trouble déficitaire de l'attention avec ou sans hyperactivité (Fryer et al., 2007), les troubles plus larges des fonctions exécutives (Vaurio et al., 2011; Rockhold et al., 2020), le trouble du développement intellectuel léger à limite (Streissguth et al., 1991; Mattson et al., 2011), le trouble d'acquisition des coordinations (Connor et al., 2006) et plus rarement ceux du langage oral (Wyper and Rasmussen, 2011; Thorne, 2017). Les troubles des apprentissages scolaires sont aussi largement cités, sans plus de précisions sur leur caractère primaire ou secondaire. L'association de troubles de l'humeur, de troubles anxieux, et surtout de troubles de la régulation émotionnelle moins bien spécifiés est particulièrement fréquente et augmente avec l'âge (Thomas et al., 1998; Franklin et al., 2008; Kully-Martens et al., 2012).

DONNÉES ÉPIDÉMIOLOGIQUES

Les TSAF sont donc maintenant une cause reconnue et identifiée comme évitable de troubles du neurodéveloppement. Leur prévalence dépend du pays, du niveau de consommation d'alcool, notamment chez les femmes en âge de procréer, et de la reconnaissance du diagnostic qui, comme cela a été exposé, a évolué depuis le début des années 2000, dépassant le cadre de la forme uniquement syndromique (Lange et al., 2017). Certains auteurs ont tout de même tenté d'estimer la prévalence des consommations d'alcool pendant la grossesse, la situant entre 8 et 9 % quelle que soit la dose consommée, et la prévalence du SAF dans la population générale entre 6 et 14 pour 10 000 personnes (Popova et al., 2017).

Les grandes études épidémiologiques de suivi prospectif d'enfants lourdement exposés nous apprennent que les sujets présentant un SAF représentent environ 10 % de l'ensemble des TSAF (Streissguth, 1978; Astley, 2010; Kuehn et al., 2012). Indirectement, il est possible d'envisager le nombre de sujets ayant un TSAF sans SAF qui ne seraient pas diagnostiqués. En France, l'Haute Autorité de Santé considère que le SAF représente 1,3 ‰ naissances vivantes par an et les TSAF dans leur ensemble, 9 ‰ (Collège de la Haute Autorité de Santé, 2013; Germanaud and Toutain, 2017). Le relevé systématique des données des codages diagnostiques des hospitalisations (PMSI) a permis d'obtenir des chiffres similaires avec des disparités importantes entre les régions (Demiguel et al., 2021). À l'échelle européenne, la prévalence du SAF était estimée à 3,7 ‰.

Le relevé des consommations pendant la grossesse peut aussi être permettre d'inférer indirectement la fréquence potentielle des TSAF. En se concentrant sur les données françaises, au début des années 2000, 52 % de femmes déclaraient avoir consommé au moins une fois de l'alcool pendant la grossesse (de Chazeron et al., 2008). Parmi ces femmes, environ 37 % déclaraient consommer plus d'une fois par mois et 7 % rapportaient un ou plusieurs épisodes de consommation excessive ponctuelle d'alcool (*binge drinking*). La prévalence des femmes enceintes qui consomment de l'alcool pendant la grossesse est le plus souvent évaluée par déclaration sur auto-questionnaire et donc sûrement sous-évaluée. En conséquence, les consommations d'alcool qui peuvent entraîner des conséquences sur le développement de l'enfant ne sont pas rares (Germanaud and Toutain, 2017).

Pour toutes ces raisons, il est logique de considérer que les TSAF sont sous-diagnostiqués surtout dans les formes non syndromiques. Il est également probable que les cliniciens restent prudents face à un diagnostic probabiliste, reposant sur un faisceau d'arguments qu'ils considéreraient comme trop pauvres et qu'il est donc nécessaire d'enrichir.

En parallèle de la reconnaissance et de la structuration des critères diagnostiques de TSAF ainsi que des travaux d'épidémiologie, les chercheurs se sont appuyés sur l'étude des modèles animaux d'exposition à l'alcool pour mieux comprendre les mécanismes de fœtotoxicité de l'éthanol.

ÉTUDE DE L'EFFET TÉRATOGENÈ DANS LES MODÈLES ANIMAUX

Les études utilisant des modèles animaux d'exposition prénatale à l'alcool ont commencé peu après l'identification du SAF, à la fin des années soixante-dix. Elles ont été essentielles pour confirmer la tératogénicité de l'alcool, refléter et étendre les travaux cliniques sur les effets comportementaux, fonctionnels et neurobiologiques de l'alcool.

Tout d'abord, les travaux de Chernoff ont permis de faire la preuve que la concentration maternelle sanguine d'alcool était corrélée au risque malformatif (Chernoff, 1977). Ceux de Sulik et al. ont prouvé qu'il existait une période critique d'exposition du premier trimestre pour le risque de malformation crâniofaciale proche de la dysmorphie faciale de l'être humain (Sulik et al., 1981). Les modèles d'exposition massive précoce du premier trimestre sont à l'origine des anomalies du massif facial, mais aussi des malformations d'organes, par exemple cardiaques (Lipinski et al., 2010). Les expositions durant le deuxième et troisième trimestre de grossesse ont des répercussions sur la croissance du cerveau (Coleman et al., 2012). En faisant varier les modalités d'administration et les dosages, Bonthius et West ont pu prouver que les expositions ponctuelles massives induisent une réduction plus importante du poids cérébral, reflet de la perte cellulaire, que des expositions chroniques continues (Bonthius and West, 1990). En plus de prouver le lien causal entre le phénotype clinique et l'exposition, les modèles animaux développés pendant les trente dernières années ont permis de mieux comprendre l'ensemble des mécanismes biologiques en jeu dans l'action toxique de l'alcool. Dans une récente revue de la littérature sur les modèles murins, Almeida et al. récapitulent qu'au cours du développement fœtal, l'ensemble des processus cellulaires clés tels que la prolifération, la migration, la différenciation, la synaptogenèse, la gliogenèse, la myélinisation et l'apoptose sont altérés par l'éthanol (Almeida et al., 2020).

Des conséquences comportementales peuvent aussi être observées chez l'animal (voir la revue de Patten et al., Patten et al., 2014). Le développement des réflexes moteurs de base et de la coordination sont systématiquement retardés, et l'apprentissage spatial ainsi que la mémoire sont altérés chez les rats exposés (Mantha et al., 2013). Les tâches d'inhibition de la réponse, d'action dans le but d'atteindre un objectif et de mémoire de travail sont échouées dans des modèles de souris exposées et permettent indirectement d'inférer l'atteinte des fonctions motrices, exécutives, mnésiques, de raisonnement de ces animaux.

Les autres facteurs pouvant avoir un effet sur l'intensité de l'expression clinique après l'exposition ont aussi fait l'objet d'études. En premier lieu, ont été incriminés les facteurs pouvant modifier la concentration sanguine maternelle en éthanol comme le polymorphisme maternel du métabolisme de l'alcool, l'âge, le poids, le statut hormonal. Puis, des facteurs nutritionnels comme des carences peuvent aggraver la restriction de croissance et les conséquences sur le comportement (Patten et al., 2014).

APPORT DE LA NEUROIMAGERIE DES TSAF

RETOUR SUR TRENTE ANS D'ÉTUDE DE LA MORPHOLOGIE CÉRÉBRALE EN IMAGERIE

Depuis les années 1990, la réalisation systématique d'imagerie par résonance magnétique (IRM) de cohortes de patients TSAF a progressivement permis de comprendre les altérations cérébrales associées à l'exposition prénatale à l'alcool chez l'humain par des moyens non invasifs. Les premières études de neuroimagerie clinique ont fait état d'anomalies de l'architecture cérébrale chez des sujets SAF, avec en premier lieu, la microcéphalie, puis les ventriculomégalies, l'agénésie partielle ou complète du corps calleux et l'hypoplasie cérébelleuse (Riley et al., 1995; Johnson et al., 1996; Swayze et al., 1997; Autti-Rämö et al., 2002). Plus récemment, de plus larges cohortes de sujets représentant l'ensemble du spectre des TSAF ou de sujets ayant été exposés à l'alcool et imagés systématiquement, ont permis d'apprécier grossièrement la fréquence de ces anomalies (Astley et al., 2009a; Boronat et al., 2017; Treit et al., 2020) : 3 à 40 % d'anomalies calleuses, 0 à 24 % d'anomalies cérébelleuses. L'étendue de la fourchette de prévalence s'explique entre autres par l'hétérogénéité des populations d'étude et l'absence de critères objectifs dans les descriptions (corps calleux jugés « dysmorphiques » par exemple). Il est tout de même déjà possible de conclure que la fréquence des anomalies visibles est plus importante chez les sujets SAF que chez les sujets exposés quel que soit le niveau d'exposition, et qu'elle dépasse le niveau des découvertes fortuites dans une population de sujets sains, mais pas celle dans une population de sujets ayant un trouble du neurodéveloppement qu'importe l'étiologie.

À côté de ces études radiologiques, des outils d'imagerie computationnelle (analyse informatisée des images) ont permis d'entreprendre la recherche d'anomalies plus subtiles à l'aide de descriptions morphométriques quantifiées plus objectives.

L'effet de l'exposition prénatale à l'alcool est, en premier lieu, attesté par la réduction de la taille globale du cerveau, caractérisé soit par du volume intérieur de la boîte crânienne, soit par du volume cérébral total, soit par du volume parenchymateux. Ainsi, la méta-analyse de Donald et al., (Donald et al., 2015) dénombre au moins 23 études sur 34 qui font état d'un déficit de taille du cerveau après l'exposition prénatale. Tous diagnostics confondus, et pour un niveau d'exposition significatif, les observations montrent une réduction d'environ 10 % du volume cérébral total par rapport à une population non exposée, ce qui, en considérant la distribution de la population normale, la situerait autour de moins deux écart-types. La réduction de volume persiste dans le temps, et est étroitement corrélée au périmètre crânien, touchant dans des proportions proches les filles et les garçons, même si une tendance de sévérité plus importante semble se dessiner chez les garçons (Day et al., 2002; Chen et al., 2011; Nardelli et al., 2011; Treit et al., 2016). Par ailleurs, plusieurs études précisent que la réduction atteint à la fois la substance grise et la substance blanche. Une minorité décrit une

diminution de volume proportionnellement plus importante dans la substance blanche (Archibald et al., 2001; Gautam et al., 2014; Fan et al., 2016). Les altérations, notamment longitudinales, de l'épaisseur corticale varient aussi d'une étude à une autre (Rajapakse et al., 1996; Zhou et al., 2011, 2018; Lebel et al., 2012; Roussotte et al., 2012; Yang et al., 2012a, 2012b; Treit et al., 2013; Marshall et al., 2022; Subramoney et al., 2022). Des différences dans les volumes et/ou l'épaisseur de la substance grise ont été signalées dans des sous-régions corticales, pointant successivement le cortex frontal, pariétal et temporal, sans qu'une zone spécifique et cohérente puisse être retenue (Sowell, 2002b; Sowell et al., 2008; Zhou et al., 2011; Lebel et al., 2012; Yang et al., 2012b; De Guio et al., 2014; Marshall et al., 2022).

Dans ces études d'imagerie anatomique chez les enfants exposés à l'alcool, des anomalies focales ont également été relevées. Plus précisément, l'altération de la forme et de la taille du corps calleux constitue l'un des résultats les plus cohérents. Étant donné que cette structure est le plus grand faisceau de substance blanche du cerveau, ainsi que la principale connexion interhémisphérique, son atteinte après exposition prénatale à un agent neuro-embryo-foetotoxique paraît logique. Des travaux sur le corps calleux ont permis de préciser qu'il s'agissait d'une réduction de taille décrite soit en surface quand seule la coupe sagittale était considérée, soit en volume lorsque plusieurs coupes parasagittales étaient ajoutées (Bookstein et al., 2002a, 2002b; Yang et al., 2012a; Gautam et al., 2014; Jacobson et al., 2017; Biffen et al., 2020). Cette réduction de taille touchait plus spécifiquement les régions postérieures : l'isthme et le splénium (Sowell et al., 2001; Dodge et al., 2009), et pouvait s'associer à des anomalies d'orientation, c'est-à-dire un déplacement antéro-postérieur ou cranio-caudal par rapport à une position moyenne du corps calleux (Sowell et al., 2001), mais leur reproductibilité est faible même au sein d'une même équipe (Sowell et al., 2001; Yang et al., 2012a).

De même, la réduction de taille du cervelet est régulièrement retrouvée dans des études de morphométrie cérébrale mettant en œuvre des outils plus ou moins complexes et semble affecter plus sévèrement la zone vermiennne (Sowell et al., 1996; O'Hare et al., 2005; Bookstein et al., 2006; Astley et al., 2009a; Cardenas et al., 2014; Sullivan et al., 2020). Ces études ont permis d'objectiver des réductions surfaciques sur le plan sagittal médian du vermis (Sowell et al., 1996; Autti-Rämö et al., 2002; O'Hare et al., 2005; Astley et al., 2009a) ou des réductions volumiques, limitées au vermis (Cardenas et al., 2014). Elles pointaient toutes, de façon plus ou moins significative, une atteinte prédominante du vermis antérieur, cohérente avec les anomalies observables en radiologie clinique. Plus récemment, une étude extensive de l'ensemble des volumes cérébelleux faisait état d'une réduction volumique du vermis et de lobules cérébelleux surtout situés dans le cervelet antérieur et inférieur (Sullivan et al., 2020).

Les structures grises profondes ont également été fréquemment rapportées comme réduites en taille, même en prenant en compte le volume total du cerveau, constituant un résultat robuste et cohérent. Les effets de l'exposition à l'alcool sur le noyau caudé ont été le plus souvent retrouvés, mais aussi et plus modestement sur le noyau lenticulaire dans son

ensemble (Riikonen et al., 1999; Astley et al., 2009a; Nardelli et al., 2011; Roussotte et al., 2012; Treit et al., 2013; Biffen et al., 2020; Nakhid et al., 2022). Récemment, l'étude canadienne de Little et Beaulieu (Little and Beaulieu, 2020) a permis, par un modèle multivarié, d'évaluer les contributions respectives des volumes de toutes les structures cérébrales sus-tentorielles pour discriminer des sujets TSAF de sujets contrôles. Le noyau caudé, le pallidum et le putamen apparaissent comme les structures dont le poids prédictif est le plus fort. L'hippocampe a aussi fait l'objet de description de réduction de sa taille (Willoughby et al., 2008; Nardelli et al., 2011) qui ne résiste pas toujours à la prise en compte de la réduction globale de taille du cerveau (Astley et al., 2009a; Coles et al., 2011; Roussotte et al., 2012; Treit et al., 2013).

Il existe donc, en plus du déficit de croissance global du cerveau, une atteinte diffuse qui peut se manifester localement, et lorsqu'elle est particulièrement marquée, être visible à l'œil nu, notamment au niveau du corps calleux et du cervelet chez les sujets ayant été exposé à l'alcool. Mais, *in fine*, radiologie clinique et imagerie computationnelle n'ont à ce jour pas permis de faire émerger de nouveaux marqueurs utiles au diagnostic.

LIMITES DE L'IMPACT DE LA NEUROIMAGERIE DANS LE RAISONNEMENT DIAGNOSTIQUE ET LA PRATIQUE CLINIQUE

Toutes ces études morphométriques n'ont pas permis de translation clinique et n'ont pas eu d'impact sur la procédure diagnostique, n'apportant pas de spécificité notamment aux formes non syndromiques, ni sur l'évaluation du pronostic. Dans les recommandations actuelles, en dehors de la microcéphalie, qui est une des caractéristiques principales du SAF, la morphologie cérébrale, si elle est prise en compte, n'impacte pas ou seulement marginalement le diagnostic final. En pratique, dans les critères diagnostiques du *4-Digit Diagnostic Code* (Astley, 2004), l'atteinte neuroanatomique est regroupée avec l'atteinte fonctionnelle, constituant un critère général d'atteinte du système nerveux central. Il met presque au même plan la microcéphalie, toute anomalie structurale cérébrale d'origine prénatale présumée sans les expliciter, les crises convulsives et l'atteinte fonctionnelle cognitive. Dans les critères de l'*Institute Of Medicine* (Hoyme et al., 2016), la microcéphalie est individualisée et les anomalies structurelles du cerveau sont citées, mais encore une fois, n'impactent que marginalement le diagnostic final. Les recommandations canadiennes séparent le critère clinique de microcéphalie, mais n'incluent pas d'autres éléments de l'anatomie cérébrale dans leur démarche. Autrement dit, à la différence des critères de morphologie faciale, les anomalies morphologiques cérébrales n'apportent étonnamment pas de spécificité étiologique dans le diagnostic de TSAF, bien que le cerveau soit l'une des cibles principales de la toxicité développementale de l'alcool. En particulier, elles ne contribuent pas au diagnostic des formes sans dysmorphie faciale qui restent non spécifiques.

Les anomalies neuroanatomiques n'ont pas rejoint explicitement les critères diagnostiques, car, en plus d'être subjectives, les plus évidentes radiologiquement sont finalement peu

fréquentes. Les raisons de l'inopérance des critères neuroanatomiques malgré une littérature notable sont à chercher dans les limites méthodologiques communes à la plupart des études. En premier lieu, l'hétérogénéité des populations étudiées limite l'extension des résultats, par exemple s'il s'agit de cohorte de sujets exposés sans diagnostic syndromique, alors les tailles d'effet sont mécaniquement moindres (Zhou et al., 2011; Sullivan et al., 2020). Ensuite, un certain nombre d'auteurs proposent des analyses à l'échelle du groupe en comparant les moyennes, ce qui ne permet pas de prendre en compte la variance individuelle. Enfin, les anomalies cérébrales peuvent être redondantes avec la réduction globale de taille du cerveau, ou bien quand la réduction de taille est prise en compte, elle l'est de façon variée pouvant rendre discutable la spécificité des résultats. Les éléments méthodologiques de ces deux dernières limites vont donc être détaillés.

ENJEUX MÉTHODOLOGIQUES

ANALYSE NORMATIVE, DÉFINIR UNE NORME ET PRENDRE EN COMPTE LA VARIANCE INTER-INDIVIDUELLE

L'essor en psychiatrie d'une approche dimensionnelle des troubles, reposant sur la conviction qu'il n'y a jamais qu'une différence de degré entre le normal et le pathologique, a poussé les neuroscientifiques de cette discipline à envisager une approche normative. Ce cadre statistique offre une méthode concrète pour étudier les différences individuelles et analyser l'hétérogénéité entre les cohortes. Il est possible de quantifier le degré dont chaque individu s'écarte du modèle normatif. La disponibilité de grandes bases de données d'imagerie de sujets sains a également permis d'accélérer la diffusion de cette démarche (Marquand et al., 2016a, 2016b; Dinga et al., 2021; Bethlehem et al., 2022; Rutherford et al., 2023). Cette approche est loin d'être nouvelle pour les cliniciens utilisant des données comportementales, cliniques et biologiques. L'exemple le plus parlant est l'utilisation quotidienne des courbes de croissance pour les pédiatres. Au-delà de la quantification nette de l'écart à la norme, il s'agit bien de considérer qu'un sujet qui s'éloigne trop de la distribution normale du groupe, considérée comme étant la référence, est « anormal », singulier, et très probablement pathologique. À noter que, tout comme pour les études de comparaison de moyennes, le choix du groupe permettant d'établir la norme revêt une importance particulière pour l'interprétation des résultats. Cette approche, qui permet d'évaluer la taille d'effet à l'échelle individuelle et donc d'intégrer la variance individuelle dans l'observation d'une variable biologique, est plus à même de s'intégrer dans une démarche de translation vers la clinique.

ANALYSE DE L'EFFET DE TAILLE DU CERVEAU

La réduction globale de taille du cerveau est l'anomalie la plus fréquente dans les TSAF. Même si la microcéphalie n'est qu'un critère diagnostique des formes syndromiques, à l'échelle du groupe, les sujets ayant une forme non syndromique présentent également une réduction de

la taille du cerveau par rapport à des sujets au développement typique (Archibald et al., 2001; Astley et al., 2009a; Rajaprakash et al., 2014; Treit et al., 2016; Boronat et al., 2017). Pour la très grande majorité des études d'imagerie de ce domaine, les réductions de taille régionales sont interprétées en intégrant linéairement la taille globale du cerveau. Le paramètre de taille du cerveau est, soit inclus dans le modèle statistique comme une covariable (Roussotte et al., 2012, par exemple), soit sa variance est retranchée au paramètre d'intérêt (Chen et al., 2011, par exemple), soit intégré sous forme de ratio (Astley et al., 2009, par exemple). La possible invariance de taille régionale pour la taille globale rend cette dernière approche dite proportionnelle, potentiellement fautive ou trompeuse, car les variations de ce ratio dépendraient uniquement de celles du volume cérébral total. Dans tous les cas, les variations de proportions sont régies par un modèle linéaire qui fait l'hypothèse d'un simple zoom entre petits et gros cerveaux, en intégrant ou non (ratio) une constante représentée par l'ordonnée à l'origine. Or, les sciences du vivant nous apprennent depuis longtemps que les proportions de sous-parties d'un objet biologique varient avec sa taille globale. La paléoanthropologie et l'étude de la neuroévolution (Finlay et al., 2001; Rutherford et al., 2023) ont réintroduit cette notion dans le champ des neurosciences (Liu et al., 2014). Les variations de tailles en fonction de la taille globale du cerveau ont ouvert le champ de ce qui est appelé les études de *scaling*². La modélisation biomathématique qui traduit au mieux la relation géométrique entre la taille de l'objet d'intérêt P_i et la taille globale du cerveau T_c est basée sur une loi de puissance qui tient compte des changements potentiels de proportion le long du gradient de taille :

$$P_i = b \times T_c^a.$$

Le coefficient de *scaling* « a » est parfois aussi appelé coefficient d'allométrie, b est le coefficient de la pente. Ce modèle inclut la stricte proportionnalité comme cas particulier, le *scaling* est isométrique avec exposant *scaling* $a = 1$. Ces modélisations de *scaling* peuvent permettre des descriptions en population saine (Germanaud et al., 2012; Reardon et al., 2016, 2018; de Jong et al., 2017; Mankiw et al., 2017; Warling et al., 2021) ou pathologique (Toro et al., 2009; Germanaud et al., 2014; Williams et al., 2020). Plus largement la communauté neuroscientifique se satisfait de moins en moins des modèles linéaires qui ne reflètent pas la complexité du vivant. L'augmentation majeure de la taille des cohortes et des capacités computationnelles permettent d'appréhender des modèles complexes avec les approches non linéaires (Chen et al., 2021).

Dans le cas spécifique des TSAF, il convient particulièrement d'utiliser un modèle biomathématique plausible avec des comportements aux limites cohérents. Dans les contextes pathologiques où les gammes de taille de cerveau ne se chevauchent que partiellement avec la population saine, la loi de puissance est utile pour projeter les modèles dans les intervalles de taille respectifs. Il a aussi été montré que ne pas utiliser un modèle sensible à l'allométrie pouvait induire en erreur en cas d'effet de taille prononcé (Toro et al.,

² La traduction de « mise à l'échelle » ne permet pas de rapporter la notion de redimensionnement dans l'espace donné, nous faisons le choix de garder le temps anglais *scaling*.

2009; Germanaud et al., 2014). Bien que certains auteurs aient marginalement appliqué cette approche dans l'analyse de la morphologie cérébrale après exposition à l'alcool (Bookstein et al., 2006; Germanaud et al., 2014), celle-ci ne fait pas encore consensus dans cette communauté et limite possiblement la portée de certains résultats.

HYPOTHÈSES, OBJECTIFS ET PLAN DE TRAVAIL

L'alcoolisation fœtale est la première cause non génétique et potentiellement évitable de handicap cognitif. Le cadre diagnostique des troubles du spectre de l'alcoolisation fœtale (TSAF) est aujourd'hui largement accepté et plusieurs formalismes établis (Astley and Clarren, 2000; Hoyme et al., 2005; Cook et al., 2016) puis mis à jour (Hoyme et al., 2016; Chudley, 2018), délimitent de manière plus ou moins stricte les formes syndromiques (SAF) des formes non syndromiques (Astley, 2006; Astley-Hemingway et al., 2019). À la différence des critères de morphologie faciale, les anomalies morphologiques cérébrales suffisamment reconnues n'apportent pas de spécificité étiologique au diagnostic de TSAF, bien que le cerveau soit l'une des cibles principales de la toxicité développementale de l'alcool. En particulier, elles ne contribuent pas au diagnostic des formes sans dysmorphie faciale, non syndromiques, pour lesquelles le lien de causalité entre l'exposition à l'alcool et le trouble du neurodéveloppement est probabiliste. En-dehors de la microcéphalie, aucun marqueur neuroanatomique utile au diagnostic ou avec une valeur pronostique, n'a émergé.

Nous avons fait l'hypothèse qu'en utilisant une population de sujets TSAF et en prenant en compte la réduction caractéristique de taille du cerveau par un modèle biomathématique non linéaire, nous pourrions caractériser les anomalies cérébelleuses et calleuses. Nous avons supposé qu'il était possible d'identifier des marqueurs qualitatifs et quantitatifs neuroanatomiques chez des sujets ayant un SAF et que ces marqueurs pourraient être retrouvés à un niveau de sévérité intermédiaire chez des sujets ayant un TSAF-NS pour contribuer au renforcement du faisceau diagnostique à l'échelle individuelle.

Pour répondre à ces hypothèses, nous avons comparé une population de TSAF à une population de sujets contrôles au neurodéveloppement typique, pour chercher à identifier les anomalies neuroanatomiques à l'échelle individuelle. Compte tenu des observations cliniques et de la littérature, nous avons concentré nos recherches sur la morphologie du cervelet et du corps calleux. Nous avons utilisé, d'une part, des outils de mesure de radiologie clinique à usage quotidien, d'autre part des outils d'imagerie computationnelle développés spécialement pour cet usage. Nous avons donc caractérisé précisément les atteintes cérébelleuses et calleuses. Puis, nous avons montré la récurrence de ces anomalies, notamment dans le sous-groupe de sujets ayant un SAF dont le diagnostic est certain, ainsi que leur prévalence chez certains sujets ayant une forme non syndromique.

Le chapitre 2 de ce manuscrit présente la série clinique d'étude ainsi que les aspects pratiques des enjeux méthodologiques évoqués. Le troisième chapitre décrit l'étude radiologique

clinique qui synthétise la démarche d'identification et de combinaison de marqueurs avec des outils utilisables *en clinique*. Le chapitre quatre détaille l'étude morphométrique de l'atteinte cérébelleuse et son utilité diagnostique. Le chapitre cinq présente 2 nouvelles approches pour caractériser la morphologie du corps calleux. La première approche utilise la parcellisation du corps calleux sur la section sagittale à partir de la segmentation corticale en lobes via le tractogramme, et la deuxième analyse le profil d'épaisseur du corps calleux selon l'axe antéro-postérieur. Le dernier chapitre synthétise et commente l'apport combiné de ces résultats et aborde les points de discussion générale.

CHAPITRE 2

CADRE MÉTHODOLOGIQUE

Dans ce chapitre, les critères d'inclusion, les données cliniques de la série de sujets TSAF ainsi constituée, les données d'imagerie et leur contrôle qualité sont détaillés. Le cadre méthodologique commun de l'analyse des données est également présenté. Le détail est repris dans la sous-partie « matériel et méthode » de chaque article.

PARTICIPANTS

PRÉAMBULE

La première partie du travail a été la constitution d'une base de données clinique et radiologique des patients présentant un trouble neurodéveloppemental en contexte d'exposition prénatale à l'alcool suivis à Robert-Debré par le Dr David Germanaud, à la suite de Pauline Garzón qui avait initié le travail (Garzón, 2017). Avec Eliot Kerdreux, nous avons mis en place un outil de recueil *RedSAF* basé sur le logiciel *RedCap*. Cet outil permet de colliger les données strictement issues du soin sur un formulaire structuré et sécurisé permettant l'exploitation pseudonymisée dans le cadre de la recherche sur les données de santé. Nous avons veillé à la compatibilité des données avec celles recueillies par le service de pédopsychiatrie de Robert-Debré pour assurer la possibilité d'une analyse transnosographique, et d'une exploitation au-delà de mon travail de thèse.

POPULATION TSAF ET CRITÈRES D'INCLUSION

Les patients âgés de 6 à 20 ans, consultant pour un trouble du neurodéveloppement en contexte d'exposition prénatale à l'alcool entre 2014 et 2020 dans le service de neuropédiatrie ou de psychiatrie de l'enfant du Centre Hospitalo-Universitaire Robert-Debré (RD) (Assistance Publique-Hôpital Publique, Paris) étaient éligibles à l'inclusion. Le critère d'inclusion était un diagnostic confirmé de TSAF dont l'enquête à la recherche d'un diagnostic différentiel était complète. Les critères d'exclusion étaient donc une exposition prénatale à l'alcool insuffisante ou trop incertaine, une exposition à un autre agent embryotoxique (notamment le valproate de sodium), un diagnostic génétique causal coïncidant, une enquête étiologique à visée différentielle incomplète à la date de l'étude, dont l'absence d'IRM, ou une IRM non exploitable.

PROCÉDURE DIAGNOSTIQUE ET PHÉNOTYPE CLINIQUE

Nous avons colligé de manière systématique les données suivantes :

- comptes rendus de consultation et d'hospitalisation reportant l'histoire prénatale, périnatale et neurodéveloppementale, l'examen physique général et neurologique, la croissance staturo-pondérale et du périmètre crânien,
- évaluation et mesures de la morphologie faciale (fentes palpébrales et lèvre supérieure) sur des photographies avec échelle systématique,
- comptes rendus d'IRM cérébrale réalisée dans le service de radiologie clinique de RD.

DIAGNOSTIC SYNDROMIQUE

Le diagnostic syndromique était établi en utilisant les deux principaux formalismes diagnostiques du *4-Digit Diagnostic Code* (Astley, 2004) et l'*Institute Of Medicine* (Hoyme et al., 2016).

Le niveau d'exposition prénatale à l'alcool était confirmé par des éléments directs (par la mère, les proches, le dossier d'adoption, ou dans le dossier du patient) ou indirects la rendant très fortement probable (triple association d'une adoption dans un pays à forte endémie de trouble chronique de l'usage de l'alcool, d'un mode de vie à haut risque d'abus d'alcool et d'une déchéance parentale). Selon le *4-Digit Diagnostic Code*, le grade 4 était attribué en cas d'exposition prénatale à l'alcool confirmée et sévère (en moyenne trois verres standards ou plus par jour pendant plus de deux à quatre semaines, ou nombreux épisodes d'ébriété, soit quatre verres ou plus occasionnellement, après la quatrième semaine de grossesse). Le grade 3 était attribué en cas d'exposition prénatale à l'alcool confirmée et modérée préoccupante (régulièrement un ou deux verres par jour, au plus, deux verres en moyenne par jour sur quatre semaines, ou plusieurs épisodes d'ébriété, après la quatrième semaine de grossesse), ou confirmée très probablement notable mais non quantifiable. Le grade 2 était attribué en cas d'exposition prénatale à l'alcool inconnue, hors situations à haut risque citées précédemment. Le grade 1 correspondant à l'absence confirmée d'exposition, de la conception à la naissance, ou certainement légère et très occasionnelle (moins d'un verre standard par semaine, et moins d'un verre standard par occasion) ou modérée simple (régulièrement entre un et quatre verres maximum par semaine, moins de deux épisodes d'ébriété) et constituait un critère d'exclusion. Dans les recommandations de l'*Institute Of Medicine*, le niveau considéré comme significatif (*documented*) correspond grossièrement au grade 3 des critères précédents, c'est-à-dire plus de six verres par semaine pendant au moins deux semaines ou plus de trois verres par occasion à au moins deux occasions. Ces recommandations établissent aussi que, la présence de problèmes sociaux ou juridiques liés à l'alcool avant ou pendant la grossesse ou certains tests biologiques, sont une documentation indirecte pertinente et qu'ils permettent de considérer le niveau d'exposition comme sûrement significatif. En pratique dans notre série clinique, la moitié des enfants étaient issus de l'adoption internationale et les autres, ne vivant plus avec leur famille biologique. Il n'était

donc pas possible de recueillir des données quantitatives rétrospectivement sur le niveau d'exposition.

Les trois critères principaux de la dysmorphie faciale (fentes palpébrales étroites, philtrum émoussé, et lèvre supérieure fine), étaient évalués pendant la consultation médicale et confirmés par l'analyse semi-quantitative sur photographie. Les fentes palpébrales étaient considérées comme étroites si le Z-score de la mesure selon les courbes de Clarrens et al. (Clarren et al., 2010) était inférieur à moins deux écart-types pour le *4-Digit Diagnostic Code* ou inférieur au dixième percentile pour l'*Institute Of Medicine*. Le relief du philtrum et la finesse de la lèvre supérieure étaient évalués par l'échelle de Likert en 5 points du Lip-Philtrum Guides en prenant en compte les différences ethniques (Astley, 2004; Hoyme et al., 2015).

Le retard de croissance staturo-pondérale était déterminé à partir des taille, poids et terme de naissance, et les mesures répétées reportées sur les courbes de Mamelle et al. (Mamelle et al., 2001) pour les nouveau-nés prématurés et les courbes du CDC (Kuczmarski et al., 2000), ajustées pour le sexe. Les troisième et dixième percentiles étaient considérés pour les grades du *4-Digit Diagnostic Code*. Les facteurs influençant postnataux (carence alimentaire par exemple), particulièrement en cas d'adoption étaient pris en compte.

L'atteinte du système nerveux central regroupe les versants structurel et fonctionnel. L'atteinte structurelle est actuellement définie lorsque le patient présente une microcéphalie, soit un périmètre crânien (tous ceux connus) inférieur à moins deux écart-types sur les courbes de Hall et al. (Hall et al., 1989) pour le *4-Digit Diagnostic Code* et inférieur ou égal au dixième percentile sur les courbes de Rollins et al. (Rollins et al., 2010) pour la classification de l'*Institute Of Medicine* et/ou une '*malformation cérébrale significative structurelle d'origine prénatale présumée et non imputable à une autre cause identifiable*'. Des crises convulsives non attribuables à une atteinte postnatale et hors crises fébriles sont aussi considérées dans le critère d'atteinte du système nerveux central, conformément aux recommandations du *4-Digit Diagnostic Code* et de l'*Institute Of Medicine*. Le versant fonctionnel implique des troubles des acquisitions ou des apprentissages correspondant à un diagnostic de trouble du neurodéveloppement ou à un déficit fonctionnel caractérisé, par exemple des fonctions exécutives ou mnésiques ou à un dysfonctionnement socio-émotionnel caractérisé, avec retentissement sur le fonctionnement adaptatif.

La concordance entre les diagnostics issus de ces deux formalismes a été étudiée. Le diagnostic final retenu pour l'ensemble des analyses était celui du *4-Digit Diagnostic Code*, connu pour être plus restrictif pour le diagnostic des formes syndromiques (Astley-Hemingway et al., 2019), puis les sujets étaient répartis en deux groupes :

- le groupe « SAF » : les sujets ayant un SAF partiel ou non,
- le groupe « TSAF-NS » : les sujets ayant un TSAF non syndromique regroupant les *Static Encephalopathy/Alcohol Exposed* et *Neurobehavioral Disorder/Alcohol Exposed* du *4-Digit Diagnostic Code* équivalent au *Alcohol Related Neurodevelopmental Disorders* de l'*Institute Of Medicine*.

DIAGNOSTIC DIFFÉRENTIEL

La recherche de diagnostic différentiel était fondée sur l'examen clinique réalisé par un neuropédiatre senior, avec, en cas de caractéristiques faciales atypiques, l'aide d'un généticien pédiatrique senior, ainsi qu'une analyse biologique standard. L'exploration génétique systématique incluait des MLPA (*Multiplex Ligation-dependent Probe Amplification*) sub-téломériques et interstitielles jusqu'à décembre 2015, puis une Analyse Chromosomique sur Puce à ADN (ACPA) de haute résolution à partir de janvier 2016 et rétrospectivement chaque fois que possible, ainsi que la recherche de mutation *FMR1* en cas de suspicion de trouble du développement intellectuel. L'IRM cérébrale était réalisée systématiquement dans le cadre du soin, compte tenu du risque d'anomalie cérébrale.

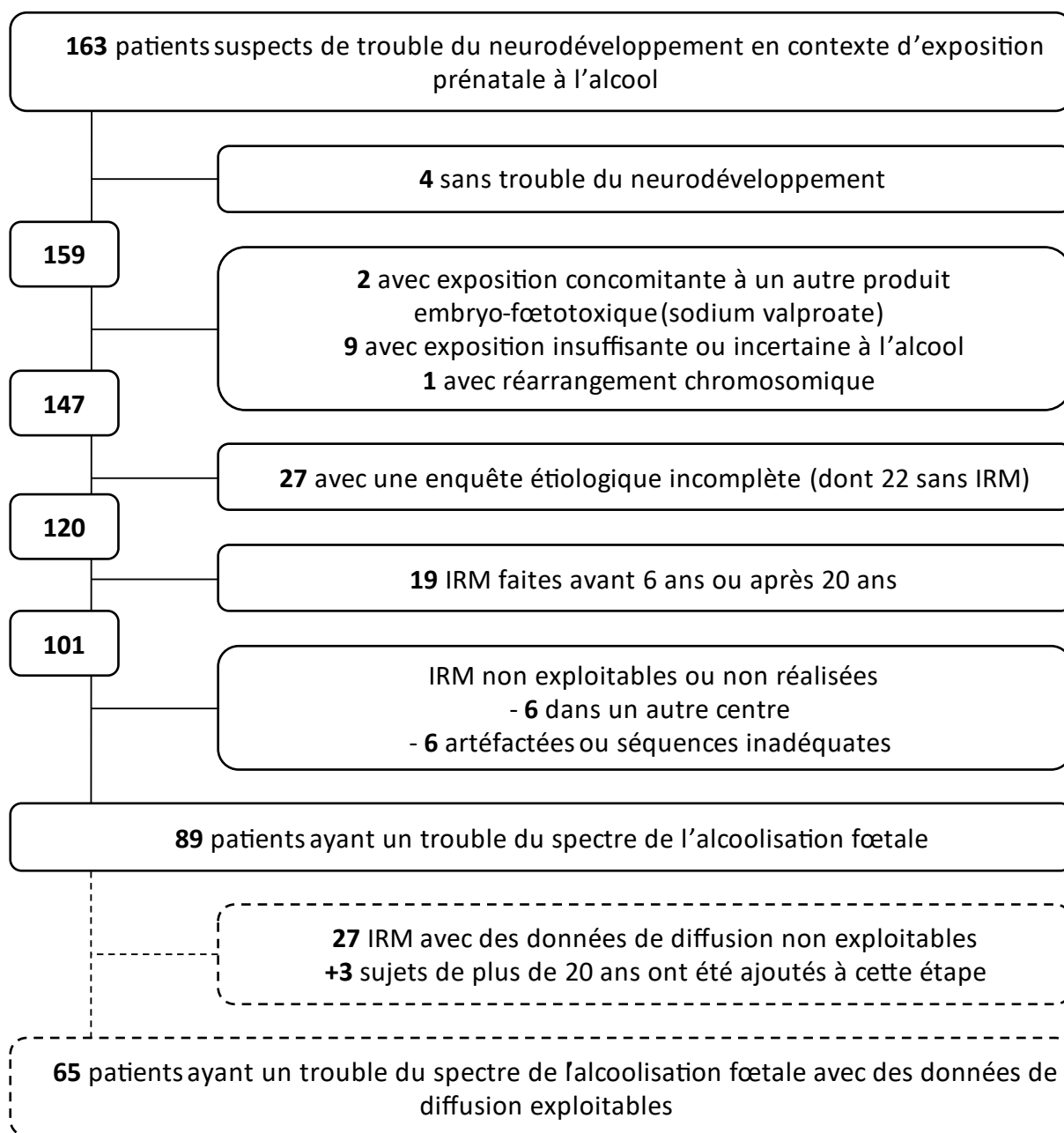


Figure 1. Diagramme de flux d'inclusion des patients de la cohorte entre 2014 et 2020.

ACQUISITION DES DONNÉES IRM

Les acquisitions IRM étaient réalisées dans le service d'imagerie pédiatrique de RD avec le scanner Philips à 1,5 T avec une séquence anatomique 3DT1 FFE-TFE (millimétrique isotrope ; TR = 8,2 ms ; TE = 3,8 ms ; TI = 0,8 s ; Flip = 8° ; SENSE = 2) et lorsque c'était possible, une séquence SE-EPI 2D pondérée en diffusion (2,5 mm isotrope, b1000 s/mm², 32 directions) et une carte de champ (**Figure 1**). Un contrôle visuel de la qualité a été systématiquement effectué pour exclure les images non exploitables. Les données IRM étaient ensuite pseudonymisées et transférées pour être traitées.

DIAGNOSTIC FONCTIONNEL

Les patients ont systématiquement bénéficié d'une évaluation psychométrique par une échelle d'intelligence de Wechsler adaptée à l'âge, réalisée ou non au sein de RD. Les autres évaluations cognitives et langagières réalisées selon les besoins cliniques étaient trop hétérogènes pour être colligées. Le diagnostic fonctionnel a été établi par un neuropédiatre senior ou un pédopsychiatre senior sur la base des données cliniques et des évaluations cognitives complémentaires selon les critères diagnostiques des troubles du neurodéveloppement du DSM-5 et de la CIM-10 (Battle, 2013).

CARACTÉRISTIQUES CLINIQUES

Les caractéristiques des 52 sujets SAF (58,4 %) et des 37 sujets TSAF-NS (41,6 %) sont détaillées dans le **Tableau** suivant.

Tableau. Caractéristiques sociodémographiques, cliniques, radiologiques et fonctionnelles des sujets TSAF. Les axes du 4-Digit Diagnostic Code apparaissent en gras et en grisé.

ET : écart-type ; SAF : syndrome d'alcoolisation fœtale ; IOM : Institute Of Medicine.

	SAF N = 52	TSAF-NS N = 37
DONNÉES SOCIODÉMOGRAPHIQUES		
Sexe (% masculin)	27 (51,9)	25 (67,6)
Âge à la consultation, moyenne en années (ET)	10,3 (3,7)	11,3 (3,9)
Âge à l'IRM, moyenne en années (ET)	10,9 (3,6)	11,9 (3,6)
Adopté (%)	32 (61,5)	22 (59,5)
Âge à l'adoption, moyenne en mois (ET)	39,3 (31,9)	30,8 (24,5)
Pays d'adoption (%)		
Russie	19 (36,5)	9 (24,3)
France	2 (3,8)	3 (8,1)
Ukraine	6 (11,5)	4 (10,8)
Autres	4 (7,7)	7 (18,9)
DONNÉES CLINIQUES		
Exposition prénatale à l'alcool (%)		

4. Confirmée et sévère	21 (40,4)	16 (43,2)
3. Confirmée et modérée préoccupante ou non quantifiée	26 (50,0)	19 (51,1)
2. Non documentée	5 (9,6)	2 (5,4)
1. Non exposé	0 (0,0)	0 (0,0)
Âge de la marche		
Connu	26 (50,0)	23 (62,2)
Moyenne en mois (ET)	16,0 (3,6)	17,4 (8,8)
Hypotrophie néonatale (%)		
Connue	32 (61,5)	30 (81,1)
Présente	16 (30,8)	4 (10,8)
Secondairement compensée	7 (13,5)	4 (10,8)
Caractéristiques faciales du SAF (%)		
4. Sévère	31 (59,6)	2 (5,4)
3. Modérée	21 (40,4)	1 (2,7)
2. Mineure	0 (0,0)	30 (81,1)
1. Aucune	0 (0,0)	4 (10,8)
Retard de croissance staturo-pondérale (%)		
4. Sévère	19 (36,5)	3 (8,1)
3. Modéré	11 (21,2)	2 (5,4)
2. Mineur	9 (17,3)	9 (24,3)
1. Aucun	13 (25,0)	23 (62,2)
ANATOMIE CÉRÉBRALE		
Périmètre crânien, le plus petit connu (%)		
Microcéphalie (< -2 ET)	34 (65,4)	13 (35,1)
≤ 10 ^{ème} percentile	46 (88,5)	21 (56,8)
Malformations cérébrales significatives, sur le compte rendu initial des radiologues (%)		
Anomalie de corps calleux	9 (17,3)	5 (13,5)
Anomalie du cervelet	6 (11,5)	5 (13,5)
Hétérotopies nodulaires	2 (3,8)	0 (0,0)
Bulbes olfactifs agénétiques ou punctiformes	2 (3,8)	1 (2,7)
Atteinte structurale du système nerveux central (%)	40 (76,9)	19 (51,4)
DONNÉES NEUROFONCTIONNELLES		
Test neuropsychologique (%)	44 (84,6)	34 (91,9)
Âge au test, moyenne en années (ET)	10,0 (2,6)	11,0 (3,6)
Type de test de l'efficacité intellectuelle (% de tests)		
WPPSI-III	1 (2,2)	0 (0,0)
WPPSI-IV	3 (6,8)	3 (8,8)
WISC-IV	27 (61,3)	21 (61,8)

WISC-V	14 (31,8)	6 (17,6)
WAIS-III	0 (0,0)	1 (2,9)
WAIS-IV	0 (0,0)	3 (8,8)
Diagnostic fonctionnel synthétique (%)		
Trouble du développement intellectuel	4 (7,7)	1 (2,7)
Efficiences intellectuelle limite	6 (11,5)	9 (24,3)
Trouble déficitaire de l'attention/hyperactivité	42 (80,8)	28 (75,7)
Trouble des fonctions exécutives	33 (63,5)	23 (62,2)
Trouble du spectre autistique	1 (1,9)	1 (2,7)
Trouble d'acquisition des coordinations	8 (15,4)	7 (18,9)
Trouble d'acquisition du langage oral	5 (9,6)	2 (5,4)
Catégorie diagnostique différente selon les critères de l'IOM	2 (3,8)	4 (10,8)

POPULATION DES CONTRÔLES

Les contrôles étaient âgés de six à vingt ans et n'avaient pas de trouble du neurodéveloppement ni d'antécédent neurologique ou psychiatrique familial au 1^{er} degré. Les acquisitions des contrôles ont été réalisées sur trois sites différents. Un sous-groupe des contrôles, apparié pour l'imageur à RD et les séquences IRM des patients, était issu d'un programme de recherche indépendant mené à l'hôpital Robert-Debré (service de psychiatrie de l'enfant). Un deuxième sous-groupe, non apparié pour l'imageur, était issu d'études précédentes. Les acquisitions ont été alors réalisées à NeuroSpin (CEA-Saclay) (Boueyre et al., 2018) avec une séquence 3DT1 Siemens MPRAGE 3 T (millimétrique isotrope ; TR = 2,3 s ; TE = 3 ms ; TI = 0,9 s ; Flip = 9° ; GRAPPA = 2) et à l'hôpital Frédéric Joliot (SHFJ, CEA-Saclay) (Germanaud et al., 2014) avec une séquence 3DT1 GE FSPGR à 1,5 T (1x1x1,2 mm ; TR = 9,9 ms ; TE = 2 ms ; TI = 0,6 s ; Flip = 10°).

ASPECTS ÉTHIQUES

Les données des patients issues du soin ont été étudiées rétrospectivement, dans le cadre de la méthodologie de référence MR-004 (déclaration de conformité 2219665v0). Elle encadre les traitements de données à caractère personnel à des fins d'étude n'impliquant pas la personne humaine, plus précisément des études ne répondant pas à la définition d'une recherche impliquant la personne humaine, en particulier les études portant sur la réutilisation des données de santé. Dans ce contexte, la possibilité d'une réutilisation anonyme des données issues du soin a été publicisée (note systématique portée au compte rendu ou information spécifique en cours de consultation) afin de permettre un refus explicite ou une demande de retrait ultérieure. L'accord d'un comité d'éthique approprié a été obtenu (CER-Paris-Saclay-2020-094).

Les données des contrôles ont été utilisées dans le cadre des autorisations éthiques des études initiales (INSERM C07-33) (Germanaud et al., 2014; Bouyeure et al., 2018).

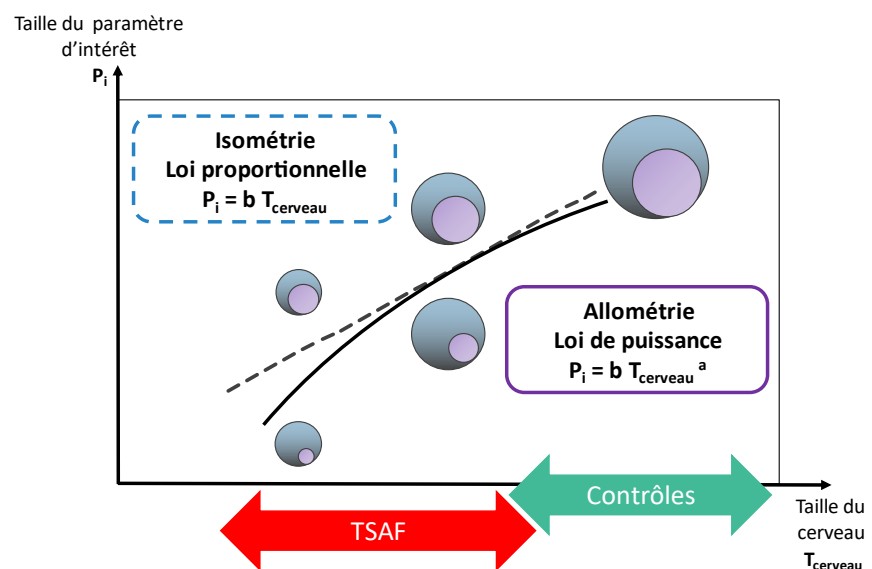
APPLICATION DES ENJEUX MÉTHODOLOGIQUES PRINCIPAUX

À partir de ces données d'imagerie, nous avons segmenté des objets anatomiques d'intérêt, mesuré des caractéristiques morphologiques de certaines régions cérébrales pour extraire des données quantitatives (volumes, surfaces, épaisseurs) en vue de les comparer entre sujets TSAF et contrôles.

MODÉLISATION DE L'EFFET DE TAILLE

Pour correctement interpréter la différence d'un paramètre morphométrique cérébral entre ces deux groupes, il faut prendre en compte le déficit global de croissance cérébrale des TSAF. L'un des moyens est de réaliser les analyses dans l'espace de *scaling*, où la taille de l'objet s'exprime en fonction de la taille globale du cerveau. La prise en compte linéaire de l'effet de la taille du cerveau dans des comparaisons peut mener à des conclusions erronées en particulier lorsque les cerveaux d'intérêt sont « trop petits ». Nous avons donc modélisé dans l'espace de *scaling*, les phénomènes d'allométrie par lesquels les proportions peuvent changer avec la taille, sur la base d'une loi de puissance non linéaire (**Figure 2**). Le coefficient de *scaling* « a » peut alors être comparé à 1, c'est-à-dire au modèle isométrique. S'il est supérieur à 1, il existe alors une allométrie positive, la taille de l'objet augmente plus vite que la taille globale. S'il est inférieur à 1, l'allométrie est négative, la taille de l'objet augmente plus faiblement que la taille globale.

Figure 2.
Modélisation de l'effet de taille, relation entre la taille du paramètre d'intérêt en fonction de la taille du cerveau ou analyse de *scaling*. Dans cette représentation, le coefficient d'allométrie a est négatif.

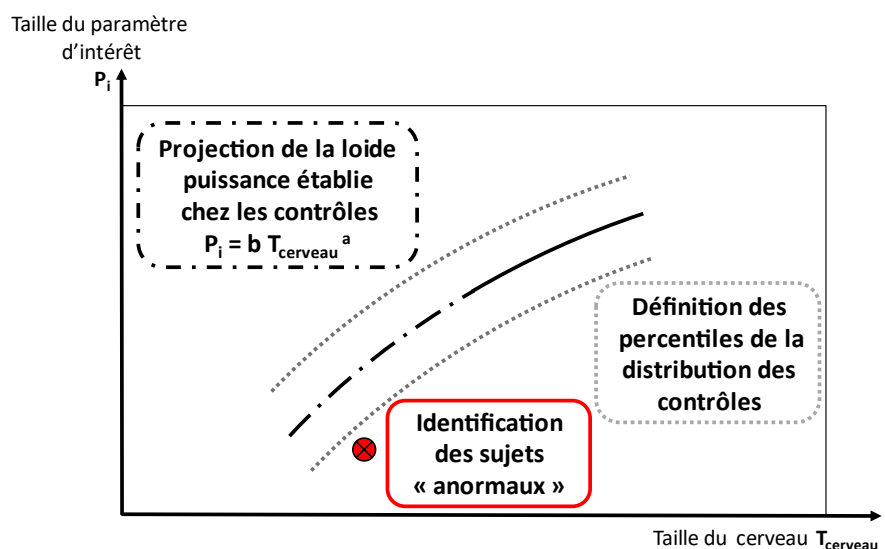


MODÈLE NORMATIF

Pour dépasser les simples comparaisons de groupes et modéliser la variance à l'échelle individuelle, nous avons utilisé une approche normative. Nous avons pu appliquer soit à l'analyse de la croissance pour décrire les variations avec l'âge soit à l'analyse de *scaling* pour décrire les variations avec la taille globale du cerveau. Dans les deux cas et quel que soit le modèle biomathématique sous-jacent, la loi a été régressée chez les contrôles pour servir alors de référence. La distance par rapport à cette référence a pu être utilisée pour quantifier la taille d'effet, comme cela est fait avec le Z-score ou l'écart-type. Cette nouvelle variable quantitative peut alors être étudiée, comparée ou permettre de classer les sujets.

Il a été aussi possible d'étudier la distribution de cette distance à la référence établie chez les contrôles pour établir un seuil normatif. Ce seuil est alors défini en percentile de la distribution des contrôles. Les sujets chez lesquels la mesure du paramètre dépasse ou ne dépasse pas ce seuil (dans le cas d'une réduction de taille) a pu être quantifié. Les sujets sont alors considérés comme « anormaux » au sens littéral, c'est-à-dire dont le paramètre étudié est excessivement trop petit ou sous-dimensionné pour la taille de leur cerveau.

Figure 3. Modélisation normative appliquée à l'analyse de *scaling* permettant l'identification des sujets anormaux, dont le paramètre d'intérêt est excessivement trop petit ou sous-dimensionné pour la taille de leur cerveau.



PRISE EN COMPTE DES COVARIABLES

Comprendre les variations de taille d'un « objet » cérébral entre les sujets contrôles et les populations de TSAF nécessite d'inclure les variables pouvant influencer ou biaiser ces variations.

Certaines covariables semblent évidentes dans l'étude du développement ou de morphologie cérébrale, comme l'âge et le sexe (Fan et al., 2010; Luders et al., 2014; Treit et al., 2017). Nous utilisons ce terme à dessein, car nous parlons ici du sexe biologique à la naissance. Ensuite, comme nous l'avons évoqué, il faut prendre en compte la taille globale du cerveau. La latéralité de la structure étudiée peut également être prise en compte, les références biographiques faisant état d'une asymétrie de morphologie cérébrale en population saine et

TSAF étant nombreuses (Sowell, 2002a; Willford et al., 2010; Zhou et al., 2018). Dans notre cas, n'ayant pas d'hypothèses sur cette question, ni de questionnement physiopathologique qui aurait nécessité cette distinction, nous avons sommé la droite et la gauche pour les structures paires. Dans le contexte clinique des TSAF, il pourrait être pertinent d'intégrer le niveau et les modalités d'exposition à l'alcool pour corrélérer quantitativement le niveau d'atteinte et le toxique en cause. Par ailleurs, le contexte socio-économique aurait pu être considérée comme une covariable d'intérêt. Dans le cadre des études en neuro-imagerie, le type d'imageur IRM, la puissance du champ, les séquences, la résolution mais aussi le lieu de l'acquisition, peuvent potentiellement introduire de variabilité dans les données.

Dans notre cas, les covariables accessibles que nous avons jugées pertinentes car potentiellement confondantes sont l'âge à l'IRM, le sexe biologique déclaré et le site d'acquisition. Nous manquons de données sur le niveau socioéconomique et le niveau d'exposition pour pouvoir les prendre en compte. Une des premières manières de minimiser l'effet d'une covariable lors de comparaison de groupes est de s'assurer qu'elle est présente dans les mêmes proportions ou avec une moyenne équivalente dans les deux groupes. À ce titre, notre groupe contrôle est apparié en âge et en sexe ratio à la population des TSAF.

L'approche classique pour prendre en compte ces covariables est de les intégrer comme variables explicatives dans une régression multiple, mais il est alors très complexe si ce n'est impossible de gérer les non-linéarités (impact des différentes covariables sur les paramètres non linéaires). Cette approche est difficilement compatible avec une analyse principale dans l'espace de *scaling* comme nous avons souhaité le faire pour prendre en compte au mieux l'effet de taille majeur dans notre population.

Il est aussi possible de retrancher au préalable au paramètre d'intérêt, la variance induite par la covariable (*residualization*, en anglais), et ce, séquentiellement covariable après covariable. L'ordre de prise en compte des covariables peut influencer le résultat final, a fortiori si elles sont colinéaires. Pour minimiser cet inconvénient, il est possible de corriger par ordre décroissant d'effet sur le paramètre d'intérêt ou d'utiliser des méthodes d'homogénéisation plus élaborées conservant la variation biologique dans les données. Enfin, et sous réserve d'effectif suffisant, pour les variables catégorielles, il est possible de réaliser les analyses en sous-groupes (par exemple, femmes et hommes séparément). Dans les études présentées, nous avons fait des choix variés dépendant de la taille des échantillons, du niveau de complexité des analyses, de la taille des effets et de l'objectif final. Nous avons pu proposer des analyses post hoc permettant de mesurer l'impact du choix proposé dans l'analyse principale.

CHAPITRE 3

ÉTUDE EN RADIOLOGIE CLINIQUE DE L'ATTEINTE DU VERMIS ET DU CORPS CALLEUX

INTRODUCTION

Dans cette première étude, nous avons recherché des marqueurs neuroanatomiques en utilisant des outils d'imagerie clinique accessibles dans la pratique quotidienne des radiologues et des cliniciens, en proposant des mesures quantitatives et semi-quantitatives. Nous avons appliqué une méthode d'analyse normative en utilisant le groupe contrôle pour établir les courbes de croissance, et de *scaling* pour prendre en compte la réduction de taille du cerveau. Nous avons pu mettre en évidence trois anomalies objectives du vermis et du corps calleux à la fois récurrentes dans le SAF et complémentaires du déficit de taille du cerveau. Nous avons montré que leur co-occurrence était fréquente, non seulement, dans le SAF, mais aussi dans les TSAF non syndromiques, alors qu'elle restait exceptionnelle chez les contrôles au développement typique. Sur cette base, nous avons proposé d'introduire un nouveau critère diagnostique neuroradiologique, en montrant comment il pourrait aider les cliniciens à mieux estimer la probabilité du lien causal entre le phénotype clinique et l'exposition prénatale à l'alcool, en particulier pour les TSAF non syndromiques où ce lien reste probabiliste.

COMBINER LES CARACTÉRISTIQUES NEUROANATOMIQUES POUR ÉTAYER LE DIAGNOSTIC DE TROUBLE DU SPECTRE DE L'ALCOOLISATION FCETALE

Fraize, J., Garzón, P., Ntorkou, A., Kerdreux, E., Boespflug-Tanguy, O., Beggiato, A., Delorme, R., Hertz-Pannier, L., Elmaleh-Berges, M., & Germanaud, D. (2023). Combining neuroanatomical features to support diagnosis of fetal alcohol spectrum disorders. *Developmental medicine and child neurology*, 65(4), 551–562. <https://doi.org/10.1111/dmcn.15411>

RÉSUMÉ

Objectif

Dans le diagnostic des troubles du spectre de l'alcoolisation fœtale (TSAF), la microcéphalie est la seule caractéristique neuroanatomique à prendre en compte. Les autres atteintes cérébrales, bien que largement décrites ne sont pas spécifiées et donc sous-exploitées, surtout en l'absence de syndrome d'alcoolisation fœtale (SAF) lorsque le diagnostic de forme non syndromique (TSAF-NS) reste probabiliste. Nous avons donc cherché, dans ce travail, à identifier les anomalies neuroanatomiques ayant une valeur diagnostique.

Matériels et méthodes

Nous avons recueilli rétrospectivement les données monocentriques de 52 sujets ayant un SAF, de 37 sujets ayant un TSAF-NS et de 94 contrôles appariés (6 - 20 ans). Sur l'IRM cérébrale, nous avons mesuré la taille du cerveau (aire d'une coupe de référence), la longueur et l'épaisseur du corps calleux, la hauteur du vermis, puis évalué la foliation du vermis (échelle de Likert). Pour chaque paramètre, nous avons établi les variations avec l'âge (courbes de croissance) et la taille du cerveau chez les contrôles (courbes de *scaling*), puis nous avons identifié les sujets présentant des mesures anormales (< 10^{ème} percentile).

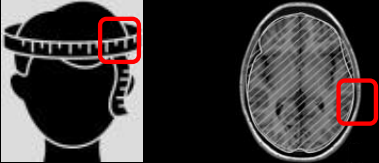
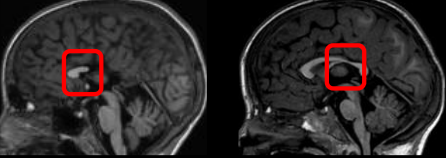
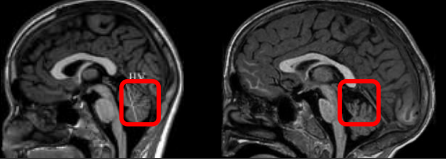
Résultats

Selon les courbes de croissance, il y avait un excès de sujets ayant un SAF avec un cerveau, un isthme, un splénium et un vermis, anormalement petits (< 10^{ème} percentile). Selon les courbes de *scaling*, cet excès ne persistait que pour l'épaisseur de l'isthme et la hauteur du vermis. La foliation du vermis était pathologique chez 18 % des sujets ayant un TSAF, et jamais chez les contrôles. Dans l'ensemble, 39 % des sujets ayant un SAF et 27 % des sujets ayant un TSAF-NS, et seulement 2 % des contrôles, présentaient deux anomalies récurrentes du SAF, et 19 % des SAF en présentaient trois. Compte tenu du nombre d'anomalies, la probabilité d'un lien de causalité avec l'alcool était renforcée pour 14 % des sujets ayant un TSAF-NS.

Conclusion


Nos résultats suggèrent que l'ajout d'un critère neuroanatomique radiologique explicite et composite pour le diagnostic de TSAF peut améliorer sa spécificité, en particulier dans le cas des formes non syndromiques.

RÉSUMÉ GRAPHIQUE

<p>Taille du cerveau Périmètre crânien/ Aire cérébrale</p>		<p>+2</p>
<p>Corps calleux Isthme fin / Agénésie</p>		<p>+1</p>
<p>Vermis Hauteur réduite / Foliation perturbée</p>		<p>+1/+1</p>
<p>Score de dommage neuroanatomique dans les troubles du spectre de l'alcoolisation fœtale</p>		<p>=</p>

ORIGINAL ARTICLE

Combining neuroanatomical features to support diagnosis of fetal alcohol spectrum disorders

Justine Fraize^{1,2}  | Pauline Garzón^{1,2} | Alexandra Ntorkou³ | Eliot Kerdreux^{1,2} |
Odile Boespflug-Tanguy⁴ | Anita Beggiano⁵ | Richard Delorme⁵ | Lucie Hertz-Pannier^{1,2} |
Monique Elmaleh-Berges^{2,3} | David Germanaud^{1,2,6}

¹CEA Paris-Saclay, Frederic Joliot Institute, NeuroSpin, UNIACT, Gif-sur-Yvette, France

²Université Paris Cité, Inserm, NeuroDiderot, InDEV, Paris, France

³Department of Paediatric Radiologic, Centre of Excellence InovAND, Robert-Debré Hospital, AP-HP, Paris, France

⁴Université Paris Cité, Inserm, NeuroDiderot, NeuroDEV, Paris, France

⁵Department of Child and Adolescent Psychiatry, Centre of Excellence InovAND, Robert-Debré Hospital, AP-HP, Paris, France

⁶Department of Genetics, Centre of Excellence InovAND, Robert-Debré Hospital, AP-HP, Paris, France

Correspondence

Justine Fraize, NeuroSpin, Bâtiment 145, CEA Paris-Saclay, 91191 Gif-sur-Yvette, France.
Email: justine.fraize@inserm.fr

Funding information

French National Agency for Research, Grant/Award Number: ANR-19-CE17-0028-01; French National Institute for Public Health research, Grant/Award Number: IRESP-19-ADDICTIONS-08

Abstract

Aim: To identify easily accessible neuroanatomical abnormalities useful for diagnosing fetal alcohol spectrum disorders (FASD) in fetal alcohol syndrome (FAS) but more importantly for the probabilistic diagnosis of non-syndromic forms (NS-FASD).

Method: We retrospectively collected monocentric data from 52 individuals with FAS, 37 with NS-FASD, and 94 paired typically developing individuals (6–20 years, 99 males, 84 females). On brain T1-weighted magnetic resonance imaging, we measured brain size, corpus callosum length and thicknesses, vermis height, then evaluated vermis foliation (Likert scale). For each parameter, we established variations with age and brain size in comparison individuals (growth and scaling charts), then identified participants with abnormal measurements (<10th centile).

Results: According to growth charts, there was an excess of FAS with abnormally small brain, isthmus, splenium, and vermis. According to scaling charts, this excess remained only for isthmus thickness and vermis height. The vermis foliation was pathological in 18% of those with FASD but in no comparison individual. Overall, 39% of those with FAS, 27% with NS-FASD, but only 2% of comparison individuals presented with two FAS-recurrent abnormalities, and 19% of those with FAS had all three. Considering the number of anomalies, there was a higher likelihood of a causal link with alcohol in 14% of those with NS-FASD.

Interpretation: Our results suggest that adding an explicit composite neuroanatomical–radiological criterion for FASD diagnosis may improve its specificity, especially in NS-FASD.

The neurodevelopmental toxicity of ethanol has long been attested by congenital brain abnormalities and the high prevalence of neurodevelopmental disorders following severe prenatal alcohol exposure (PAE).¹ Yet, it remains a

frequent and underdiagnosed cause of cognitive and behavioural disabilities.² Grouped under the umbrella diagnosis of fetal alcohol spectrum disorder (FASD), the pathological consequences of PAE range from fetal alcohol

Abbreviations: ACC, agenesis of corpus callosum; FAS, fetal alcohol syndrome; FASD, fetal alcohol spectrum disorder; NS-FASD, non-syndromic fetal alcohol spectrum disorder; PAE, prenatal alcohol exposure; RBA, reference brain area (axial).

This is an open access article under the terms of the [Creative Commons Attribution-NonCommercial-NoDerivs](https://creativecommons.org/licenses/by-nc-nd/4.0/) License, which permits use and distribution in any medium, provided the original work is properly cited, the use is non-commercial and no modifications or adaptations are made.

© 2022 The Authors. *Developmental Medicine & Child Neurology* published by John Wiley & Sons Ltd on behalf of Mac Keith Press.

syndrome (FAS) with its specific association of facial features, body, and brain growth deficiency, to non-specific non-syndromic FASD (NS-FASD) when these physical criteria are absent or incomplete, but a probabilistic causal link can be assumed between neurodevelopmental disorders and PAE. Several guidelines for diagnosing FASD have been published^{3–5} and revised,⁶ which now share a common backbone of key clinical criteria among which the dysmorphic facial features have a well-codified evaluation and a decisive value. The full facial phenotype consensually involves a more specific diagnostic category with a more certain causal link with PAE. The cerebral phenotype is more diversely considered for both the features deemed relevant and their diagnostic significance. Anatomical and functional impairments are either grouped or treated separately depending on guidelines or versions with little impact on diagnosis.

The most patent neuroanatomical abnormality in FASD is a global brain growth deficiency that frequently results in clinical microcephaly.^{7,8} More focal brain abnormalities have also been described,^{9–11} most of them rarely or hardly apparent on individual magnetic resonance imaging (MRI) scans: abnormalities of the corpus callosum^{11–14} or the cerebellum, particularly the vermis,^{15–17} or nodular heterotopias. However, neither clinical radiology nor computational imaging findings have so far enabled FASD-relevant brain abnormalities to be unambiguously discriminated from incidental or non-suggestive ones, let alone warranted a consensual well-codified distinct neuroanatomical criterion influencing diagnosis. Currently, any structural brain abnormality of presumed prenatal origin is considered like any severe functional impairment,⁴ or given a higher diagnostic weight,⁵ or else considered a distinct item, with an emphasis on microcephaly mainly for its frequency-driven practical value,⁶ but with little influence on the final diagnosis. Unlike dysmorphic facial features, neuroanatomical abnormalities provide very little,⁶ if any,^{4,5} etiological specificity in FASD diagnosis, even though the brain is a major target of ethanol developmental toxicity.

In our study, we aimed to characterize recurrent anomalies on brain MRI whose combination could be of diagnostic value in FASD. We first considered measurements of brain size, corpus callosum, and vermis, and compared the individual values observed in FAS with the distributions according to age and then brain size in typically developing comparison individuals, to identify which of these measures were frequently abnormal in individuals with FAS, while not being trivially explained by brain growth deficiency. Beyond vermis height measurement, we established the ability of a semi-quantitative Likert scale, describing the shape of the upper vermis, to accurately distinguish typical from atypical vermis. We then investigated whether individuals with FAS and NS-FASD presented a combination of small brain size with one or more of the callosal and vermis abnormalities we showed to be recurrent in FAS, while comparison individuals did not. Finally, we sought to establish whether

What this paper adds

- Neuroanatomical anomalies independent of microcephaly can be measured with clinical-imaging tools.
- Small-for-age brain, small-for-brain-size callosal isthmus or vermian height, and disrupted vermis foliation are fetal alcohol syndrome (FAS)-recurrent anomalies.
- Associations of these anomalies are frequent in fetal alcohol spectrum disorder (FASD) even without FAS, while exceptional in typically developing individuals.
- These associations support higher likelihood of causal link with alcohol in some individuals with non-syndromic FASD.
- A new explicit and composite neuroanatomical-radiological criterion can improve the specificity of FASD diagnosis.

taking such combinations into account in the diagnosis could constitute an additional argument to estimate the causal link with PAE.

METHOD

Participants

We performed a retrospective case–control study with monocentric recruitment for participants with FASD and bicentric for comparison individuals. Eighty-nine participants with FASD, aged 6 to 20 years, were included among the 149 diagnosed between 2014 and 2020 at Robert-Debré University Hospital (AP-HP, Paris, France) (Figure S1). Ninety-four typically developing comparison individuals aged 6 to 20 years, with no report of PAE nor family history of neurological or psychiatric condition (in first-degree relatives) recruited as part of independent research programmes, were included.

This study was not a clinical trial and the use of previous data sets was approved by the appropriate ethics committees (CER-Paris-Saclay 2020–094 for participants with FASD, Inserm 08–029 and 11–008 for comparison individuals) ensuring proper consent of participants.

FASD diagnostic procedure

Positive diagnosis was established according to the 4-Digit Diagnostic Code⁵ and the revised guidelines of the Institute of Medicine⁶ leading to distinguish two groups of FASD: the syndromic or FAS (including partial FAS), and the non-syndromic or NS-FASD (static encephalopathy and

neurobehavioural disorder/alcohol exposed⁵ or alcohol-related neurodevelopmental disorder⁶) (Figure S1). Our differential diagnosis work-up included systematic brain MRI and genetic testing. We evaluated the concordance (Cohen's kappa coefficient, κ) of between-group assignment using one or the other guideline. As it proved to be high in our population, only the 4-Digit Diagnostic Code was used in subsequent analyses.

MRI data acquisition

MRI acquisitions were performed on a 1.5 Tesla Philips Ingenia MRI scanner (Philips Healthcare, Amsterdam, the Netherlands) with a millimetric isotropic three-dimensional T1-weighted fast field echo-turbo field echo sequence (repetition time = 8.2 ms; echo time = 3.8 ms; inversion time = 0.8 s; Flip = 8°; SENSitivity Encoding [SENSE] = 2) for participants with FASD and 41 scanner-matched comparison individuals, and on a 3 Tesla Siemens Trio MRI scanner (Siemens Healthineers, Oxford, UK) with a millimetric isotropic three-dimensional T1-weighted magnetization prepared rapid gradient-echo sequence for the remaining comparison individuals.¹⁹

Neuroanatomical quantitative measurements

Measurements were manually performed using the PACS measurement tools (Carestream, New York, NY, USA) by one operator (J.F.) blind to diagnosis. An axial reference brain area (RBA) (Figure 1a,b) was used as a proxy of brain size, as it is strongly correlated with the actual total brain volume ($R^2 = 74.9\%$; Figure S2). The square root of the RBA was used for the sake of dimensional homogeneity (other measurements being lengths). The length of the corpus callosum, the genu thickness, body thickness, isthmus thickness, splenium thickness, and height of the vermis (Figure 1c–e) were measured according to previously validated methods^{20,21} and we ensured that there was no scanner effect in the comparison group (Table S1). For two individuals with obvious partial agenesis of corpus callosum (ACC), the thicknesses were

measured as zero for the agenetic parts. A post hoc robustness analysis excluding these individuals was systematically proposed for callosal parameters.

Semi-quantitative assessment of upper vermis foliation

A five-point Likert scale was proposed to evaluate the upper vermis foliation (Figure 2). Three experts performed blind and independent ranking of the participants with FASD and the scanner-matched comparison individuals only (to avoid lifting the blind reading process). Observer agreement was assessed with κ considering the five ranks separately and then grouping ranks 1 to 3. The rank finally assigned was the nearest-rounded average of the three observers.

Modelling and statistical analysis

Statistical analyses were performed in R (R Foundation for Statistical Computing, Vienna, Austria), using packages 'stats', 'graphics', and 'irr'. Alpha risk was set at 0.05 and adjusted to 0.007 in the case of multiple comparisons on the seven measured parameters (Bonferroni correction).

The effects of groups or covariates (sex) on quantitative variables were tested by analysis of variance (ANOVA; F -test) and comparisons of means between two groups were performed with Student's t -tests. Comparisons of proportions between groups for qualitative variables were performed either with a χ^2 test (two groups) or proportion test (more).

Growth and scaling charts in typically developing comparison individuals

The growth relationships between measured parameters (P) and age were modelled by a linear law with slope a and intercept b ($P = a \times \text{age} + b$), justified by asymptotically linear growth after 6 years old already described in the typically developing paediatric population.^{20,21} The scaling

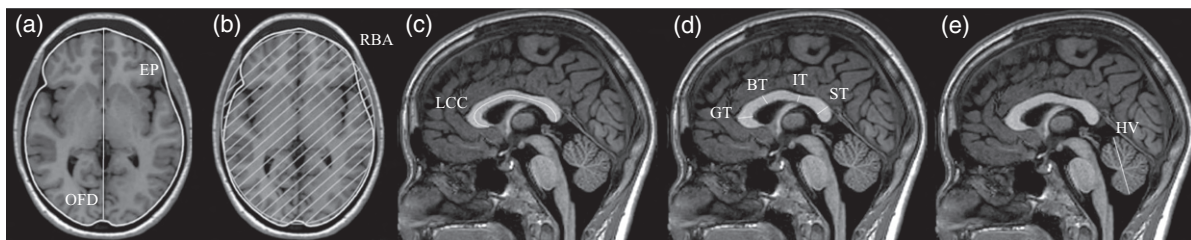


FIGURE 1 Neuroanatomical quantitative measurements. (a) Encephalic perimeter (EP), occipitofrontal diameter (OFD) on the axial referential section through the anterior and posterior commissures. (b) Reference brain area $\left(RBA = \pi \cdot OFD \cdot d; EP \approx 2\pi \sqrt{\frac{OFD^2 + d^2}{2}} \right)$, d being an intermediate

parameter corresponding to the smaller of the two diameters of the ellipse (the other being the OFD). (c) Length of the corpus callosum (LCC). (d) Genu thickness (GT), body thickness (BT), isthmus thickness (IT), and splenium thickness (ST). (e) Height of the vermis (HV).

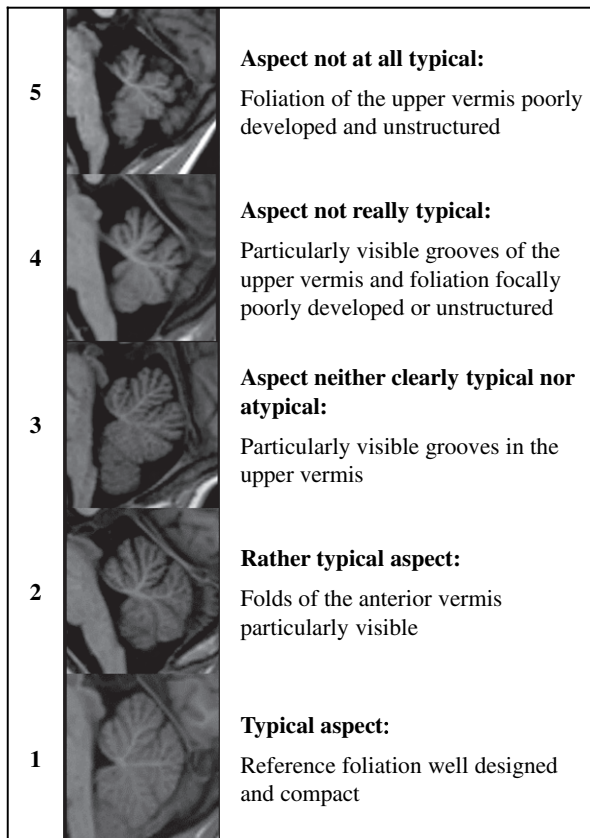


FIGURE 2 Five-point Likert scale of upper vermis foliation. Anterior vermis: up to and including the primary fissure; upper vermis: above the horizontal fissure. Examples are 'medium' for their rank. Assessment was performed on median sagittal and left/right $-1/-2$ sections; overall size of the vermis was not considered per se.

relationships between measured parameters (P) and brain size (RBA) were modelled by a power law with scaling coefficient a and constant b ($P = b \times \sqrt{\text{RBA}}^a$) to take into account expected allometric effects^{22,23} (changes in proportions with size). For each measured parameter, we established growth and scaling normative charts by fitting those two models in the comparison group, then estimated the 10th centile curve under the assumption of homogeneous variance along the age or brain size interval. We tested age or brain size effect by comparing the fitted models with constant model (F -test, nested models) and estimated the part of variance of P explained by age or brain size with the coefficient of determination (R^2). As an alternative analysis, we also established charts in male and female groups.

Abnormal measurement detection in participants with FASD (normative analysis)

For each parameter, individuals with measurements below the 10th centile curve were counted as normatively too small for age or for brain size. An FAS-recurrent abnormality was considered when the number of too-small measurements in FAS exceeded the theoretically expected 10% of the

individuals (one-sided Fisher's test) and were finally retained only if persistent for brain size (with scaling charts). Lastly, the number of participants with FAS and NS-FASD presenting with combinations of these FAS-recurrent abnormalities was compared with the typically developing individuals to assess the discriminative value.

Neuroanatomical diagnostic criteria and probabilistic link with PAE

We incorporated the combination of FAS-recurrent neuroanatomical abnormalities in a radiological-clinical diagnostic criterion, both explicit and quantitative, inspired by the revised Institute of Medicine decision tree and the 4-Digit Diagnostic Code severity ranking. Assuming that the greater the number of recurrent abnormalities observed in an individual with FASD, the stronger the probabilistic causal link with PAE, we also associated the different combinations of non-facial criteria with a six-level scale of causal link ranging from unlikely to certain. We finally sought how many participants with NS-FASD had a high probability.

RESULTS

Population

Among the 89 participants with FASD, 58.4% had FAS and 41.6% had NS-FASD. Their clinical characteristics are detailed in Table 1. There was no significant group effect for sex ratio ($p = 0.179$) and mean age ($p = 0.140$). The 4-Digit Diagnostic Code and revised Institute of Medicine guidelines were discordant only for six individuals (6.7%, $\kappa = 0.86$), with no effect on further results (Table 1).

Comparison of mean measurements

There were group differences for all measurements except the genu thickness ($p = 0.063$), even after excluding the two with ACC (data not shown), and we found no sex effect. The NS-FASD group's measurements were intermediate between comparison individuals and the group with FAS. FAS and NS-FASD groups differed only for height of the vermis measurements ($p = 0.002$) (Table 2).

Growth deficiency: individual measurements as a function of age

In the 94 comparison individuals, callosal and vermian measurements did not change significantly with age, except for the splenium thickness ($p = 0.003$); the determination coefficient R^2 was always lower than 10% (Figure S3). Among the 89 participants with FASD, brain size (RBA) was below the 10th centile of comparison individuals in 74.2%

TABLE 1 Sociodemographic, clinical, radiological, and functional characteristics of participants with FASD and comparison individuals, and group comparison

	FAS <i>n</i> = 52	NS-FASD <i>n</i> = 37	Typically developing <i>n</i> = 94	Group comparison	
				Group effect, <i>p</i> ^a	FAS vs NS-FASD, <i>p</i> ^b
Sociodemographic assessment					
Sex (% male)	27 (51.9)	25 (67.6)	47 (50.0)	0.179	0.209
Age at first consultation, mean (SD), years:months	10:4 (3:8)	11:4 (3:11)	—	—	0.217
Age at MRI, mean (SD), years:months	10:1 (3:7)	11:11 (3:7)	12:1 (3:5)	0.140	0.219
Adopted (%)	32 (61.5)	22 (59.5)	0 (0.0)	<0.001	1.000
Age at adoption, mean (SD), years:months	3:3 (2:8)	2:7 (2:5)	—	—	0.237
Clinical assessment					
(1) Prenatal alcohol exposure (%)					
4. Confirmed, severe	21 (40.4)	16 (43.2)	—	—	0.959
3. Confirmed, moderate or unquantified	26 (50.0)	19 (51.1)	—	—	1.000
2. Not documented	5 (9.6)	2 (5.4)	—	—	0.743
(2) FAS facial features (%)					
4. Severe	31 (59.6)	2 (5.4)	—	—	<0.001
3. Moderate	21 (40.3)	1 (2.7)	—	—	<0.001
2. Mild	0 (0.0)	30 (81.1)	—	—	<0.001
1. None	0 (0.0)	4 (10.8)	—	—	0.057
(3) Growth deficiency (%)					
4. Significant	19 (36.5)	3 (8.1)	—	—	0.005
3. Moderate	11 (21.2)	2 (5.4)	—	—	0.077
2. Mild	9 (17.3)	9 (24.3)	—	—	0.586
1. None	13 (25.0)	23 (62.2)	—	—	0.001
Brain anatomy					
Head circumference, smallest known (%)					
≤ -2 SD: microcephaly	34 (65.4)	13 (35.1)	—	—	<i>0.009</i>
< 10th centile	46 (88.5)	21 (56.8)	—	—	0.002
Structural brain anomalies from first radiologist report (%)					
Corpus callosum abnormality	9 (17.3)	5 (13.5)	—	—	0.850
Cerebellum abnormality	7 (13.5)	5 (13.5)	—	—	1.000
Nodular heterotopia	2 (3.8)	0 (0.0)	—	—	0.630
Agenetic/punctiform olfactory bulb	2 (3.8)	1 (2.7)	—	—	1.000
(4) Structural brain damage (%)	40 (76.9)	19 (51.4)	—	—	0.290
Functional brain assessment					
IQ median (10th centile)	<i>n</i> = 39; 80 (65.8)	<i>n</i> = 30; 79 (64.0)	—	—	/
GAI median (10th centile)	<i>n</i> = 43; 82 (64.2)	<i>n</i> = 29; 86 (68.2)	—	—	/
(4) Brain damage (%)					
4. Certain	39 (75.0)	15 (40.5)	—	—	0.002
3. Probable	13 (25.0)	17 (45.9)	—	—	0.067
2. Possible	0 (0.0)	5 (13.5)	—	—	<i>0.024</i>
Discordant diagnostic with revised Institute of Medicine guidelines	2 (3.8)	4 (10.8)	—	—	
Cohen's Kappa coefficient	$\kappa = 0.86$				

Four diagnostic criteria of the 4-Digit Diagnostic Code described in Figure S1. Concordance between the two guidelines (Cohen's Kappa coefficient, κ).

Bold type, $p < 0.007$, after Bonferroni correction; italic type, $p < 0.05$.

Abbreviations: FAS, fetal alcohol syndrome; FASD, fetal alcohol spectrum disorder; NS-FASD, non-syndromic fetal alcohol spectrum disorder; GAI, General Ability Index; SD, standard deviation.

^a p -value from analysis of variance (F -test) or proportion test.

^b p -value from Student's t -test or χ^2 test.

TABLE 2 Neuroanatomical quantitative measurements of brain size, corpus callosum length and thicknesses, and vermis height (group comparison and sex effect on group comparison)

	FAS <i>n</i> = 52	NS-FASD <i>n</i> = 37	Typically developing <i>n</i> = 94	Group effect, <i>p</i> ^a	Sex effect, <i>p</i> ^a	FAS vs NS-FASD, <i>p</i> ^b
Brain size, mean in cm ² (SD)						
Reference brain area	160.5 (11.7)	167.1 (12.2)	184.6 (11.1)	<0.001	0.138	0.013
Corpus callosum, mean in mm (SD)						
Length of the corpus callosum	76.7 (11.9)	79.8 (6.0)	86.8 (6.5)	<0.001	0.703	0.104
Genu thickness	10.0 (1.4)	10.6 (1.5)	10.6 (1.5)	0.063	0.904	0.071
Body thickness	5.9 (1.3)	6.4 (1.0)	6.6 (1.0)	0.003	0.361	0.098
Isthmus thickness	3.4 (1.0)	3.9 (0.8)	4.3 (0.9)	<0.001	0.138	0.037
Splenium thickness	9.2 (2.6)	10.4 (1.5)	10.5 (1.4)	<0.001	0.544	0.008
Vermis, mean in mm (SD)						
Height of the vermis	41.5 (5.0)	44.5 (4.0)	46.1 (3.0)	<0.001	0.546	0.002

Bold type, $p < 0.007$, after Bonferroni correction; italic type, $p < 0.05$.

Abbreviations: FAS, fetal alcohol syndrome; NS-FASD, non-syndromic fetal alcohol spectrum disorder; SD, standard deviation.

^a p -value from analysis of variance (F -test).

^b p -value from Student's t -test.

(Figure 3a) and there was an excess of individuals with FAS with an abnormally small length of the corpus callosum, isthmus thickness, splenium thickness, and height of the vermis measurements for age ($p < 0.001$ and $p = 0.002$ for splenium thickness) (Table 3).

Scaling anomalies: individual measurements as a function of brain size

To identify anomalies independent of the overall brain size deficit (RBA), we established scaling curves for comparison individuals. The only measurement significantly correlated with brain size was length of the corpus callosum ($p < 0.001$; $R^2 = 20.4\%$), with a trend for body thickness, splenium thickness, and height of the vermis ($p = 0.012$, $p = 0.020$, $p = 0.023$; $R^2 = 6.6\%$, 5.7% , 5.4% respectively) (Figure S3). There was an excess of individuals with FAS below the 10th centile for isthmus thickness and height of the vermis only ($p = 0.003$ after excluding the two with ACC, $p < 0.001$ respectively) (Table 3 and Figure 3b,c), which was also found in the alternative analysis separating females and males (Figure S4).

Semi-quantitative assessment of the upper vermis foliation

The agreement along the five-rank scale between the three observers was moderate ($\kappa = 0.44$) but increased to strong ($\kappa = 0.65$) when it came to differentiating individuals with 'not very typical' or 'not at all typical' foliation (4 or 5) from the others, with no comparison individual ever ranked 4 or 5 (Figure S5). Eleven individuals ranked 4 (eight with FAS, three with NS-FASD) and five ranked 5 (three with FAS, two with NS-FASD), totalling 18.0% considered to have

disrupted upper vermis foliation. Notably, four individuals who ranked 4 or 5 did not show a small vermis for brain size (Figure 3c, blue points), making this semi-quantitative assessment non-redundant with height of the vermis.

Combination of neuroanatomical abnormalities

We identified four recurrent neuroanatomical abnormalities in FAS not trivially associated with each other and particularly not plain consequences of brain size deficit, illustrated in Figure 4.

We grouped the clinical and radiological evidence of FAS-related neuroanatomical damage as follows: (1) brain size deficit for age—clinically (head circumference) and/or radiologically (RBA); (2) corpus callosum abnormalities—partial ACC or narrowed callosal isthmus for brain size; (3) vermis abnormalities—disrupted upper vermis foliation and/or insufficient vermian height for brain size.

There were 38.5% with FAS, 27.0% with NS-FASD, and only 2.1% of comparison individuals with two out of these three abnormalities, and 19.2% with FAS with all three (Table 4), showing both a discriminative value of the association of FAS-recurrent neuroanatomical abnormalities and its possible observation in NS-FASD.

Integration into a neuroanatomical criterion

A diagnostic tree, including a distinct and quantified neuroanatomical criterion that gives double weight to the well-documented and frequent brain size deficiency, is proposed in Figure 5. An assumption of the strength of the causal link with PAE is associated with each combination of non-facial criteria within each tree branch. We found

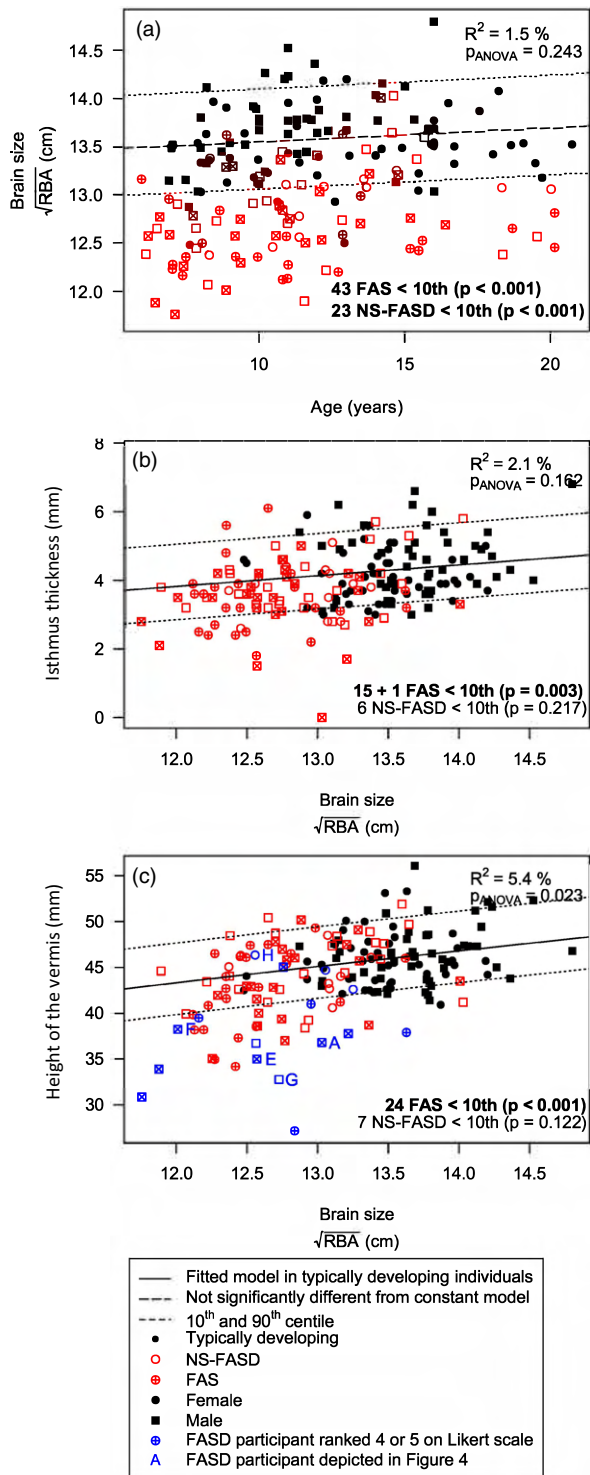


FIGURE 3 Fetal alcohol syndrome (FAS)-recurrent abnormal measurements. (a) Growth chart for brain size. (b,c) Scaling charts for isthmus thickness and the height of the vermis. Top: determination coefficient R^2 and p_{ANOVA} (p -value of comparison of fitted model vs constant) in comparison individuals. Bottom: number of fetal alcohol spectrum disorder (FASD) < 10th centile (p -value of one-sided Fisher's test). Bold type, $p < 0.007$.

that 18.0% of participants with NS-FASD were associated with high levels of causal link with PAE (very likely, almost certain).

DISCUSSION

In this study, we have described recurrent excessive narrowing of the callosal isthmus and insufficient vermian height associated with FAS, not explained by brain size deficit, using validated neuroanatomical measurements^{20,21} that are accessible in a clinical–radiological setting on routine T1-weighted MRI. We also introduced a simple and reliable tool to evaluate the foliation of the upper vermis and showed its usefulness in identifying disrupted foliation associated with FAS, never observed in typically developing comparison individuals, and not always related to insufficient vermian height. Lastly, we demonstrated that the association of two or three of either brain size, callosal or vermian abnormalities was frequent not only in FAS but also in NS-FASD, while remaining exceptional in comparison individuals. These results strongly favour the addition of a composite neuroanatomical criterion to the current FASD clinical diagnostic procedure, including specified and objective radiological assessment, as it can improve the estimation of the causal link with PAE and open the path to a better diagnostic specificity in the absence of FAS.

Accounting for brain size

Brain size deficit is the most obvious and recurrent neuroanatomical abnormality in individuals with FASD.^{1,8,9} The head circumference has shown only a moderate correlation to the actual brain volume in the typically developing and the PAE populations beyond the age of 6 years ($R^2 = 36\text{--}43\%$).⁸ As brain volume is not yet easily accessible in routine MRI, we proposed the measurement of RBA as a useful radiological proxy of brain size, strongly correlated with it ($R^2 = 74.9\%$; Figure S2) and geometrically more sensitive than length or perimeter.⁸ Associating RBA with present or former clinical measurements of head circumference¹⁸ would eventually increase the sensitivity of detection of brain growth deficiency.

Brain size must be considered when interpreting other neuroanatomical measurements that correlate with it in the general population²⁴ and thus are plainly reduced in small brains. Thus, to interpret the reduction in callosal and vermian size observed in FASD at the individual level, we complemented the classical normative analysis on growth charts (effect of age) with an analysis on scaling charts (effect of size). Because of the partial overlap between FASD and comparison individuals' ranges of brain sizes, we had to ensure that the scaling model fitted in comparison individuals correctly projected to the smaller FASD range. Allometric scaling modelled by a power law captures the gradual change in proportions along size range and has been shown to be the rule rather than the exception in neuroanatomy.^{16,22} Not taking it into account can be misleading²⁵ and, in our situation, a simple affine model would have dubiously increased abnormal FASD measurements, whereas the power-law model is more conservative. Lastly, most of the participants with FASD with

TABLE 3 Number of participants with FASD below the 10th centile on growth and scaling normative charts established in comparison individuals for each measured parameter

FASD <i>n</i> = 89	Growth				Scaling			
	FAS <10th centile	<i>p</i>	NS-FASD <10th centile	<i>p</i>	FAS <10th centile	<i>p</i>	NS-FASD <10th centile	<i>p</i>
Brain size								
Reference brain area	43	<0.001	23	<0.001				
Corpus callosum								
Length of the corpus callosum	27 (+2)	<0.001	17	<0.001	7 (+2)	0.294	4	0.529
Genu thickness	10	0.082	5	0.354	3	0.870	3	0.715
Body thickness	<i>13 (+1)</i>	<i>0.012</i>	7	0.122	6 (+1)	0.440	2	0.873
Isthmus thickness	20 (+1)	<0.001	9	<i>0.031</i>	15 (+1)	0.003	6	0.217
Splenium thickness	15 (+2)	0.002	4	0.529	9 (+2)	0.118	0	1.000
Vermis								
Height of the vermis	32	<0.001	9	<i>0.031</i>	24	<0.001	7	0.122

p-value from one-sided Fisher's test. In brackets, the excluded individuals with agenesis of corpus callosum. Bold type, $p < 0.007$, after Bonferroni correction; italic type, $p < 0.05$. For the charts used to establish these results, see Figure S3.

Abbreviations: FAS, fetal alcohol syndrome; FASD, fetal alcohol spectrum disorder; NS-FASD, non-syndromic fetal alcohol spectrum disorder.

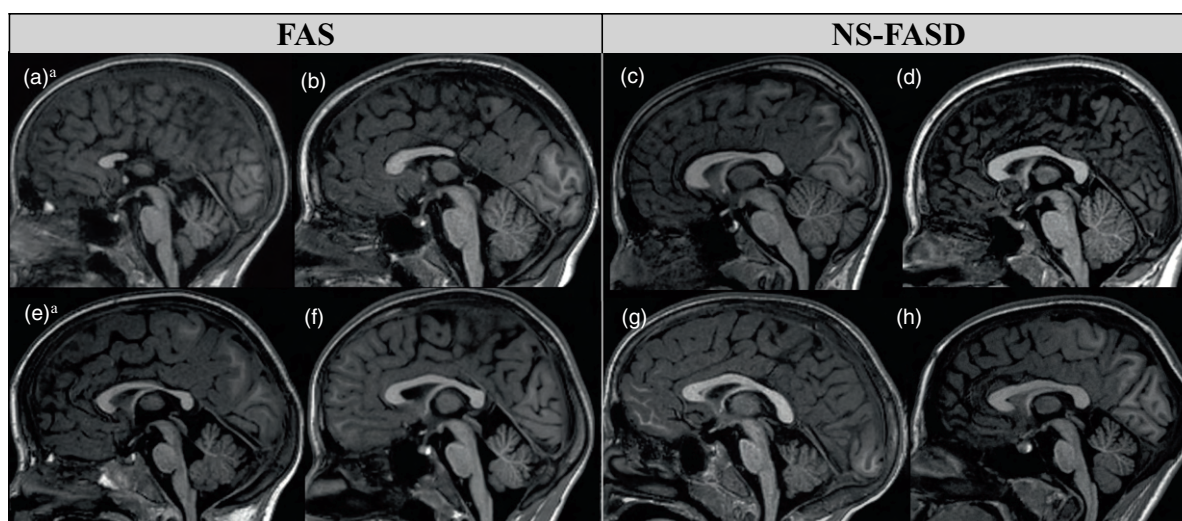


FIGURE 4 Individuals with fetal alcohol spectrum disorder (FASD) with identified fetal alcohol spectrum (FAS)-recurrent anomalies. (a,b) Partial agenesis of corpus callosum. (c,d) Narrowed callosal isthmus for brain size. (e,g) Upper vermis ranked 5; (f,h) ranked 4. Note that for (h) the height of the vermis is normal for brain size (Figure 3). ^a Association of three abnormalities.

either vermian or callosal measurements too small for age showed normal values for brain size, as was flagrant for the length of the corpus callosum (Table 3). The reduction of isthmus thickness and height of the vermis were the only ones not strictly redundant with brain size reduction. In terms of non-redundancy of abnormal features, we also showed that disrupted upper foliation could be found in a normal-sized vermis (Figure 3c, individual H). Ultimately, this scaling normative approach helped discover abnormalities that were complementary enough to be combined with brain size deficit within an FAS neuroanatomical pattern and possible diagnostic criterion.

Specificity of the abnormalities

We identified frequent height (44.9%) and/or foliation (18.0%) vermian abnormalities. Surprisingly, this result was not highlighted in most published FASD clinical-radiological studies,^{11,26} except in a recent qualitative large series,¹⁰ though that study provided little description. Yet, several computer-assisted neuroimaging studies have reported a size reduction of the anterior vermis (area, volume) following PAE^{7,15,17} at the group level, generally taking brain size effect linearly into account. Our results suggest that there might also be a qualitative disruption of vermian foliation

TABLE 4 Recurrent neuroanatomical abnormalities identified in FAS, counted in each group FAS, NS-FASD, and combination of two or three of the abnormalities, versus comparison individuals

	FAS	<i>p</i>	NS-FASD	<i>p</i>	Typically developing
Recurrent neuroanatomical abnormalities					
Brain size deficit					
Reference brain area < 10th centile and/or head circumference < 10th centile	48 (92.3%)	<0.001	27 (73.0%)	<0.001	9 (9.6%)
Corpus callosum abnormalities					
Partial ACC and/or narrowed callosal isthmus (isthmus thickness < 10th centile)	17 (32.7%)	0.001	6 (16.2%)	0.217	9 (9.6%)
Vermis abnormalities					
Insufficient vermian height (<10th centile)	25 (48.1%)	<0.001	10 (27.0%)	<i>0.014</i>	9 (9.6%)
Disrupted upper vermis foliation (Likert 4, 5)	24		7		9 (9.6%)
	11		5		0 (0.0%)
Combination of neuroanatomical abnormalities					
Brain size deficit associated with corpus callosum or vermis abnormalities	20 (38.5%)	<0.001	10 (27.0%)	<0.001	2 (2.1%)
Brain size deficit associated with corpus callosum and vermis abnormalities	10 (19.2%)	<0.001	0 (0.0%)	1.000	0 (0.0%)

p-value from one-sided Fisher's test. Bold type, *p* < 0.007, after Bonferroni correction; italic type, *p* < 0.05.

Abbreviations: ACC, agenesis of corpus callosum; FAS, fetal alcohol syndrome; NS-FASD, non-syndromic fetal alcohol spectrum disorder.

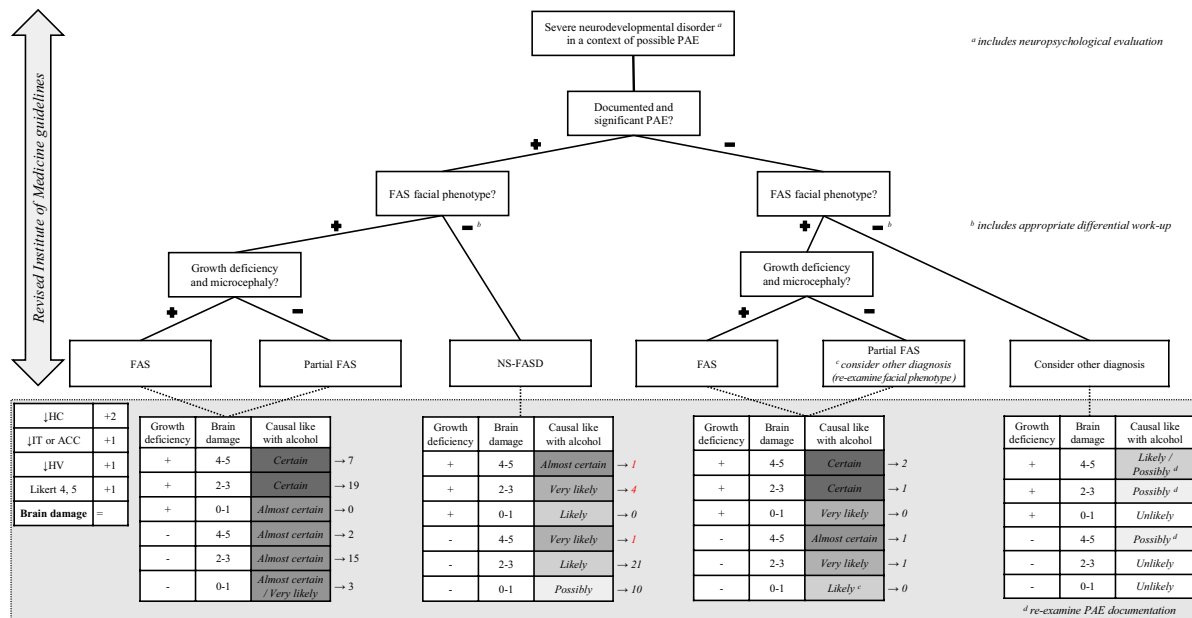


FIGURE 5 Proposition of revised FASD diagnostic algorithm (based on the revised Institute of Medicine guidelines) with an estimate of the probability of a causal link between clinical phenotype and PAE, based on documentation of consumption, FAS facial phenotype, growth deficiency, as well as a specified neuroanatomical criterion as a 'brain damage' score: brain growth deficiency (↓HC), ACC or narrowing of the callosal isthmus for brain size (↓IT) and insufficient vermian height for brain size (↓HV) or disrupted upper vermis foliation (Likert 4, 5). Number of participants with FASD in each category noted on the right; red type, high level of probability in participants with NS-FASD. Abbreviations: ACC, agenesis of corpus callosum; FAS, fetal alcohol syndrome; FASD, fetal alcohol spectrum disorder; HC, head circumference; HV, height of the vermis; IT, isthmus thickness; NS-FASD, non-syndromic fetal alcohol spectrum disorder; PAE, prenatal alcohol exposure.

(branching, length, thickness of the folia). The Likert scale we propose was based on the formalism adopted in the literature for FASD facial morphology.^{5,6} Under the proposed conditions, ranking 1, 2, or 3 is not very robust, but the relevance of this scale is supported by the strong agreement

between observers in distinguishing typical from atypical aspects that should be considered pathological, without misclassification of comparison individuals. Indeed, as for facial morphology, it is the distinction of the two pathological ranks that is relevant to clinical use, and the effectiveness

of the Likert scale probably relies on its spreading over five ranks.

In FASD, cases of ACC have been repeatedly reported.^{7,10,11} In these three large recent cohorts, the prevalence of ACC did not exceed 3% (2.2% in ours), while it is rated from 0.02% to 0.7% in the general population²⁷ to around 1% in individuals with neurodevelopmental disorders.²⁸ Qualitatively abnormal or atypical shapes may be reported in up to 38% of cases,¹⁰ but criteria are subjective and difficult to interpret. Using computerized analysis tools, subtle anomalies were found at the group level: differences in volume, surface, length, or position^{12–14} versus typically developing individuals. Unfortunately, these results are heterogeneous or difficult to replicate.^{12,29} We found a clear excess of abnormally thin isthmus. Considering the reports of posterior partial ACC and possibly of splenic anomalies at the group level, we expected to find a similar excess of narrowed splenium, but it was not significant in our population. Despite well-codified measurement criteria,²⁰ the complex shape variability of the splenium (rounded, curved, short without being thin) may have limited the sensitivity of abnormality detection.

To our knowledge, none of the previous studies on callosal and vermian abnormalities have so far attempted to propose any practical and normative use at the individual level.

Interest of a neuroanatomical diagnostic criterion

Over time, the evolution of FASD diagnostic guidelines has given variable importance to neuroanatomical features, sometimes discounting them,⁴ often mixing them with neurofunctional impairment,^{3,5,6} always with little, if any, impact on diagnostic specificity. Yet, the triple association of the FAS-recurrent abnormalities we described was repeatedly observed in FAS (19.2%), the double associations were frequent in FAS (38.5%), and repeatedly observed in NS-FASD (27.0%), while both situations were either unobserved or exceptional (2.1%) in typically developing individuals (Table 3). Provided that FAS-specificity and extendibility to some NS-FASD are confirmed by other large-scale studies, such a brain signature could form the basis of a specified and independent neuroanatomical diagnostic criterion that would be worth discussing beyond a simply descriptive value (Figure 5). Within the framework of existing diagnostic categories and respecting the preeminent specificity of the facial phenotype, we showed that adding this type of criterion can help refine the estimation of the probabilistic link between neurodevelopmental disorders and PAE, and contribute to identify a sub-category of NS-FASD in which this estimated link is particularly strong. Thus, without being indispensable in cases sufficiently supported by the clinic, brain MRI could find its place in the diagnostic work-up when a strengthening of the probabilistic diagnosis of FASD-NS is desirable.

Limitations

As for any retrospective study on FASD,^{10,11,29} the representativeness of the population is an important issue. In this regard, our series included a high proportion of adopted children (60.7%) for whom PAE was documented but poorly quantified and perinatal comorbidities were difficult to exclude.

One could question the way the 10th centile of the scaling curves was established for normative analysis. First, we relied on a power-law scaling model, the most theoretically correct choice,^{22,23} which allows for both nonlinear allometric and linear proportional relationships ($P = b \times \sqrt{RBA}^{a-1}$). Yet, low coefficients of determination R^2 associated with a moderate population size ($n = 94$) probably limited the statistical power to assess model fits. That said, keeping a very general model seemed appropriate as it tended to best fit for many parameters before Bonferroni correction and proved to be more conservative (limiting false positives). Finally, to robustly establish the centiles of the distributions in our medium-sized comparison group, we had to assume homogeneous variance over the studied intervals.

The absence of sex distinction, even if sex effect on brain size is well known,^{8,18} might also be questioned. In this study, pooling males and females resulted from a trade-off between statistical power and robustness (model fit) linked to the size of the comparison group, and adequacy of normative limits at the individual level (charts) brought by adding the sex covariate. We explored the extent to which this choice would affect our results and first verified that there was no significant effect of sex on the raw measurements excepted for brain size (Table 2), which was consistent with the strongly negative allometric relationship between brain size and these parameters²² (significant variations of RBA between males and females, associated with very subtle or insignificant variations of callosal and vermian measurements; Table S1). Bearing in mind that the analyses would be less robust, we also showed that the alternative choice of separating males and females did not significantly change our final results, with concordant identification of both FAS-related neuroanatomical abnormalities (Figure S4) and participants with pathological FASD on the normative charts. In the end, the use of a common growth chart for RBA potentially caused only three false negatives in males and one false positive in females (Figure 3 vs Figure S4), which would have been counted as one FAS and two NS-FASD with a combination of two anomalies, thus not changing the conclusions.

The choice of a 10th centile thresholding over a lower one is also questionable, especially because it has been a source of controversy in the field³⁰ for other diagnostic parameters. Since we intended to combine the abnormalities, we considered that this threshold would not be too permissive in the end, which proved to be correct as double or triple combinations dropped almost below the detection level in about 100 typically developing individuals. Eventually, a third centile-threshold alternative analysis consistently showed a significant excess of isthmus thickness and height of the vermian abnormality for brain size (data not shown).

All these concerns advocate complementary studies for more accurate standardization of the scaling curves, including sex differentiation and extending age ranges to adult charts, taking advantage of larger samples or multisite designs. However, the relatively large excess of abnormal isthmus thickness and height of the vermis values with a nonetheless conservative model gives us confidence in our results.

CONCLUSION

Explicit and quantitative FAS-recurrent anomalies (small brain size for age, narrowed callosal isthmus for brain size, and disrupted upper vermis foliation or reduced vermian height for brain size) can be associated into a composite neuroanatomical–radiological criterion. It is likely to benefit the diagnostic process for NS-FASD, bringing confidence where some lack of specificity can deter diagnosis, for the sake of diagnosis rate and eventually patient care.

ACKNOWLEDGMENTS

We thank the volunteers, patients, and families, the French supportive association for FASD-affected families ‘*Vivre avec le SAF*’, and Elizabeth Rowley-Jolivet for English proofreading.

FUNDING INFORMATION

The French National Agency for Research (ANR-19-CE17-0028-01) and the French National Institute for Public Health research (IRESP-19-ADDICTIONS-08).

CONFLICT OF INTEREST

The authors have stated that they had no interests that might be perceived as posing a conflict or bias.

DATA AVAILABILITY STATEMENT

The data that support the findings of this study are available on request from the corresponding author. The data are not publicly available due to privacy or ethical restrictions.

ORCID

Justine Fraize  <https://orcid.org/0000-0001-6434-7992>

REFERENCES

- Kuehn D, Aros S, Cassorla F, Avaria M, Unanue N, Henriquez C, et al. A prospective cohort study of the prevalence of growth, facial, and central nervous system abnormalities in children with heavy prenatal alcohol exposure. *Alcohol Clin Exp Res*. 2012; 36(10):1811–9.
- Lange S, Probst C, Gmel G, Rehm J, Burd L, Popova S. Global Prevalence of Fetal Alcohol Spectrum Disorder Among Children and Youth: A Systematic Review and Meta-analysis. *JAMA Pediatr*. 2017; 171(10):948–956.
- Chudley AE. Diagnosis of fetal alcohol spectrum disorder: current practices and future considerations. *Biochem Cell Biol*. 2018; 96(2):231–236.
- Cook JL, Green CR, Lilley CM, Anderson SM, Baldwin ME, Chudley AE, et al. Fetal alcohol spectrum disorder: a guideline for diagnosis across the lifespan. *CMAJ*. 2016; 188(3):191–197.
- Astley SJ. Diagnostic Guide for Fetal Alcohol Spectrum Disorders: The 4-Digit Diagnostic Code. 3rd edition University of Washington Publication Services, Seattle, WA: 2004. Available from: <http://depts.washington.edu/fasdpn/pdfs/guide04.pdf>
- Hoyme HE, Kalberg WO, Elliott AJ, Blankenship J, Buckley D, Marais AS, et al. Updated Clinical Guidelines for Diagnosing Fetal Alcohol Spectrum Disorders. *Pediatrics*. 2016; 138(2):e20154256.
- Astley SJ, Aylward EH, Olson HC, Kerns K, Brooks A, Coggins TE, et al. Magnetic resonance imaging outcomes from a comprehensive magnetic resonance study of children with fetal alcohol spectrum disorders. *Alcohol Clin Exp Res*. 2009; 33(10):1671–89.
- Treit S, Zhou D, Chudley AE, Andrew G, Rasmussen C, Nikkel SM, et al. Relationships between Head Circumference, Brain Volume and Cognition in Children with Prenatal Alcohol Exposure. *PLoS One*. 2016; 11(2):e0150370.
- Nguyen VT, Chong S, Tieng QM, Mardon K, Galloway GJ, Kurniawan ND. Radiological studies of fetal alcohol spectrum disorders in humans and animal models: An updated comprehensive review. *Magn Reson Imaging*. 2017; 43:10–26.
- Boronat S, Sánchez-Montañez A, Gómez-Barros N, Jacas C, Martínez-Ribot L, Vázquez E, et al. Correlation between morphological MRI findings and specific diagnostic categories in fetal alcohol spectrum disorders. *Eur J Med Genet*. 2017; 60(1):65–71.
- Treit S, Jeffery D, Beaulieu C, Emery D. Radiological Findings on Structural Magnetic Resonance Imaging in Fetal Alcohol Spectrum Disorders and Healthy Controls. *Alcohol Clin Exp Res*. 2020; 44(2):455–462.
- Sowell ER, Mattson SN, Thompson PM, Jernigan TL, Riley EP, Toga AW. Mapping callosal morphology and cognitive correlates: effects of heavy prenatal alcohol exposure. *Neurology*. 2001; 57(2):235–244.
- Bookstein FL, Connor PD, Huggins JE, Barr HM, Pimentel KD, Streissguth AP. Many infants prenatally exposed to high levels of alcohol show one particular anomaly of the corpus callosum. *Alcohol Clin Exp Res*. 2007; 31(5):868–879.
- Biffen SC, Warton CMR, Dodge NC, Molteno CD, Jacobson JL, Jacobson SW, et al. Validity of automated FreeSurfer segmentation compared to manual tracing in detecting prenatal alcohol exposure-related subcortical and corpus callosal alterations in 9- to 11-year-old children. *Neuroimage Clin*. 2020; 28:102368.
- O'Hare ED, Kan E, Yoshii J, Mattson SN, Riley EP, Thompson PM, et al. Mapping cerebellar vermal morphology and cognitive correlates in prenatal alcohol exposure. *Neuroreport*. 2005; 16(12):1285–90.
- Bookstein FL, Streissguth AP, Connor PD, Sampson PD. Damage to the human cerebellum from prenatal alcohol exposure: the anatomy of a simple biometrical explanation. *Anat Rec B New Anat*. 2006; 289(5):195–209.
- Cardenas VA, Price M, Infante MA, Moore EM, Mattson SN, Riley EP, et al. Automated cerebellar segmentation: Validation and application to detect smaller volumes in children prenatally exposed to alcohol. *Neuroimage Clin*. 2014; 4:295–301.
- Rollins JD, Collins JS, Holden KR. United States head circumference growth reference charts: birth to 21 years. *J Pediatr*. 2010; 156(6):907–913.e2.
- Bouyeure A, Germanaud D, Bekha D, Delattre V, Lefèvre J, Pinabiaux C, et al. Three-Dimensional Probabilistic Maps of Mesial Temporal Lobe Structures in Children and Adolescents' Brains. *Front Neuroanat*. 2018; 12:98.
- Garel C, Cont I, Alberti C, Josserand E, Moutard ML, Ducou le Pointe H. Biometry of the corpus callosum in children: MR imaging reference data. *AJNR Am J Neuroradiol*. 2011; 32(8):1436–43.
- Jandeaux C, Kuchcinski G, Ternynck C, Riquet A, Leclerc X, Pruvo JP, et al. Biometry of the Cerebellar Vermis and Brain Stem in Children: MR Imaging Reference Data from Measurements in 718 Children. *AJNR Am J Neuroradiol*. 2019; 40(11):1835–1841.
- de Jong LW, Vidal JS, Forsberg LE, Zijdenbos AP, Haight T, Alzheimer's Disease Neuroimaging Initiative, et al. Allometric scaling of brain regions to intra-cranial volume: An epidemiological MRI study. *Hum Brain Mapp*. 2017; 38(1):151–164.
- Germanaud D, Lefèvre J, Fischer C, Bintner M, Curie A, des Portes V, et al. Simplified gyral pattern in severe developmental microcephalies?

- New insights from allometric modeling for spatial and spectral analysis of gyrification. *Neuroimage*. 2014; 102 Pt 2:317–31.
24. Giedd JN, Rapoport JL. Structural MRI of Pediatric Brain Development: What Have We Learned and Where Are We Going? *Neuron*. 2010; 67(5):728–734.
 25. Toro R, Chupin M, Garnero L, Leonard G, Perron M, Pike B, et al. Brain volumes and Val66Met polymorphism of the BDNF gene: local or global effects? *Brain Struct Funct*. 2009; 213(6):501–9.
 26. Autti-Rämö I, Autti T, Korkman M, Kettunen S, Salonen O, Valanne L. MRI findings in children with school problems who had been exposed prenatally to alcohol. *Dev Med Child Neurol*. 2002; 44(2):98–106
 27. Glass HC, Shaw GM, Ma C, Sherr EH. Agenesis of the corpus callosum in California 1983–2003: a population-based study. *Am J Med Genet A*. 2008; 146A(19):2495–2500.
 28. Jeret JS, Serur D, Wisniewski K, Fisch C. Frequency of agenesis of the corpus callosum in the developmentally disabled population as determined by computerized tomography. *Pediatr Neurosci*. 1985; 12(2):101–103.
 29. Yang Y, Phillips OR, Kan E, Sulik KK, Mattson SN, Riley EP, et al. Callosal thickness reductions relate to facial dysmorphology in fetal alcohol spectrum disorders. *Alcohol Clin Exp Res*. 2012; 36(5):798–806.
 30. Hemingway SJA, Bledsoe JM, Brooks A, Davies JK, Jirikowic T, Olson E, et al. Comparison of the 4-Digit Code, Canadian 2015, Australian 2016 and Hoyme 2016 fetal alcohol spectrum disorder diagnostic guidelines. *Adv Pediatr Res*. 2019; 6(2):31.

SUPPORTING INFORMATION

The following additional material may be found online:

Figure S1 Flow chart and diagnostic procedure.

Figure S2 Correlation between reference brain area (RBA) and total brain volume obtained with *volBrain*.

Figure S3 Growth charts (left), scaling charts (right).

Figure S4 Charts of female (left) and male (right).

Figure S5 Semi-quantitative assessment of the upper vermis foliation.

Table S1 Effect of scanner, age, and sex on measured parameters in the comparison group.

How to cite this article: Fraize J, Garzón P, Ntorkou A, Kerdreux E, Boespflug-Tanguy O, Beggiato A, et al. Combining neuroanatomical features to support diagnosis of fetal alcohol spectrum disorders. *Dev Med Child Neurol*. 2022;00:1–12. <https://doi.org/10.1111/dmcn.15411>

MATÉRIELS SUPPLÉMENTAIRES

Figure S1. Flow chart and diagnostic procedure.

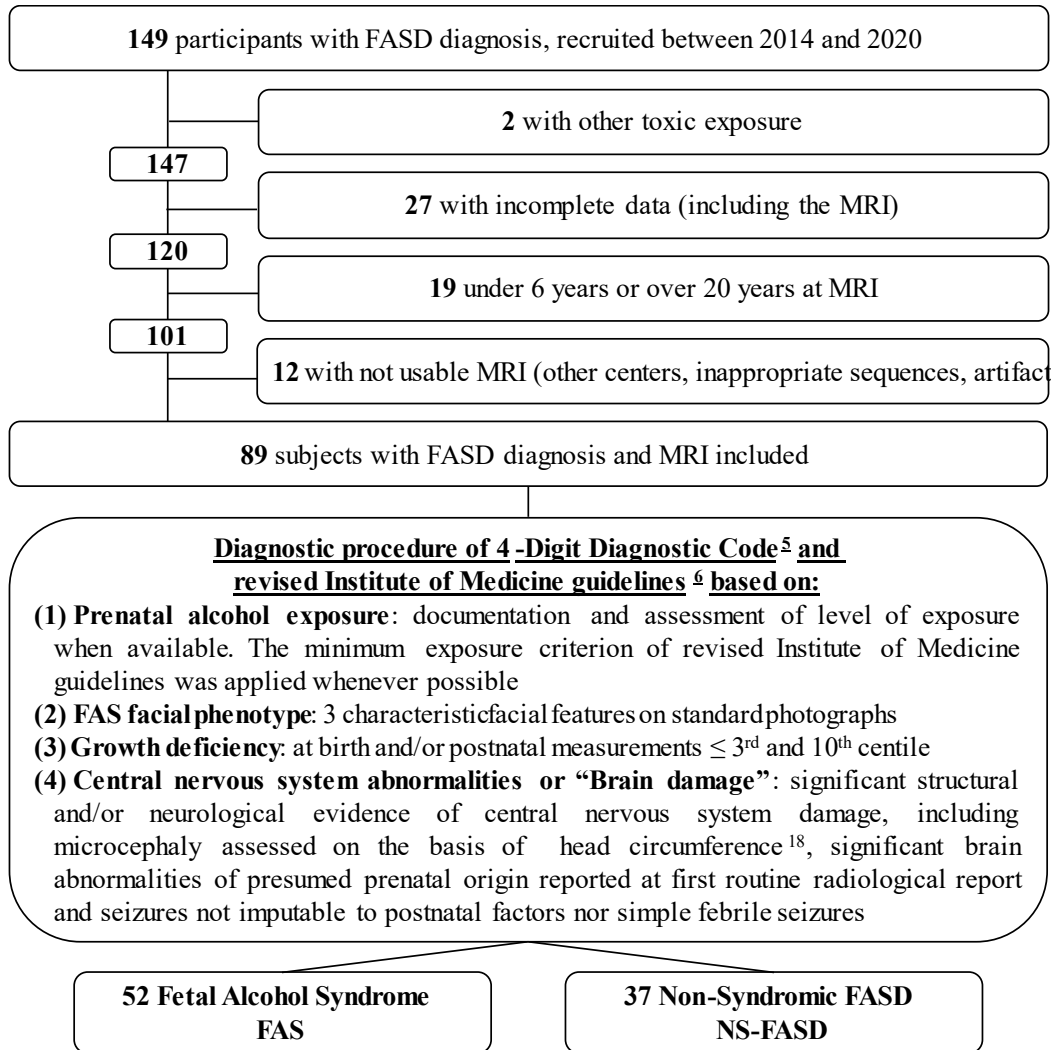


Figure S2. Correlation between reference brain area (RBA) and total brain volume obtained with volBrain.

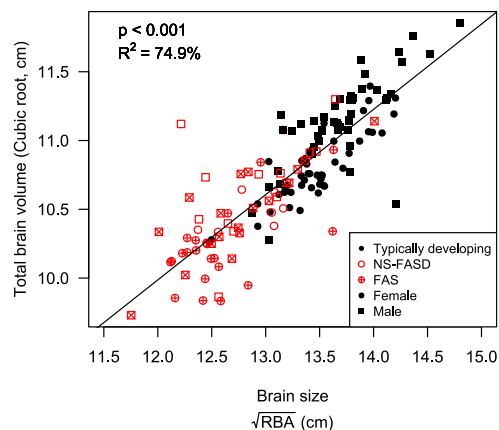
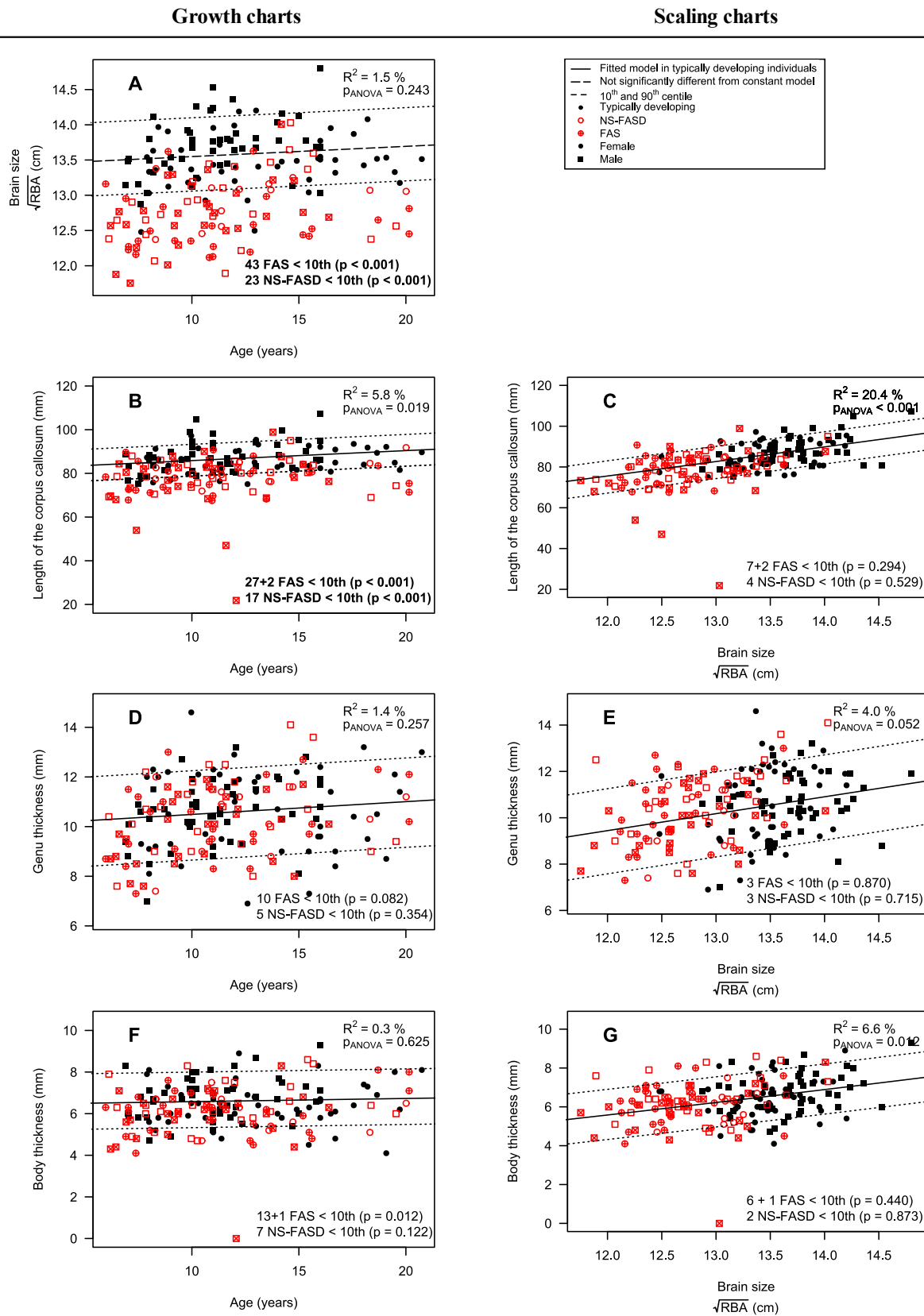


Figure S3. Growth charts (left), scaling charts (right).



Growth charts

Scaling charts

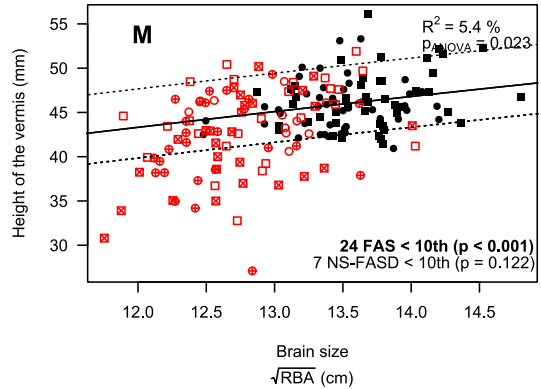
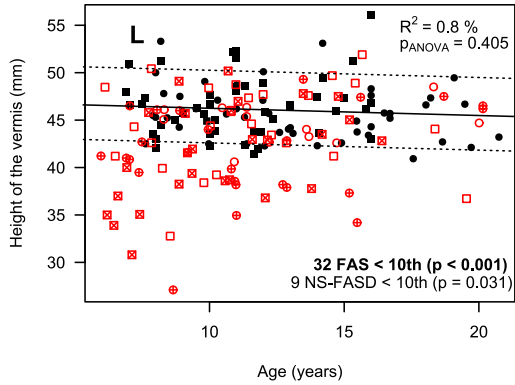
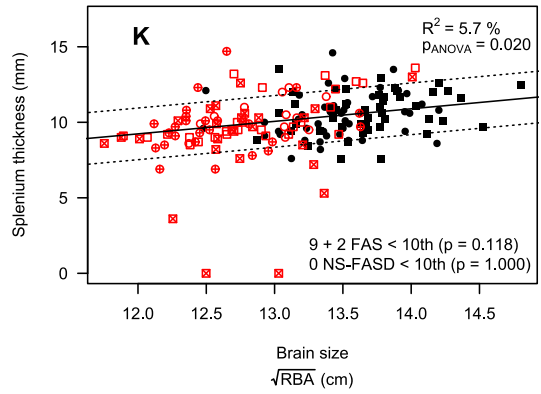
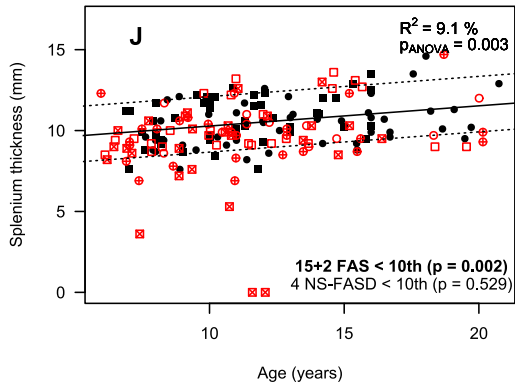
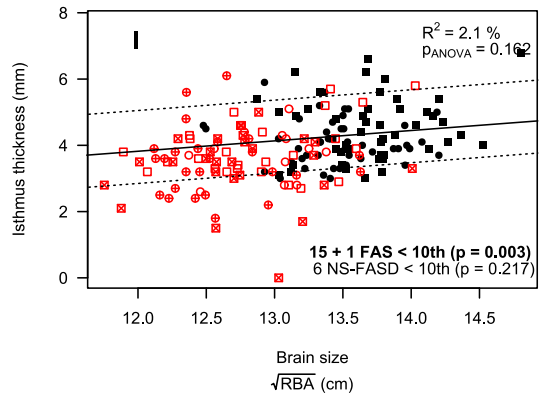
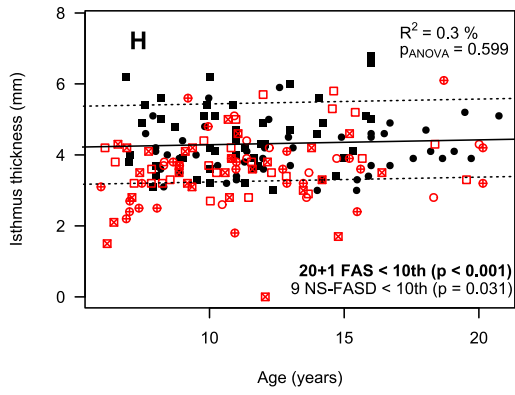
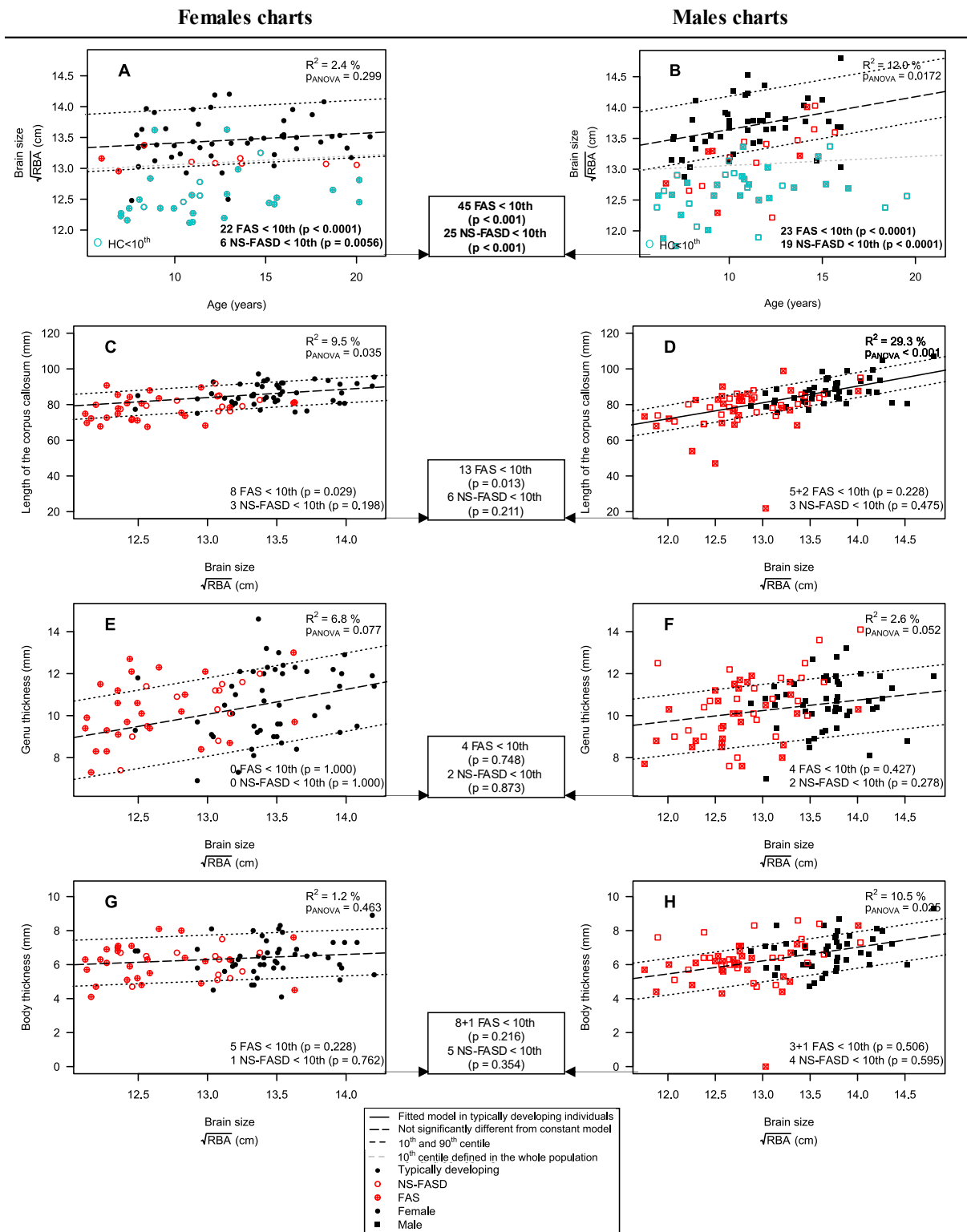
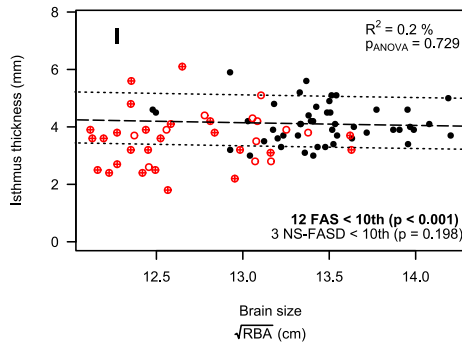


Figure S4. Charts of female (left) and male (right).

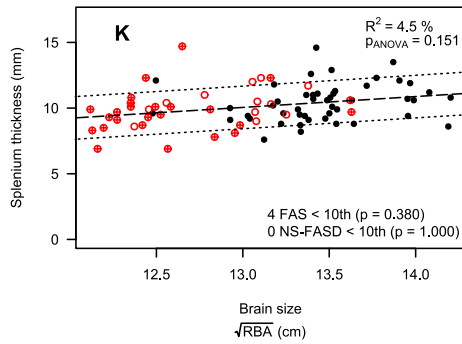
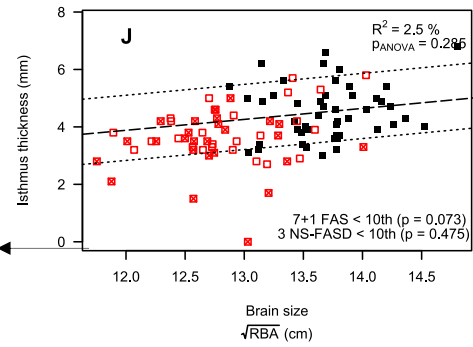


Females charts

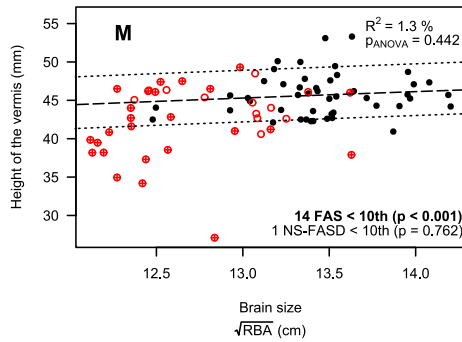
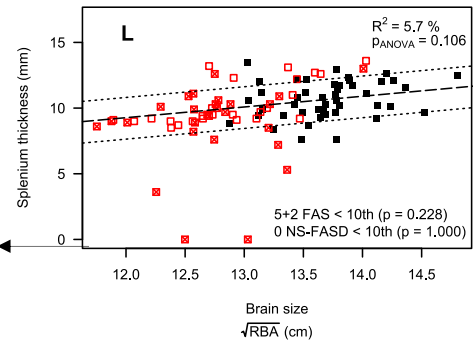
Males charts



19 FAS < 10th
($p = 0.001$)
6 NS-FASD < 10th
($p = 0.217$)



9 FAS < 10th
($p = 0.137$)
0 NS-FASD < 10th
($p = 1.000$)



26 FAS < 10th
($p < 0.001$)
6 NS-FASD < 10th
($p = 0.217$)

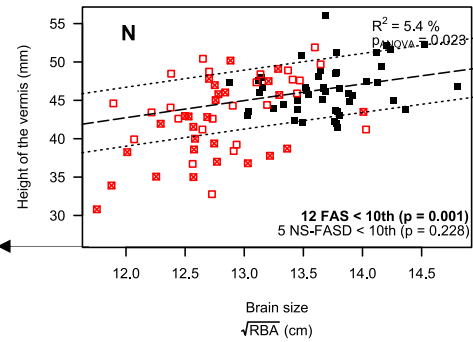

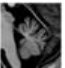





Figure S5. Semi-quantitative assessment of the upper vermis foliation.

Likert Rank	FAS				NS-FASD				Typically developing			
	A	B	C	Mean	A	B	C	Mean	A	B	C	Mean
 5	3	3	4	3	2	2	2	2	0	0	0	0
 4	12	10	10	8	4	2	2	3	0	2	0	0
 3	12	10	2	11	14	9	6	7	13	7	7	9
 2	13	12	15	16	0	6	7	12	17	13	15	17
 1	12	17	21	14	8	18	20	13	10	18	18	14

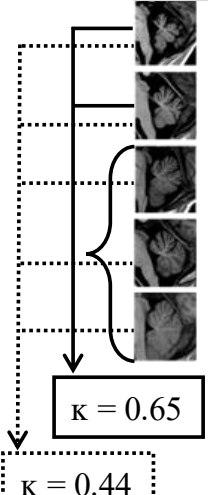


Table S1. Effect of scanner, age, and sex on measured parameters in the comparison group.

	Scanner effect, <i>p</i> ^a	Age effect, <i>p</i> ^a	Sex effect, <i>p</i> ^a
Brain size			
Reference brain area	0.190	<i>0.026</i>	0.001
Corpus callosum			
Length of the corpus callosum	<i>0.023</i>	0.003	0.140
Genu thickness	0.062	0.254	0.662
Body thickness	0.521	0.266	0.070
Isthmus thickness	0.335	0.335	<i>0.015</i>
Splenium thickness	<i>0.008</i>	0.006	0.052
Vermis			
Height of the vermis	0.168	0.586	0.380

Multivariate linear regression.

Bold type, $p < 0.007$, after Bonferroni correction; italic type, $p < 0.05$.

^a *p*-value from the generalized linear model including scanner, age, and sex as covariate for each measured parameter.

COMPLÉMENTS DE DISCUSSION

Cette première étude nous a permis de montrer qu'avec des outils simples et en prenant en compte la réduction de taille du cerveau, des anomalies neuroanatomiques pouvaient être identifiées comme récurrentes chez les patients avec SAF et qu'elles pouvaient aussi être retrouvées chez un certain nombre de sujets ayant une forme non syndromique de TSAF. En les conjuguant, nous avons montré qu'elles pouvaient constituer un critère diagnostique composite qui peut s'intégrer directement dans l'arbre décisionnel diagnostique. Nous avons proposé un score permettant de mieux estimer le lien causal entre les troubles du neurodéveloppement et l'exposition prénatale à l'alcool. Cette proposition est particulièrement pertinente en pratique clinique dans le cas des formes non syndromiques où ce lien est probabiliste et a besoin d'être renforcé.

Ce travail s'est appuyé sur trois éléments méthodologiques que nous souhaitons mettre en avant : (1) la prise en compte de la variance à l'échelle individuelle, (2) l'interprétation en fonction de la taille globale du cerveau et l'introduction de la notion de courbe de *scaling* (3) la translation des formes SAF aux formes non syndromiques pour faire la preuve de l'intérêt diagnostique.

Les deux premiers points sont amplement discutés dans l'article. En revanche, la proposition d'ajout à l'arbre diagnostique actuel que nous avons faite (Fraize et al., 2023c, **Figure 5**), mérite plus d'explications. Pour intégrer nos résultats à la démarche clinique, il fallait les incorporer dans un format qui correspond aux recommandations actuelles et d'attester de leur intérêt pratique. Nous avons proposé un score quantitatif, basé sur l'importance relative de chacun des marqueurs neuroanatomiques qui le constituent (voir **résumé graphique**). L'item 'taille du cerveau' (noté HC↓) associe la mesure clinique du périmètre crânien et la mesure radiologique de la taille du cerveau, par la mesure de l'aire cérébrale de référence, est coté à +2, compte tenu du fait qu'il s'agit d'un signe cardinal déjà reconnu dans les TSAF. L'item 'atteinte vermienne' associe la mesure de la hauteur vermienne (notée ↓HV) et la qualification de la foliation (notée Likert 4, 5) cotées chacune +1. L'item 'atteinte calleuse' est coté +1 et inclus l'amincissement de l'isthme du corps calleux (noté ↓IT) et l'agénésie du corps calleux (noté avec l'abréviation ACC). La distribution des points associés à chaque item de ce score est donc empirique et l'attribution du niveau de certitude diagnostique correspondant est fondé sur une hypothèse cumulative très simple, mais constituant un raisonnement clinique habituel : *l'accumulation d'arguments fait augmenter la conviction diagnostique (notion de faisceau d'arguments)*. Cette proposition est surtout pertinente dans le cas de sujets avec trouble du neurodéveloppement en contexte d'exposition prénatale à l'alcool qui présenteraient un phénotype radiologique de SAF : le lien causal à l'alcool se verrait alors renforcé. Dans notre cohorte, ils sont six sur 37, soit 16 % des sujets, pour lesquels l'utilisation de ces outils simples appliqués à une IRM cérébrale de routine, permettrait de renforcer la conviction diagnostique.

En parallèle de cette application dont nous avons déjà défendu l'intérêt, nous avons aussi proposé d'envisager deux autres situations. Tout d'abord, dans le cas où l'exposition prénatale serait insuffisamment documentée, elle devrait être réexaminée si le phénotype radiologique est très en faveur (score 4 ou 5) ou à l'inverse, la piste d'un TSAF pourrait être écartée ou fortement remise en question dans le cas où aucun signe radiologique ne serait retrouvé. Un tel usage serait ambitieux, car il suppose la spécificité de ce phénotype radiologique dont nous n'avons pas, avec cette étude, fait la preuve formelle. Pour cela, il serait nécessaire de faire des comparaisons transnosographiques. Il faut également considérer la dimension dynamique du diagnostic étiologique, la possibilité qu'il soit revu à la lumière d'éléments anamnestiques, radiologiques ou génétiques, non pas pour changer la catégorie syndromique, mais plutôt pour pondérer la certitude du lien causal. Le fait d'échelonner à l'intérieur même d'une catégorie diagnostique, la certitude avec laquelle il est effectivement établi, s'accorde assez mal avec les classifications parfois rigides qui sont nécessaires à la recherche.

Dans la continuité de ce travail, nous avons mis à disposition de l'équipe de radiologie clinique de l'hôpital Robert-Debré une fiche de calcul permettant d'obtenir à partir des mesures faites à la console, l'aire cérébrale de référence, le positionnement des sujets sur les courbes de *scaling* de l'isthme du corps calleux et de la hauteur vermienne, ainsi que d'une version française de l'échelle de Likert (**Annexe**).

Nous avons proposé, à la suite de cette étude radio-clinique, d'étudier spécifiquement le cervelet puis le corps calleux avec des outils d'imagerie assistée par ordinateur. Ces études sont présentées dans les chapitres suivants 4 et 5.

ÉTUDE EN IMAGERIE COMPUTATIONNELLE DE L'ATTEINTE DU CERVELET

INTRODUCTION

Plusieurs arguments ont convergé pour nous pousser à porter nos efforts de recherche de marqueurs neuroanatomiques sur le cervelet en premier lieu. La littérature pointe de manière récurrente le cervelet comme zone de vulnérabilité à l'exposition prénatale à l'alcool. Plusieurs cas de dysgénésie vermienne majeure parmi les patients suivis ont renforcé cette conviction (Garzón, 2017). Enfin, Pauline Garzón, dans un travail préliminaire de volumétrie à l'échelle lobaire avec une analyse d'allométrie, a confirmé que le volume cérébelleux était plus petit qu'attendu (Garzón et al., 2017) ce qui nous a encouragés à utiliser des outils dédiés pour préciser cette atteinte cérébelleuse.

Dans cette étude, nous avons montré que dans le SAF, où la microcéphalie est un signe cardinal, le cervelet est plus petit que ce qui est attendu compte tenu de la taille du cerveau et qu'à l'intérieur même du cervelet, la réduction de taille suit un gradient de sévérité antérieur-postérieur-inférieur. Un classificateur construit pour différencier les sujets SAF des sujets contrôles au développement typique les discrimine efficacement en incluant ce gradient cérébelleux. Il peut également être appliqué aux sujets ayant une forme non syndromique, et ainsi catégoriser un tiers d'entre eux comme ayant une atteinte cérébelleuse caractéristique du SAF, ce qui renforce alors la probabilité et la spécificité du diagnostic.

AMÉLIORATION DU DIAGNOSTIC DES TROUBLES DU SPECTRE DE L'ALCOOLISATION FŒTALE GRÂCE À UN CLASSIFICATEUR BASÉ SUR LE GRADIENT INTRACÉRÉBELLEUX DU SOUS-DIMENSIONNEMENT VOLUMÉTRIQUE

Fraize, J., Fischer, C., Elmaleh-Bergès, M., Kerdreux, E., Beggiato, A., Ntorkou, A., Duchesnay, E., Bekha, D., Boespflug-Tanguy, O., Delorme, R., Hertz-Pannier, L., & Germanaud, D. (2023). Enhancing fetal alcohol spectrum disorders diagnosis with a classifier based on the intracerebellar gradient of volumetric undersizing. *Human brain mapping*, 10.1002/hbm.26348. Advance online publication. <https://doi.org/10.1002/hbm.26348>

RÉSUMÉ

Introduction

Dans les troubles du spectre de l'alcoolisation fœtale (TSAF), le déficit de croissance cérébrale est une caractéristique commune des sujets atteints du syndrome d'alcoolisation fœtale (SAF) ou de TSAF non syndromique (TSAF-NS). Cependant, bien qu'il ait été suggéré que le cervelet est plus sévèrement affecté que le reste du cerveau, ce trait ne s'est pas encore vu attribuer une valeur spécifique dans les critères diagnostiques de TSAF, où les caractéristiques neuroanatomiques comptent encore peu voire pas du tout dans la spécificité du diagnostic.

Matériels et méthodes

Nous avons appliqué une combinaison d'outils de segmentation cérébelleuse à un jeu de données d'IRM cérébrale à 1,5 T de type 3DT1 provenant d'une population monocentrique de 89 personnes atteintes de TSAF (52 SAF, 37 TSAF-NS) et de 126 contrôles au développement typique (âgés de 6 à 20 ans). La chaîne d'analyses fournissait les mesures volumiques du cervelet, du vermis et de ses 3 sous-parties et des 3 lobes (antérieur, postérieur, inférieur), plus le volume total du cerveau. Après ajustement des facteurs de confusion, la relation d'échelle allométrique entre ces volumes cérébelleux (V_i) et le volume total du cerveau ou du cervelet (V_t) a été régressée ($V_i = bV_t^a$), et l'effet du groupe (SAF, contrôle) sur l'échelle allométrique a été évalué. Nous avons ensuite estimé, pour chaque volume cérébelleux de la population SAF, l'écart par rapport à la loi de *scaling* typique (\sqrt{DTS}) établie chez les contrôles. Enfin, nous avons entraîné et testé deux classificateurs pour discriminer les sujets SAF des contrôles, l'un basé sur le \sqrt{DTS} total du cervelet uniquement, l'autre basé sur tous les \sqrt{DTS} cérébelleux, en comparant leurs performances à la fois dans le groupe SAF et TSAF-NS.

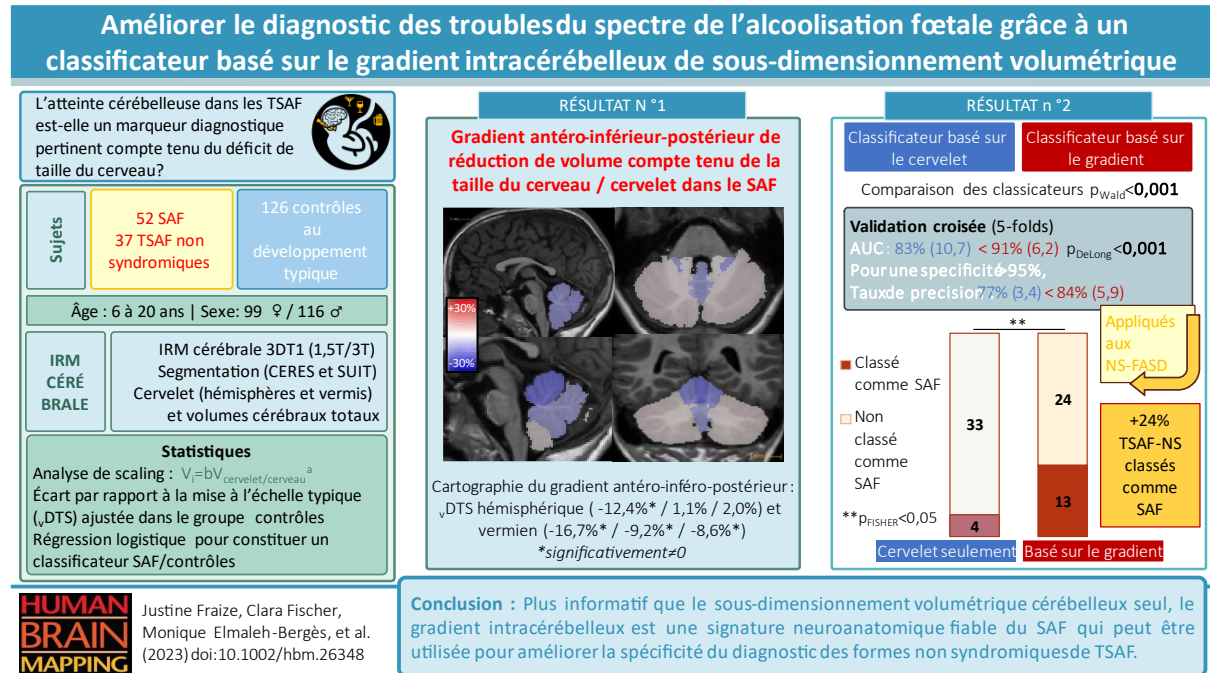
Résultats

Le *scaling* allométrique était significativement différent entre le groupe SAF et le groupe contrôle pour tous les volumes cérébelleux ($p < 0,001$). Nous avons confirmé l'excès de déficit du volume total du cervelet ($\sqrt{DTS} = -10,6\%$) et révélé un gradient antéro-inféro-postérieur de sous-dimensionnement volumétrique dans les hémisphères ($-12,4\%$, $1,1\%$, $2,0\%$ respectivement) et le vermis ($-16,7\%$, $-9,2\%$, $-8,6\%$ respectivement). Le classificateur basé sur le gradient intracérébelleux de \sqrt{DTS} s'est révélé plus efficace que celui basé sur le \sqrt{DTS} total du cervelet uniquement (AUC = 92% vs. 82% , $p = 0,001$). En fixant un seuil de probabilité élevé pour une spécificité des classificateurs $> 95\%$, celui basé sur le gradient a identifié 35% des TSAF-NS comme ayant un phénotype cérébelleux de SAF, comparé à 11% avec le classificateur basé sur le cervelet seul ($p_{\text{FISHER}} = 0,027$).











Conclusion

Dans une grande série de TSAF et en utilisant un modèle allométrique de *scaling*, cette étude détaille le sous-dimensionnement volumétrique du cervelet au niveau lobaire et vermien, révélant un gradient antéro-inféro-postérieur de vulnérabilité à l'exposition prénatale à l'alcool. Elle suggère aussi fortement que ce gradient intracérébelleux de sous-dimensionnement volumétrique puisse constituer une signature neuroanatomique fiable du SAF qui pourrait être utilisée pour améliorer la spécificité du diagnostic de TSAF-NS.

RÉSUMÉ GRAPHIQUE



Enhancing fetal alcohol spectrum disorders diagnosis with a classifier based on the intracerebellar gradient of volumetric undersizing

Justine Fraize^{1,2}  | Clara Fischer³ | Monique Elmaleh-Bergès^{2,4}  |
 Eliot Kerdreux^{1,2}  | Anita Beggiato⁵  | Alexandra Ntorkou⁴  |
 Edouard Duchesnay³  | Dhaif Bekha^{1,2} | Odile Boespflug-Tanguy⁶  |
 Richard Delorme⁵  | Lucie Hertz-Pannier^{1,2}  | David Germanaud^{1,2,7} 

¹CEA Paris-Saclay, Joliot Institute, NeuroSpin, UNIACT, Centre d'études de Saclay, Gif-sur-Yvette, France

²Université Paris Cité, Inserm, U1141 NeuroDiderot, inDEV, Paris, France

³CEA Paris-Saclay, Joliot Institute, NeuroSpin, BAOBAB, Centre d'études de Saclay, Gif-sur-Yvette, France

⁴Department of Pediatric Radiology, Centre of Excellence InovAND, AP-HP, Robert-Debré Hospital, Paris, France

⁵Department of Child and Adolescent Psychiatry, Centre of Excellence InovAND, AP-HP, Robert-Debré Hospital, Paris, France

⁶Université Paris Cité, U1141 NeuroDiderot, NeuroDEV, Paris, France

⁷Department of Genetics, Centre of Excellence InovAND, AP-HP, Robert-Debré Hospital, Paris, France

Correspondence

Justine Fraize and David Germanaud, CEA Paris-Saclay, Joliot Institute, NeuroSpin, UNIACT, Centre d'études de Saclay, Bâtiment 145, 91191, Gif-sur-Yvette, France.
 Email: justine.fraize@inserm.fr and david.germanaud@cea.fr

Funding information

French National Agency for Research; French National Institute for Public Health research

Abstract

In fetal alcohol spectrum disorders (FASD), brain growth deficiency is a hallmark of subjects both with fetal alcohol syndrome (FAS) and with non-syndromic FASD (NS-FASD, i.e., those without specific diagnostic features). However, although the cerebellum was suggested to be more severely undersized than the rest of the brain, it has not yet been given a specific place in the FASD diagnostic criteria where neuro-anatomical features still count for little if anything in diagnostic specificity. We applied a combination of cerebellar segmentation tools on a 1.5 T 3DT1 brain MRI dataset from a monocentric population of 89 FASD (52 FAS, 37 NS-FASD) and 126 typically developing controls (6–20 years old), providing 8 volumes: cerebellum, vermis and 3 lobes (anterior, posterior, inferior), plus total brain volume. After adjustment of confounders, the allometric scaling relationship between these cerebellar volumes (V_i) and the total brain or cerebellum volume (V_t) was fitted ($V_i = bV_t^a$), and the effect of group (FAS, control) on allometric scaling was evaluated. We then estimated for each cerebellar volume in the FAS population the deviation from the typical scaling (Δ DTS) learned in the controls. Lastly, we trained and tested two classifiers to

Abbreviations: AIC, Akaike information criterion; BIC, Bayesian information criterion; Δ DTS, deviation from the typical scaling; FASD, fetal alcohol spectrum disorder; FAS, fetal alcohol syndrome; FDR, false discovery rate; MRI, magnetic resonance imaging; NDD, neurodevelopmental disorders; NS-FASD, non-syndromic FASD; PAE, prenatal alcohol exposure; ROC, receiver operating characteristic.

This is an open access article under the terms of the [Creative Commons Attribution-NonCommercial-NoDerivs](https://creativecommons.org/licenses/by-nc-nd/4.0/) License, which permits use and distribution in any medium, provided the original work is properly cited, the use is non-commercial and no modifications or adaptations are made.

© 2023 The Authors. *Human Brain Mapping* published by Wiley Periodicals LLC.

discriminate FAS from controls, one based on the total cerebellum $\sqrt{\text{DTS}}$ only, the other based on all the cerebellar $\sqrt{\text{DTS}}$, comparing their performance both in the FAS and the NS-FASD group. Allometric scaling was significantly different between FAS and control group for all the cerebellar volumes ($p < .001$). We confirmed the excess of total cerebellum volume deficit ($\sqrt{\text{DTS}} = -10.6\%$) and revealed an antero-inferior-posterior gradient of volumetric undersizing in the hemispheres (-12.4% , 1.1% , 2.0% , respectively) and the vermis (-16.7% , -9.2% , -8.6% , respectively). The classifier based on the intracerebellar gradient of $\sqrt{\text{DTS}}$ performed more efficiently than the one based on total cerebellum $\sqrt{\text{DTS}}$ only (AUC = 92% vs. 82%, $p = .001$). Setting a high probability threshold for >95% specificity of the classifiers, the gradient-based classifier identified 35% of the NS-FASD to have a FAS cerebellar phenotype, compared to 11% with the cerebellum-only classifier ($p_{\text{FISHER}} = 0.027$). In a large series of FASD, this study details the volumetric undersizing within the cerebellum at the lobar and vermian level using allometric scaling, revealing an anterior-inferior-posterior gradient of vulnerability to prenatal alcohol exposure. It also strongly suggests that this intracerebellar gradient of volumetric undersizing may be a reliable neuroanatomical signature of FAS that could be used to improve the specificity of the diagnosis of NS-FASD.

KEYWORDS

cerebellum morphometry, diagnostic imaging, fetal alcohol spectrum disorders, fetal alcohol syndrome, microcephaly, prenatal alcohol exposure, scaling analysis

1 | INTRODUCTION

The clinical consequences of prenatal alcohol exposure (PAE) are grouped under the diagnostic continuum of fetal alcohol spectrum disorder (FASD), ranging from the specific form called fetal alcohol syndrome (FAS) to nonspecific forms called non-syndromic FASD (NS-FASD). FASD diagnosis relies on four criteria: growth deficiency, facial dysmorphism, anatomical (mainly brain growth deficiency) and functional neurological abnormalities, in conjunction with PAE. In NS-FASD, the physical features of FAS are absent or insufficient, and the probabilistic diagnosis is based on the combination of compatible neurodevelopmental disorders (NDD) and sufficient PAE. This distinction and the diagnostic criteria of these two conditions were formalized by Astley (2004) in the 4-digit diagnostic code, by Hoyme et al. for the Institute of Medicine (Hoyme et al., 2016) and in the Canadian guidelines by Cook et al. (2016). Yet there is still a need for additional markers particularly to ensure a high likelihood of causal link between observed NDD and PAE in the absence of FAS, and thus support the use of the whole diagnosis spectrum, as NS-FASD are still underdiagnosed.

The most obvious and widely reported consequence of PAE on the brain is growth deficiency (Archibald et al., 2001; Astley et al., 2009; Boronat et al., 2017; Nardelli, Lebel, Rasmussen, Andrew, & Beaulieu, 2011; Rajaprakash, Chakravarty, Lerch, & Rovet, 2014; Roebuck, Mattson, & Riley, 1998; Treit et al., 2014; Treit, Jeffery, Beaulieu, & Emery, 2020). It can result in microcephaly, a clinical feature

that may (Hoyme et al., 2016), or may not (Astley, 2004; Cook et al., 2016), be considered a distinct diagnostic criterion. Although the brain is one of the main targets of alcohol developmental toxicity, no other neuroanatomical anomaly is specified in the diagnostic guidelines, let alone used to improve diagnostic certainty. Yet, some focal anomalies have now been reported in an interestingly high number of subjects with FAS or FASD, particularly cerebellar anomalies, initially just described on clinical magnetic resonance imaging (MRI) (Astley et al., 2009; Boronat et al., 2017; Treit et al., 2020), and more recently specified by our team as at least vermian hypoplasia and/or anterior dysgeneses (Fraize et al., 2022).

MRI-based computational neuroanatomy has enabled the description of damage not identified by the radiologist but significant in quantitative group analysis, supporting the existence of and further specifying cerebellar involvement in FASD (Astley et al., 2009; Bookstein, Streissguth, Connor, & Sampson, 2006; Cardenas et al., 2014; O'Hare et al., 2005; Sowell et al., 1996). These first studies relied on small samples and on tools of increasing sophistication to characterize these abnormalities. Only in one recent study did Sullivan et al. (2020) implement a comprehensive automated segmentation of the cerebellum (yet without full individualization of anterior segments), in a large cohort of subjects with FASD, to characterize lower intracerebellar volume. After linear correction for sex, age and noteworthily brain size, they showed significantly lower volume of both the anterior part of the cerebellum and some posterior lobules (VIIIa and X lobules) in the FASD group compared to controls. Yet, despite a breakthrough in

cerebellar lesion mapping, no relevant clinical translation of these average group-level effects was proposed.

Indeed, any clinical application requires the analysis to result not only in group characterization but in individual assessment. At least, it should lead to the identification of subjects bearing neuroanatomical features that are both recurrent and distant enough from a normative reference to be considered as markers of FASD (such as the FAS clinical features); at best, it should provide a probability of being fetal alcohol-related. In a previous study, we identified several anomalies recurrent in FAS from a set of manual clinical-radiological measurements. We proposed to aggregate these multifocal neuroanatomical features into a composite phenotype to identify subjects with FASD with improved specificity (Fraize et al., 2022). With the same idea of multivariate analysis of neuroanatomical features for the discrimination of subjects with FASD, Little and Beaulieu (Little & Beaulieu, 2020), recently introduced a machine learning strategy considering a rather broad brain phenotype: using all supra-tentorial brain volumes in a classifier, they sought to identify brain regions with the greatest predictive contribution to FASD diagnosis but without FAS vs. non-FAS distinction.

In addition to sample size, type of anatomical segmentation or individualization of analysis, a final pitfall may have limited the success in identifying useful neuroanatomical markers of FASD: in most studies, the local size deficits were interpreted by taking global brain size into account with a linear or even sometimes a strictly proportional (ratio) model (Astley et al., 2009). Yet the relevance of the power law to describe the phenomena associated with brain size variations (scaling), especially age-independent size polymorphism, is well advocated (Bookstein et al., 2006; de Jong et al., 2017; Germanaud et al., 2012; Liu, Johnson, Long, Magnotta, & Paulsen, 2014). This scaling model allows for variation in shape and proportions with brain size (allometric scaling), including the strictly proportional model as a special case (isometric scaling with scaling exponent = 1). Even more, it has been shown that not using an allometry-sensitive model could be misleading in the case of pronounced size effects (Germanaud et al., 2014; Toro et al., 2009). In the general population, the cerebellum has been shown to scale with very negative allometry with brain size, that is, larger brains have relatively smaller cerebellums (de Jong et al., 2017; Warling et al., 2021). This nonlinear size effect should be considered in any comparison between FASD versus typically developing individuals, where brain size ranges only partially overlap, to interpret the volume variations of affected subjects according to the typical scaling of controls.

In this study, we searched for volumetric abnormalities in the cerebellum, vermis, and their lobar sub-parts, in FASD individuals compared with typically developing controls, taking into account the allometric cerebellar scaling, so as to exploit the detailed profile of cerebellar and intracerebellar anomalies to better characterize subjects with FASD. After proper anatomical segmentation, the scaling laws of the cerebellar volume (as a function of total brain volume) and each of its sub-volumes (as a function of the cerebellar volume) were estimated in the typically developing group, to be compared to the scaling laws estimated in the FASD group, but mostly to serve as

references to evaluate the deviation from typical scaling of these volumes in each subject with FASD. This normative-like approach aimed at both estimating a comprehensive profile of cerebellar volumetric undersizing, identifying the regions more or less affected by the global cerebral or cerebellar volume deficit, and providing individual profiles to be integrated in a logistic classifier of FAS versus typically developing controls. Lastly, we estimated the effectiveness of this FAS versus control classifier, and particularly whether it could help identify a significant subgroup of subjects with NS-FASD with a FAS-like cerebellar pattern.

2 | METHODS

2.1 | Participants

Eighty-nine consecutive subjects with FASD, aged 6 to 20 years, were retrospectively included from a clinical series of patients attending the NDD-dedicated child neurology consultation at Robert-Debré University Hospital (RD) between 2014 and 2020. FASD diagnostic was established using the two main guidelines (Astley, 2004; Hoyme et al., 2016) and a full differential diagnosis work-up was completed, including a systematic brain MRI. Individuals prenatally exposed to another embryo-fetotoxic agent were not included, nor were those who explicitly refused to participate in the study (see details in supplementary material Figure A.1). Subjects with FASD were split into two groups: the syndromic or FAS (including partial FAS) and the non-syndromic or NS-FASD. We evaluated the concordance (Cohen's kappa coefficient, κ) of between-group assignment using one or the other guideline. This cohort and the diagnostic procedure have already been described in a previous study (Fraize et al., 2022). Clinical and radiological characteristics of the 52 subjects with FAS (58.4%) and the 37 subjects with NS-FASD (41.6%) are detailed in Table 1.

One hundred and twenty-six typically developing subjects, aged 6 to 20 years, with no report of PAE, developmental delay or family history of neurological or psychiatric condition (1st degree) were included for comparison (supplementary material Figure A.1 and Table A.1). A subgroup of 40 subjects was matched with the FASD group for the acquisition site (MRI scanner and sequence) as part of a research program on autism in the RD Psychiatry Department. Other typically developing subjects were part of previously published studies (Boueyre et al., 2018; Germanaud et al., 2014).

There were no significant differences in the control group compared to the FASD group for sex (50.8% vs. 58.4% of male respectively, $p = .334$) and age at MRI (12.08 vs. 11.32 years of age respectively, $p = .116$).

2.2 | Ethics statement

This study was conducted in accordance with the principles of the Declaration of Helsinki. Subjects' data were studied in accordance

TABLE 1 Demographic, clinical, radiological data of subjects with FASD.

	FAS (n = 52)	NS-FASD (n = 37)	FASD groups comparison (p-value)
Sociodemographic assessment			
Sex: male, n (%)	27 (51.9)	25 (67.6)	.209
Age at MRI, mean in years (SD)	10.93 (3.57)	11.88 (3.55)	.219
Clinical assessment, n (%)			
(1) Prenatal alcohol exposure			
4.Confirmed, severe	21 (40.4)	16 (43.2)	.959
3.Confirmed, moderate or unquantified	26 (50.0)	19 (51.1)	1.000
2.Not documented	5 (9.6)	2 (5.4)	.748
1.No exposure	0 (0.0)	0 (0.0)	–
(2) FAS facial features			
4.Severe	31 (59.6)	2 (5.4)	<.001
3.Moderate	21 (40.3)	1 (2.7)	<.001
2.Mild	0 (0.0)	30 (81.1)	<.001
1.None	0 (0.0)	4 (10.8)	.057
(3) Growth deficiency			
4.Significant	19 (36.5)	3 (8.1)	.005
3.Moderate	11 (21.2)	2 (5.4)	.077
2.Mild	9 (17.3)	9 (24.3)	.586
1.None	13 (25.0)	23 (62.2)	.001
Brain anatomy			
(4) Structural central nervous system damage	40 (76.9)	19 (51.4)	.290
Head circumference (smallest known)			
(4) ≤ -2 SD: microcephaly	34 (65.4)	13 (35.1)	.009
Diagnostic agreement with revised Institute of Medicine Guidelines	50 (96.2)	33 (89.2)	
Cohen's Kappa coefficient	$\kappa = 0.86$		

Note: In bold, p-values <0.05.

Abbreviations: FAS, fetal alcohol syndrome; FASD, fetal alcohol spectrum disorder; NS-FASD, non-syndromic fetal alcohol spectrum disorder; SD, standard deviation.

with French regulation (MR-004, declaration of conformity n°2059980v0), following approval by the Paris-Saclay research ethics committee (CER-Paris-Saclay-2020-094). Controls' data were used within the framework of the ethical authorizations of the primary studies (Gene and autism, Inserm C07-33, 08-029 and 11-008).

2.3 | MRI acquisition

For both subjects with FASD and site-matched controls, MRI acquisitions were performed in the Department of Pediatric Radiology of RD Hospital at 1.5 T (Ingenia, Philips Healthcare, Amsterdam, the Netherlands) with a 3DT1 FFE-TFE sequence (1 mm isotropic; TR = 8.2 ms; TE = 3.8 ms; TI = 0.8 s; Flip = 8°; SENSE = 2). Another group of controls was acquired at the Frédéric Joliot Hospital (SHFJ, CEA-Saclay) at 1.5 T (Signa, GE Healthcare, Milwaukee, US) with a 3DT1 GE FSPGR sequence (1 × 1 × 1.2 mm; TR = 9.9 ms; TE = 2 ms; TI = 0.6 s; Flip = 10°) and a third one on a 3 T (Siemens

Trio, Siemens Healthineers, Oxford, UK) at NeuroSpin (NS, CEA-Saclay) with a 3DT1 Siemens MPRAGE sequence (1 mm isotropic; TR = 2.3 s; TE = 3 ms; TI = 0.9 s; Flip = 9°; GRAPPA 2). A visual quality check was systematically performed (Justine Fraize and David Germanaud) to exclude images of insufficient quality (detailed in supplementary material Figure A.1).

2.4 | MRI processing and cerebellar segmentation

We applied the automated segmentation of the cerebellum into lobules proposed by CERES (Romero et al., 2017), in volBrain (<http://volbrain.upv.es>, Manjón & Coupé, 2016). CERES is based on multi-atlas label fusion, known to minimize labelling errors due to inaccurate affine or non-linear registration. CERES has proven its superiority over other methods (Carass et al., 2018) but does not individualize the vermis. Thus, we also extracted the mask of the vermis from the single individual reference “Scalable Brain Atlas” (Bakker, Tiesinga, &

Kötter, 2015) and for each subject, we applied *SUIT* (Diedrichsen, Balsters, Flavell, Cussans, & Ramnani, 2009), a spatial normalization tool optimized for the cerebellum, to perform a mono-atlas segmentation based on our high-resolution atlas of the vermis. Then we merged the mask of the vermis with the *CERES* segmentation in each subject space. We extended the lobules' "cortical" labels in the deep cerebellum by applying a Voronoi front propagation algorithm available in the *Morphologist* software suite (*BrainVISA*) (<https://brainvisa.info>). We finally combined lobules to obtain sub-volumes, according to Schmahmann's anatomical description (Schmahmann et al., 1999) and merged the right and left sides, providing eight volumes and sub-volumes: the whole cerebellum, whole vermis and their subdivisions into anterior, posterior, and inferior lobes (hereinafter referred to as anterior, posterior and inferior hemisphere or vermis). All steps were followed by a visual quality check and manual corrections of obvious errors of segmentation (Figure 1). The total brain volume was obtained by *volBrain* (Manjón & Coupé, 2016).

2.5 | Statistical analysis

The statistics were computed using the R software (R Foundation for Statistical Computing, Vienna, Austria). Subject characteristics and volumes were analyzed using proportion test or independent samples

t-tests. For each analysis step, p-values were corrected to achieve a false discovery rate (FDR) of 5% (Benjamini & Hochberg, 1995).

2.5.1 | Adjusting for confounders

Raw volumes were corrected for confounders (site, sex, age) using ComBat (Fortin et al., 2018) based on an empirical Bayes method for correction of batch effects (Johnson, Li, & Rabinovic, 2007). We sequentially corrected for site (RD, SHFJ, NS) then for sex, integrating into the model correction sex, age (quadratic effect) and diagnostic (FASD, control) as covariates to be spared. The residual effect of age was no longer significant and was not corrected. In a robustness *post-hoc* analysis, we performed all analyses described below with the raw unadjusted data.

2.5.2 | Evaluating the effect of FAS on scaling

We performed scaling analyses modeling both the effect of brain size on the cerebellar volume, and at the cerebellar scale, the effect of cerebellum size (total cerebellum volume) on the cerebellar sub-volumes. We used a non-linear power law that accounts for allometric effects, i.e. the variation of proportion with size by comparison with a strictly

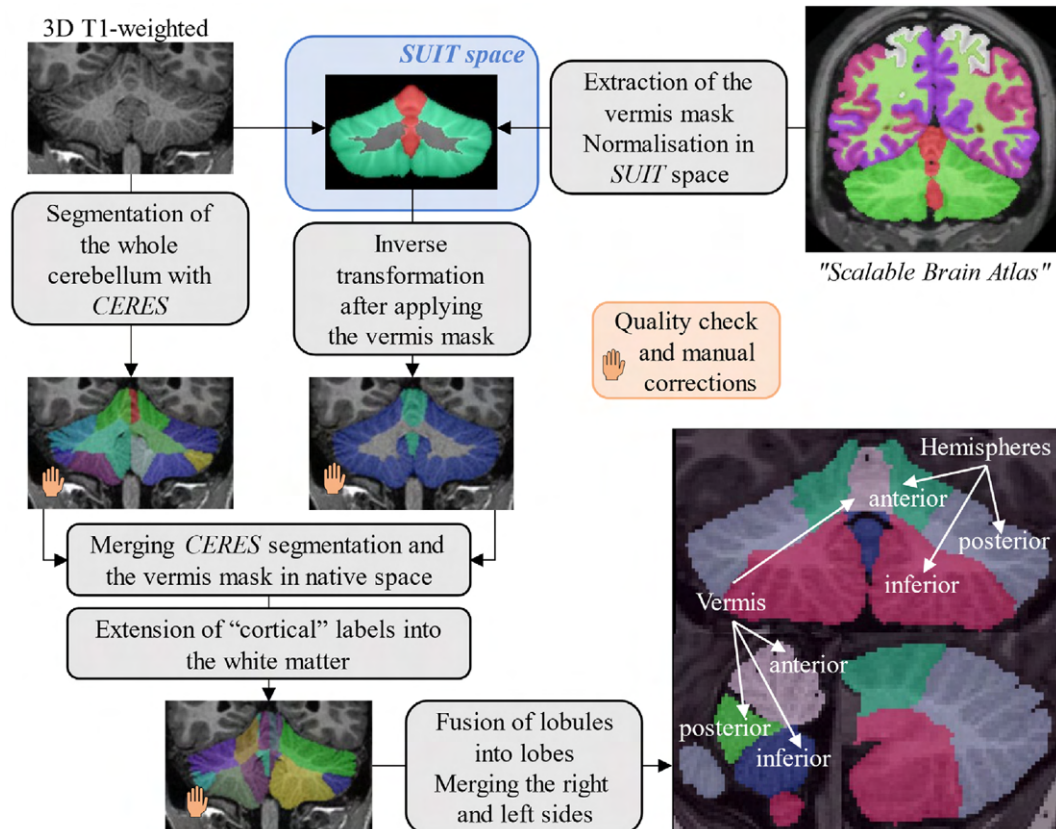


FIGURE 1 Cerebellar segmentation pipeline.

proportional relationship called isometry (Bookstein et al., 2006; de Jong et al., 2017; Germanaud et al., 2012; Liu et al., 2014). To assess this scaling relationship between cerebellar volumes (V_i) and total volume (V_t = total brain or cerebellum volume), we fitted $V_i = bV_t^a$, in the FAS and the control groups, after log-linearization ($\log_{10} V_i = a \log_{10} V_t + \log_{10} b$). Scaling coefficients 'a' in the FAS (a_{FAS}) and control ($a_{Controls}$) groups were compared to 1, to determine whether the fit was different from isometry. We evaluated the effect of FAS diagnosis on allometric laws by comparing nested models with and without a FAS diagnosis covariate ($\log_{10} V_i = a \log_{10} V_t + a_{FAS} \text{ FAS}$ $\log_{10} V_t + \log_{10} b + \text{FAS} \log_{10} b_{FAS}$) with a Wald test. We also estimated the determination coefficient R^2 of the global model and its difference with the model with the FAS diagnosis covariate δR^2 .

2.5.3 | Quantifying the degree of volumetric undersizing in FASD compared to control

Using the scaling model fitted in the typically developing group as a reference, we established the individual deviations from the predicted value for each subject (FAS, NS-FASD and controls). As a metric of this deviation, we proposed a "deviation from typical scaling" (\sqrt{DTS}), which corresponds to the distance from the typical/reference scaling prediction, relative to the mean volume of the controls, as $\sqrt{DTS} = (V_{observed} - V_{norm}) / \sqrt{V_{control}}$. For the sake of neuroanatomical clarity, we mapped the \sqrt{DTS} values with a color scale on the cerebellar segmentation of selected subjects.

To perform normative analysis, \sqrt{DTS} and confidence intervals were evaluated in the FAS group taking into account both the variance of the estimation of the reference model in controls and the variance of the FAS observations with two embedded bootstrap resamplings ($n = 1000$). We established the distribution of the mean difference between the \sqrt{DTS} in the control (≈ 0 expected) and in the FAS group in a total of 10^6 bootstrapped observations. The proportion of observations in which the null hypothesis (controls-FAS $\neq 0$, $\alpha = 5\%$) was rejected among the bootstrapped observations enabled calculation of the p -value. The differences between each sub-part of the cerebellum were investigated two-by-two by estimating if the distribution of their difference in \sqrt{DTS} included 0 or not.

2.5.4 | Classifying the subjects with FASD

Based on \sqrt{DTS} , we fitted logistic regression models to estimate the probability of belonging to the FAS group. We built two nested models, the first using only the \sqrt{DTS} of the cerebellum (cerebellum-only classifier) and the second adding the six cerebellar sub-volumes \sqrt{DTS} (gradient-based classifier). The benefit of adding the intracerebellar \sqrt{DTS} to the classifier was tested successively in several ways. First, the fitting quality of the logistic regressions was tested by using the Wald test and comparing both the Akaike information criterion (AIC) and the Bayesian information criterion (BIC). Then the inherent performance of the classifiers was evaluated in the whole FAS

+ control population by computing the area under the receiver operating characteristic (ROC) curves (AUC_{global}) and comparing them with the DeLong method (DeLong, DeLong, & Clarke-Pearson, 1988). As our aim was to obtain a classifier able to improve the diagnosis likelihood, we decided that the specificity ought to be high, thus we set the one-decimal threshold probability for a diagnostic prediction of FAS to achieve a specificity $>95\%$ at least, in both classifiers used in the whole population. Second, to further assess the performance of each classifier, we performed a 5-fold cross-validation (Mosteller, 1968). Over the five validation folds, we estimated the mean of the performance criteria (AUC_{CV}) and of both effective specificity and accuracy under the previously defined diagnosis threshold.

Finally, each high-specificity classifier (cerebellum-only and gradient-based classifiers) fitted in the whole population was applied to the FAS and NS-FASD populations to estimate and compare the proportion of subjects classified as FAS on neuroanatomical features only, that is to say for subjects with NS-FASD those showing a FAS-like cerebellar or intracerebellar profile of \sqrt{DTS} .

3 | RESULTS

3.1 | Mean volume comparison between groups

Group of subjects with FAS or NS-FASD showed lower raw (data not shown) and adjusted volumes (total brain, total cerebellum, and all cerebellar sub-parts) compared to the control group (Figure 2). The volumes in NS-FASD group were intermediate between controls and FAS groups.

3.2 | Cerebellar scaling analysis: Accounting for the brain size effect

3.2.1 | Reference scaling laws in controls

In controls, the global scaling of the cerebellum volume relative to the total brain volume showed the expected strong negative allometry ($a_{control} = 0.40$, $p < .001$), illustrated in Figure 3a. Relative to the cerebellum volume, the intracerebellar scaling of the sub-parts was not significantly different from isometry ($a \approx 1$), except for the posterior vermis ($a_{control} = 0.62$, $p = .034$) (Figure 3).

3.2.2 | Effect of FAS on cerebellar scaling laws

In the FAS group, the global scaling of the cerebellum volume relative to the total brain volume was isometric (i.e., proportional, $a_{FAS} = 1.02$, $p = .899$). The intracerebellar scaling analysis showed positive allometry for the anterior hemispheres ($a_{FAS} = 1.38$; $p = .013$) and its vermis ($a_{FAS} = 2.05$; $p < .001$), negative allometry for the posterior hemispheres ($a_{FAS} = 0.86$; $p = .001$) and isometry for the inferior

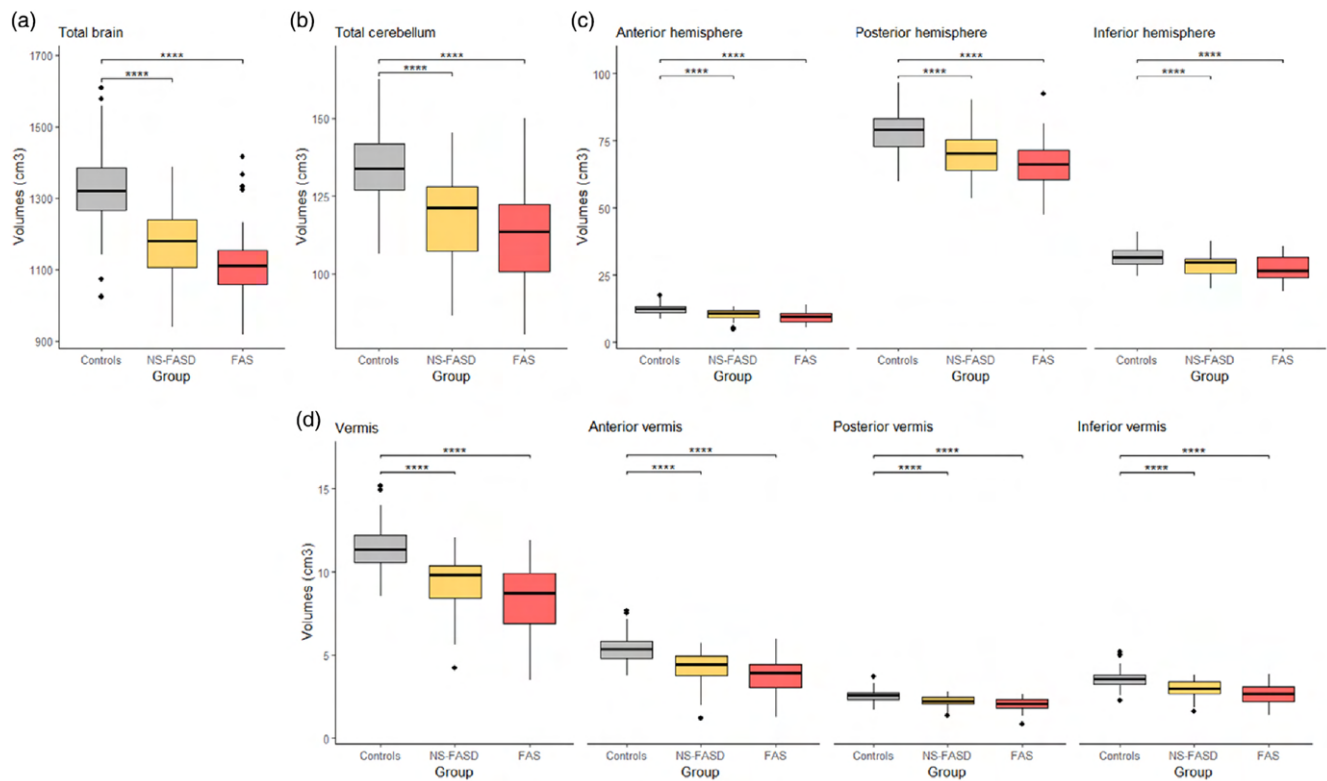


FIGURE 2 Cerebral and cerebellar adjusted volumes for control, FAS and NS-FASD groups. (a) Total brain, (b) total cerebellum, (c) cerebellar hemispheres, (d) vermis and its sub-parts volumes. NS-FASD, non-syndromic fetal alcohol spectrum disorder. The difference between FASD and controls groups was significant for all the volumes (**** for $p < .01$).

hemispheres ($a_{FAS} = 1.08$; $p = .279$). Some of the vermis sub-volumes exhibited a different scaling from that of their corresponding hemispheres: isometry for the posterior vermis ($a_{FAS} = 1.18$; $p = .237$) and positive allometry for the inferior vermis ($a_{FAS} = 1.51$; $p < .001$).

The effect of FAS diagnosis as a covariate on the scaling exponent was significant for every volume and sub-volume ($p_{DIAG} < 0.05$) (Figure 3).

3.3 | Normative analysis: Undersized volumes in FAS

In FAS, the cerebellum showed an excessively small volume relative to the whole brain one, an undersizing that did not distribute equally between cerebellar sub-volumes. The “deviation from typical scaling” (\sqrt{DTS}) was used to quantify the degree of volumetric undersizing considering what would be expected from the law established in controls.

The cerebellar volume was 10.6% smaller than expected considering the cerebral volume (Table 2). Within the cerebellum, a gradient of severity was identified: the \sqrt{DTS} was largely negative in the anterior hemispheres (-12.4% , $p < .001$), null in the inferior (1.1% , $p = .657$) and positive in the posterior hemispheres ($+2.0\%$, $p = .010$). Thus, there was an anterior-inferior-posterior gradient of severity of volume restriction in the hemispheres. The vermis was smaller than expected (-11.6% ; $p < .001$) and this undersizing followed the same decreasing anterior-inferior-posterior gradient (-16.7% , -9.2% , -8.6% , $p < .001$) (Table 2). The \sqrt{DTS} were significantly different two-by-two ($p < .001$), except the posterior vermis with the

inferior vermis ($p = .355$) and the posterior hemispheres with the inferior hemispheres ($p = .273$). The average antero-infero-posterior gradient identified in subjects with FAS is shown using a colored scale on a subject with FAS's cerebellar segmentation (Figure 4C).

3.4 | Cerebellar-based classifiers

3.4.1 | Classification efficiency: Subjects with FAS versus typically developing controls

The logistic model including the six intracerebellar \sqrt{DTS} was significantly more efficient in explaining the diagnostic status (FAS or control) than the one based on the cerebellar \sqrt{DTS} only ($p_{WALD} < 0.001$, lower AIC and BIC).

The ROC curves established for the two classifiers were used to define the AUC_{global} and the classifier including the intracerebellar \sqrt{DTS} (gradient-based classifier) was found to perform better than the one based on the cerebellum \sqrt{DTS} only (cerebellum-only classifier) ($AUC_{global} = 92\%$ vs. 82% , $p < .001$). The final threshold probability for a specificity of FAS prediction of at least $>95\%$ was 0.7 for both classifiers used in the whole population.

The five-fold cross-validation confirmed the higher AUC for the gradient-based classifier ($AUC_{CV} = 91\%$ vs. 83%). The estimated accuracy was also improved by the adjunction of the intracerebellar \sqrt{DTS} (84% vs. 77%) (Figure 5).

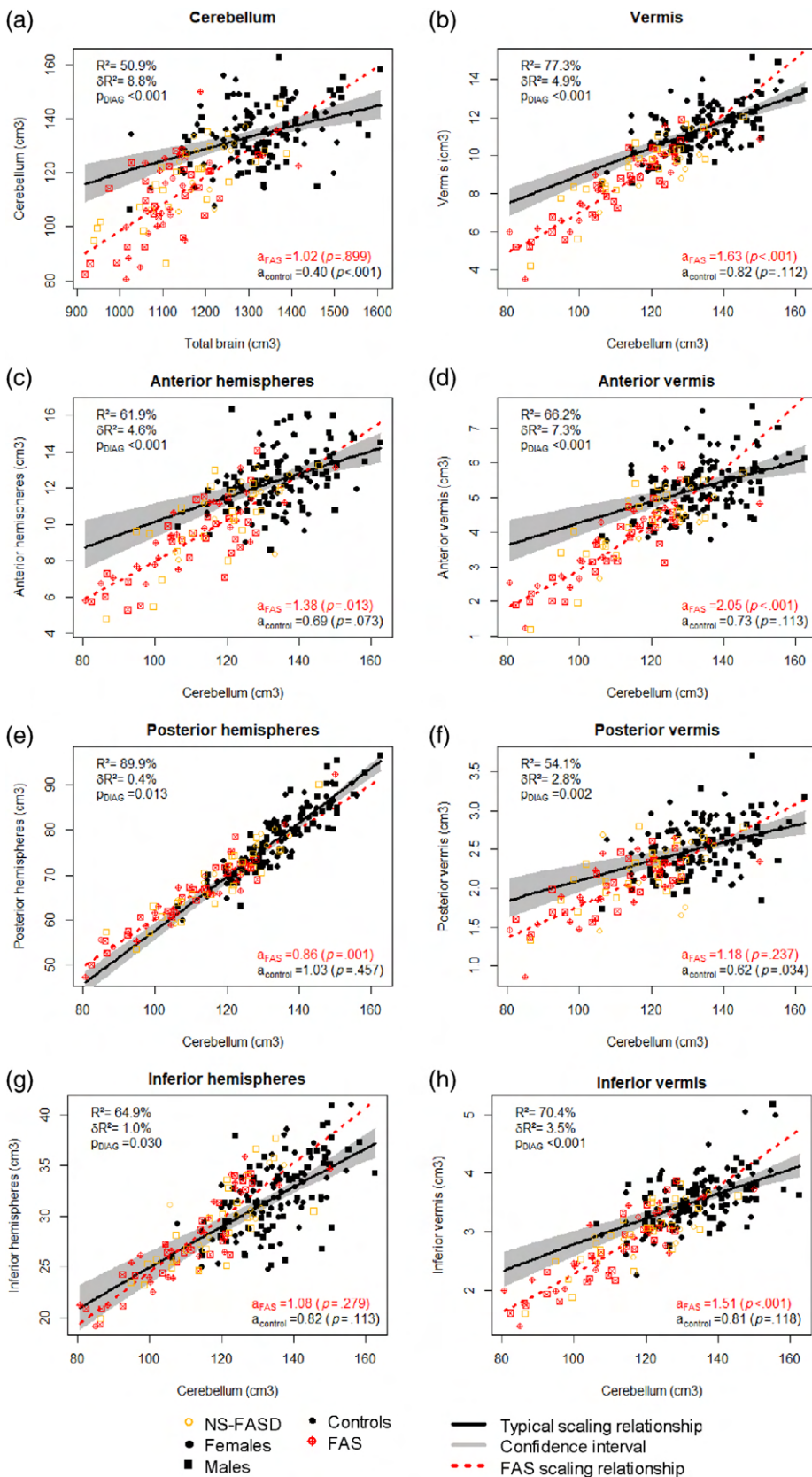


FIGURE 3 Brain scaling charts of cerebellar volumes with total brain volume (a) and cerebellar scaling charts of cerebellar sub-volumes with total cerebellum volume (B to H), in the FAS group (red) compared to the control group (black). NS-FASD represented in orange. Bottom left: Scaling coefficients $a_{FAS}/a_{Controls}$. Top right: Determination coefficient R^2 and δR^2 , FAS diagnosis effect (P_{DIAG}). Confidence interval (95%) of fitted model in the control group in grey. All p -values are adjusted to achieve a $FDR = 5\%$.

3.4.2 | Application to the NS-FASD population

The two classifiers trained in the FAS and control samples with the classification threshold set for high diagnostic specificity (>95%) correctly

classified 27% and 60% of subjects with FAS respectively (Figure 6a). The use of the gradient-based classifier resulting in a 33% increase in well-classified subjects with FAS. When applied to the NS-FASD sample, the classifier including intracerebellar ν DTS identified 13 NS-FASD (35%)

TABLE 2 Deviation from typical scaling ($\sqrt{\text{DTS}}$) of cerebellar volume and sub-volumes, in subjects with FAS, with 95% confidence interval estimated by bootstrap resampling.

	$\sqrt{\text{DTS}}$ (%)	IC95%	<i>p</i> -value
Cerebellum	-10.6	[-13.2; -8.1]	<.001
Anterior hemispheres	-12.4	[-15.4; -9.3]	<.001
Posterior hemispheres	2.0	[1.0; 3.0]	.010
Inferior hemispheres	1.1	[-0.8; 3.0]	.657
Vermis	-11.6	[-14.1; -9.1]	<.001
Anterior vermis	-16.7	[-20.3; -13.1]	<.001
Posterior vermis	-8.6	[-11.4; -5.9]	<.001
Inferior vermis	-9.2	[-11.9; -6.4]	<.001

Note: Comparison of the FAS and controls $\sqrt{\text{DTS}}$ by embedded bootstrap resampling. All *p*-values are adjusted to achieve a FDR = 5%, in bold *p*-values <0.05.

as probable FAS, compared to only 4 (11%) on the basis of total cerebellum $\sqrt{\text{DTS}}$ alone ($p_{\text{FISHER}} = 0.027$) (see subject E in Figure 4).

4 | DISCUSSION

Our study is the first to compare the allometric variations of cerebellar lobar and vermian volumes in 126 typically developing controls and 89 subjects with FASD aged 6–20 years. Our results confirm that the cerebellum is particularly affected by volumetric undersizing in FAS compared to typically developing subjects and describe an intracerebellar gradient of volumetric undersizing from over-impaired vermis and anterior regions to less affected inferior and posterior ones. Used as a multidimensional neuroanatomical marker in a logistic classifier, this gradient is more efficient than the sole cerebellar volume undersizing to discriminate FAS from non-FAS healthy controls. Trained in the FAS and control population, the gradient-based classifier also

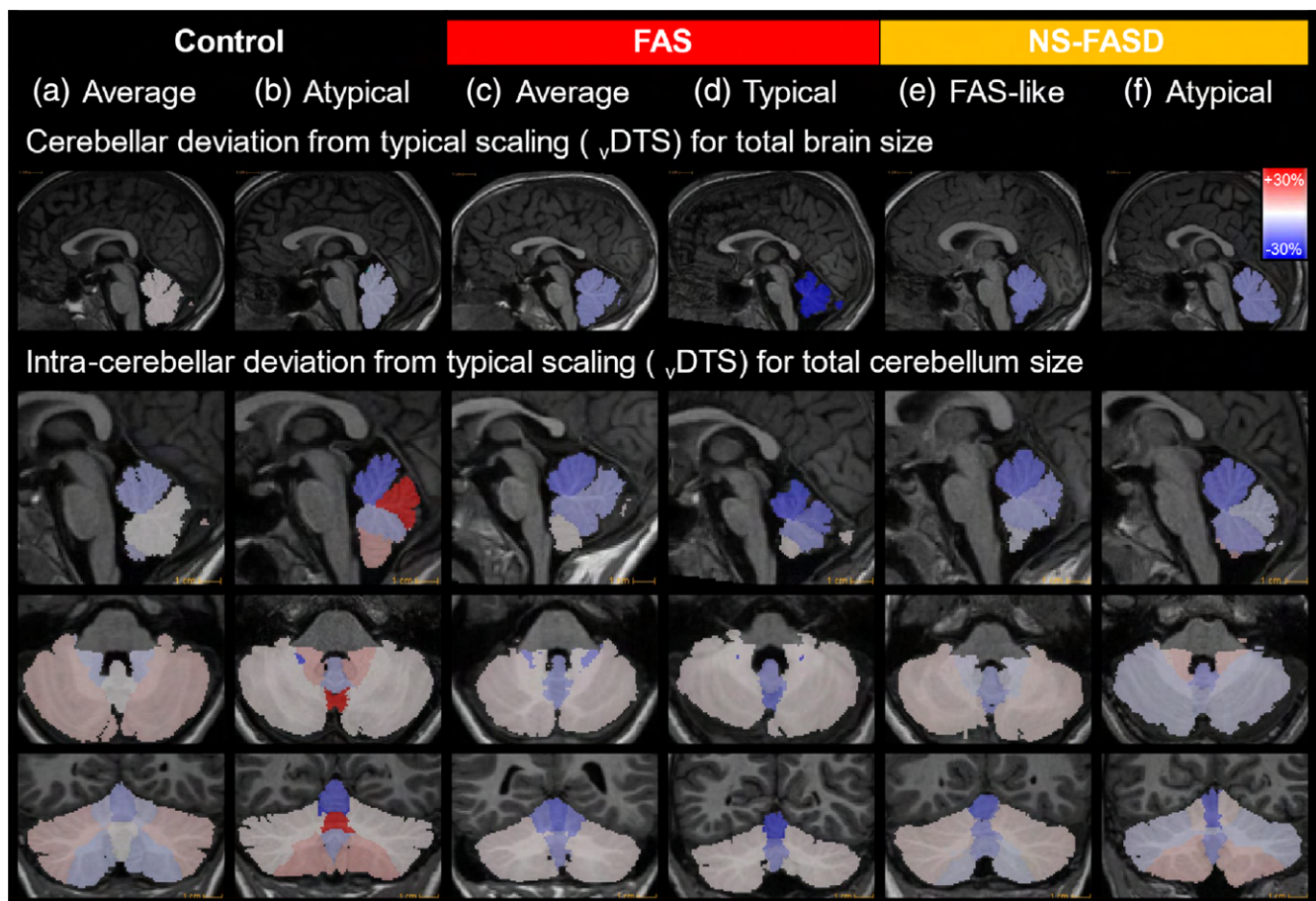


FIGURE 4 Mapping the “deviation from typical scaling” ($\sqrt{\text{DTS}}$) in selected subjects. (a) Control subject close to the norm (almost null $\sqrt{\text{DTS}}$). (b) Control subject with small cerebellum but without the specific gradient of FAS. (c) Average antero-infero-posterior gradient of Subjects with FAS (Table 2). (d) Subject with FAS with obvious dysgenesis of the anterior vermis; the typical antero-infero-posterior gradient is amplified. (e) Subject with NS-FASD with the same typical antero-infero-posterior gradient (classified as FAS). (f) Subject with NS-FASD with a small vermis for the size of the cerebellum but without the specific gradient (not classified as FAS). Note the similarity of the gradient between C, D, and E.

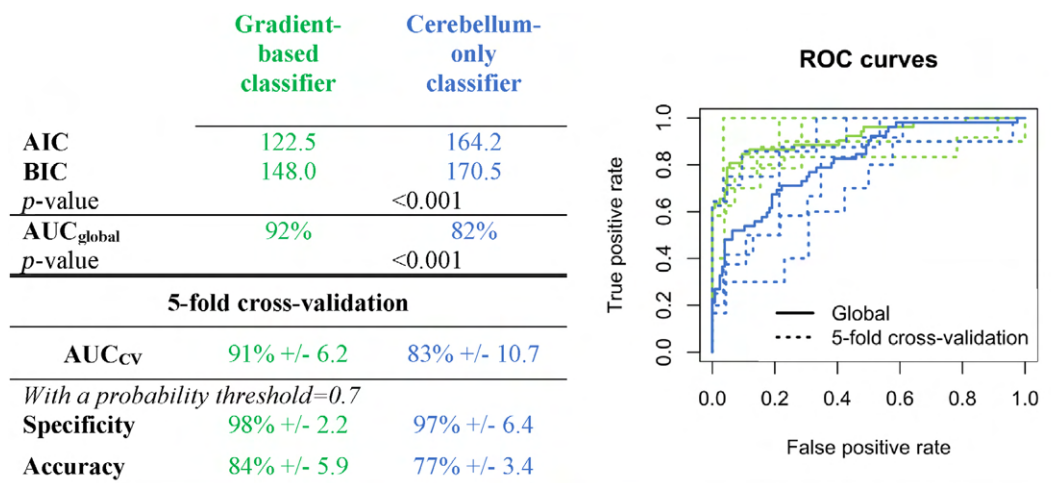


FIGURE 5 Comparison of FAS vs. controls classifiers using either the cerebellar vDTS only (blue) or adding the six intracerebellar vDTS (green). Left: AIC, BIC and *p*-value of the Wald test. AUC and *p*-value of comparison with the DeLong method. Right: ROC curves of each classifier in the whole sample (solid line) and in the 5-fold cross-validation samples (dotted), mean of the performance indices of the 5-fold cross-validation with the standard deviation. AIC, Akaike information criterion; AUC, area under the curve; BIC, Bayesian information criterion; DTS, deviation from typical scaling; ROC, receiver operating characteristic.

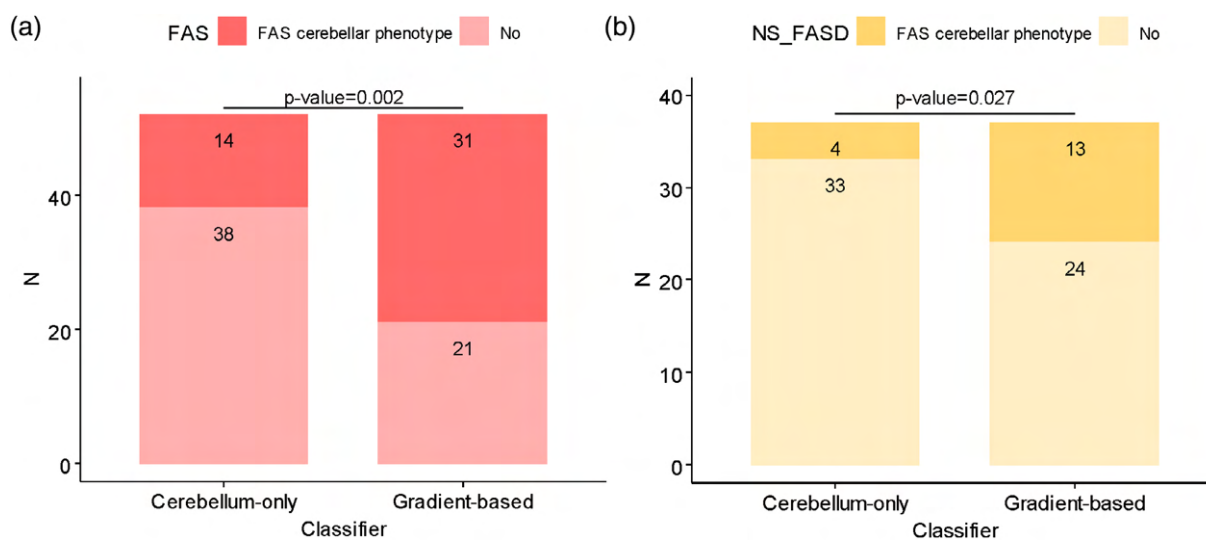


FIGURE 6 Proportion of FAS (a) and NS-FASD (b) classified as FAS cerebellar phenotype with the cerebellum-only classifier (left, dark color) and gradient-based classifier (right, dark color), with the classification threshold of 0.7 corresponding to a 95% diagnostic specificity.

identifies more than a third of NS-FASD as having a FAS-like pattern of intracerebellar volumetric undersizing.

4.1 | Presence and significance of an intracerebellar gradient of volumetric undersizing in subjects with FAS/FASD

The historical descriptions of vermis abnormalities in FASD (O'Hare et al., 2005; Sowell et al., 1996) showed a smaller area of the vermis than control, on the sagittal midsection ($N = 9$ subjects with PAE and $N = 21$ subjects with PAE and FAS, respectively). Cardenas

et al. (2014) strongly suggested the whole cerebellum and hemispheric volume to be undersized, taking into account brain size (intracranial volume) linearly in a small cohort of subjects ($N = 11$ subjects with PAE, no correction for multiple comparisons). In a sizeable cohort, Astley et al. (2009) also highlighted a smaller vermian area, affecting more severely its anterior part. Despite small sample sizes or sometimes simple tools, these studies already pointed to both anterior damage of the cerebellar vermis with relative preservation of its posterior part and more severe damage in subjects with FAS than in "affected" subjects without facial features. In the present study on 89 subjects with FASD (52 FAS), we confirm that the whole cerebellum is smaller than expected in subjects with FAS (−10.6%),

considering non-linear allometric scaling. We also clearly demonstrate that this volumetric undersizing, compared to what would be expected on the basis of the controls, is not homogeneously distributed within the cerebellum between anterior, posterior, and inferior regions of the vermis and the hemispheres: the most affected regions are the anterior vermis (−16.7%) then the anterior hemispheres (−12.4%), but also the rest of the vermis (−11.6% as a whole), while the inferior and posterior hemispheres are less affected if not relatively preserved respectively (Table 2 and Figure 3). Therefore, we propose to consider the cerebellar damage as a complex neuroanatomical phenotype reflecting an intracerebellar anterior-inferior-posterior gradient of volumetric undersizing both at the vermic and hemispheric levels and characterizing the pathologically small cerebellum of subjects with FAS (Figure 4).

This gradient of cerebellar damage is probably the result of a prenatal extreme alcohol sensitivity of cerebellar cells. The reasons for the spatial heterogeneity of damage are to be sought in experimental science and animal models. A recent review of studies in murine models (Almeida et al., 2020) confirmed that all developmental stages of the cerebellum (gliogenesis, cell differentiation, synaptogenesis and myelination) could be hindered by prenatal ethanol exposure. Studies of animal models, both murine and ovine, have shown that PAE, whether occasional or repeated, results in massive loss of Purkinje cells in the vermis in utero (Idrus & Napper, 2012; Marcussen, Goodlett, Mahoney, & West, 1994; Nirgudkar, Taylor, Yanagawa, & Valenzuela, 2016; Sawant et al., 2013), and a lower volume of the vermic lobules, with differences in affected regions depending on the term at exposure (Nirgudkar et al., 2016; Sawant et al., 2013). However, these few experiments did not consider the global deficit in size, nor did they systematically investigate the whole cerebellum. They were thus unable to show a specifically vermic damage, nor did they systematically show a more anterior cerebellar damage. One hypothesis, in addition to an overall sensitivity of Purkinje cells, could be a graduated sensitivity related to differential cell maturation, such as in the posterior cerebellar hemispheres, which mature earlier and may be therefore less sensitive to cell loss (Sawant et al., 2013). In human studies, however, the timing and level of exposure at each stage of pregnancy, retrospectively and/or by statement, are necessarily biased or inaccessible, making assumptions about a possible link illusory.

Understanding the significance of cerebellar damage observed after PAE also means interrogating the functional consequences to be expected. FASD subjects have cognitive profiles that variably combine impairments in cognitive functions (intellectual efficiency, coordination, language, executive functions, etc.) as well as in emotional regulation, often associated in a complex multidimensional disorder (Lange, Rovet, Rehm, & Popova, 2017). Interestingly, these NDDs, although non-specific, could be related to the affective-cognitive cerebellar syndrome described by Schmahmann & Sherman Schmahman and Sherman (1998) and Schmahmann Schmahmann (2010) and to the now well-known cognitive role of the cerebellum (Schmahmann, 2019). A developmental form of this functional syndrome has been proposed by some authors (Brossard-Racine &

Limperopoulos, 2016). However, functional studies on the cerebellum strongly suggest that the “cognitive cerebellum” is mainly located in the posterior part of the cerebellum, and that the anterior cerebellum mostly has a motor role (Stoodley & Schmahmann, 2009) which is in apparent contradiction with our observations, but also with those of Sullivan et al. (2020). Some authors attempted to correlate anatomical damage with cognitive functioning: O'Hare et al. (2005) found a correlation between the degree of vermic displacement and verbal learning and memory functioning in subjects with PAE and Sullivan et al. (2020) found a statistical relationship between lobe VIIb volumes and intellectual quotient performance and lobe X and verbal performance. This is still quite an open field for investigations and in any case, the cerebral damage—primarily a global brain size deficit—is diffuse in subjects with FASD, so even if this size deficit is heterogenous, one could hardly expect a unicast structural-functional explanation.

4.2 | Towards the clinical relevance of a cerebellar signature of FAS

After ascertaining the specificity of this gradient, we were keen to see whether this identification could be of any clinically relevant use. To avoid making an obvious redundant statement, it was of course important for the neuroanatomical anomalies to be independent from the whole brain growth deficiency, considering allometric phenomena in the scaling (size effect) analysis (Bookstein et al., 2006; de Jong et al., 2017; Germanaud et al., 2012; Liu et al., 2014). Beyond theoretical concerns, we ensured that the power-law model always fitted the data at least as well as the strictly proportional model (data not shown). Overall, we observed a coefficient of determination R^2 of at least 51% (Figure 4), which suggests fair adequacy of the scaling fit. It can also be noted that while we are the first to describe intracerebellar allometric laws, we confirmed the strong negative allometry of the whole cerebellum to total brain ($a = 0.40$ in our control population) that was previously described in larger healthy cohorts ($a = 0.54$) (de Jong et al., 2017; Warling et al., 2021). Lastly, we proved that the cerebellar and intracerebellar scaling laws were different in controls and in subjects with FAS for all the cerebellar and intracerebellar volumes (Figure 3).

To move from classical group comparisons towards describing individual differences with respect to a common reference model (Marquand et al., 2019; Marquand, Wolfers, Mennes, Buitelaar, & Beckmann, 2016), we established reference scaling curves similarly to long-standing growth curves in pediatric medicine (Garel et al., 2011; Rollins, Collins, & Holden, 2010). We were then able to estimate how much the observed volumes deviated from the expected ones according to the typical scaling laws (“volumetric deviation from typical scaling,” \sqrt{DTS}) and used these distances in the scaling space as measures of the undersizing (or oversizing) of cerebellar and intracerebellar volumes in FAS. Our approach to making these deviations relevant at the individual level consisted less in a directly normative approach than in the training of a multidimensional classifier on the basis of the \sqrt{DTS} . In this way, for each subject, we obtained a diagnostic

probability of presenting with an anatomical cerebellar phenotype of FAS rather than a typical one. This classification strategy began to emerge in the field of FASD neuroanatomy and diagnosis (Little & Beaulieu, 2020) but it has mainly been used as a way to identify brain areas with a high FASD predictive weight rather than to qualify subjects. Our first step at the individual level was to show that a univariate classification based on total cerebellum $\sqrt{\text{DTS}}$ only was already relevant for discerning FAS from controls ($\text{AUC}_{\text{global}} = 82\%$), consistently with the singular isometric scaling observed in FAS. Moreover, we showed that the newly identified gradient phenotype provides valuable additional information to distinguish between FAS and typically developing subjects, leading to a significant improvement of the classifier ($\text{AUC}_{\text{global}} = 92\%$, $p < .001$, +33% of FAS subjects correctly classified). This result argues for the use of such a multidimensional cerebellar marker that is not redundant with the whole brain size anomaly nor with the cerebellum one.

In addition to showing that the multidimensional cerebellar gradient-based classifier was more effective than the one considering only the cerebellum, we also wanted to evaluate its applicability and value at the individual level on subjects with NS-FASD. FASD imaging studies often report that subjects with non-syndromic FASD have an intermediate degree of neuroanatomical changes at the group level (comparison of means) (Archibald et al., 2001; Astley et al., 2009; Inkelis, Moore, Bischoff-Grethe, & Riley, 2020; O'Hare et al., 2005; Sullivan et al., 2020). In our cohort, subjects with NS-FASD also presented an intermediate severity of impairment (orange dots, Figure 4) in an overlapping range between subjects with FAS and typically developing controls. It was therefore logical to investigate whether what could be considered a FAS cerebellar signature, or at least a cerebellar morphology strongly suggestive of FAS, in view of the high level of specificity set for the classification (>95%), was also observed in some subjects with NS-FASD. We indeed found that the gradient-based classifier tagged 35% of the NS-FASD group as FAS-like (three times more than the 11% tagged with the cerebellum-only classifier). For all these FAS-like subjects, it seems reasonable to consider that the likelihood of a causal link with PAE is significantly higher, even in the absence of a clinical FAS (see subject E in Figure 4).

In current diagnostic procedures (Astley, 2004; Cook et al., 2016; Hoyme et al., 2016), the neuroanatomical impairments other than microcephaly that should be taken into account are not clearly listed, and in any case do not provide an argument for or against a FASD diagnosis. For subjects with NS-FASD, the link between functional impairment (NDD) and PAE remains a probabilistic diagnosis, after a thorough differential diagnosis work-up. Here, we have demonstrated that a gradient of cerebellar hemispheric and vermian damage can be used to train an efficient classifier on 178 subjects of which 30% had a positive specific FAS diagnosis (Astley, 2004). Since this classifier identified 35% subjects with NS-FASD as having a FAS-like cerebellar phenotype, we think that it advocates for a more objective and independent neuroanatomical FASD diagnosis criterion, in line with what we proposed in our previous study based on more directly available radiological-clinical measurements (Fraize et al., 2022). Were they to

be confirmed by other works, these results could provide an additional diagnostic argument and ease the way to more confident diagnoses in certain subjects presenting FASD without FAS, and therefore prompt a larger use of the full spectrum of FASD diagnosis in some medical communities where a full FAS diagnosis often remains the only option.

4.3 | Dealing with confounding covariates

For the sake of robustness of the fit of the reference typical scaling laws, we gathered a population of 126 controls from three different acquisition sites (sequence and imager), a third only being site- and sequence-matched to the FASD group. As expected (Takao, Hayashi, & Ohtomo, 2011), there was a site bias (see control group data, supplementary material Table A.1) that we corrected beforehand using a batch effect correcting method (Fortin et al., 2017). ComBat has proven to be a method superior to other correction methods, especially for imaging data and when using logistic regression (Fortin et al., 2018; Horng et al., 2022). However, to test the robustness of our results (potential loss of information, information bias), we performed a full *post-hoc* analysis on the raw data set (without correcting for site or sex effect), that showed very similar results in terms of gradient and reached the same conclusions on the classifier potential (supplementary material Figure A.2).

To be as rigorous and informative as possible, it would have been interesting to establish differential reference charts for females and males, since a differential sex effect is expected on volumes (Fan et al., 2010; Sullivan et al., 2020). We chose to privilege the statistical power provided by a group of 126 controls, that we would have lost by dividing the number by two. As a first precaution, we ensured that there was no difference in sex-ratio between the subgroups (Table 1). Then, we applied the same method of confounders correction as for the site. In the end, even if this choice of correction possibly erases informative sex differences, at least the result of the *post-hoc* analysis is reassuring in terms of quality of adjustment, and we trust our sex-independent results (supplementary material Figure A.2). However, a replication study on a larger sample, differentiating between females and males, would be of real interest, with the prospect of a more efficient analysis and classifier due to more finely adjusted reference scaling laws.

Lastly, choosing the scaling model and this "size-for-size" space means not including the classical normative analysis "size-for-age." Again, we first ensured that there was no difference in mean age between the groups (Table 1), and after adjusting for site and sex confounders, we found no effect of age, even with a rather biologically accurate model preserving a possible interaction with age and quadratic age (Giedd & Rapoport, 2010; Nardelli et al., 2011). This was not surprising since in the age range we studied, long after the fast growth of the first years of life and before significant adulthood shrinking, the effect of age was expected to be negligible (Inkelis et al., 2020; Jandeaux et al., 2019).

4.4 | Anatomical considerations

In Schmahmann's original description of cerebellar anatomy (Schmahmann et al. 1999) the lateral boundaries of the anterior vermis were considered virtual; thus, the vermis is not individualized in many current segmentation tools (Diedrichsen et al., 2009). Yet, other neuroanatomical consensus atlases, such as the "Scalable Brain Atlas" (Bakker et al., 2015), propose a delimitation of the whole vermis lateral boundaries. Besides, the FASD literature suggests a predominantly sagittal involvement of the anterior cerebellum. That is why we proposed a combination of the currently most accurate CERES lobular segmentation (Romero et al., 2017) with a mono-atlas segmentation of the vermis optimized by the SUIT cerebellar-dedicated spatial normalization, which circumvented the lack of a completely validated tool and met our requirements to individualize the whole vermis. Given the manageable size of our cohort, systematic verification, and correction of lobar boundaries by an expert (JF) for obvious segmentation errors ensured the anatomical reliability of the studied sub-volumes, in particular when the anatomy was very abnormal (Figure 4c,d). In this context, we were not able to corroborate our results with several segmentation methods as others duly did (Biffen et al., 2020; Sullivan et al., 2020; Sullivan, Zahr, Saranathan, Pohl, & Pfefferbaum, 2019), which would have unrealistically required several combinations of tools. Among the other choices related to cerebellar anatomy, we found it unnecessary to perform a lateralized sub-volume analysis (left and right comparison). The results of the lateralized analyses of Zhou et al. (2018), confirmed by the asymmetry index study of Sullivan et al. (Sullivan et al., 2020), did not suggest cerebellar volume asymmetry in subjects exposed prenatally to alcohol. In the same spirit of a parsimonious, anatomically accurate and power-optimized study, we chose to work at the scale of the cerebellar lobes, not lobules, keeping the possibility of verification and correction of the boundaries when necessary. We also chose not to individualize the white and grey matter. In fact, the grey-white junction is sensitive to the configuration of the T1 sequence, to the maturation effect of age until late adolescence (Drakulich et al., 2021), and in any case, the cerebellar grey/white boundary is not positioned at the same place in the different cerebellar segmentations proposed for millimetric T1-weighted conventional images.

4.5 | Other limitations

The retrospective design of our study led to the exclusion of a significant number of potential subjects with FASD due to incomplete data (supplementary material Figure A.1). However, it is important to emphasize that brain MRI was systematically performed on FASD-suspected subjects in the Robert-Debré reference center as part of the recommended work-up, so there was no bias was expected in terms of severity or type of subjects with FASD in our studied population. In the diagnosis procedure, we also duly considered a "relevant" threshold of PAE (Cook et al., 2016; Hoyme

et al., 2016), even if we did not have retrospective access to detailed timing and quantification. Therefore we were unable to correlate our finding with the level of PAE (Jacobson, Jacobson, Stanton, Meintjes, & Molteno, 2011; May et al., 2013). Another limitation related to the retrospective construct of this study is that MRI data were acquired in the context of clinical care, on a 1.5 T imager, which may be seen as not optimum for brain imaging. This is a grounded concern for a structure such as the cerebellum even if it should be pointed out that 60% of participants shared the same site and sequence, and that all sequences were high-quality millimetric IR-prep ultra-fast gradient echo sequences. One could also question the fact that inferior parts of the cerebellum may have suffered from a mild signal drop-off, not visible in quality-check steps, that could have tempered with our ability to reveal a group difference in this area. The last important methodological limitation, which is often found in human studies on NDD, is the choice of the control population. The comparison between subjects with FASD and typically developing controls (no alcohol, no neurological, psychiatric or learning condition) appears as a necessary step, but to ensure a real specificity of any cerebellar phenotype in FASD, it would be necessary to compare with a population of subjects with a non-alcohol related NDD and/or a population of "small brains" not related to alcohol (any type of microcephaly of paired severity). Future studies consequently should focus on separate female/male groups, use multiple segmentation tools, and compare results with various samples of subjects with NDD or small brain populations, as to the best of the authors' knowledge this has not yet been proposed in other comparable studies.

5 | CONCLUSION

Our study is the first to consider allometric scaling to describe the cerebellar damage in a large cohort of FASD, revealing an anterior-inferior-posterior gradient of sensitivity to PAE both in hemispheres and vermis. More informative than cerebellar undersizing alone, the intracerebellar gradient could constitute an advance towards a first neuroanatomical signature of FAS to be searched in NS-FASD to try and improve the specificity of the diagnosis.

ACKNOWLEDGMENTS

The authors would like to thank the volunteers, patients and families, and the French supportive association for FASD-affected families "Vivre avec le SAF."

FUNDING INFORMATION

This study was supported by the French National Agency for Research (ANR-19-CE17-0028-01) and the French National Institute for Public Health research (IRESP-19-ADDICTIONS-08).

CONFLICT OF INTEREST STATEMENT

The authors have no conflicts of interest to disclose.

DATA AVAILABILITY STATEMENT

The data that support the findings of this study are available on request from the corresponding author. The data are not publicly available due to privacy or ethical restrictions.

ORCID

Justine Fraize  <https://orcid.org/0000-0001-6434-7992>

Monique Elmaleh-Bergès  <https://orcid.org/0000-0001-8190-8202>

Eliot Kerdreux  <https://orcid.org/0000-0002-4071-2008>

Anita Beggiato  <https://orcid.org/0000-0002-7374-0275>

Alexandra Ntorkou  <https://orcid.org/0000-0001-7454-4316>

Edouard Duchesnay  <https://orcid.org/0000-0002-4073-3490>

Odile Boespflug-Tanguy  <https://orcid.org/0000-0003-2389-1232>

Richard Delorme  <https://orcid.org/0000-0002-5614-3663>

Lucie Hertz-Pannier  <https://orcid.org/0000-0003-4952-7009>

David Germanaud  <https://orcid.org/0000-0001-5055-4624>

REFERENCES

- Almeida, L., Andreu-Fernández, V., Navarro-Tapia, E., Aras-López, R., Serra-Delgado, M., Martínez, L., García-Algar, O., & Gómez-Roig, M. D. (2020). Murine models for the study of fetal alcohol spectrum disorders: An overview. *Frontiers in Pediatrics*, 8, 359. <https://doi.org/10.3389/fped.2020.00359>
- Archibald, S. L., Fennema-Notestine, C., Gamst, A., Riley, E. P., Mattson, S. N., & Jernigan, T. L. (2001). Brain dysmorphology in individuals with severe prenatal alcohol exposure. *Developmental Medicine and Child Neurology*, 43, 148–154. <https://doi.org/10.1111/j.1469-8749.2001.tb00179.x>
- Astley, S. J. (2004). *Diagnostic guide for fetal alcohol spectrum disorders: The 4-digit diagnostic code* (3rd ed.). University of Washington.
- Astley, S. J., Aylward, E. H., Olson, H. C., Kerns, K., Brooks, A., Coggins, T. E., Davies, J., Dorn, S., Gendler, B., Jirikowic, T., Kraegel, P., Maravilla, K., & Richards, T. (2009). Magnetic resonance imaging outcomes from a comprehensive magnetic resonance study of children with fetal alcohol spectrum disorders. *Alcoholism, Clinical and Experimental Research*, 33, 1671–1689. <https://doi.org/10.1111/j.1530-0277.2009.01004.x>
- Bakker, R., Tiesinga, P., & Kötter, R. (2015). The scalable brain atlas: Instant web-based access to public brain atlases and related content. *Neuroinformatics*, 13, 353–366. <https://doi.org/10.1007/s12021-014-9258-x>
- Benjamini, Y., & Hochberg, Y. (1995). Controlling the false discovery rate: A practical and powerful approach to multiple testing. *Journal of the Royal Statistical Society: Series B: Methodological*, 57, 289–300. <https://doi.org/10.1111/j.2517-6161.1995.tb02031.x>
- Biffen, S. C., Warton, C. M. R., Dodge, N. C., Molteno, C. D., Jacobson, J. L., Jacobson, S. W., & Meintjes, E. M. (2020). Validity of automated FreeSurfer segmentation compared to manual tracing in detecting prenatal alcohol exposure-related subcortical and corpus callosal alterations in 9- to 11-year-old children. *NeuroImage Clinical*, 28, 102368. <https://doi.org/10.1016/j.nicl.2020.102368>
- Bookstein, F. L., Streissguth, A. P., Connor, P. D., & Sampson, P. D. (2006). Damage to the human cerebellum from prenatal alcohol exposure: The anatomy of a simple biometrical explanation. *Anatomical Record. Part B, New Anatomist*, 289, 195–209. <https://doi.org/10.1002/ar.b.20114>
- Boronat, S., Sánchez-Montañez, A., Gómez-Barros, N., Jacas, C., Martínez-Ribot, L., Vázquez, E., & del Campo, M. (2017). Correlation between morphological MRI findings and specific diagnostic categories in fetal alcohol spectrum disorders. *European Journal of Medical Genetics*, 60, 65–71. <https://doi.org/10.1016/j.ejmg.2016.09.003>
- Bouyeure, A., Germanaud, D., Bekha, D., Delattre, V., Lefèvre, J., Pinabiaux, C., Mangin, J.-F., Rivière, D., Fischer, C., Chiron, C., Hertz-Pannier, L., & Noulhiane, M. (2018). Three-dimensional probabilistic maps of mesial temporal lobe structures in children and Adolescents' brains. *Frontiers in Neuroanatomy*, 12, 98. <https://doi.org/10.3389/fnana.2018.00098>
- Brossard-Racine, M., & Limperopoulos, C. (2016). Normal cerebellar development by qualitative and quantitative MR imaging. *Neuroimaging Clinics of North America*, 26, 331–339. <https://doi.org/10.1016/j.nic.2016.03.004>
- Carass, A., Cuzzocreo, J. L., Han, S., Hernandez-Castillo, C. R., Rasser, P. E., Ganz, M., Beliveau, V., Dolz, J., Ben Ayed, I., Desrosiers, C., Thyreau, B., Romero, J. E., Coupé, P., Manjón, J. V., Fonov, V. S., Collins, D. L., Ying, S. H., Onyike, C. U., Crocetti, D., ... Prince, J. L. (2018). Comparing fully automated state-of-the-art cerebellum parcellation from magnetic resonance images. *NeuroImage*, 183, 150–172. <https://doi.org/10.1016/j.neuroimage.2018.08.003>
- Cardenas, V. A., Price, M., Infante, M. A., Moore, E. M., Mattson, S. N., Riley, E. P., & Fein, G. (2014). Automated cerebellar segmentation: Validation and application to detect smaller volumes in children prenatally exposed to alcohol. *NeuroImage Clinical*, 4, 295–301. <https://doi.org/10.1016/j.nicl.2014.01.002>
- Cook, J. L., Green, C. R., Lilley, C. M., Anderson, S. M., Baldwin, M. E., Chudley, A. E., Conry, J. L., LeBlanc, N., Loock, C. A., Lutke, J., Mallon, B. F., McFarlane, A. A., Temple, V. K., & Rosales, T. (2016). Fetal alcohol spectrum disorder: A guideline for diagnosis across the lifespan. *Canadian Medical Association Journal*, 188, 191–197. <https://doi.org/10.1503/cmaj.141593>
- de Jong, L. W., Vidal, J.-S., Forsberg, L. E., Zijdenbos, A. P., Haight, T., Alzheimer's Disease Neuroimaging Initiative, Sigurdsson, S., Gudnason, V., van Buchem, M. A., & Launer, L. J. (2017). Allometric scaling of brain regions to intra-cranial volume: An epidemiological MRI study. *Human Brain Mapping*, 38, 151–164. <https://doi.org/10.1002/hbm.23351>
- DeLong, E. R., DeLong, D. M., & Clarke-Pearson, D. L. (1988). Comparing the areas under two or more correlated receiver operating characteristic curves: A nonparametric approach. *Biometrics*, 44, 837–845. <https://doi.org/10.2307/2531595>
- Diedrichsen, J., Balsters, J. H., Flavell, J., Cussans, E., & Ramnani, N. (2009). A probabilistic MR atlas of the human cerebellum. *NeuroImage*, 46, 39–46. <https://doi.org/10.1016/j.neuroimage.2009.01.045>
- Drakulich, S., Thiffault, A.-C., Olafson, E., Parent, O., Labbe, A., Albaugh, M. D., Khundrakpam, B., Ducharme, S., Evans, A., Chakravarty, M. M., & Karama, S. (2021). Maturational trajectories of pericortical contrast in typical brain development. *NeuroImage*, 235, 117974. <https://doi.org/10.1016/j.neuroimage.2021.117974>
- Fan, L., Tang, Y., Sun, B., Gong, G., Chen, Z. J., Lin, X., Yu, T., Li, Z., Evans, A. C., & Liu, S. (2010). Sexual dimorphism and asymmetry in human cerebellum: An MRI-based morphometric study. *Brain Research*, 1353, 60–73. <https://doi.org/10.1016/j.brainres.2010.07.031>
- Fortin, J.-P., Cullen, N., Sheline, Y. I., Taylor, W. D., Aselcioglu, I., Cook, P. A., Adams, P., Cooper, C., Fava, M., McGrath, P. J., McInnis, M., Phillips, M. L., Trivedi, M. H., Weissman, M. M., & Shinohara, R. T. (2018). Harmonization of cortical thickness measurements across scanners and sites. *NeuroImage*, 167, 104–120. <https://doi.org/10.1016/j.neuroimage.2017.11.024>
- Fortin, J.-P., Parker, D., Tunç, B., Watanabe, T., Elliott, M. A., Ruparel, K., Roalf, D. R., Satterthwaite, T. D., Gur, R. C., Gur, R. E., Schultz, R. T., Verma, R., & Shinohara, R. T. (2017). Harmonization of multi-site diffusion tensor imaging data. *NeuroImage*, 161, 149–170. <https://doi.org/10.1016/j.neuroimage.2017.08.047>
- Fraize, J., Garzón, P., Ntorkou, A., Kerdreux, E., Boespflug-Tanguy, O., Beggiato, A., Delorme, R., Hertz-Pannier, L., Elmaleh-Berges, M., & Germanaud, D. (2022). Combining neuroanatomical features to support diagnosis of fetal alcohol spectrum disorders. *Developmental Medicine and Child Neurology*, 65, 551–562. <https://doi.org/10.1111/dmcn.15411>

- Garel, C., Cont, I., Alberti, C., Josserand, E., Moutard, M. L., & Ducou le Pointe, H. (2011). Biometry of the corpus callosum in children: MR imaging reference data. *American Journal of Neuroradiology*, 32, 1436–1443. <https://doi.org/10.3174/ajnr.A2542>
- Germanaud, D., Lefèvre, J., Fischer, C., Bintner, M., Curie, A., des Portes, V., Eliez, S., Elmaleh-Bergès, M., Lamblin, D., Passemard, S., Operto, G., Schaer, M., Verloes, A., Toro, R., Mangin, J. F., & Hertz-Pannier, L. (2014). Simplified gyral pattern in severe developmental microcephalies? New insights from allometric modeling for spatial and spectral analysis of gyrification. *NeuroImage*, 102(Pt 2), 317–331. <https://doi.org/10.1016/j.neuroimage.2014.07.057>
- Germanaud, D., Lefèvre, J., Toro, R., Fischer, C., Dubois, J., Hertz-Pannier, L., & Mangin, J.-F. (2012). Larger is twistier: Spectral analysis of gyrification (SPANGY) applied to adult brain size polymorphism. *NeuroImage*, 63, 1257–1272. <https://doi.org/10.1016/j.neuroimage.2012.07.053>
- Giedd, J. N., & Rapoport, J. L. (2010). Structural MRI of pediatric brain development: What have we learned and where are we going? *Neuron*, 67, 728–734. <https://doi.org/10.1016/j.neuron.2010.08.040>
- Hornig, H., Singh, A., Yousefi, B., Cohen, E. A., Haghighi, B., Katz, S., Noël, P. B., Shinohara, R. T., & Kontos, D. (2022). Generalized ComBat harmonization methods for radiomic features with multi-modal distributions and multiple batch effects. *Scientific Reports*, 12, 4493. <https://doi.org/10.1038/s41598-022-08412-9>
- Hoyme, H. E., Kalberg, W. O., Elliott, A. J., Blankenship, J., Buckley, D., Marais, A.-S., Manning, M. A., Robinson, L. K., Adam, M. P., Abdul-Rahman, O., Jewett, T., Coles, C. D., Chambers, C., Jones, K. L., Adnams, C. M., Shah, P. E., Riley, E. P., Charness, M. E., Warren, K. R., & May, P. A. (2016). Updated clinical guidelines for diagnosing fetal alcohol spectrum disorders. *Pediatrics*, 138, e20154256. <https://doi.org/10.1542/peds.2015-4256>
- Idrus, N. M., & Napper, R. M. A. (2012). Acute and long-term Purkinje cell loss following a single ethanol binge during the early third trimester equivalent in the rat. *Alcoholism, Clinical and Experimental Research*, 36, 1365–1373. <https://doi.org/10.1111/j.1530-0277.2012.01743.x>
- Inkelis, S. M., Moore, E. M., Bischoff-Grethe, A., & Riley, E. P. (2020). Neurodevelopment in adolescents and adults with fetal alcohol spectrum disorders (FASD): A magnetic resonance region of interest analysis. *Brain Research*, 1732, 146654. <https://doi.org/10.1016/j.brainres.2020.146654>
- Jacobson, S. W., Jacobson, J. L., Stanton, M. E., Meintjes, E. M., & Molteno, C. D. (2011). Biobehavioral markers of adverse effect in fetal alcohol spectrum disorders. *Neuropsychology Review*, 21, 148–166. <https://doi.org/10.1007/s11065-011-9169-7>
- Jandeaux, C., Kuchcinski, G., TERNYNCK, C., Riquet, A., Leclerc, X., Pruvo, J.-P., & Soto-Ares, G. (2019). Biometry of the cerebellar vermis and brain stem in children: MR imaging reference data from measurements in 718 children. *AJNR. American Journal of Neuroradiology*, 40, 1835–1841. <https://doi.org/10.3174/ajnr.A6257>
- Johnson, W. E., Li, C., & Rabinovic, A. (2007). Adjusting batch effects in microarray expression data using empirical Bayes methods. *Biostatistics*, 8, 118–127. <https://doi.org/10.1093/biostatistics/kxj037>
- Lange, S., Rovet, J., Rehm, J., & Popova, S. (2017). Neurodevelopmental profile of fetal alcohol spectrum disorder: A systematic review. *BMC Psychology*, 5, 22. <https://doi.org/10.1186/s40359-017-0191-2>
- Little, G., & Beaulieu, C. (2020). Multivariate models of brain volume for identification of children and adolescents with fetal alcohol spectrum disorder. *Human Brain Mapping*, 41, 1181–1194. <https://doi.org/10.1002/hbm.24867>
- Liu, D., Johnson, H. J., Long, J. D., Magnotta, V. A., & Paulsen, J. S. (2014). The power-proportion method for intracranial volume correction in volumetric imaging analysis. *Frontiers in Neuroscience*, 8, 356. <https://doi.org/10.3389/fnins.2014.00356>
- Manjón, J. V., & Coupé, P. (2016). volBrain: An online MRI brain volumetry system. *Frontiers in Neuroinformatics*, 10, 30. <https://doi.org/10.3389/fninf.2016.00030>
- Marcussen, B. L., Goodlett, C. R., Mahoney, J. C., & West, J. R. (1994). Developing rat Purkinje cells are more vulnerable to alcohol-induced depletion during differentiation than during neurogenesis. *Alcohol*, 11, 147–156.
- Marquand, A. F., Kia, S. M., Zabihi, M., Wolfers, T., Buitelaar, J. K., & Beckmann, C. F. (2019). Conceptualizing mental disorders as deviations from normative functioning. *Molecular Psychiatry*, 24, 1415–1424. <https://doi.org/10.1038/s41380-019-0441-1>
- Marquand, A. F., Wolfers, T., Mennes, M., Buitelaar, J., & Beckmann, C. F. (2016). Beyond lumping and splitting: A review of computational approaches for stratifying psychiatric disorders. *Biological Psychiatry Cognitive Neuroscience Neuroimaging*, 1, 433–447. <https://doi.org/10.1016/j.bpsc.2016.04.002>
- May, P. A., Blankenship, J., Marais, A.-S., Gossage, J. P., Kalberg, W. O., Joubert, B., Cloete, M., Barnard, R., de Vries, M., Hasken, J., Robinson, L. K., Adnams, C. M., Buckley, D., Manning, M., Parry, C. D. H., Hoyme, H. E., Tabachnick, B., & Seedat, S. (2013). Maternal alcohol consumption producing fetal alcohol spectrum disorders (FASD): Quantity, frequency, and timing of drinking. *Drug and Alcohol Dependence*, 133, 502–512. <https://doi.org/10.1016/j.drugalcdep.2013.07.013>
- Mosteller, F. (1968). *Data analysis, including statistics*. Handb. Soc.
- Nardelli, A., Lebel, C., Rasmussen, C., Andrew, G., & Beaulieu, C. (2011). Extensive deep gray matter volume reductions in children and adolescents with fetal alcohol spectrum disorders: Reduced deep gray matter volume in FASD. *Alcohol: Clinical & Experimental Research*, 35, 1404–1417. <https://doi.org/10.1111/j.1530-0277.2011.01476.x>
- Nirgudkar, P., Taylor, D. H., Yanagawa, Y., & Valenzuela, C. F. (2016). Ethanol exposure during development reduces GABAergic/Glycinergic neuron numbers and lobule volumes in the mouse cerebellar vermis. *Neuroscience Letters*, 632, 86–91. <https://doi.org/10.1016/j.neulet.2016.08.039>
- O'Hare, E. D., Kan, E., Yoshii, J., Mattson, S. N., Riley, E. P., Thompson, P. M., Toga, A. W., & Sowell, E. R. (2005). Mapping cerebellar vermal morphology and cognitive correlates in prenatal alcohol exposure. *Neuroreport*, 16, 1285–1290. <https://doi.org/10.1097/01.wnr.0000176515.11723.a2>
- Rajaprakash, M., Chakravarty, M. M., Lerch, J. P., & Rovet, J. (2014). Cortical morphology in children with alcohol-related neurodevelopmental disorder. *Brain and Behavior: A Cognitive Neuroscience Perspective*, 4, 41–50. <https://doi.org/10.1002/brb3.191>
- Roebuck, T. M., Mattson, S. N., & Riley, E. P. (1998). A review of the neuroanatomical findings in children with fetal alcohol syndrome or prenatal exposure to alcohol. *Alcoholism, Clinical and Experimental Research*, 22, 339–344. <https://doi.org/10.1111/j.1530-0277.1998.tb03658.x>
- Rollins, J., Collins, J. S., & Holden, K. (2010). United States head circumference growth reference charts: Birth to 21 years. *The Journal of Pediatrics*, 156, 907–913.e2. <https://doi.org/10.1016/j.jpeds.2010.01.009>
- Romero, J. E., Coupé, P., Giraud, R., Ta, V.-T., Fonov, V., Park, M. T. M., Chakravarty, M. M., Voineskos, A. N., & Manjón, J. V. (2017). CERES: A new cerebellum lobule segmentation method. *NeuroImage*, 147, 916–924. <https://doi.org/10.1016/j.neuroimage.2016.11.003>
- Sawant, O. B., Lunde, E. R., Washburn, S. E., Chen, W.-J. A., Goodlett, C. R., & Cudd, T. A. (2013). Different patterns of regional Purkinje cell loss in the cerebellar vermis as a function of the timing of prenatal ethanol exposure in an ovine model. *Neurotoxicology and Teratology*, 35, 7–13. <https://doi.org/10.1016/j.ntt.2012.11.001>
- Schmahman, J. D., & Sherman, J. C. (1998). 1998. The cerebellar cognitive affective syndrome. *Brain: A Journal of Neurology*, 121, 561–579.
- Schmahmann, J. D. (2010). The role of the cerebellum in cognition and emotion: Personal reflections since 1982 on the dysmetria of thought hypothesis, and its historical evolution from theory to therapy. *Neuropsychology Review*, 20, 236–260. <https://doi.org/10.1007/s11065-010-9142-x>

- Schmahmann, J. D. (2019). The cerebellum and cognition. *Neuroscience Letters*, 688, 62–75. <https://doi.org/10.1016/j.neulet.2018.07.005>
- Schmahmann, J. D., Doyon, J., McDonald, D., Holmes, C., Lavoie, K., Hurwitz, A. S., Kabani, N., Toga, A., Evans, A., & Petrides, M. (1999). Three-dimensional MRI atlas of the human cerebellum in proportional stereotaxic space. *NeuroImage*, 10, 233–260. <https://doi.org/10.1006/nimg.1999.0459>
- Sowell, E. R., Jernigan, T. L., Mattson, S. N., Riley, E. P., Sobel, D. F., & Jones, K. L. (1996). Abnormal development of the cerebellar vermis in children prenatally exposed to alcohol: Size reduction in lobules I–V. *Alcoholism, Clinical and Experimental Research*, 20, 31–34. <https://doi.org/10.1111/j.1530-0277.1996.tb01039.x>
- Stoodley, C. J., & Schmahmann, J. D. (2009). Functional topography in the human cerebellum: A meta-analysis of neuroimaging studies. *NeuroImage*, 44, 489–501. <https://doi.org/10.1016/j.neuroimage.2008.08.039>
- Sullivan, E. V., Moore, E. M., Lane, B., Pohl, K. M., Riley, E. P., & Pfefferbaum, A. (2020). Graded cerebellar lobular volume deficits in adolescents and young adults with fetal alcohol Spectrum disorders (FASD). *Cerebral Cortex*, 30, 4729–4746. <https://doi.org/10.1093/cercor/bhaa020>
- Sullivan, E. V., Zahr, N. M., Saranathan, M., Pohl, K. M., & Pfefferbaum, A. (2019). Convergence of three parcellation approaches demonstrating cerebellar lobule volume deficits in alcohol use disorder. *NeuroImage Clinical*, 24, 101974. <https://doi.org/10.1016/j.nicl.2019.101974>
- Takao, H., Hayashi, N., & Ohtomo, K. (2011). Effect of scanner in longitudinal studies of brain volume changes. *Journal of Magnetic Resonance Imaging*, 34, 438–444. <https://doi.org/10.1002/jmri.22636>
- Toro, R., Chupin, M., Garnero, L., Leonard, G., Perron, M., Pike, B., Pitiot, A., Richer, L., Veillette, S., Pausova, Z., & Paus, T. (2009). Brain volumes and Val66Met polymorphism of the BDNF gene: Local or global effects? *Brain Structure and Function*, 213, 501–509. <https://doi.org/10.1007/s00429-009-0203-y>
- Treit, S., Jeffery, D., Beaulieu, C., & Emery, D. (2020). Radiological findings on structural magnetic resonance imaging in fetal alcohol Spectrum disorders and healthy controls. *Alcoholism, Clinical and Experimental Research*, 44, 455–462. <https://doi.org/10.1111/acer.14263>
- Treit, S., Zhou, D., Lebel, C., Rasmussen, C., Andrew, G., & Beaulieu, C. (2014). Longitudinal MRI reveals impaired cortical thinning in children and adolescents prenatally exposed to alcohol. *Human Brain Mapping*, 35, 4892–4903. <https://doi.org/10.1002/hbm.22520>
- Warling, A., McDermott, C. L., Liu, S., Seidlitz, J., Rodrigue, A. L., Nadig, A., Gur, R. C., Gur, R. E., Roalf, D., Moore, T. M., Glahn, D., Satterthwaite, T. D., Bullmore, E. T., & Raznahan, A. (2021). Regional white matter scaling in the human brain. *The Journal of Neuroscience*, 41, 7015–7028. <https://doi.org/10.1523/jneurosci.1193-21.2021>
- Zhou, D., Rasmussen, C., Pei, J., Andrew, G., Reynolds, J. N., & Beaulieu, C. (2018). Preserved cortical asymmetry despite thinner cortex in children and adolescents with prenatal alcohol exposure and associated conditions. *Human Brain Mapping*, 39, 72–88. <https://doi.org/10.1002/hbm.23818>

SUPPORTING INFORMATION

Additional supporting information can be found online in the Supporting Information section at the end of this article.

How to cite this article: Fraize, J., Fischer, C., Elmaleh-Bergès, M., Kerdreux, E., Beggiano, A., Ntorkou, A., Duchesnay, E., Bekha, D., Boespflug-Tanguy, O., Delorme, R., Hertz-Pannier, L., & Germanaud, D. (2023). Enhancing fetal alcohol spectrum disorders diagnosis with a classifier based on the intracerebellar gradient of volumetric undersizing. *Human Brain Mapping*, 1–16. <https://doi.org/10.1002/hbm.26348>

MATÉRIELS SUPPLÉMENTAIRES

Table S1. Characteristics of the control population, in the 3 sites of acquisitions (NS, SHFJ, RD). SD: standard deviation.

Site	RD	SHFJ	NS	Total	p-value
Field	1.5T	1.5T	3T		
n	40	31	55	126	
Sex: male n (%)	18 (45.0)	17 (54.8)	29 (52.7)	50.8	0.663
Age at MRI, mean in years (SD)	12.69 (4.06)	11.72 (2.83)	11.84 (2.83)	12.07 (3.27)	0.360

Figure S1. Flow charts of FASD and control groups.

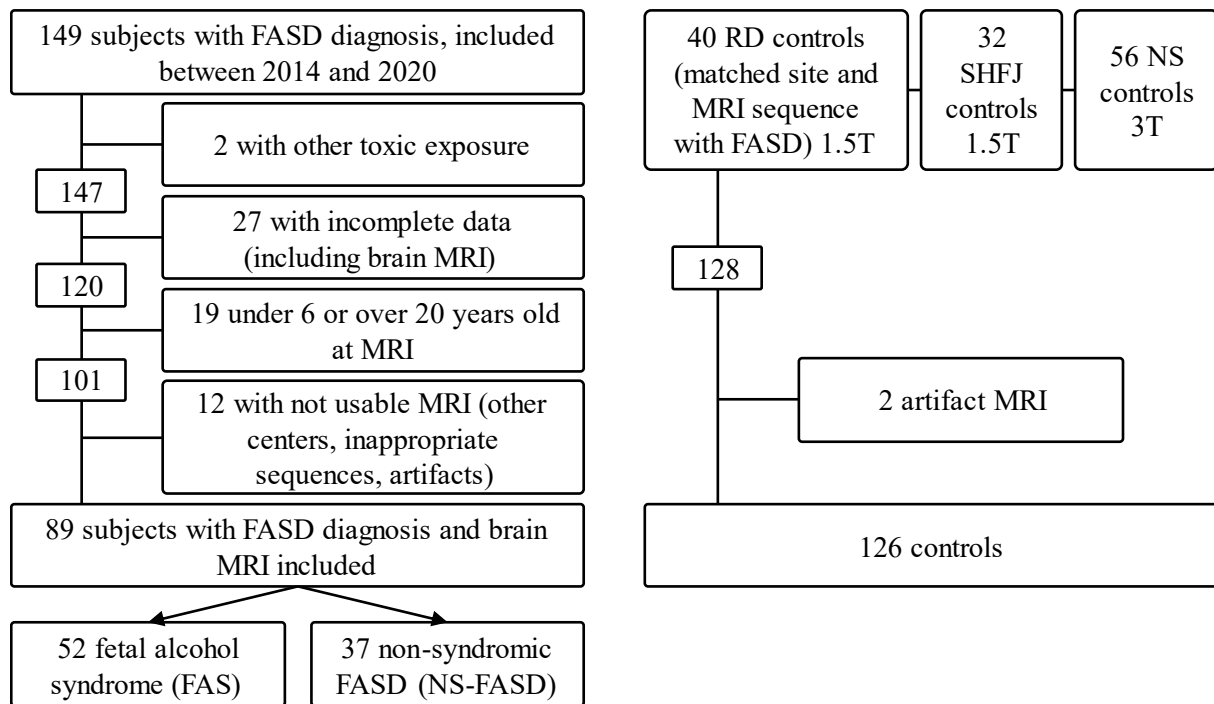
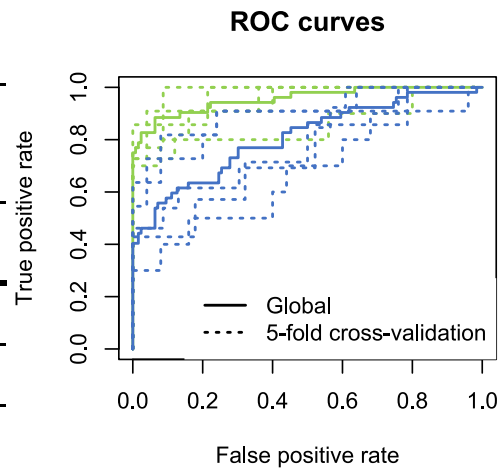


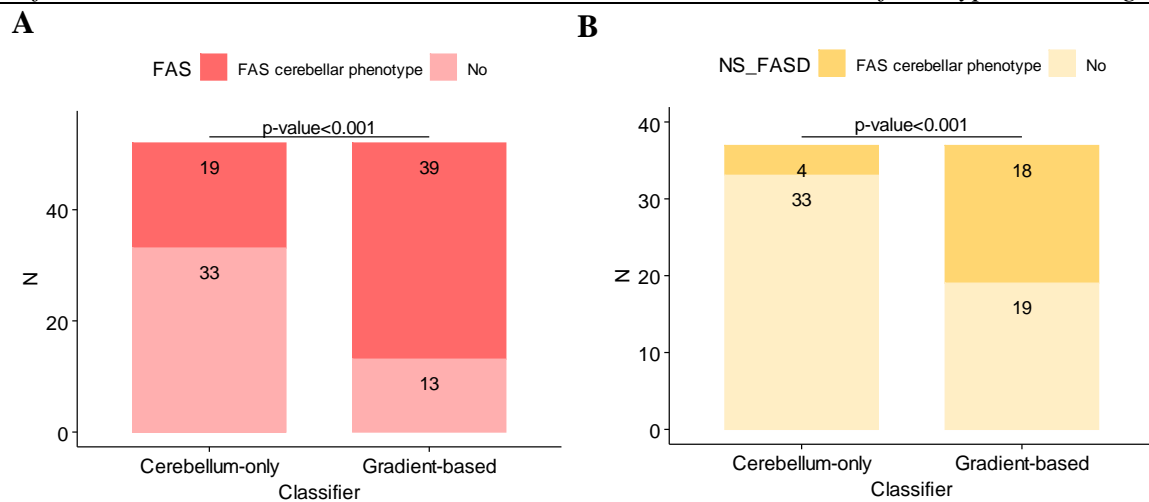
Figure S2. Summary of the main results of the post hoc study on the raw unadjusted data.

	$\sqrt{\text{DTS}}$ (%)	IC95%	p-value	Deviation from typical scaling ($\sqrt{\text{DTS}}$) of cerebellar volume and sub-volumes, in FAS subjects, with the 95% confidence interval estimated by bootstrap resampling. Comparison of the FAS and controls $\sqrt{\text{DTS}}$ by embedded bootstrap resampling. All p-values are adjusted to achieve a FDR = 5%, in bold p-values <5%.
Cerebellum	-10.8	[-13.5 ; -8.1]	<0.001	
Anterior hemispheres	-12.4	[-15.9 ; -8.9]	<0.001	
Posterior hemispheres	2.9	[1.7 ; 4.0]	0.008	
Inferior hemispheres	3.4	[1.5 ; 5.3]	0.629	
Vermis	-14.3	[-17.1 ; -11.4]	<0.001	
Anterior vermis	-18.5	[-22.4 ; -14.5]	<0.001	
Posterior vermis	-12.2	[-15.5 ; -8.9]	<0.001	
Inferior vermis	-8.4	[-11.3 ; -5.6]	<0.001	

	Gradient-based classifier	Cerebellum-only classifier
AIC	88.0	162.7
BIC	113.5	169.0
p-value	<0.001	
AUC_{global}	96%	81%
p-value	<0.001	
5-fold cross-validation		
AUC_{cv}	94% +/- 4.9	80% +/- 8.7
<i>With a probability threshold=0.7</i>		
Specificity	97% +/- 3.9	100% +/- 0.0
Accuracy	90% +/- 3.1	61% +/- 3.2



Comparison of FAS vs. control classifiers using either the cerebellar ν DTS only (blue) or adding the 6 intracerebellar ν DTS (green). Left: AIC, BIC and p-value of the Wald test. AUC and p-value of comparison with the DeLong method. Right: ROC curves of each classifier in all samples (solid line) and in the 5-fold cross-validation samples (dotted line), mean of the performance indices of the 5-fold cross-validation with the standard deviation. *ROC: receiver operating characteristic; AIC: Akaike information criterion; BIC Bayesian information criterion; AUC: area under the curve; ν DTS: deviation from typical scaling.*



Proportion of FAS (A) and NS-FASD (B) classified as FAS cerebellar phenotype with the cerebellum-only classifier (left, dark color) and gradient-based classifier (right, dark color), with the classification threshold of 0.7 corresponding to a 95% diagnostic specificity.

Note that the 12 of the 13 subjects identified in the main analysis (Figure 6) with the adjusted volumes are included in the 18, the latter having a probability very close to the probability threshold (0.7).

COMPLÉMENT DE DISCUSSION

Dans cette étude, nous avons fait la preuve de l'existence d'un gradient de gravité antéro-inféro-postérieur de l'atteinte cérébelleuse des TSAF qui pourrait être utile au diagnostic notamment des formes non syndromiques.

L'ensemble des points qui nous semblait nécessaire de discuter apparaissent dans l'article tel que publié.

La dernière étape permettant la translation à la clinique est un dernier point plus pragmatique que vaut la peine d'être discuté. L'application concrète des outils de mesure, complexe à mettre en œuvre, pourrait limiter la portée clinique de nos résultats. En effet, dans cette étude, nous avons combiné deux méthodes de segmentation cérébelleuse pour obtenir les volumes d'intérêt, notamment les sous-parties du vermis, limitant l'implémentation radio-clinique directe. Depuis la sortie de la deuxième version de *volBrain*, *vol2brain* (Manjón et al., 2022), la segmentation du vermis en trois parties est incluse, et avec CERES, tous les volumes cérébelleux sont accessibles en quelques clics, si aucune correction manuelle n'est nécessaire. Étant donné l'existence de grandes bases de données d'IRM pédiatrique, qui permettraient d'établir des courbes de *scaling* robustes, l'implémentation en clinique de la démarche que nous proposons semble être un futur envisageable.

CHAPITRE 5

ÉTUDE EN IMAGERIE COMPUTATIONNELLE DE L'ATTEINTE DU CORPS CALLEUX

INTRODUCTION COMMUNE

Nous avons étudié la morphologie du corps calleux grâce à deux méthodes apportant des informations complémentaires sur l'atteinte calleuse dans les TSAF.

Dans la première partie, la méthode de parcellisation du corps calleux basée sur la parcellisation corticale et la connectivité en diffusion a été élaborée, appliquée et finalisée par Gabrielle Convert et Yann Leprince, ingénieurs de recherche dans l'équipe InDEV. J'ai colligé, analysé, interprété les données issues de cette méthode et rédigé l'article issu de ce travail. La deuxième partie est le fruit d'une collaboration avec Julien Lefèvre, chercheur à l'Université d'Aix-Marseille. Il a conçu et finalisé la méthode de mesure entièrement automatisée de l'épaisseur calleuse. Il a rédigé un article de conférence pour présenter les apports théoriques associés à l'élaboration de cette méthode (**Contributions non incluses**). J'ai aidé à l'amélioration de certains points de cette technique. J'ai appliqué les traitements à l'ensemble de la cohorte, analysé les données en proposant des méthodes statistiques adaptées et interprété les résultats finaux. J'ai rédigé l'article qui est en cours de soumission.

CARTOGRAPHIE DE LA RÉDUCTION DE LA SURFACE DU CORPS CALLEUX DANS LES TROUBLES DU SPECTRE DE L'ALCOOLISATION FŒTALE À L'AIDE DES SILLONS ET D'UNE PARCELLISATION BASÉE SUR LA CONNECTIVITÉ

Fraize, J., Convert, G., Leprince, Y., Sylvestre-Marconville, F., Kerdreux, E., Auzias, G., Lefèvre, J., Delorme, R., Elmaleh-Bergès, M., Hertz-Pannier, L., & Germanaud, D. (2023). Mapping corpus callosum surface reduction in fetal alcohol spectrum disorders with sulci and connectivity-based parcellation. *Frontiers in Neuroscience*, 17. <https://doi.org/10.3389/fnins.2023.1188367>

RÉSUMÉ

Introduction

Les troubles du spectre de l'alcoolisation fœtale (TSAF) vont du syndrome d'alcoolisation fœtale (SAF) aux formes non spécifiques non syndromiques (TSAF-NS) qui sont encore sous-diagnostiquées et pourraient bénéficier de nouveaux marqueurs neuroanatomiques. La principale manifestation neuroanatomique de la toxicité développementale de l'exposition prénatale à l'alcool est la réduction de la taille du cerveau. Les observations répétées en imagerie ont longtemps attiré l'attention sur le corps calleux (CC), sans pour autant être toutes convergentes. Notre étude propose une nouvelle segmentation du CC qui repose à la fois sur une segmentation corticale basée sur les sillons et sur l'organisation « hémisphérotopique » des fibres transcalleuses.

Matériels et méthodes

Nous avons recueilli une série monocentrique de 37 sujets atteints de SAF, 28 sujets atteints de TSAF-NS et 38 sujets au développement typique (de 6 à 25 ans) ayant eu une IRM cérébrale (1,5T). En associant l'imagerie pondérée en T1 et en diffusion, nous avons projeté une segmentation corticale des hémisphères basée sur les sillons sur la coupe sagittale médiane du CC, produisant sept parcelles homologues antéro-postérieures (frontopolaire, préfrontale antérieure et postérieure, précentrale, postcentrale, pariétale et occipitale). Nous avons mesuré l'effet du TSAF sur la surface des parcelles calleuses et corticales en considérant l'âge, le sexe et la taille du cerveau comme des covariables. La proportion de surface de la parcelle corticale correspondante sur la surface corticale totale a été introduite comme covariable supplémentaire. Nous avons effectué une analyse normative pour identifier les sujets ayant une parcelle anormalement petite.

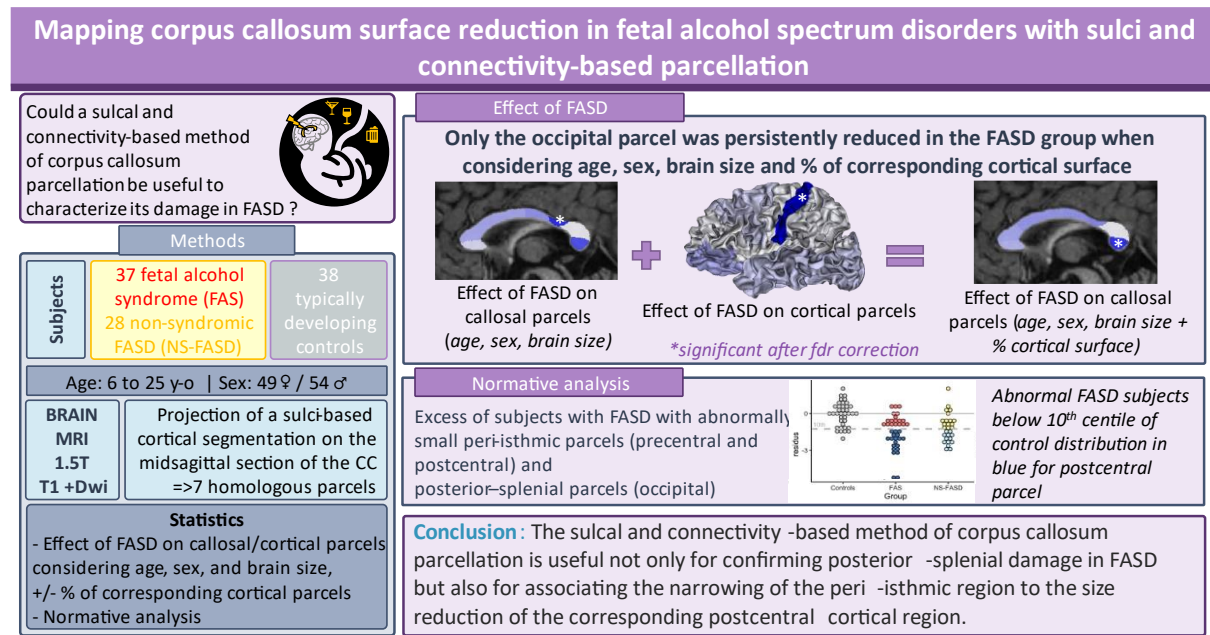
Résultats

Toutes les parcelles du CC et corticales étaient plus petites dans le groupe TSAF que chez les contrôles. En tenant compte de l'âge, du sexe et de la taille du cerveau (surface corticale totale), seul la parcelle du CC postcentrale ($R^2 = 6,5 \%$, $p_{FDR} = 0,032$) et le pourcentage de la parcelle corticale postcentrale ($R^2 = 8,9 \%$, $p_{FDR} = 0,007$) étaient encore plus petits. En ajoutant au modèle la proportion de surface corticale correspondante, seule la parcelle occipitale était réduite de façon persistante dans le groupe TSAF ($R^2 = 5,7 \%$, $p_{FDR} = 0,014$). Dans l'analyse normative, nous avons trouvé un excès de sujets atteints de TSAF avec des parcelles pré et postcentrales (péri-isthmiques) et spléniales postérieures anormalement petites ($p_{FDR} < 0,05$).

Conclusion

La méthode objective de parcellisation du CC basée sur les sillons et la connectivité s'est avérée utile, non seulement, pour confirmer les anomalies spléniales postérieures dans le TSAF, mais aussi le rétrécissement de la région péri-isthmique fortement associé à une réduction spécifique de la taille de la région corticale postcentrale correspondante (gyrus postcentral). L'analyse normative a montré que ce type de segmentation du CC pouvait fournir un endophénotype neuroanatomique cliniquement pertinent, même chez les personnes ayant une forme non syndromique de TSAF.

RÉSUMÉ GRAPHIQUE



frontiers in Neuroscience, Neurodevelopment Section. J. Fraize, G. Convert, YLeprince, et al. (2023) doi: 10.3389/fnins.2023.1188367



OPEN ACCESS

EDITED BY

Kirsten A. Donald,
University of Cape Town, South Africa

REVIEWED BY

Anish Kumar Simhal,
Memorial Sloan Kettering Cancer Center,
United States

Lijia Zhang,
Duke University, United States

*CORRESPONDENCE

Justine Fraize

✉ justine.fraize@inserm.fr

David Germanaud

✉ david.germanaud@cea.fr

†These authors have contributed equally to this work

RECEIVED 17 March 2023

ACCEPTED 17 May 2023

PUBLISHED 09 June 2023

CITATION

Fraize J, Convert G, Leprince Y,
Sylvestre-Marconville F, Kerdreux E, Auzias G,
Lefèvre J, Delorme R, Elmaleh-Bergès M,
Hertz-Pannier L and Germanaud D (2023)
Mapping corpus callosum surface reduction in
fetal alcohol spectrum disorders with sulci and
connectivity-based parcellation.
Front. Neurosci. 17:1188367.
doi: 10.3389/fnins.2023.1188367

COPYRIGHT

© 2023 Fraize, Convert, Leprince,
Sylvestre-Marconville, Kerdreux, Auzias,
Lefèvre, Delorme, Elmaleh-Bergès,
Hertz-Pannier and Germanaud. This is an
open-access article distributed under the terms
of the [Creative Commons Attribution License
\(CC BY\)](https://creativecommons.org/licenses/by/4.0/). The use, distribution or reproduction
in other forums is permitted, provided the
original author(s) and the copyright owner(s)
are credited and that the original publication in
this journal is cited, in accordance with
accepted academic practice. No use,
distribution or reproduction is permitted which
does not comply with these terms.

Mapping corpus callosum surface reduction in fetal alcohol spectrum disorders with sulci and connectivity-based parcellation

Justine Fraize^{1,2*†}, Gabrielle Convert^{1,2†}, Yann Leprince¹,
Florent Sylvestre-Marconville^{1,2}, Eliot Kerdreux^{1,2},
Guillaume Auzias³, Julien Lefèvre³, Richard Delorme⁴,
Monique Elmaleh-Bergès⁵, Lucie Hertz-Pannier^{1,2} and
David Germanaud^{1,2,6*}

¹UNIACT, NeuroSpin, Frederic Joliot Institute, Centre d'études de Saclay, CEA Paris-Saclay, Gif-sur-Yvette, France, ²InDEV, NeuroDiderot, Inserm, Université Paris Cité, Paris, France, ³Institut de Neurosciences de La Timone, CNRS, Aix-Marseille Université, Marseille, France, ⁴Department of Child and Adolescent Psychiatry, Robert-Debré Hospital, AP-HP, Centre of Excellence InovAND, Paris, France, ⁵Department of Pediatric Radiologic, Robert-Debré Hospital, AP-HP, Centre of Excellence InovAND, Paris, France, ⁶Department of Genetics, Robert-Debré Hospital, AP-HP, Centre de Référence Déficiences Intellectuelles de Causes Rares, Centre of Excellence InovAND, Paris, France

Introduction: Fetal alcohol spectrum disorders (FASD) range from fetal alcohol syndrome (FAS) to non-syndromic non-specific forms (NS-FASD) that are still underdiagnosed and could benefit from new neuroanatomical markers. The main neuroanatomical manifestation of prenatal alcohol exposure on developmental toxicity is the reduction in brain size, but repeated imaging observations have long driven the attention on the corpus callosum (CC), without being all convergent. Our study proposed a new segmentation of the CC that relies on both a sulci-based cortical segmentation and the “hemispherotopic” organization of the transcallosal fibers.

Methods: We collected a monocentric series of 37 subjects with FAS, 28 with NS-FASD, and 38 with typical development (6 to 25 years old) using brain MRI (1.5T). Associating T1- and diffusion-weighted imaging, we projected a sulci-based cortical segmentation of the hemispheres on the midsagittal section of the CC, resulting in seven homologous anterior–posterior parcels (frontopolar, anterior and posterior prefrontal, precentral, postcentral, parietal, and occipital). We measured the effect of FASD on the area of callosal and cortical parcels by considering age, sex, and brain size as linear covariates. The surface proportion of the corresponding cortical parcel was introduced as an additional covariate. We performed a normative analysis to identify subjects with an abnormally small parcel.

Results: All callosal and cortical parcels were smaller in the FASD group compared with controls. When accounting for age, sex, and brain size, only the postcentral ($\eta^2 = 6.5\%$, $p_{FDR} = 0.032$) callosal parcel and % of the cortical parcel ($\eta^2 = 8.9\%$, $p_{FDR} = 0.007$) were still smaller. Adding the surface proportion (%) of the corresponding cortical parcel to the model, only the occipital parcel was persistently reduced in the FASD group ($\eta^2 = 5.7\%$, $p_{FDR} = 0.014$). In the normative analysis, we found an excess of subjects with FASD with abnormally small precentral and postcentral (peri-isthmic) and posterior–splenial parcels ($p_{FDR} < 0.05$).

Conclusion: The objective sulcal and connectivity-based method of CC parcellation proved to be useful not only in confirming posterior–splenial

damage in FASD but also in the narrowing of the peri-isthmic region strongly associated with a specific size reduction in the corresponding postcentral cortical region (postcentral gyrus). The normative analysis showed that this type of callosal segmentation could provide a clinically relevant neuroanatomical endophenotype, even in NS-FASD.

KEYWORDS

fetal alcohol spectrum disorder (FASD), corpus callosum, segmentation, cortical sulci, connectivity, microcephaly

1. Introduction

The pathological consequences of prenatal alcohol exposure (PAE) are grouped under the diagnosis of fetal alcohol spectrum disorders (FASD) that range from fetal alcohol syndrome (FAS) to non-syndromic, non-specific forms (NS-FASD) (Astley, 2004; Cook et al., 2016; Hoyme et al., 2016). The positive diagnosis of FAS is based on a consensual set of clinical features, including facial dysmorphism, growth retardation, and microcephaly, while the positive diagnosis of NS-FASD remains probabilistic. One of the main targets of the teratogenic effects of ethanol is the brain; subjects with FASD tend to have not only a smaller brain but also recurrent focal brain abnormalities detectable with magnetic resonance imaging (MRI). However, no specific neuroanatomical criterion has been added to the diagnostic guidelines.

One of the more frequently reported of these focal brain abnormalities occurs in the corpus callosum (CC) (for reviews, see: Lebel et al., 2011; Donald et al., 2015; Nguyen et al., 2017; Moore and Xia, 2021). In Astley et al.'s cohort of 65 children with FASD (6 to 16 years old), two had hypoplasia or agenesis of the CC (Astley et al., 2009). Autti-Rämö et al. described two adolescents of approximately 14 years among the 17 adolescents who were prenatally exposed to alcohol with anomalies of the CC (one thinning and one hypoplasia) (Autti-Rämö et al., 2002). Similarly, Boronat et al. (2017) listed among the 62 subjects aged between 4 and 18 years old with FASD, 24 with hypoplasia of the CC, and two with partial agenesis. Recently, Treit et al. (2020) described five subjects with dysmorphic CC, associated with the asymmetry of the lateral ventricles among 124 subjects with FASD from school age to adulthood. In a previous radiological-clinical study, we reported two cases of partial agenesis of the CC over 89 subjects with FASD from school age to early adulthood and described, with manual measurements and normative scaling analysis, an isthmus narrowing as a recurrent abnormality in both FAS and non-syndromic FASD (Fraize et al., 2022). In addition to these radiological descriptions, computational neuroimaging has searched for more subtle anomalies or more

objective morphometric descriptions. Several studies of the CC in the FASD population recommended a reduction in the midsagittal CC area (Riley et al., 1995; Sowell et al., 2001; Astley et al., 2009; Dodge et al., 2009), thickness (Yang et al., 2012), volume (Gautam et al., 2014; Biffen et al., 2020; Inkelis et al., 2020), or shape with a flattened or misshapen appearance (Sowell et al., 2001; Bookstein et al., 2002) that could be correlated to the amount of prenatal alcohol consumption (Biffen et al., 2017; Jacobson et al., 2017). Within the callosal structure itself, it appears that the size reduction affected the posterior region more severely, notably the isthmus and the splenium size (Sowell et al., 2001; Dodge et al., 2009; Fraize et al., 2022) or position (Sowell et al., 2001; Bookstein et al., 2002). Note that while several studies of the last 20 years, mostly in children and young adults, tend to converge toward a global reduction in the size of the CC, affecting its posterior part in particular, this result has proved difficult to fully or systematically replicate, even within large cohorts (Sowell et al., 2001; Yang et al., 2012; Marshall et al., 2022).

The CC is a large white matter fiber bundle consisting of axonal projections between homologous cortical regions and crossing the interhemispheric plane as a compact well-individualized midsagittal structure. Midsagittal CC fibers mainly have a “hemispherotopic” organization and two adjacent CC fibers corresponding to two adjacent points on the hemisphere (Pandya et al., 1971; Friedrich et al., 2020), and the frontal connectivity is largely overrepresented, accounting for the anterior two-third of the structure (Park et al., 2008; Chao et al., 2009; Wang et al., 2020). At first approximation, the midsagittal section of the CC is often proposed as a proxy for the much larger and more complex 3D whole CC bundle. It can be divided into several regions to be compared across subjects in terms of area, length, or thickness. These divisions are commonly determined by neuroradiologists based on the arbitrary geometrical processes deemed to guarantee homology between subjects (Witelson, 1989; Hofer and Frahm, 2006). Relying only on the midsagittal anatomy or geometry, such approaches are not related to the actual anatomical connectivity. In fact, they may be not only irrelevant in the case of the pathological shortening (partial agenesis of the CC) that occurs in FASD but also insensitive to the interindividual variations of relative cortical representation in the midsagittal section. Even if the results are still ambiguous concerning FASD-associated regional anomalies of hemispheric volume (Archibald et al., 2001; Astley et al., 2009), cortical thickness (Sowell et al., 2008; Zhou et al., 2011; Yang et al., 2012; Treit et al., 2014; Marshall et al., 2022), or

Abbreviations: PAE, prenatal alcohol exposure; FASD, fetal alcohol spectrum disorders; FAS, fetal alcohol syndrome; NS-FASD, non-syndromic fetal alcohol spectrum disorders; MRI, magnetic resonance imaging; CC, corpus callosum; CxPS, cortical parcel surface area; TCxS, total cortical surface area; CcPS, callosal parcel surface area.

extension (Rajaprakash et al., 2014; Hendrickson et al., 2018), any midsagittal anomaly of the CC should raise questions about either cortical or white matter damage (Gautam et al., 2014; Fan et al., 2016; Ghazi Sherbaf et al., 2019; Kar et al., 2022), prompting a conjoint analysis of both cortical and callosal anatomy. Hence, it appears important to introduce and use parcellation of the CC into as many parcels as relevant in the regions defined on the cortical surface anatomy and projected on the midsagittal section through the real hemispherotopic callosal–cortical connectivity. A few implementations have been proposed during the past 20 years (Huang et al., 2005; Styner et al., 2005; Chao et al., 2009) without resulting in a consensual use for callosal parcellation and morphometry, but they have never been applied to the study of developmental conditions, let alone FASD.

Therefore, we aimed to describe the anatomy of the midsagittal section of the CC in a large monocentric cohort of FASD and typically developing control subjects, by means of its automatic anterior–posterior parcellation into seven parcels, achieved at the individual level from T1- and diffusion-weighted images, reflecting a fan-shaped segmentation of the cortex along six major sulcal meridians. The comparison between FASD or FAS and typical callosal anatomy was performed not only by considering covariates, including the cortical extension, as a brain size proxy but also a relative representation of the reference cortical parcel to better disentangle pathological phenomena and increase sensitivity in the detection of FASD singularity. In addition to the group comparison, we completed the analysis of our models of the callosal surfaces by a normative approach to show the detectability at the individual level of likely focal callosal anomalies.

2. Material and methods

2.1. Population and MRI data

A total of 65 subjects with FASD, aged between 6 and 25 years, were included retrospectively from a clinical series of patients with neurodevelopmental disorders who were admitted to the Child Neurology Department at Robert-Debré University Hospital between 2014 and 2020. FASD diagnosis was established using the two main guidelines (Astley, 2004; Hoyme et al., 2016), and a full differential diagnosis work-up was completed, notably a systematic brain MRI. The exclusion criteria were participants who were prenatally exposed to another embryo-fetotoxic agent or who explicitly disagreed with the study participation. Finally, subjects with FASD were separated into two groups: the syndromic or FAS (including partial FAS) and the non-syndromic or NS-FASD. The clinical and radiological characteristics of the 65 subjects with FASD are detailed in Table 1. This cohort and the diagnostic procedure were already described in a previous study (Fraize et al., 2022, 2023).

A total of 38 typically developing subjects, aged between 6 and 25 years, with no report of PAE, developmental delay, or family history of the neurological or psychiatric condition (1st degree) were included for comparison (control group), as part of a research program on autism in the Department of Child and Adolescent

TABLE 1 Sociodemographic, clinical, radiological data of subjects with FASD.

	FAS	NS-FASD	<i>p</i> -value
n =	37	28	
Sociodemographic assessment			
Sex: male <i>n</i> (%)	17 (47.2)	15 (57.7)	0.578
Age at MRI, mean in years (SD)	11.17 (3.72)	13.06 (4.97)	0.098
Clinical assessment, <i>n</i> (%)			
(1) Prenatal alcohol exposure			
4. Confirmed, severe	15 (40.5)	13 (46.4)	0.825
3. Confirmed, moderate or unquantified	20 (54.1)	13 (46.4)	0.720
2. Not documented	2 (5.4)	2 (7.1)	1.000
1. No exposition	0 (0.0)	0 (0.0)	-
(2) FAS facial features			
4. Severe	22 (59.5)	2 (7.1)	<0.001
3. Moderate	15 (40.5)	0 (0.0)	<0.001
2. Mild	0 (0.0)	23 (82.1)	<0.001
1. None	0 (0.0)	3 (10.7)	0.075
(3) Growth deficiency			
4. Significant	14 (37.8)	3 (10.7)	0.020
3. Moderate	8 (21.6)	2 (7.1)	0.175
2. Mild	6 (16.2)	6 (21.4)	1.000
1. None	9 (24.3)	17 (60.7)	0.012
Brain anatomy			
(4) Structural central nervous system damage	29 (78.4)	17 (60.7)	0.097
Head circumference, smallest known			
(4) ≤ - 2 SD: microcephaly	26 (70.3)	14 (50.0)	0.086

Diagnostic criteria of the 4-Digit Diagnostic Code are numbered from (1) to (4). FAS, fetal alcohol syndrome; FASD, fetal alcohol spectrum disorder; NS-FASD, non-syndromic FASD; SD, standard deviation. In bold, *p*-values <5%.

Psychiatry of Robert-Debré University Hospital. There were no significant sex or age differences in the control groups compared with the FASD group (*p* = 0.813 and *p* = 0.479 respectively) (Table 2).

MRI data acquisition was performed in the Department of Pediatric Radiology of Robert-Debré University Hospital on the same 1.5T scanner (Ingenia, Philips Healthcare, Amsterdam, the Netherlands) including a 3D T1-weighted FFE-TFE sequence (1 mm isotropic; TR = 8.2ms; TE = 3.8ms; TI = 0.8s; Flip = 8°; SENSE = 2), a 2D diffusion-weighted SE-EPI (2.5 mm isotropic, b1,000 s/mm², 32 directions), and a field map. A visual quality check was systematically performed to exclude images of insufficient quality.

TABLE 2 Clinical characteristics of the two groups of subjects.

	Controls	FASD	<i>p</i> -value
<i>n</i>	38	65	
Sex: male <i>n</i> (%)	17 (0.45)	32 (0.49)	0.813 [†]
Age at MRI, mean in years (SD)	12.63 (4.15)	12.02 (4.37)	0.479 ^{††}

FASD, fetal alcohol spectrum disorder; SD, standard deviation. [†] *p*-value of the comparison of proportions for sex, ^{††} *p*-value of the comparison of means by Student's *t*-test.

2.2. Image processing

We combined the existing tools for sulcal-based cortical segmentation and tractography to perform an original parcellation of the midsagittal section of the CC into seven parcels along the anterior–posterior axis, achieved at the individual level in the native space without any template-based normalization process. The delineation and further inter-individual homology of the cortical and callosal parcels rely on the identification of major sulcal landmarks previously described as “sulcal meridians” (Auzias et al., 2013).

T1-weighted MRI data were processed within the *BrainVISA/Anatomist* (RRID:SCR_007354), using *Morphologist2015* (Rivière et al., 2009; Perrot et al., 2011) for tissue segmentation, inner cortical surface meshing, sulci modeling, and identification. All the MRI processing steps explained below are summed up in Figure 1.

2.2.1. Midsagittal section of the corpus callosum

The mask of the midsagittal section of the CC was obtained within the *Morphologist2015* framework after oversampling of the T1-weighted images at 0.5 mm isotropic resolution, by intersecting the white matter mask with the midsagittal plane in the Talairach space, localizing the section in the interhemispheric plane. The mask was checked systematically for any obvious segmentation error that could be manually corrected.

2.2.2. Sulcal-based parcellation of the cortical surface

The cortical parcellation was obtained individually for each subject in its own image space, with an adaptation of the *MarsAtlas* parcellation (Auzias et al., 2016), which is based on the *Hip-Hop* model (Auzias et al., 2013) of the geodesic representation of the cortex, where the CC wraps around a cingular pole and a set of well-identified major sulci are used as “meridians,” linking the cingular pole to the insular pole, and others as orthogonal “parallels.” We added the anterior (*aka* horizontal) ramus of the lateral fissure and anterior perpendicular ramus of the cingular sulcus (*aka* anterior vertical paracingulate sulcus) (Amiez et al., 2019) to the original *Hip-Hop* model to increase the constraints on the first and second sulcal meridian, respectively. The *Morphologist2015* identification and projection on the inner cortical surface of all the meridian sulci were systematically quality-checked and corrected for obvious errors by an expert (GD). Seven cortical parcels separated by the sulcal meridians were obtained by fusion of the original

MarsAtlas parcels along the parallels, schematically corresponding to the following classical lobar and sub-lobar hemispheric regions: frontopolar, anterior prefrontal, posterior prefrontal, precentral, postcentral, parietal, and occipital. The corresponding cortical parcel surface area (CxPS, cm²) was computed, as well as the total cortical surface area (TCxS, cm²). The cortical parcellation and the binary mask of the midsagittal section of the CC were realigned to the diffusion space using FSL FLIRT (Jenkinson et al., 2002).

2.2.3. Diffusion-weighted image processing and whole-brain tractography

Preprocessing of the diffusion-weighted image data was performed using tools from *FSL* (RRID:SCR_002823) (Jenkinson et al., 2012) and *MRtrix3* (RRID:SCR_006971) (Tournier et al., 2019). *FSL eddy* (Andersson and Sotiropoulos, 2016; Andersson et al., 2016) corrects for motion, eddy currents, and susceptibility distortions related to the magnetic field B₀, based on a field map acquired along with the diffusion. Fiber orientation distributions were estimated using the constrained spherical deconvolution method (Tournier et al., 2007). With the orientation distribution functions (ODF) thus obtained, the iFOD2 algorithm was used to perform probabilistic tractography (Tournier et al., 2010). We imposed biological constraints to optimize the quality of the tractograms, reducing the number of biologically aberrant “fibers” based on the segmentation of five distinct tissues of the T1-weighted image (Anatomically Constrained Tractography) (Zhang et al., 2001; Smith et al., 2012). A dynamic seeding strategy was used to generate 10⁷ streamlines (or fibers) per subject, and the *SIFT2* filter was employed to weigh streamlines according to their density (Smith et al., 2015).

2.2.4. Hemispherotopic parcellation of the midsagittal section of the CC

The entire CC bundle was automatically extracted from the whole-brain tractography using the crossing of the midsagittal section of the CC as the positive selection criterion. Any CC fiber connecting two homologous parcels from our seven sulcal-based cortical parcellations was labeled accordingly, resulting in the segmentation of the CC into seven sub-bundles corresponding to its bilateral homologous interhemispheric connectivity. A volumetric fiber density map was then computed and restricted to the midsagittal section of the CC for each of the seven CC sub-bundles. Finally, a subdivision of the midsagittal section of the CC was obtained by assigning to each of its voxels the label of the cortical parcel that sent the most fibers by majority voting on density maps. A weighting of the vote by the eight nearest neighbors (half weight for the concerned voxel, a twelfth for the neighbors) was implemented to regularize a few isolated voxels observed with simple majority voting. The final parcellation of all subjects was quality-checked visually: No aberrant segmentation was observed, and no manual correction was performed. The final metric was the callosal surface area for the total CC surface and the frontopolar, anterior prefrontal, posterior prefrontal, precentral, postcentral, parietal, and occipital callosal parcel surface (CcPS, mm²). The code used to perform the selection of the CC bundle

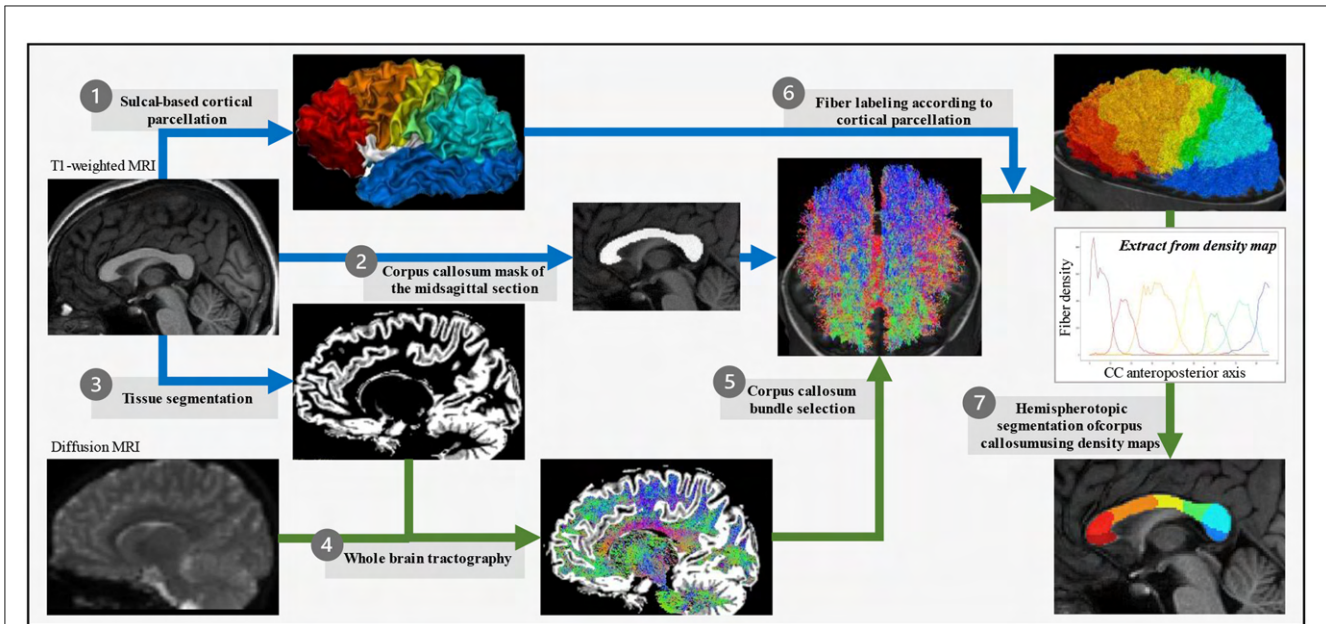


FIGURE 1 Corpus callosum parcellation pipeline. For each subject in its own image space, T1-weighted images were used to obtain the cortical surface (*Morphologist*) that was then divided into seven parcels based on the *Hip-Hop* model of geodesic representation of the cortex (adapted from *MarsAtlas*) (1), the mask of the midsagittal section of the corpus callosum (*Morphologist*) (2), and the white vs. gray matter segmentation (*FSL*) (3). Diffusion-weighted images were used to generate the whole-brain tractography (*MRtrix3*) (4) from which the corpus callosum fiber bundle was selected for passing through the midsagittal section of the corpus callosum (*MRtrix3*) (5), and then its fibers connecting two homologous parcels of the sulcal-based cortical parcellation labeled according to this bilateral homologous interhemispheric connectivity (*MRtrix3*) (6). Finally, a regularized majority vote on the labeled-fibers density map allowed to assign a cortical-based label to each voxel of the midsagittal section of the corpus callosum (7).

and the parcellation of the midsagittal section is released on <https://github.com/neurospin/CC-parcellation-from-tractography>.

2.3. Statistical analysis

Statistics were performed using R Project for Statistical Computing (RRID:SCR_001905), with a 5% alpha risk with both uncorrected (*p*-value) and corrected (*q*-value) FDR for multiple comparisons (Benjamini and Hochberg, 1995).

Group differences in clinical characteristics and callosal and cortical surface areas (CcPS and CxPS) were evaluated using two-sample *t*-tests for continuous variables and a chi-squared test for categorical variables.

To examine the surface area reduction in the callosal parcels (CcPS) in FASD subjects by comparison to typically developing controls, we performed multiple regression, including age at MRI, sex, and the TCxS as a proxy of brain size, using the following model (1):

$$CcPS = DIAG * b_{DIAG} + SEX * b_{SEX} + AGE * b_{AGE} + TCxS * b_{TCxS} + b_0 \quad (1)$$

where *b* is the unstandardized regression coefficient for each predictor.

Given the potential effect of FASD on the size of each cortical parcel surface area (CxPS), expressed in model (2) and their mechanical correlation with the corresponding callosal parcel surface area (CcPS), an additional model (3) was also tested, which included the CxPS expressed as a percentage of the total surface (%CxSP = CxPS/TCxS) as a covariate. The *p*-values and *t*-values associated with the unstandardized regression coefficients were used to assess the effect of each covariate and the eta-squared (η^2) for the effect size.

$$\%CxPS = DIAG * b_{DIAG} + SEX * b_{SEX} + AGE * b_{AGE} + TCxS * b_{TCxS} + b_0 \quad (2)$$

$$CcPS = DIAG * b_{DIAG} + SEX * b_{SEX} + AGE * b_{AGE} + TCxS * b_{TCxS} + \%CxPS * b_{\%CxPS} + b_0 \quad (3)$$

For the normative analysis at the individual level, the model of CcPS as a function of sex, age, and brain size was regressed in the control group (4). The values of the regression coefficients ($b_{AGE/control}$, $b_{SEX/control}$, $b_{TCxS/control}$) thus obtained were applied to the two FASD populations to obtain “residues” or deviations from the control model.

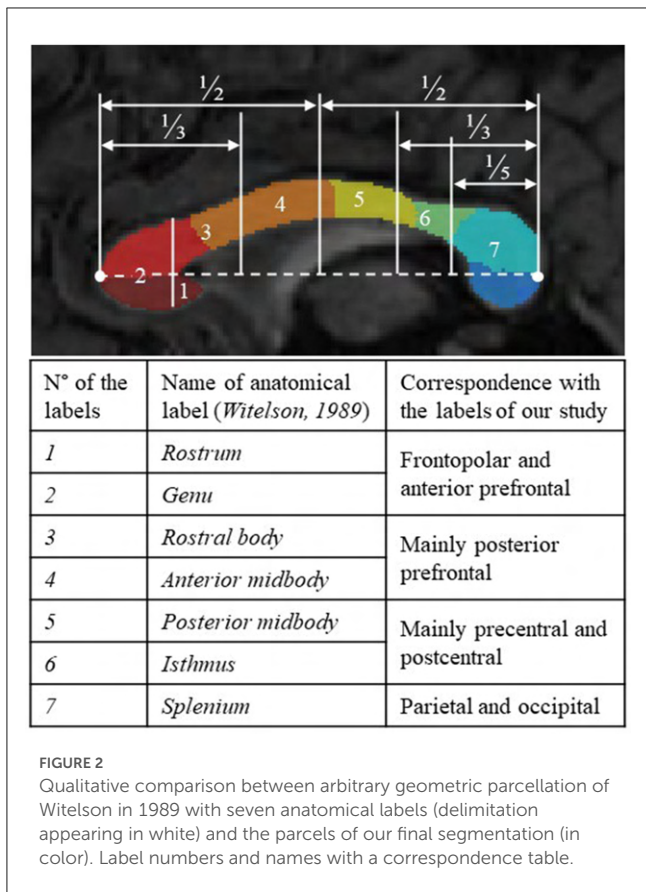


FIGURE 2 Qualitative comparison between arbitrary geometric parcellation of Witelson in 1989 with seven anatomical labels (delimitation appearing in white) and the parcels of our final segmentation (in color). Label numbers and names with a correspondence table.

$$CcPS [control] = SEX * b_{SEX/control} + AGE * b_{AGE/control} + TCxS * b_{TCxS/control} + b_0 \quad (4)$$

Finally, the numbers of subjects with FASD below the 10th percentile of the control distribution, a threshold deemed of clinical relevance for potential anomaly detection, were tagged and counted and compared to the number of controls (Fisher’s exact test).

3. Results

3.1. Anatomical analysis of CC parcellation

For all the FASD and control subjects, the parcellation process resulted in one-piece parcels which were comparable in size (from ~10% to 25% of the total callosal surface), with clear-cut radial boundaries, regularly sampling the whole midsagittal section of the CC along its anterior–posterior axis. The parcellation was not similar but consistent with more classical geometric segmentations (Witelson, 1989), highlighting the large representation of frontal and pericentral projections (Figure 2). It was also successfully applied to the cases of partial agenesis, with the process being robust to the reductional abnormalities, showing which parcels still occupy the residual CC (Figures 3C–H).

3.2. Group comparison

3.2.1. FASD vs. controls

Mean callosal and cortical parcel surface areas were all significantly different between FASD and control groups (q -value < 0.05) (Figure 4).

When age, sex, and brain size (TCxS) covariates were included in the analysis of callosal surfaces (model 1), a negative effect of FASD was found on the total CC surface, the precentral, postcentral, and occipital CcPS areas ($\eta^2 = 2.7, 2.3, 6.5,$ and 4.1% , respectively), that remained significant after FDR correction only for the postcentral one (q -value = 0.032). With the same covariates (model 2), a strong negative effect of FASD was found on the postcentral %CxPS ($\eta^2 = 8.9\%$, q -value = 0.007). Adding the corresponding %CxPS to the analysis of each CcPS (model 3), a negative effect of FASD was observed on the anterior and posterior prefrontal, the precentral and postcentral CcPS areas, increasing from $\eta^2 = 1.9$ to 2.6% , but not remaining after FDR correction and a stronger negative effect on the occipital CcPS area ($\eta^2 = 5.7\%$, q -value = 0.014) (Figure 5, Table 3). Note that no effect at all was observed in the frontopolar and parietal callosal or cortical parcels.

3.2.2. FAS vs. controls

In the FAS group, the effect of the FAS diagnosis was also found only on the postcentral CcPS area using (model 1) ($\eta^2 = 12.8\%$, q -value = 0.008). A strong negative effect of FAS was observed on the postcentral CxPS area ($\eta^2 = 20.4\%$, q -value < 0.001). In model 3, the effect of FAS on CcPS followed the same prefrontal to postcentral gradient (from $\eta^2 = 3.3\%$ to 4.2%) and affected the occipital CcPS ($\eta^2 = 4.9\%$, $p = 0.014$, q -value = 0.059) but did not remain significant after FDR correction (Figure 5, Table 4).

3.3. Normative analysis

This last step aimed at identifying subjects with one or other of the parcels abnormally small (10th centile threshold) considering the distribution in controls. The distribution of the “residues” from model 4 fitted in controls (age, sex, and brain size as covariates) is presented in Figure 6, in each group (controls, FAS, and NS-FASD) for each parcel, identifying the subjects below the 10th percentile and comparing their proportion between patients and controls.

Subjects with FAS were significantly in excess below the 10th percentile, for total CC surface ($n = 11$, $q = 0.006$), precentral CcSP ($n = 10$, $q = 0.025$), postcentral CcSP ($n = 19$, $q = 0.004$), and occipital CcSP ($n = 12$, $q = 0.008$) (Figure 6). The two subjects with FAS showing radiologically evident callosal agenesis, whose corresponding CcSP areas were equal to zero, were counted (Figures 3C, D). In a *post hoc* analysis excluding these two subjects, these results persisted except for the precentral CcSP ($q > 0.05$). Subjects with NS-FASD were significantly in excess below the 10th percentile, for total CC surface ($n = 9$, $q = 0.005$), anterior prefrontal CcSP ($n = 10$, $q = 0.028$), precentral CcSP ($n = 11$, $q = 0.005$), postcentral CcSP ($n = 13$, $q = 0.009$), and occipital CcSP ($n = 10$, $q = 0.007$).

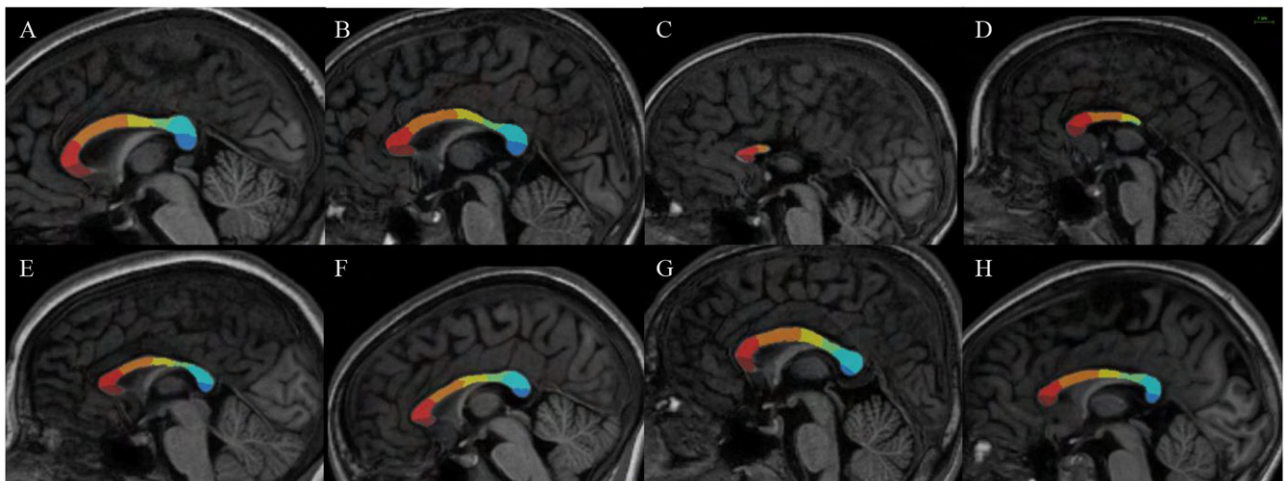


FIGURE 3 Results of our new segmentation pipeline of the corpus callosum in selected subjects, with the seven parcels (antero-posterior): frontopolar (dark red), anterior prefrontal (red), posterior prefrontal (orange), precentral (yellow) postcentral (green), parietal (light blue), occipital (dark blue). **(A, B)** Parcellation on control subjects. **(C, D)** Subjects with FAS with partial agenesis of the corpus callosum. **(E)** Subject with FAS. **(F–H)** Subjects with NS-FASD. The scale common to all images appears at the top right.

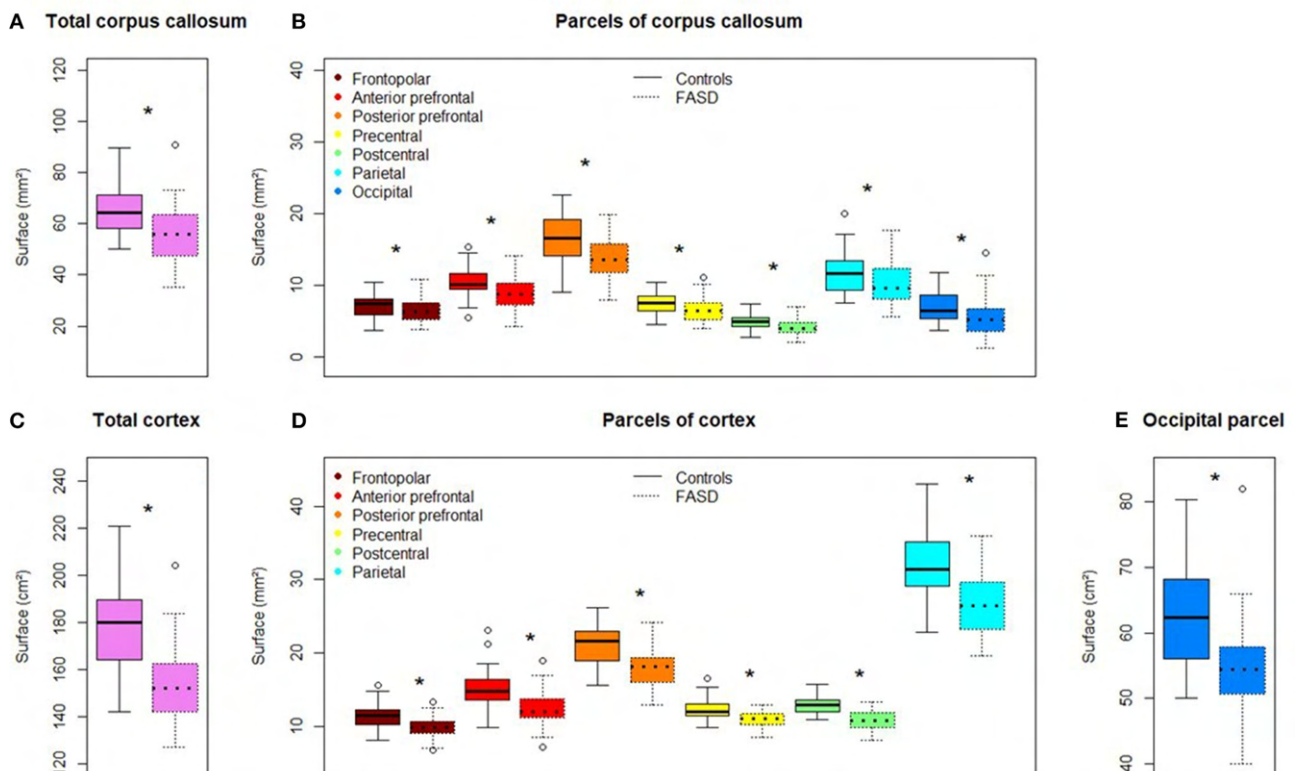


FIGURE 4 Comparison of callosal and cortical parcel surface areas of controls (left) and subjects with FASD (right, dotted line). **(A)** Total corpus callosum surface area. **(B)** All parcels, right to left: frontopolar, anterior prefrontal, posterior prefrontal, precentral, postcentral, parietal, occipital. **(C)** Total cortical surface area. **(D)** Frontopolar, anterior prefrontal, posterior prefrontal, precentral, postcentral, parietal cortical surface area. **(E)** Occipital cortical surface area. *Significantly different between FASD and control group (FDR corrected p -value: q -value < 0.05).

The reduction in the size of the postcentral CcSP was the most frequent. We tagged in blue the subjects presenting with this abnormally small postcentral CcPS on all other parcel plots to see whether they presented or not with other abnormally

small CcSP. The subjects with FAS showing an abnormally small precentral CcSP had also too small a postcentral one (dark blue), but it was not the case for all those with an abnormally small occipital CsSP (Figure 6). We can also note that there

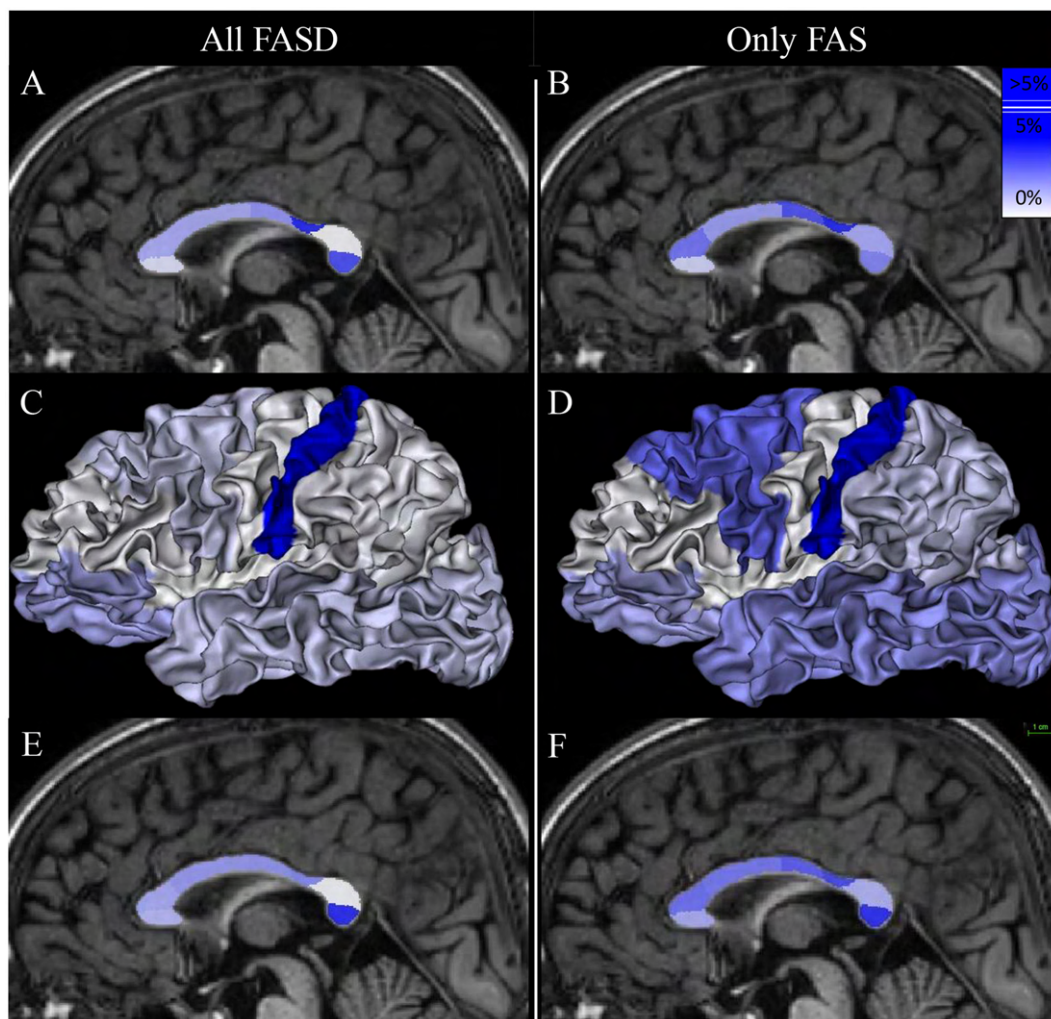


FIGURE 5

Mapping of the group effect size (FASD vs. control on the left and FAS vs. control on the right) on callosal parcel surface area [(A, B, E, F), respectively] and cortical parcel surface area (C, D). Eta-squared (η^2) associated with b_{DIAG} in each model are listed in Tables 3, 4. The scale appears at the top right of (F).

were more subjects with FASD identified below the 10th for the postcentral CcSP than for the global CC size reduction (20 vs. 32).

4. Discussion

Our study compared the morphology of the CC between 65 subjects with FASD and 38 typically developing controls, aged between 6 and 25 years old, by means of a sulci and connectivity-based segmentation of its midsagittal section into seven parcels. We were able to show two main significant spots of surface reduction in the callosal section, one in the peri-isthmic and especially post-isthmic region (precentral and postcentral parcels), the other in the posterior terminal end (occipital parcel). Though mainly posterior, these focal shrinkages were separated by a more preserved section (parietal parcel) and our results suggested progressive damage from the more anterior regions corresponding to the prefrontal parcels to the much reduced post-isthmic region. Furthermore, the hemispherotopic segmentation allowed for an increased understanding of the nature of this callosal section damage showing

that the post-isthmic reduction is highly associated with a shrinkage of the corresponding postcentral cortical surface parcel, while, conversely, the very terminal posterior reduction was all the more visible considering the relative preservation of the corresponding occipital-temporal cortical surface parcel. Finally, we suggested how such group results could translate to individual analysis through normative identification of subjects with post-isthmic and terminal callosal parcels that were too small compared to the control distribution, the two markers being not always redundant to each other, and in any case more sensitive than the whole callosal section reduction alone.

4.1. Bimodal damage mostly in the posterior half of the corpus callosum

4.1.1. Considering the callosal section only

The surface of the midsagittal section of the CC was globally reduced in our FASD population compared with controls (Figure 4), which is consistent with previous reports, a reduction

TABLE 3 Group effect (FASD vs. control) on callosal parcel surface area (CcPS in models 1 and 3) and cortical parcel surface area (CxPS in model 2).

All subjects with FASD	b_{DIAG} in model 1 (CcPS)				b_{DIAG} in model 2 (CxPS)				b_{DIAG} in model 3 (CcPS)			
	η^2	t (98)	p -value	q -value	η^2	t (98)	p -value	q -value	η^2	t (97)	p -value	q -value
Total CC	2.7	-1.90	0.030	0.080	-	-	-	-	-	-	-	-
Frontopolar	0.6	-0.81	0.211	0.241	1.4	1.20	0.116	0.333	1.5	-1.36	0.088	0.103
Anterior prefrontal	1.8	-1.49	0.070	0.093	0.0	0.05	0.480	0.492	1.9	-1.73	0.044	0.062
Posterior prefrontal	1.8	-1.54	0.064	0.093	0.7	0.89	0.187	0.333	2.2	-1.72	0.044	0.062
Precentral	2.3	-1.72	0.044	0.088	0.0	0.02	0.492	0.492	2.3	-1.77	0.040	0.062
Postcentral	6.5	-2.75	0.004	0.032	8.9	-3.17	0.001	0.007	2.6	-1.82	0.036	0.062
Parietal	0.0	-0.14	0.445	0.445	0.2	-0.50	0.308	0.431	0.0	-0.04	0.486	0.486
Occipital	4.1	-2.17	0.016	0.064	0.8	0.88	0.190	0.333	5.7	-2.87	0.002	0.014

Eta-squared (η^2), t -value, p -value, and q -value (FDR corrected p -value) associated with b_{DIAG} in each model. In bold, p -value and FDR-corrected p -value (q -value) <0.05. Effect sizes (η^2) are mapped in Figures 5A, C, E.

TABLE 4 Group effect (FAS vs. control) on callosal parcel surface area (CcPS in models 1 and 3) and cortical parcel surface area (CxPS in model 2).

All subjects with FAS	b_{DIAG} in model 1 (CcPS)				b_{DIAG} in model 2 (CxPS)				b_{DIAG} in model 3 (CcPS)			
	η^2	t (98)	p -value	q -value	η^2	t (98)	p -value	q -value	η^2	t (97)	p -value	q -value
Total CC	4.6	-2.09	0.020	0.069	-	-	-	-	-	-	-	-
Frontopolar	0.9	-0.84	0.202	0.202	1.4	1.03	0.154	0.270	1.8	-1.28	0.103	0.114
Anterior prefrontal	3.2	-1.65	0.052	0.102	0.0	0.05	0.479	0.479	3.3	-1.85	0.034	0.059
Posterior prefrontal	2.1	-1.42	0.081	0.108	2.8	1.57	0.061	0.214	3.0	-1.73	0.044	0.062
Precentral	4.0	-1.97	0.026	0.069	0.1	-0.31	0.378	0.441	3.7	-1.94	0.028	0.059
Postcentral	12.8	-3.36	0.001	0.008	20.4	-4.40	<0.001	<0.001	4.2	-1.98	0.026	0.059
Parietal	1.9	-1.30	0.100	0.114	0.8	-0.76	0.224	0.314	1.7	-1.21	0.114	0.114
Occipital	2.8	-1.54	0.064	0.102	1.9	1.18	0.120	0.270	4.9	-2.24	0.014	0.059

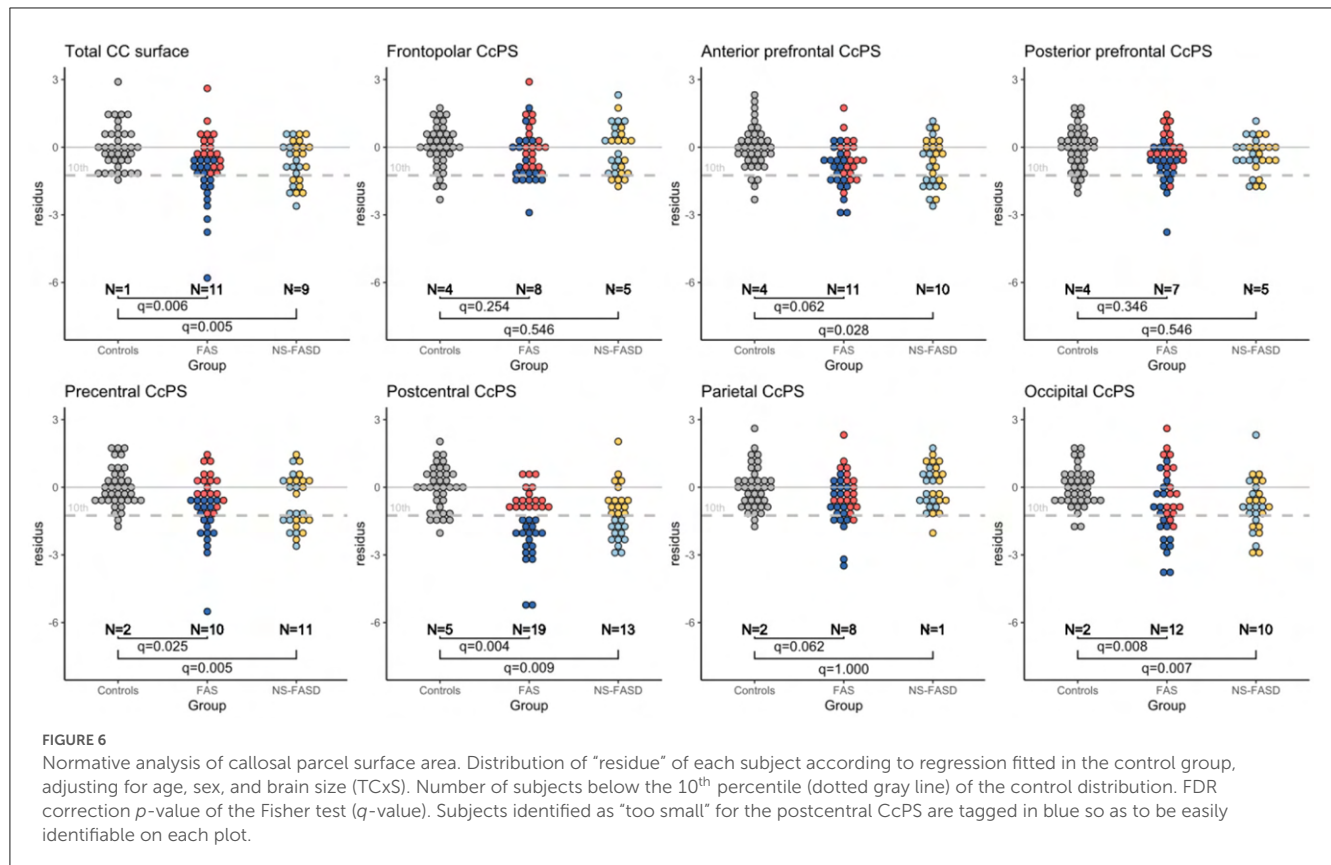
Eta-squared (η^2), t -value, p -value, and q -value (FDR-corrected p -value) associated with b_{DIAG} in each model. In bold, p -value and FDR-corrected p -value (q -value) <0.05. Effect sizes (η^2) are mapped in Figures 5B, D, F.

that affected all the parcels we defined on the anterior-posterior axis. In the first step of our analysis, we searched for an effect that was independent of obvious confounding factors, including age, sex, and a brain size parameter reflecting the amount of hemispheric cortex to be connected through the CC (here TCxS), to detect any heterogeneous damage. The main effect is an anterior-posterior U-shape gradient of surface reduction, bottoming around the isthmus, and is more precisely posterior to the typical narrowing in the postcentral parcel. In fact, this gradient is very probably not unimodal as this first analysis strongly demonstrated another spot of focal surface reduction at the very end of the CC in the terminal occipital parcel, with the parietal parcel being fully preserved in between (Figure 5, Table 3). We found similar results in the FAS-only subgroup even if the terminal reduction was not significant (Figure 5, Table 4).

Hence, we confirmed the previous data of the literature that pointed out a reduction in the midsagittal CC area (Riley et al., 1995; Sowell et al., 2001; Dodge et al., 2009; Jacobson et al., 2017), affecting the posterior isthmic and splenial regions more severely (Sowell et al., 2001; Dodge et al., 2009; Fraize et al., 2022) but

demonstrating a more complex landscape of surface reduction in the posterior half of the CC with the preservation of the anterior part of the splenium in between a post isthmic nadir and a terminal splenial dip.

We were able to replicate our previous results (Fraize et al., 2022), which highlighted the narrowing of the isthmus as a recurrent FAS anomaly in a subset of the original MRI dataset, but with a computational automatic imaging approach. Consistently, we showed a major reduction in the callosal surface in the post-isthmic parcel (postcentral) controlling for brain size. At the same time and with simple manual measurements, we failed to show an effect of the FASD on the splenium thickness, incriminating the necessarily noisy measurement of this plump object that is highly variable in shape. The difference with the present study is twofold: First, we have a better proxy of the splenium with surface measurement than only a middle thickness, but more importantly, the splenium is now divided into an anterior part (parietal parcel) and a posterior one (occipital parcel), revealing a differential involvement.



4.1.2. Considering cortical–callosal surface correlations

One main contribution of our callosal parcellation based on sulci landmarks and cortical–callosal connectivity was to allow for the analysis of the focal surface variations of the midsagittal section not only according to the global hemispheric size (TCxS) but more precisely according to the focal extension of the connectivity-related cortical surfaces, with two outcomes for the study.

The primary outcome was that a second step of analysis of the callosal parcel surfaces, including the relative cortical parcel surface as a covariate, emphasized the relative terminal reduction in the callosal section while mitigating the post-isthmic one, both in the FASD group and, to a lesser extent, in the FAS group. Within the limits of statistical power, this analysis also revealed a potential prefrontal-postcentral gradient of relative callosal reduction that could be tackled in a larger study, conducted perhaps at a higher resolution (more parcels or even continuous shape analysis).

A secondary outcome of this parcellation strategy was that, our study, designed to target the CC, revealed a very significant focal cortical surface reduction in FASD and FAS, electively affecting the postcentral gyrus. To our knowledge, this has not been reported yet. The two studies of cortical surface extension in FASD reported discordant observations in other regions: It was decreased in the right temporal surface area in 36 participants with ARND (equivalent to NS-FASD) compared to 52 controls (Rajaprakash et al., 2014), whereas a larger surface area of the right precentral gyrus was observed in a large cohort of exposed subjects but without PAE threshold (Marshall et al., 2022). An indirect insight could also come from gyrification studies: For instance, a reduced sulcal depth was found in the intraparietal sulci, including the

postcentral one, of 24 children with FASD correlating with the level of PAE (De Guio et al., 2014), and a reduction in local gyrification was observed in bilateral parietal clusters, including the superior part of the postcentral gyrus and the inferior part of the right one in 30 alcohol-exposed adolescents (Infante et al., 2015). However, in both studies, the postcentral involvement was neither elective nor exclusive, and it would, in any case, only be an indirect correlate of postcentral cortical surface reduction. The heterogeneity of the populations and analyses makes it difficult to put our cortical result further in perspective. Regarding the structure and shape of the CC, the question of the directionality of the observed correlation between the reduction in callosal and cortical parcels also remains open, as it would make sense not only if a defect in interhemispheric connectivity affected the size of the concerned gyrus but also if a primary defect in the cortical extension of this gyrus led to a reduction in the size of the associated callosal sub-bundle.

4.1.3. Insight from preclinical models with callosal damage

The profile of damage in the midsagittal section of the CC that we report should be compared with what has been observed in animal models of PAE, mostly in rodents, even if the choice of species, strain, type of exposure, and measurements are likely to trigger different results (Parnell et al., 2014; Zhang et al., 2019; Milbocker et al., 2022). Interestingly, we found reports not only of global and recurrent terminal reduction in the midsagittal corpus callosum in rats (Moreland et al., 2002) but also of global and middle “isthmic” thinning in mice (O’Leary-Moore et al., 2011), both consistent with our bimodal mostly terminal profile.

4.2. Quantitative anomalies of the corpus callosum as a potential diagnostic marker

Pragmatically, we also sought to identify callosal abnormalities that could be found at the individual level. We looked for FASD subjects with callosal parcels that could be considered too small once the appropriate covariates were taken into account. We performed a normative-like analysis by computing the residual for each subject and each callosal surface to the model fitted in the controls while considering all the covariates of interest. We were then able to identify the subjects with FAS or NS-FASD with values below the 10th percentile of the control distribution. Though exploratory due to the limited size of our control group, this individual analysis found global, peri-isthmic (pre and postcentral), and terminal anomalies (<10th percentile) to be recurrent (in excess) not only in FAS but also in NS-FASD. More interestingly, this individual analysis showed that anomalies in the postcentral or occipital callosal parcel surfaces were more frequent than in the total callosal section alone (for instance in the FAS group, 19+2 vs. 11 subjects), making them better candidate markers of the disease. Besides, if all the patients with FAS showing abnormal precentral values had a postcentral anomaly, this was not the case for the occipital value that tended to add new subjects (Figure 6). This phenomenon appeared to be even more complex in NS-FASD in any case, highlighting the probably multimodal nature of the callosal damage already illustrated by our study.

The question of the specificity of our findings as of any callosal marker in the FASD population is worth raising. Agenesis of the CC is not extremely rare in the general population (0.02%–0.7%) (Glass et al., 2008) and could be as high as approximately 1% in a population of subjects with neurodevelopmental disorders (Jeret et al., 1985). One could therefore expect an additional comparison group of subjects with neurodevelopmental disorders or microcephaly without PAE for a better assessment of specificity. Even in the absence of this type of study, the sheer number of subjects with FAS concerned by at least one peri-isthmic or terminal quantitative anomaly of the CC gives our result a much broader potential for clinical use than visually assessed agenesis of the CC. Indeed, with a reduction in the midsagittal callosal section following the bimodal profile, we found that positively diagnosed FAS could be a relevant feature to strengthen the probabilistic diagnosis of non-syndromic non-specific FASD. In that respect, our result argues for more precise and meaningful neuroanatomical criteria in FASD diagnostic guidelines.

4.3. Interest and limitations of the sulci and connectivity-based parcellation

The intrinsic limitations of the purely geometric parcellations in the midsagittal section of the CC, such as Witelson's (Witelson, 1989), have prompted the use of connectivity-based ones, relying on objective and anatomically grounded cortical segmentations (Huang et al., 2005; Styner et al., 2005; Chao et al., 2009; Friedrich et al., 2020). These methods are relevant even when there is no guarantee of the integrity of the extremities, especially the posterior one which is difficult to verify morphologically, and ensure an adequate proxy of inter-individual variations in the

relative representation of the different cortical regions at the level of the medial CC. However, there were very few implementations in the field of neurodevelopmental imaging (Lebel et al., 2010), and to our knowledge, our study is the first in a neurodevelopmental condition such as FASD. Relying on the *Hip-Hop* and *MarsAtlas* cortical parcellation, with the homology of the parcels being supported by the reasonable assumption of homology between the large sulci that define the geodesic meridians, our implementation proved to be highly appropriate to sample the anterior–posterior axis of the CC. It also allowed, as previously discussed, the conjoint analysis of cortical and callosal parcels.

Other methodological limitations could be discussed, such as the use of a segmentation tool as *MarsAtlas* initially developed for a healthy adult cohort. The first steps of the *MarsAtlas/Hip-Hop* process rely on the *Morphologist* segmentation pipeline that has currently been successfully used in typically developing or impaired children and adolescents (Borst et al., 2014; Cachia et al., 2016; Kersbergen et al., 2016). Then, the *MarsAtlas* method is essentially based on the identification of homologous sulci in each subject space, without any normalization step. Our cohort was composed of children above 6 years of age whose gyrification has been shown to be very similar to that of adults (White et al., 2010). However, the use of such a method in a pathological population raises the question of the integrity of the main cortical sulci in FASD. Indeed, we lack the knowledge of any reports on FASD, showing that the sulcal pattern may be so impaired as to prevent the use of sulcal landmarks, with the few sulcal modifications reported being mostly quantitative and small-sized (Infante et al., 2015; Hendrickson et al., 2017; Kilpatrick et al., 2021). Besides, the parcellation process was carefully quality checked to avoid mis-segmentation or misclassification of the sulci that would affect the final callosal parcellation (Figure 1). Finally, it should be emphasized that the proposed method is purely object-based morphometry and thus does not rely on any template normalization or averaging in the image domain, which may have unpredictable consequences in pathological populations and raise methodological questions in dysgenetic CC.

Our implementation of this strategy led to a sampling of the midsagittal section of the CC into seven parcels, with subdivisions that proved to be quite relevant in some regions (for instance, isthmus and splenium), but this may still be insufficient. Much more subtle spatial resolution could be achieved with the same rationale using higher resolution cortical atlases, not only in both the large parcels (for instance prefrontal ones) and possibly complex regions, such as the splenium, but also within the thickness of the CC (Park et al., 2008). Provided that a dataset with sufficient statistical power is available, such an increase in spatial resolution and a number of parcels might have revealed a more subtle pattern of surface area reduction.

4.4. Other limitations and future directions

With hundred subjects and only a third of typically developing controls, the size of our dataset may have limited the power of the study and the scope of the results, at least because of the risk of sampling bias. However, it can be recalled that the relatively small number of subjects allowed a particularly thorough

quality control that would not have been possible with a larger data set, mitigating, in part, the disadvantage of the limitation in group size and that this is a homogeneous monocentric study in terms of both clinical recruitment and MRI acquisitions. However, some potentially interesting results are still exploratory as they did not remain after FDR correction to limit type I risk (for instance, the prefrontal–postcentral gradient) and that, conversely, some interesting small-sized effects may have been missed due to insufficient power.

Our choice of a linear model to regress the data, and in particular, the effect of brain size is debatable since the use of a power model in which the proportions can vary with the size (allometry) (de Jong et al., 2017; Fraize et al., 2023) is more correct and less prone to mismodeling (covering the linear one). The small size of the control group and the low-shared variance share between brain size and callosal section area led us to consider that non-linear modeling was not appropriate for our dataset and to apply only an affine approximation of the scaling effect. A more complex non-linear account for scaling could be used in a replication study with a larger sample.

Last, it is also an understandable but real limitation not to be able to analyze the observed variance with respect to the level of PAE. While PAE is documented to be above a relatively consensual threshold in our population, we do not have further insight into the timing and extent of this exposure.

Hence, in light of our results, we considered that there is a real interest for future studies to implement our segmentation or any similar cortical and connectivity-based one, with a high FAS to NS-FASD ratio to ensure specificity of the findings and a large control group to provide normative data for potential clinical use at the individual level. It could also be of interest to focus on younger samples or even a prenatal population, as to the authors' knowledge, only one ultrasound imaging study has suggested the early damage of the splenium as a diagnostic or prognostic marker of the consequences of PAE in neonates (Bookstein et al., 2005).

5. Conclusion

Our study described the surface reduction in the midsagittal section of the corpus callosum in a series of 65 patients with FASD. A unique combination of anatomical and diffusion tensor imaging was used to provide a sulci and connectivity-based parcellation into seven regions, designed to account for the cortical connectivity of the structure and its possible partial agenesis or marked dysgenesis. We demonstrated bimodal damage mostly in the posterior half of the corpus callosum, with a strong post-isthmic narrowing and relative terminal splenium damage, of which only the latter was independent of the reduction in the connected cortical parcel. These anomalies were more frequently and sensitively observed than the reduction in the whole section area and, interestingly, were frequent not only in FAS but also in NS-FASD, opening the field for a clinical application as a diagnostic marker.

Data availability statement

The datasets presented in this article are not readily available because the data that support the findings of this study are available on request from the corresponding author. The data are not publicly available due to privacy or ethical restrictions. Requests to access the datasets should be directed to JF, justine.fraize@inserm.fr.

Ethics statement

This study was conducted in accordance with the principles of the Declaration of Helsinki. Subjects' data were studied in accordance with French regulation (MR-004, declaration of conformity n 2059980v0), following approval by the Paris-Saclay research ethics committee (CER-Paris-Saclay-2020-094). Written informed consent from the FASD participants' legal guardian/next of kin was not required to participate in this study in accordance with the national legislation and the institutional requirements. Controls' data were used within the framework of the ethical authorizations of the primary studies (Gene and autism, Inserm C07-33). Written informed consent from the control participants' legal guardian/next of kin was required to participate in the initial study in accordance with the national legislation and the institutional requirements.

Author contributions

JF, GC, and DG contributed to the conception and design of the study. JF and EK collected and organized the database. GC, FS-M, and YL ensured data processing. JF performed the statistical analysis. JF and DG wrote the manuscript. All authors contributed to manuscript revision, read, and approved the submitted version.

Funding

This study was supported by the French National Agency for Research (ANR-19-CE17-0028-01) and the French National Institute for Public Health Research (IRES-19-ADDICTIONS-08).

Acknowledgments

The authors would like to thank the volunteers, patients and families, and the French supportive association for FASD-affected families *Vivre avec le SAF*.

Conflict of interest

The authors declare that the research was conducted in the absence of any commercial or financial relationships that could be construed as a potential conflict of interest.

Publisher's note

All claims expressed in this article are solely those of the authors and do not necessarily represent those of their affiliated

organizations, or those of the publisher, the editors and the reviewers. Any product that may be evaluated in this article, or claim that may be made by its manufacturer, is not guaranteed or endorsed by the publisher.

References

- Amiez, C., Sallet, J., Hopkins, W. D., Meguerditchian, A., Hadj-Bouziane, F., Ben Hamed, S., et al. (2019). Sulcal organization in the medial frontal cortex provides insights into primate brain evolution. *Nat. Commun.* 10, 3437. doi: 10.1038/s41467-019-11347-x
- Andersson, J. L. R., Graham, M. S., Zsoldos, E., and Sotiropoulos, S. N. (2016). Incorporating outlier detection and replacement into a non-parametric framework for movement and distortion correction of diffusion MR images. *Neuroimage* 141, 556–572. doi: 10.1016/j.neuroimage.06058
- Andersson, J. L. R., and Sotiropoulos, S. N. (2016). An integrated approach to correction for off-resonance effects and subject movement in diffusion MR imaging. *Neuroimage* 125, 1063–1078. doi: 10.1016/j.neuroimage.10019
- Archibald, S. L., Fennema-Notestine, C., Gamst, A., Riley, E. P., Mattson, S. N., and Jernigan, T. L. (2001). Brain dysmorphology in individuals with severe prenatal alcohol exposure. *Dev. Med. Child Neurol.* 43, 148–154. doi: 10.1111/j.1469-8749.2001.tb00179.x
- Astley, S. J. (2004). Diagnostic guide for fetal alcohol spectrum disorders: The 4-digit diagnostic code. Astley S. J. Diagnostic Guide for Fetal Alcohol Spectrum Disorders: The 4-Digit Diagnostic Code. 3rd edition University of Washington Publication Services, Seattle, WA: 2004. Available online at: <http://depts.washington.edu/fasdpn/pdfs/guide04.pdf>, 123
- Astley, S. J., Aylward, E. H., Olson, H. C., Kerns, K., Brooks, A., Coggins, T. E., et al. (2009). Magnetic resonance imaging outcomes from a comprehensive magnetic resonance study of children with fetal alcohol spectrum disorders. *Alcohol. Clin. Exp. Res.* 33, 1671–1689. doi: 10.1111/j.1530-0277.2009.01004.x
- Autti-Rämö, I., Autti, T., Korkman, M., Kettunen, S., Salonen, O., Valanne, L., et al. (2002). MRI findings in children with school problems who had been exposed prenatally to alcohol. *Dev. Med. Child Neurol.* 44, 98–106. doi: 10.1017/s0012162201001748
- Auzias, G., Coulon, O., and Brovelli, A. (2016). MarsAtlas: A cortical parcellation atlas for functional mapping. *Hum. Brain Mapp.* 37, 1573–1592. doi: 10.1002/hbm.23121
- Auzias, G., Lefèvre, J., Le Troter, A., Fischer, C., Perrot, M., Régis, J., et al. (2013). Model-driven harmonic parameterization of the cortical surface: HIP-HOP. *IEEE Trans. Med. Imaging* 32, 873–887. doi: 10.1109/TMI.2013.2241651
- Benjamini, Y., and Hochberg, Y. (1995). Controlling the false discovery rate: a practical and powerful approach to multiple testing. *J. Royal Stat. Soc. Series B (Methodol.)* 57, 289–300. doi: 10.1111/j.2517-6161.1995.tb02031.x
- Biffen, S. C., Warton, C. M. R., Dodge, N. C., Molteno, C. D., Jacobson, J. L., Jacobson, S. W., et al. (2020). Validity of automated FreeSurfer segmentation compared to manual tracing in detecting prenatal alcohol exposure-related subcortical and corpus callosal alterations in 9- to 11-year-old children. *Neuroimage Clin.* 28, 102368. doi: 10.1016/j.nicl.2020.102368
- Biffen, S. C., Warton, C. M. R., Lindinger, N. M., Randall, S. R., Lewis, C. E., Molteno, C. D., et al. (2017). Reductions in corpus callosum volume partially mediate effects of prenatal alcohol exposure on IQ. *Front. Neuroanat.* 11, 132. doi: 10.3389/fnana.2017.00132
- Bookstein, F. L., Connor, P. D., Covell, K. D., Barr, H. M., Gleason, C. A., Sze, R. W., et al. (2005). Preliminary evidence that prenatal alcohol damage may be visible in averaged ultrasound images of the neonatal human corpus callosum. *Alcohol* 36, 151–160. doi: 10.1016/j.alcohol.07007
- Bookstein, F. L., Sampson, P. D., Connor, P. D., and Streissguth, A. P. (2002). Midline corpus callosum is a neuroanatomical focus of fetal alcohol damage. *Anat. Rec.* 269, 162–174. doi: 10.1002/ar.10110
- Boronat, S., Sánchez-Montañez, A., Gómez-Barros, N., Jacas, C., Martínez-Ribot, L., Vázquez, E., et al. (2017). Correlation between morphological MRI findings and specific diagnostic categories in fetal alcohol spectrum disorders. *Eur. J. Med. Genet.* 60, 65–71. doi: 10.1016/j.ejmg.09003
- Borst, G., Cachia, A., Vidal, J., Simon, G., Fischer, C., Pineau, A., et al. (2014). Folding of the anterior cingulate cortex partially explains inhibitory control during childhood: a longitudinal study. *Dev. Cogn. Neurosci.* 9, 126–135. doi: 10.1016/j.dcn.02006
- Cachia, A., Borst, G., Tissier, C., Fisher, C., Plaze, M., Gay, O., et al. (2016). Longitudinal stability of the folding pattern of the anterior cingulate cortex during development. *Dev. Cogn. Neurosci.* 19, 122–127. doi: 10.1016/j.dcn.02011
- Chao, Y.-P., Cho, K.-H., Yeh, C.-H., Chou, K.-H., Chen, J.-H., Lin, C.-P., et al. (2009). Probabilistic topography of human corpus callosum using cytoarchitectural parcellation and high angular resolution diffusion imaging tractography. *Hum. Brain Mapp.* 30, 3172–3187. doi: 10.1002/hbm.20739
- Cook, J. L., Green, C. R., Lilley, C. M., Anderson, S. M., Baldwin, M. E., Chudley, A. E., et al. (2016). Fetal alcohol spectrum disorder: a guideline for diagnosis across the lifespan. *Can. Med. Assoc. J.* 188, 191–197. doi: 10.1503/cmaj.141593
- De Guio, Mangin, F., Rivière, J.-F., Perrot, D., Molteno, M., Jacobson, C. D., et al. S. W., et al. (2014). A study of cortical morphology in children with fetal alcohol spectrum disorders: cortical morphology in fetal alcohol spectrum disorders. *Hum. Brain Mapp.* 35, 2285–2296. doi: 10.1002/hbm.22327
- de Jong, Vidal, L. W., Forsberg, J.-S., Zijdenbos, L. E., and Haight, A. P. T., Alzheimer's Disease Neuroimaging Initiative, et al. (2017). Allometric scaling of brain regions to intra-cranial volume: an epidemiological MRI study. *Hum. Brain Mapp.* 38, 151–164. doi: 10.1002/hbm.23351
- Dodge, N. C., Jacobson, J. L., Molteno, C. D., Meintjes, E. M., Bangalore, S., Diwadkar, V., et al. (2009). Prenatal alcohol exposure and interhemispheric transfer of tactile information: detroit and cape town findings. *Alcohol. Clin. Exp. Res.* 33, 1628–1637. doi: 10.1111/j.1530-0277.2009.00994.x
- Donald, K. A., Eastman, E., Howells, F. M., Adnams, C., Riley, E. P., Woods, R. P., et al. (2015). Neuroimaging effects of prenatal alcohol exposure on the developing human brain: a magnetic resonance imaging review. *Acta Neuropsychiatr.* 27, 251–269. doi: 10.1017/neu.2015.12
- Fan, J., Jacobson, S. W., Taylor, P. A., Molteno, C. D., Dodge, N. C., Stanton, M. E., et al. (2016). White matter deficits mediate effects of prenatal alcohol exposure on cognitive development in childhood. *Hum. Brain Mapp.* 37, 2943–2958. doi: 10.1002/hbm.23218
- Fraize, J., Fischer, C., Elmaleh-Bergès, M., Kerdreux, E., Beggiano, A., Ntorkou, A., et al. (2023). Enhancing fetal alcohol spectrum disorders diagnosis with a classifier based on the intra-cerebellar gradient of volume reduction. *Hum. Brain Mapp.* doi: 10.1002/hbm.26348. [Epub ahead of print].
- Fraize, J., Garzón, P., Ntorkou, A., Kerdreux, E., Boespflug-Tanguy, O., Beggiano, A., et al. (2022). Combining neuroanatomical features to support diagnosis of fetal alcohol spectrum disorders. *Dev. Med. Child Neurol.* 3, 5411. doi: 10.1111/dmnc.15411
- Friedrich, P., Fraenz, C., Schlüter, C., Ocklenburg, S., Mädler, B., Güntürkün, O., et al. (2020). The relationship between axon density, myelination, and fractional anisotropy in the human corpus callosum. *Cerebral Cortex* 30, 2042–2056. doi: 10.1093/cercor/bhz221
- Gautam, P., Nuñez, S. C., Narr, K. L., Kan, E. C., and Sowell, E. R. (2014). Effects of prenatal alcohol exposure on the development of white matter volume and change in executive function. *NeuroImage: Clinical* 5, 19–27. doi: 10.1016/j.nicl.05010
- Ghazi Sherbaf, F., Aarabi, M. H., Hosein Yazdi, M., and Haghshomar, M. (2019). White matter microstructure in fetal alcohol spectrum disorders: a systematic review of diffusion tensor imaging studies. *Hum. Brain Mapp.* 40, 1017–1036. doi: 10.1002/hbm.24409
- Glass, H. C., Shaw, G. M., Ma, C., and Sherr, E. H. (2008). Agenesis of the corpus callosum in California 1983–2003: a population-based study. *Am. J. Med. Genet. A* 146A, 2495–2500. doi: 10.1002/ajmg.a.32418
- Hendrickson, T. J., Mueller, B. A., Sowell, E. R., Mattson, S. N., Coles, C. D., Kable, J. A., et al. (2017). (2017). Cortical gyrification is abnormal in children with prenatal alcohol exposure. *Neuroimage Clin* 15, 391–400. doi: 10.1016/j.nicl.05015
- Hendrickson, T. J., Mueller, B. A., Sowell, E. R., Mattson, S. N., Coles, C. D., Kable, J. A., et al. (2018). 2-year cortical trajectories are abnormal in children and adolescents with prenatal alcohol exposure. *Dev. Cogn. Neurosci.* 30, 123–133. doi: 10.1016/j.dcn.02008
- Hofer, S., and Frahm, J. (2006). (2006). Topography of the human corpus callosum revisited—Comprehensive fiber tractography using diffusion tensor magnetic resonance imaging. *Neuroimage* 32, 989–994. doi: 10.1016/j.neuroimage.05044
- Hoyme, H. E., Kalberg, W. O., Elliott, A. J., Blankenship, J., Buckley, D., Marais, A. S., et al. (2016). Updated clinical guidelines for diagnosing fetal alcohol spectrum disorders. *Pediatrics* 138, 4256. doi: 10.1542/peds.2015-4256

- Huang, H., Zhang, J., Jiang, H., Wakana, S., Poetscher, L., Miller, M. I., et al. (2005). (2005). DTI tractography based parcellation of white matter: application to the mid-sagittal morphology of corpus callosum. *Neuroimage* 26, 195–205. doi: 10.1016/j.neuroimage.01019
- Infante, M. A., Moore, E. M., Bischoff-Grethe, A., Migliorini, R., Mattson, S. N., Riley, E. P., et al. (2015). Atypical cortical gyrification in adolescents with histories of heavy prenatal alcohol exposure. *Brain Res.* 1624, 446–454. doi: 10.1016/j.brainres.08002
- Inkelis, S. M., Moore, E. M., Bischoff-Grethe, A., and Riley, E. P. (2020). Neurodevelopment in adolescents and adults with fetal alcohol spectrum disorders (FASD): a magnetic resonance region of interest analysis. *Brain Res.* 1732, 146654. doi: 10.1016/j.brainres.2020.146654
- Jacobson, S. W., Jacobson, J. L., Moltano, C. D., Warton, C. M. R., Wintermark, P., Hoyme, H. E., et al. (2017). Heavy prenatal alcohol exposure is related to smaller corpus callosum in newborn MRI scans. *Alcohol. Clin. Exp. Res.* 41, 965–975. doi: 10.1111/acer.13363
- Jenkinson, M., Bannister, P., Brady, M., and Smith, S. (2002). Improved optimization for the robust and accurate linear registration and motion correction of brain images. *Neuroimage* 17, 825–841. doi: 10.1016/s1053-8119(02)91132-8
- Jenkinson, M., Beckmann, C. F., Behrens, T. E. J., Woolrich, M. W., and Smith, S. M. (2012). FSL. *Neuroimage* 62, 782–790. doi: 10.1016/j.neuroimage.09015
- Jeret, J. S., Serur, D., Wisniewski, K., and Fisch, C. (1985). Frequency of agenesis of the corpus callosum in the developmentally disabled population as determined by computerized tomography. *Pediatr. Neurosci.* 12, 101–103. doi: 10.1159/000120229
- Kar, P., Reynolds, J. E., Gibbard, W. B., McMorris, C., Tortorelli, C., Lebel, C., et al. (2022). Trajectories of brain white matter development in young children with prenatal alcohol exposure. *Hum. Brain Mapp.* 43, 4145–4157. doi: 10.1002/hbm.25944
- Kersbergen, K. J., Leroy, F., Išgum, I., Groenendaal, F., Vries, d. e., Claessens, L. S., et al. (2016). Relation between clinical risk factors, early cortical changes, and neurodevelopmental outcome in preterm infants. *Neuroimage* 142, 301–310. doi: 10.1016/j.neuroimage.07010
- Kilpatrick, L. A., Joshi, S. H., O'Neill, J., Kalender, G., Dillon, A., Best, K. M., et al. (2021). Cortical gyrification in children with attention deficit-hyperactivity disorder and prenatal alcohol exposure. *Drug Alcohol. Depend.* 225, 108817. doi: 10.1016/j.drugalcdep.2021.108817
- Lebel, C., Caverhill-Godkewitsch, S., and Beaulieu, C. (2010). Age-related regional variations of the corpus callosum identified by diffusion tensor tractography. *Neuroimage* 52, 72. doi: 10.1016/j.neuroimage.03072
- Lebel, C., Roussotte, F., and Sowell, E. R. (2011). Imaging the impact of prenatal alcohol exposure on the structure of the developing human brain. *Neuropsychol. Rev.* 21, 102–118. doi: 10.1007/s11065-011-9163-0
- Marshall, A. T., Bodison, S. C., Uban, K. A., Adise, S., Jonker, D., Charles, W., et al. (2022). The impact of prenatal alcohol and/or tobacco exposure on brain structure in a large sample of children from a South African birth cohort. *Alcohol. Clin. Exp. Res.* 46, 1980–1992. doi: 10.1111/acer.14945
- Milbocker, K. A., LeBlanc, G. L., Brengel, E. K., Hekmatyar, K. S., Kulkarni, P., Ferris, C. F., et al. (2022). Reduced and delayed myelination and volume of corpus callosum in an animal model of fetal alcohol spectrum disorders partially benefit from voluntary exercise. *Sci. Rep.* 12, 10653. doi: 10.1038/s41598-022-14752-3
- Moore, E. M., and Xia, Y. (2021). neurodevelopmental trajectories following prenatal alcohol exposure. *Front. Hum. Neurosci.* 15, 695855. doi: 10.3389/fnhum.2021.695855
- Moreland, N., La Grange, L., and Montoya, R. (2002). Impact of in utero exposure to EtOH on corpus callosum development and paw preference in rats: protective effects of silymarin. *BMC Complement. Altern. Med.* 2, 10. doi: 10.1186/1472-6882-2-10
- Nguyen, V. T., Chong, S., Tieng, Q. M., Mardon, K., Galloway, G. J., Kurniawan, N. D., et al. (2017). (2017). Radiological studies of fetal alcohol spectrum disorders in humans and animal models: an updated comprehensive review. *Magn. Reson. Imaging* 43, 10–26. doi: 10.1016/j.mri.06012
- O'Leary-Moore, S. K., Parnell, S. E., Lipinski, R. J., and Sulik, K. K. (2011). Magnetic resonance-based imaging in animal models of fetal alcohol spectrum disorder. *Neuropsychol. Rev.* 21, 167–185. doi: 10.1007/s11065-011-9164-z
- Pandya, D. N., Karol, E. A., and Heilbronn, D. (1971). The topographical distribution of interhemispheric projections in the corpus callosum of the rhesus monkey. *Brain Res.* 32, 31–43. doi: 10.1016/0006-8993(71)90153-3
- Park, H.-J., Kim, J. J., Lee, S.-K., Seok, J. H., Chun, J., Kim, D. I., et al. (2008). Corpus callosal connection mapping using cortical gray matter parcellation and DT-MRI. *Hum. Brain Mapp.* 29, 503–516. doi: 10.1002/hbm.20314
- Parnell, S. E., Holloway, H. E., Baker, L. K., Styner, M. A., and Sulik, K. K. (2014). Dysmorphogenic effects of first trimester-equivalent ethanol exposure in mice: a magnetic resonance microscopy-based study. *Alcohol. Clin. Exp. Res.* 38, 2008–2014. doi: 10.1111/acer.12464
- Perrot, M., Rivière, D., and Mangin, J.-F. (2011). (2011). Cortical sulci recognition and spatial normalization. *Med. Image Anal.* 15, 529–550. doi: 10.1016/j.media.02008
- Rajaprakash, M., Chakravarty, M. M., Lerch, J. P., and Rovet, J. (2014). Cortical morphology in children with alcohol-related neurodevelopmental disorder. *Brain Behav.* 4, 41–50. doi: 10.1002/brb3.191
- Riley, E. P., Mattson, S. N., Sowell, E. R., Jernigan, T. L., Sobel, D. F., Jones, K. L., et al. (1995). Abnormalities of the corpus callosum in children prenatally exposed to alcohol. *Alcohol. Clin. Exp. Res.* 19, 1198–1202. doi: 10.1111/j.1530-0277.1995.tb01600.x
- Rivière, D., Geffroy, D., Denghien, I., Souedet, N., and Cointepas, Y. (2009). BrainVISA: an extensible software environment for sharing multimodal neuroimaging data and processing tools. *Neuroimage* 47, 3. doi: 10.1016/S1053-8119(09)71720-3
- Smith, R. E., Tournier, J.-D., Calamante, F., and Connelly, A. (2012). (2012). Anatomically-constrained tractography: improved diffusion MRI streamlines tractography through effective use of anatomical information. *Neuroimage* 62, 1924–1938. doi: 10.1016/j.neuroimage.06005
- Smith, R. E., Tournier, J.-D., Calamante, F., and Connelly, A. (2015). (2015). SIFT2: enabling dense quantitative assessment of brain white matter connectivity using streamlines tractography. *Neuroimage* 119, 338–351. doi: 10.1016/j.neuroimage.06092
- Sowell, E. R., Mattson, S. N., Kan, E., Thompson, P. M., Riley, E. P., Toga, A. W., et al. (2008). Abnormal cortical thickness and brain-behavior correlation patterns in individuals with heavy prenatal alcohol exposure. *Cereb. Cortex* 18, 136–144. doi: 10.1093/cercor/bhm039
- Sowell, E. R., Mattson, S. N., Thompson, P. M., Jernigan, T. L., Riley, E. P., Toga, A. W., et al. (2001). Mapping callosal morphology and cognitive correlates: effects of heavy prenatal alcohol exposure. *Neurology* 57, 235–244. doi: 10.1212/wnl.57.2.235
- Styner, M. A., Oguz, I., Smith, R. G., Cascio, C., and Jomier, M. (2005). Corpus callosum subdivision based on a probabilistic model of inter-hemispheric connectivity. *Med. Image Comput. Assist. Interv.* 8, 765–772. doi: 10.1007/11566489_94
- Tournier, J.-D., Calamante, F., and Connelly, A. (2007). (2007). Robust determination of the fibre orientation distribution in diffusion MRI: non-negativity constrained super-resolved spherical deconvolution. *Neuroimage* 35, 1459–1472. doi: 10.1016/j.neuroimage.02016
- Tournier, J. D., Calamante, F., and Connelly, A. (2010). Improved probabilistic streamlines tractography by 2nd order integration over fibre orientation distributions. *Proc. Intl. Soc. Mag. Reson. Med. (ISMRM)*, 18, 25.
- Tournier, J.-D., Smith, R., Raffelt, D., Tabbara, R., Dhollander, T., Pietsch, M., et al. (2019). MRtrix3: A fast, flexible and open software framework for medical image processing and visualisation. *Neuroimage* 202, 116137. doi: 10.1016/j.neuroimage.2019.116137
- Treit, S., Jeffery, D., Beaulieu, C., and Emery, D. (2020). Radiological findings on structural magnetic resonance imaging in fetal alcohol spectrum disorders and healthy controls. *Alcohol. Clin. Exp. Res.* 44, 455–462. doi: 10.1111/acer.14263
- Treit, S., Zhou, D., Lebel, C., Rasmussen, C., Andrew, G., Beaulieu, C., et al. (2014). Longitudinal MRI reveals impaired cortical thinning in children and adolescents prenatally exposed to alcohol. *Hum. Brain Mapp.* 35, 4892–4903. doi: 10.1002/hbm.22520
- Wang, X., Cuzon Carlson, V. C., Studholme, C., Newman, N., Ford, M. M., Grant, K. A., et al. (2020). In utero MRI identifies consequences of early-gestation alcohol drinking on fetal brain development in rhesus macaques. *Proc. Natl. Acad. Sci. USA.* 117, 10035–10044. doi: 10.1073/pnas.1919048117
- White, T., Su, S., Schmidt, M., Kao, C.-Y., and Sapiro, G. (2010). The development of gyrification in childhood and adolescence. *Brain Cogn.* 72, 36–45. doi: 10.1016/j.bandc.10009
- Witelson, S. F. (1989). Hand and sex differences in the isthmus and genu of the human corpus callosum. A postmortem morphological study. *Brain* 112(Pt 3), 799–835. doi: 10.1093/brain/112.3.799
- Yang, Y., Phillips, O. R., Kan, E., Sulik, K. K., Mattson, S. N., Riley, E. P., et al. (2012). Callosal thickness reductions relate to facial dysmorphology in fetal alcohol spectrum disorders. *Alcohol. Clin. Exp. Res.* 36, 798–806. doi: 10.1111/j.1530-0277.2011.01679.x
- Zhang, C. R., Kurniawan, N. D., Yamada, L., Fleming, W., Kaminen-Ahola, N., Ahola, A., et al. (2019). Early gestational ethanol exposure in mice: effects on brain structure, energy metabolism and adiposity in adult offspring. *Alcohol* 75, 1–10. doi: 10.1016/j.alcohol.04008
- Zhang, Y., Brady, M., and Smith, S. (2001). Segmentation of brain MR images through a hidden Markov random field model and the expectation-maximization algorithm. *IEEE Trans. Med. Imaging* 20, 45–57. doi: 10.1109/42.906424
- Zhou, D., Lebel, C., Lepage, C., Rasmussen, C., Evans, A., Wyper, K., et al. (2011). Developmental cortical thinning in fetal alcohol spectrum disorders. *Neuroimage* 58, 16–25. doi: 10.1016/j.neuroimage.06026

PROFILAGE SPECTRAL DE L'ÉPAISSEUR DU CORPS CALLEUX DANS LES TROUBLES DU SPECTRE DE L'ALCOOLISATION FŒTALE

Fraize, J., Leprince, Y., Auzias, G., Elmaleh-Bergès, M., Hertz-Pannier, L., Lefèvre, J., & Germanaud, D. (2023). Spectral-based thickness profiling of the corpus callosum in fetal alcohol spectrum disorders. *Human Brain Mapping, Submitted*

RÉSUMÉ

Introduction

Le diagnostic de troubles du spectre de l'alcoolisation fœtale (TSAF) englobe les conséquences pathologiques de l'exposition prénatale à l'alcool, qui vont du syndrome d'alcoolisation fœtale (SAF) aux formes non syndromiques (TSAF-NS). La cible principale des effets tératogènes de l'éthanol est le cerveau, ce qui conduit les sujets atteints de TSAF à présenter non seulement un plus petit cerveau, mais aussi des anomalies cérébrales focales visibles et récurrentes, comme des anomalies du corps calleux (CC) communément rapportées. Nous avons déjà montré le rétrécissement du CC pour la taille du cerveau, en utilisant des mesures manuelles et son apport dans un critère neuroanatomique composite pour alimenter la certitude diagnostique. Le but de cette étude est d'automatiser ces mesures du CC et d'identifier les anomalies récurrentes chez les sujets atteints de SAF, indépendamment de la réduction de la taille du cerveau.

Matériels et méthodes

Nous présentons une méthode innovante, rapide, entièrement automatisée et sans normalisation, pour mesurer l'épaisseur du CC en continu et en des points singuliers (genou, corps, isthme et splénium), en plus de sa longueur (LCC). Nous avons développé et appliqué ce profilage de l'épaisseur basé sur le spectre à la section sagittale médiane du CC extraite d'IRM cérébrale 3DT1 de 1,5T d'une population monocentrique de 89 TSAF (52 SAF, 37 TSAF-NS) et de 126 contrôles au développement typique (6-20 ans). Après ajustement pour l'effet de site, nous avons comparé les profils moyens et les épaisseurs des points singuliers dans les trois groupes. Pour chaque paramètre, nous avons établi les variations en fonction de l'âge (courbe de croissance) et de la taille du cerveau dans le groupe contrôle (courbe de *scaling*), puis nous avons identifié les participants dont les mesures étaient anormales (< 10^{ème} percentile).

Résultats

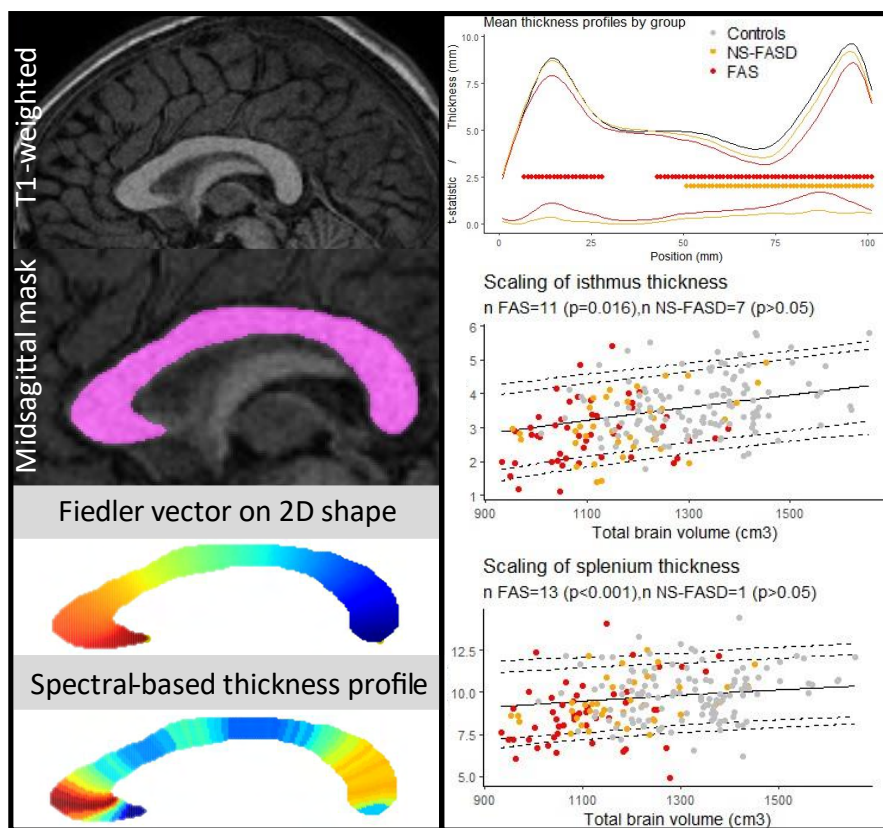
Nous avons confirmé l'amincissement de la moitié postérieure du CC dans les deux groupes de TSAF, et du genou dans le groupe des SAF, par rapport au groupe contrôles. Nous avons trouvé un effet de groupe significatif pour la LCC, les épaisseurs du genou, du corps, de l'isthme et du splénium ($p < 0,05$). Nous avons décrit une bosse au niveau du corps dont la morphologie ne diffère pas entre les groupes. Selon les courbes de croissance de chaque paramètre, il y a un excès de sujets TSAF avec une LCC et un isthme, anormalement petits et

seulement des sujets SAF pour le genou et le splénium. Selon les courbes de *scaling*, cet excès ne subsiste que pour la LCC, les épaisseurs de l'isthme et du splénium.

Conclusion

Dans une large série de TSAF, nous avons caractérisé des anomalies indépendantes de la taille du cerveau, de la partie postérieure de la CC avec une méthode entièrement automatisée, confirmant et élargissant notre étude précédente. Notre nouvel outil rapproche l'utilisation d'un critère neuroanatomique incluant l'atteinte du CC de la pratique clinique et nos résultats renforcent la conviction qu'une signature du SAF pourrait être recherchée chez les TSAF-NS, ce qui pourrait améliorer la spécificité du diagnostic.

RÉSUMÉ GRAPHIQUE



Spectral-based thickness profiling of the corpus callosum in fetal alcohol spectrum disorders

Justine Fraize^{1,2*} | Yann Leprince¹ | Guillaume Auzias³ | Monique Elmaleh-Bergès⁴ | Lucie Hertz-Pannier^{1,2} | Julien Lefèvre^{†3} | David Germanaud^{†1,2,5*}

¹ CEA Paris-Saclay, Frederic Joliot Institute, NeuroSpin, UNIACT, Centre d'études de Saclay, Gif-sur-Yvette, France

² Université Paris Cité, Inserm, NeuroDiderot, InDEV, Paris, France

³ Aix-Marseille Université, CNRS, Institut de Neurosciences de La Timone, UMR7289, Marseille, France

⁴ Department of Pediatric Radiology, Centre of Excellence InovAND, AP-HP, Robert-Debré Hospital, Paris, France

⁵ Centre de Référence Déficiences Intellectuelles de Causes Rares, Department of Genetics, Centre of Excellence InovAND, Robert-Debré Hospital, AP-HP, Paris, France

[†]These authors have contributed equally to this work

*Correspondence:

Justine Fraize and David Germanaud, CEA Paris-Saclay, Joliot Institute, NeuroSpin, UNIACT, Centre d'études de Saclay, Bâtiment 145, 91191, Gif-sur-Yvette, France. Email: justine.fraize@inserm.fr and david.germanaud@cea.fr

Funding information:

French National Agency for Research; French National Institute for Public Health research

Abstract

Introduction

The diagnosis of fetal alcohol spectrum disorders (FASD) encompasses the pathological consequences of prenatal alcohol exposure, which range from fetal alcohol syndrome (FAS) to non-syndromic forms (NS-FASD). The main target of the teratogenic effects of ethanol is the brain, leading subjects with FASD to exhibit not only a smaller brain but also recurrent visible focal brain abnormalities such as the commonly reported abnormal corpus callosum (CC). We previously showed the narrowing of the CC for brain size, using manual measurement and its usefulness in a composite neuroanatomical criterion for diagnostic certainty. The aim of this study was to automate these measurements of the CC and identify recurrent abnormalities in FAS subjects, independently of brain size reduction.

Methods

We introduce an innovative, fast, fully automated, and normalization-free method to measure thicknesses of the corpus callosum continuously and at singular points (genu, body, isthmus, and splenium), in addition to its length (LCC)

We developed and applied this spectral-based thickness profiling to the midsagittal section of the CC extracted from a 1.5T 3DT1 brain MRI dataset of a monocentric population of 89 FASD (52 FAS, 37 NS-FASD) and 126 typically developing controls (6-20 years old). After adjusting for batch effect, we compared the mean profiles and thicknesses of the singular points across the 3 groups. For each parameter, we established variations with age (growth charts) and brain size in the control group (scaling charts), then identified participants with abnormal measurements (<10th percentile).

Results

We confirmed the thinning of the posterior half of the CC in both FASD groups, and of the genu section in the FAS group, compared to the control group. We found a significant group effect for the LCC, the genu, the median body, the isthmus, and the splenium thicknesses ($p < 0.05$). We described a body hump whose morphology did not differ between groups. According to the growth charts of each parameter, there was an excess of FASD subjects with abnormally small LCC, isthmus, and of FAS subjects only for the genu and the splenium. According to the scaling charts, this excess remained only for the LCC, the isthmus and the splenium thickness.

Conclusion

In a large series of FASD, we characterized size-independent anomalies of the posterior part of the CC with a fully automated method, confirming and extending our previous study. Our new tool brings the use of a neuroanatomical criterion including CC damage closer to clinical practice and our results reinforce the conviction that a signature of FAS can be searched for in NS-FASD, thereby improving the specificity of the diagnosis.

Keywords: Corpus callosum, fetal alcohol spectrum disorders, fetal alcohol syndrome, Spectral analysis

Abbreviations:

FASD, fetal alcohol spectrum disorder; FAS, fetal alcohol syndrome; FDR, false discovery rate; MRI, magnetic resonance imaging; NDD, neurodevelopmental disorders; NS-FASD, non-syndromic FASD.

1 | Introduction

The diagnosis of fetal alcohol spectrum disorders (FASD) encompasses the pathological consequences of prenatal alcohol exposure, which range from fetal alcohol syndrome (FAS) to non-syndromic, non-specific forms (NS-FASD) (Astley, 2004; Cook et al., 2016; Hoyme et al., 2016). The diagnosis of fetal alcohol syndrome (FAS) is determined by a consensual set of clinical features, which include facial dysmorphia, growth retardation, and microcephaly. On the other hand, the diagnosis of non-syndromic fetal alcohol spectrum disorder (NS-FASD), which associates neurodevelopmental disorders with prenatal alcohol exposure, remains probabilistic. The main target of the teratogenic effects of ethanol is the brain, leading individuals with FASD to exhibit not only a smaller brain but also recurrent focal brain abnormalities that are detectable via magnetic resonance imaging (MRI).

One of the most commonly reported focal brain abnormalities is the corpus callosum. This large bundle of white matter fibers composed of interhemispheric homotopic axonal projections turns out to be a privileged indicator of the consequences of prenatal alcohol exposure. The last four large radiological description studies reported thinning, hypoplasia, complete or partial agenesis of the corpus callosum in series composed of children either prenatally exposed or with a diagnosis of FASD (Autti-Rämö et al., 2002; Astley, 2004; Boronat et al., 2017; Treit et al., 2020; Fraize et al., 2023c). The prevalence of corpus callosum anomalies that are visible to the naked eye, although partly subjective, could approach 3 to 10% in the FASD population. Computational neuroimaging has sought to uncover more subtle anomalies or more objective morphometric descriptions. Several studies conducted on subjects with FASD

have suggested that the midsagittal corpus callosum area (Riley et al., 1995; Sowell et al., 2001; Astley et al., 2009; Dodge et al., 2009; Fraize et al., 2023c), thickness (Yang et al., 2012a), and volume (Gautam et al., 2014; Biffen et al., 2020; Inkelis et al., 2020) may be reduced compared to controls. These changes have also been correlated with the amount of prenatal alcohol consumption (Biffen et al., 2017; Jacobson et al., 2017). In addition to a global reduction in the size of the corpus callosum in FASD, the posterior region appears to be more severely affected in size (Sowell et al., 2001; Dodge et al., 2009; Fraize et al., 2023a) or in shape, resulting in a flattened or misshapen appearance (Sowell et al., 2001; Bookstein et al., 2002). However, these results need to be qualified, because even within the same team, they were not always confirmed. In the study by Yang et al., where three series from different sites were pooled, the thinning on the posterior part initially described (Sowell et al., 2001) was found to be significant in only one subgroup (Yang et al., 2012a). Despite these detailed descriptions, no neuroanatomical criterion referring explicitly to specific anomalies of the corpus callosum has been added to the diagnostic guidelines (Astley, 2004; Cook et al., 2016; Hoyme et al., 2016). Yet, we recently reported the narrowing of the isthmus to be a recurrent anomaly in FAS, using objective manual measurements of callosal thickness and normative scaling analysis (Fraize et al., 2023c), and proposed to integrate it into an explicit compound neuroanatomical marker in the diagnostic decision tree so that neuroanatomy can contribute to the clinical assessment at least of non-syndromic forms.

To our knowledge, there is no fully automated reference tool for the measurement of the corpus callosum thickness, let alone automated analysis

methods to tag and obtain individual measurements for singular points. Semi-automated measurement tools currently exist. For instance, Luders et al. proposed a technique beginning with manually delineating the corpus callosum on the sagittal midsection manually (Luders et al., 2006a). The upper and lower contours are then differentiated to compute the mean distance and generate the median line. The thickness of the corpus callosum is subsequently derived from this median line and compared at each interval. Following this pioneering study, the approach was implemented in the analysis of correlation with gender, IQ, and attention (Luders et al., 2006b, 2009, 2014; Westerhausen et al., 2011). Adamson et al. proposed another more automated method, albeit still involving human intervention (Adamson et al., 2011). Firstly, the two extremities are manually placed on the contour of the corpus callosum which is automatically generated. These two points are then adjusted to maximize the length of the center line. Subsequently, the center line is divided into 40 points. Finally, the thickness of the corpus callosum is determined by using either the orthogonality to the center line or by applying the Laplace equation. A fully automated method was proposed by Herron et al. based on a series of radial lines emanating from a centroid and intersecting the corpus callosum that are verticalized to unwrap the structure, define a median line and measure thickness (Herron et al., 2012; Li et al., 2017). The process relies on spatial normalization, the measurements being obtained in the *Montreal Neurological Institute* (MNI) space and transformed back to native anatomical space by inverting the affine spatial normalization transformation.

Regardless of how the thickness profile was obtained in these different studies (Sowell

et al., 2001; Luders et al., 2009; Yang et al., 2012b; Danielsen et al., 2020), the subsequent analyses and comparisons required normalization into a common space. This normalization step comes with a more or less explicit assumption on how callosal thickness is expected to vary with size, the reference for normalization being either a whole brain parameter or at least the corpus callosum length. It is also difficult to anticipate how these analyses would accommodate incompleteness of the structure, for instance posterior agenesis for the corpus callosum, in terms of distortions or loss of signal, depending on the choice of normalization or template (Mangin et al., 2016). Normalization-based procedures and the hypotheses that go with them are perfectly legitimate, but questionable when studying pathological populations, particularly when there is an impairment of the overall size of the brain or a risk of major dysgenesis of the structure being studied, which is the case with FASD and corpus callosum. At the very least, this encourages strategies of generation and analysis of the corpus callosum thickness profile that minimize the need for spatial normalization, let alone spatial averaging, and enable explicit size effect models to be implemented. Indeed, the local size deficits must be interpreted by taking global brain size into account (scaling analysis) with a model that allows proportions to vary with brain size (allometric scaling). The relevance of the power law to describe the phenomena associated with brain size variations is firmly established (Toro et al., 2009; Germanaud et al., 2012; Liu et al., 2014; de Jong et al., 2017; Warling et al., 2021; Fraize et al., 2023b).

In this study, we first introduce a new method that is fast and fully automated, based on a first step of spectral analysis of the shape of the corpus callosum, which

makes it possible to define and measure a continuous thickness profile at the individual level. We then propose a normalization-free strategy of analysis of this profile based on automatically defined local singular extrema. Lastly, we apply this spectral-based thickness profiling to a series of subjects with FASD and controls. We characterize brain size independent callosal anomalies in a fully automated manner, that were compared with the ones previously manually characterized in the same population (Fraize et al., 2023c).

2 | Materiel and methods

2.1 | Participants

Eighty-nine consecutive subjects with FASD, aged 6 to 20 years, were retrospectively included from a clinical series of patients attending the dedicated child neurology consultation for neurodevelopmental disorders at Robert-Debré University Hospital (RD) between 2014 and 2020. FASD diagnosis was established on the basis of the guidelines of Astley (Astley, 2004) and a full differential diagnosis work-up was completed, including a systematic brain MRI. Individuals prenatally exposed to another embryo-fetotoxic agent were not included. FASD subjects were split into two groups: the syndromic FAS (including partial FAS) and the non-syndromic ones (NS-FASD). This series and the precise diagnostic procedure have already been described in previous studies (Fraize et al., 2023b, 2023c). Clinical and radiological characteristics of the 52 FAS subjects (58.4%) and the 37 NS-FASD subjects (41.6%) are detailed in **Table 1**.

One hundred and twenty-six typically developing subjects, aged 6 to 20 years, with no report of PAE, developmental delay or family history of neurological or psychiatric condition (1st degree) were

included for comparison. A subgroup of 40 subjects was matched with the FASD group for the acquisition site (MRI scanner and sequence) as part of a research program on autism in the RD Psychiatry Department. Other typically developing subjects were part of previously published studies (Germanaud et al., 2014; Bouyeure et al., 2018).

There were no significant differences in the control group compared to the FASD group for sex (50.8% vs. 58.4% of males respectively, $p=0.334$) and age at MRI (12.08 vs.11.32 years of age respectively, $p=0.116$).

This study was conducted in accordance with the principles of the Declaration of Helsinki. Subjects' data were studied in accordance with French regulation (MR-004, declaration of conformity n°2059980v0), following approval by the Paris-Saclay research ethics committee (CER-Paris-Saclay-2020-094). Controls' data were used within the framework of the ethical authorizations of the primary studies (Gene and autism, Inserm C07-33, 08-029 and 11-008).

2.2 | MRI data

For both FASD subjects and 40 site-matched controls, MRI acquisitions were performed in the Department of Pediatric Radiology of RD Hospital at 1.5T (Ingenia, Philips Healthcare, Amsterdam, the Netherlands) with a 3DT1 FFE-TFE sequence (1 mm isotropic; TR = 8.2ms; TE = 3.8ms; TI = 0.8s; Flip = 8°; SENSE = 2). Another group of 31 controls was acquired at the Frédéric Joliot Hospital (SHFJ, CEA-Saclay) at 1.5T (Signa, GE Healthcare, Milwaukee, US) with a 3DT1 GE FSPGR sequence (1x1x1.2 mm; TR = 9.9ms; TE = 2ms; TI = 0.6s; Flip = 10°) and a third one of 55 controls subjects on a 3T (Siemens Trio, Siemens Healthineers, Oxford, UK) at

NeuroSpin (NS, CEA-Saclay) with a 3DT1 Siemens MPRAGE sequence (1mm isotropic; TR=2.3s; TE = 3ms; TI = 0.9s; Flip = 9°; GRAPPA 2). A visual quality check was systematically performed (JF, DG) to exclude images of insufficient quality.

2.3 | MRI processing

2.3.1 | Total brain volume

The total brain volume was obtained by *volBrain* (Manjón and Coupé, 2016), and was highly correlated ($R^2 = 75\%$) with the previously used proxy of brain size, that is, the axial reference brain surface (**sup. mat., Figure S1**)(Fraize et al., 2023c).

2.3.2 | Midsagittal section of the corpus callosum

The mask of the midsagittal section of the corpus callosum was obtained within the *Morphologist2015* framework of *BrainVisa* (<https://brainvisa.info/>) after oversampling of the T1-weighted images at 0.5 mm isotropic resolution. This section was localized in the interhemispheric plane by intersecting the white matter mask with the midsagittal plane in the Talairach space. The mask was checked systematically for any obvious segmentation error that could be manually corrected.

	FAS n = 52	NS-FASD n = 37	FASD groups comparison p-value
Sociodemographic assessment			
Sex: male n (%)	27 (51.9)	25 (67.6)	0.209
Age at MRI, mean in years (SD)	10.93 (3.57)	11.88 (3.55)	0.219
Clinical assessment, n (%)			
(1) Prenatal alcohol exposure			
4. Confirmed, severe	21 (40.4)	16 (43.2)	0.959
3. Confirmed, moderate or unquantified	26 (50.0)	19 (51.1)	1.000
2. Not documented	5 (9.6)	2 (5.4)	0.748
1. No exposure	0 (0.0)	0 (0.0)	-
(2) FAS facial features			
4. Severe	31 (59.6)	2 (5.4)	<0.001
3. Moderate	21 (40.3)	1 (2.7)	<0.001
2. Mild	0 (0.0)	30 (81.1)	<0.001
1. None	0 (0.0)	4 (10.8)	0.057
(3) Growth deficiency			
4. Significant	19 (36.5)	3 (8.1)	0.005
3. Moderate	11 (21.2)	2 (5.4)	0.077
2. Mild	9 (17.3)	9 (24.3)	0.586
1. None	13 (25.0)	23 (62.2)	0.001
Brain anatomy			
(4) Structural central nervous system damage	40 (76.9)	19 (51.4)	0.290
Head circumference (smallest known)			
(4) $\leq - 2$ SD: microcephaly	34 (65.4)	13 (35.1)	0.009

Table 1. Demographic, clinical, radiological data of FASD subjects. FAS: fetal alcohol syndrome; FASD: fetal alcohol spectrum disorder; NS-FASD: non-syndromic fetal alcohol spectrum disorder; SD: standard deviation. *In bold, p-values <0.05.*

2.3.3 | Spectral analysis of the shape using the Fiedler vector

From the mask of the midsagittal section of the corpus callosum, we built a graph based on 26-connectivity. We used the Fiedler vector of this graph, the first non-trivial eigenvector of the Laplacian matrix, to compute a quasi-isometric parameterization. This mathematical tool tracked the main elongation vector and identified extremal points. We added a simple algorithm to reposition the rostrum so that it was optimal (see details in **sup. mat., Figure S2**). The Laplacians graph were perturbed to create a 'new' Fiedler vector that followed the correct elongation (Lefèvre et al. 2023). We finally obtained a map of the corpus callosum thickness on regularly and optimally spaced slices (between 50 and 80) following the longitudinal orientation of the shape. The code used to perform spectral analysis of the corpus callosum midsagittal section is released on <https://github.com/JulienLefevreMars/CorpusCallosumParameterization>.

2.3.4 | Thickness profile and singular points

The first parameter of interest extracted was the length of the corpus callosum (LCC) obtained from the length of the curvilinear abscissa between the two extreme points. Then, we targeted the local singular extrema on the continuous thickness profile curve fitted with cubic smoothing spline (`smooth.spline()` R function). The smoothing parameters were set at the same level for each subject. *Spar* is the smoothing parameter controlling the trade-off between fidelity to the data and roughness of the function estimate. It is derived from the lambda parameter, scaled between 0 and 1. Here, we fixed the *spar* parameter at 0.4. We then extracted the positions and the thicknesses of the genu (GT) and the splenium (ST), the local

maximums of the two extremities, and of the isthmus (IT), the local minimum between these two points. In addition, we looked for localized thickening, a hump, within the body. As the amplitude of this thickening could potentially be small and to make sure that it was independent of curve smoothing variations, we sought it on the thickness profile curve between the genu and the isthmus, by varying the level of smoothing (10 levels in addition to the one initially chosen, from 0.2 to 0.7). To locate the body hump, we identified the local maximum(s) whose position was consensual on the curvilinear abscissa on more than 8 of the smoothing levels. We extracted the body hump thickness (BHT) or the mean thickness if there were several humps (no more than two). We also extracted the median of the thicknesses between the genu and the isthmus, as the median body thickness (MBT). All these processing steps are summed up in **Figure 1**.

These length and thickness parameters were correlated with available gold standard manual measures using the PACS measurement tools (Carestream, New York, NY, USA) (Fraize et al., 2023c) by establishing the coefficient of determination R^2 and the mean percentage error (MPE= mean of the difference between manual and automated measurements divided by manual measurement).

2.4 | Modeling and statistical analysis

Statistics were performed using R Project for Statistical Computing (RRID:SCR_001905), with a 5% alpha risk. A False Discovery Rate (FDR) method was systematically applied to correct for multiple comparisons (Benjamini and Hochberg, 1995) at each analysis step (all parameters together). Group differences in clinical characteristics and parameters were evaluated using two-sample *t*-tests

for continuous variables, and a Chi-square test for categorical variables, ANOVA for group effect.

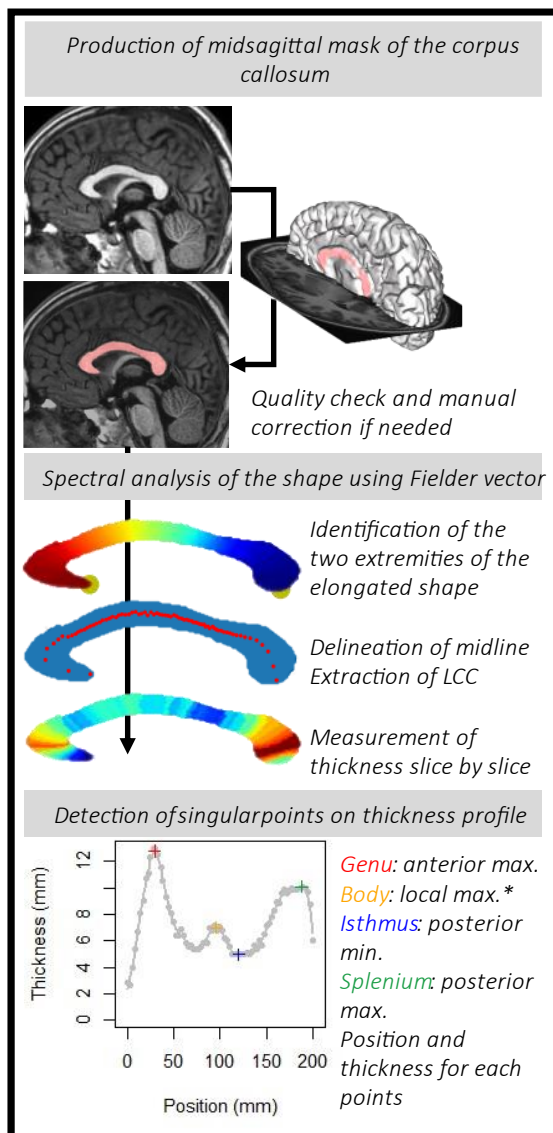


Figure 1. Pipeline to obtain the thickness profile for each subject and identify the points of interest: the genu, the body hump (*see details in the text and in Figure 3), the isthmus and the splenium.

Since the data were acquired on 3 sites, we adjusted for batch effect prior to analyses using ComBat, a method based on an empirical Bayes framework (Johnson et al., 2007; Fortin et al., 2018), integrating into the model sex, age, and diagnosis as covariates to be spared. We then performed unifactorial group comparisons

between FASD and controls knowing that these groups were matched for age and sex: first on the whole thickness profile after rigid length normalization to provide a continuous quantitative comparison of the radiological aspect of the corpus callosum, second on the five parameters previously defined (callosal length and the thickness of the 4 singular points). Lastly, we implemented clinically inspired normative analysis to provide an individual-based comparison of these five parameters, accounting for two major covariates i.e., age and brain size: first a normative growth analysis (age) then a normative scaling analysis (brain size).

2.4.1 | Unifactorial group comparison

We compared the thickness profiles of the controls with those of the two FASD groups. After rigid spatial normalization in the curvilinear abscissa axis, we oversampled thicknesses along this normed axis ($n = 100$) then adjusted for site effect. We studied the effect of FASD, using a linear mixed model considering diagnosis (controls vs. FAS or NS-FASD) as a fixed effect and random effect for each subject. Nonparametric cluster-based permutation analyses were carried out using a method inspired by EEG-MEG analysis to locate and group zones of significantly different thicknesses for spatial consistency (originally, time-points with temporal consistency in EEG signals), considering corrections for multiple comparisons (Maris and Oostenveld, 2007). Significance probability was calculated using the cluster-mass statistic (cluster-forming $\alpha = 0.05$, randomizations = 1000).

2.4.2 | Normative analyses

To define the growth curves, the relationships between measured parameters (LCC and thicknesses at singular points adjusted for site effect) and

age were modelled in the control group. We applied a general additive model considering homoscedasticity over the age range to fit the model and obtain percentiles of the distribution (Wood and Fasiolo, 2017; Dinga et al., 2021).

To define the scaling curves, the relationships between measured parameters (P) and brain size (total brain volume, TBV) were modelled by a power law with scaling coefficient a and constant b ($P = b \times TBV^a$) to take into account expected allometric effects (changes in proportions with size) (Liu et al., 2014; de Jong et al., 2017; Warling et al., 2021). Using bootstrap resampling and empirical quantiles, we obtained the unbiased prediction intervals (90th and 10th percentiles) (Guenther, 1971; Lee and Scholtes, 2014).

For each parameter, FASD subjects with measurements below the 10th percentile curve were counted as normatively too small for age or for brain size. An abnormality was considered recurrent when the number of too-small measurements in the FAS or NS-FASD group exceeded the theoretically expected 10% of the individuals (binomial test).

3 | Results

3.1 | Identification of singular points

The method was successfully applied to all subjects. For the two FAS subjects with posterior agenesis and the one with an obvious posterior thinning, the thickness profile was also extracted and analyzed (Figure 2). They were not included for

further analysis as they were obvious outliers with missing singular points.

From the thickness profiles, we were able to identify for each subject the position and thickness of the genu, isthmus and splenium automatically.

We divided the subjects into 4 types to define the presence or not of the body hump. In type 1, the position of the body hump was obvious and consensual for all smoothing levels, accounting for 78 subjects (36.8%). In type 2, the position of the body hump was obvious and consensual for more than 8 smoothing levels, accounting for 70 subjects (33.0%). In type 3, two body humps were obvious and consensual for more than 8 smoothing levels, accounting for 30 subjects (14.2%). In type 4, no body hump was identified, accounting for 34 subjects (16.0%) (Figure 3). The BHT was thus only considered for type 1, 2 and 3 subjects (n=178).

The measurements obtained by our method were strongly correlated ($R^2 > 50\%$), with the gold standard of manual measurements, the most highly correlated being that of the LCC ($R^2 = 90.3\%$) (Figure 4). For this measurement, the error was minimal (mean percentage error MPE=1.6%). This error was moderate for the isthmus, genu and splenium but systematically underestimated (positive MPE < 15%). The manual location for the body thickness measurement (at the central point) did not directly correspond to the measurements collected in the current study, resulting in larger MPE (~20%).

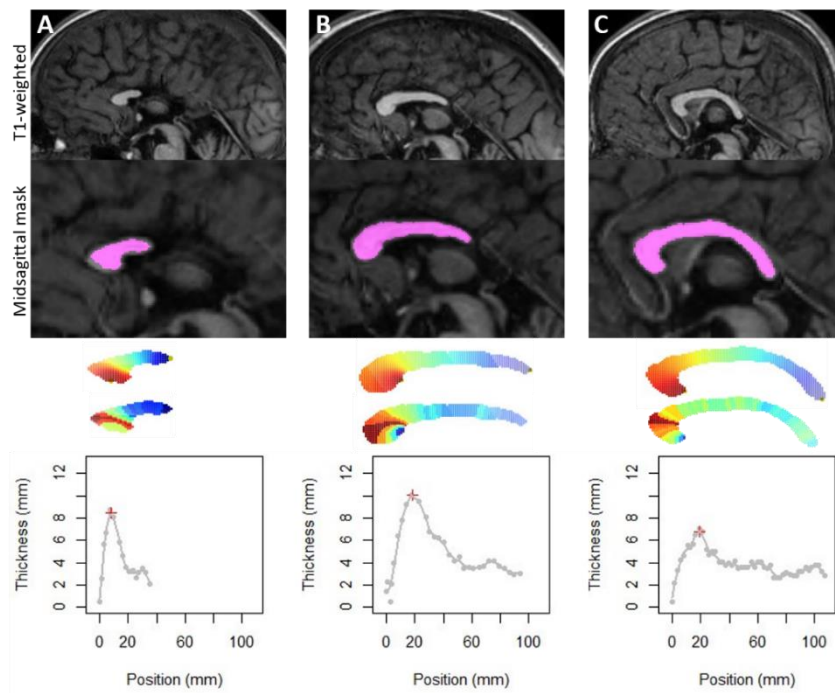


Figure 2. Application of the method on the three FAS subjects with partial agenesis (A, B) or with too thin corpus callosum (C), which could also be considered as a very posterior agenesis of the splenium. Note that our method detects the longest elongation and allows us to obtain thicknesses by slice. On the other hand, detection of singular points was not possible.

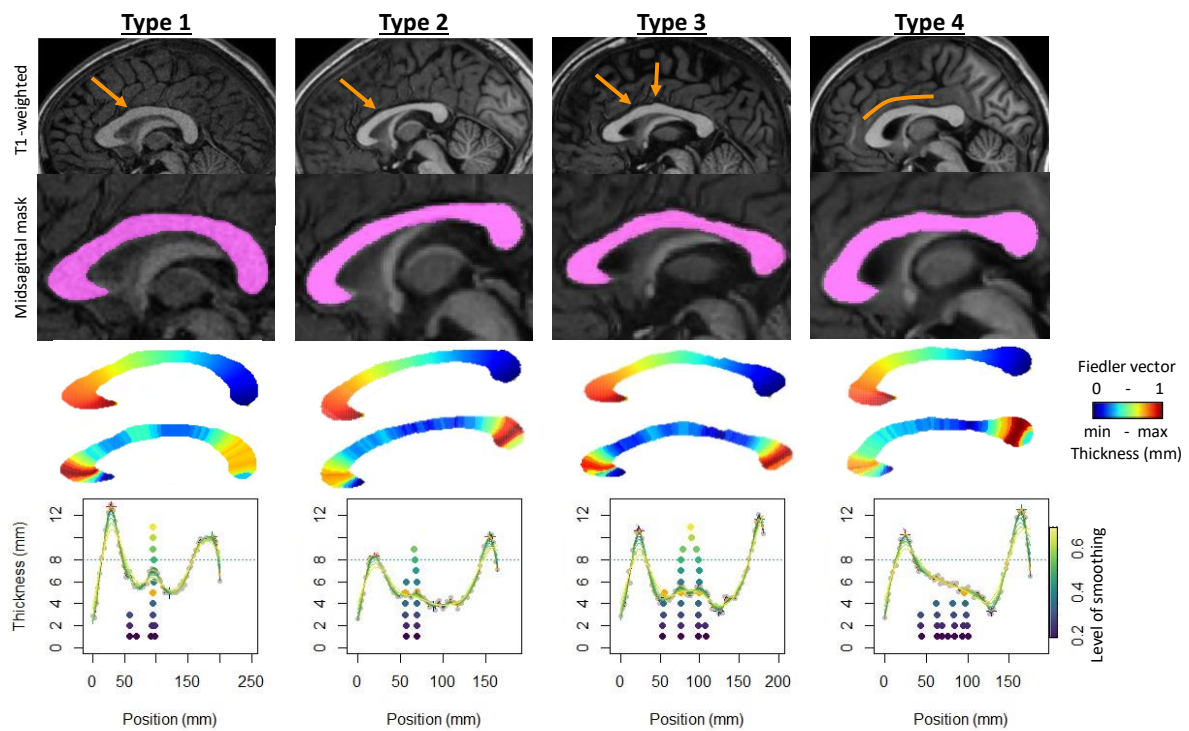


Figure 3. Body hump identification. Example of subject by group, variation of smoothing level to identify local maximums. First row: T1 anatomical image with location of the hump (orange arrow). Second row: the corpus callosum mask on sagittal midsection. Third row: Fiedler vector value (posterior-anterior gradient from 0 to 1). Fourth row: slice thickness (scaled gradient from red greatest to blue smallest thickness). Fifth row: thickness profile as a function of position along the curvilinear abscissa. Variation in smoothing level (colored curves) and position of local maximums between genu and isthmus, from lowest smoothing level (bottom dark purple point) to highest (top light-yellow point). Type I: position of the

body hump obvious and consensual for all smoothing levels. Type 2: position of the body hump obvious and consensual for more than 8 smoothing levels. Type 3: two body humps obvious and consensual for more than 8 smoothing levels. Type 4: no body hump.

Distribution of types by group control (C) and FASD (FAS and NS-FASD). Comparison of proportion of type between groups. ns: f not significant, p-value <0.05; p-values were adjusted for multiple comparisons using the FDR method.

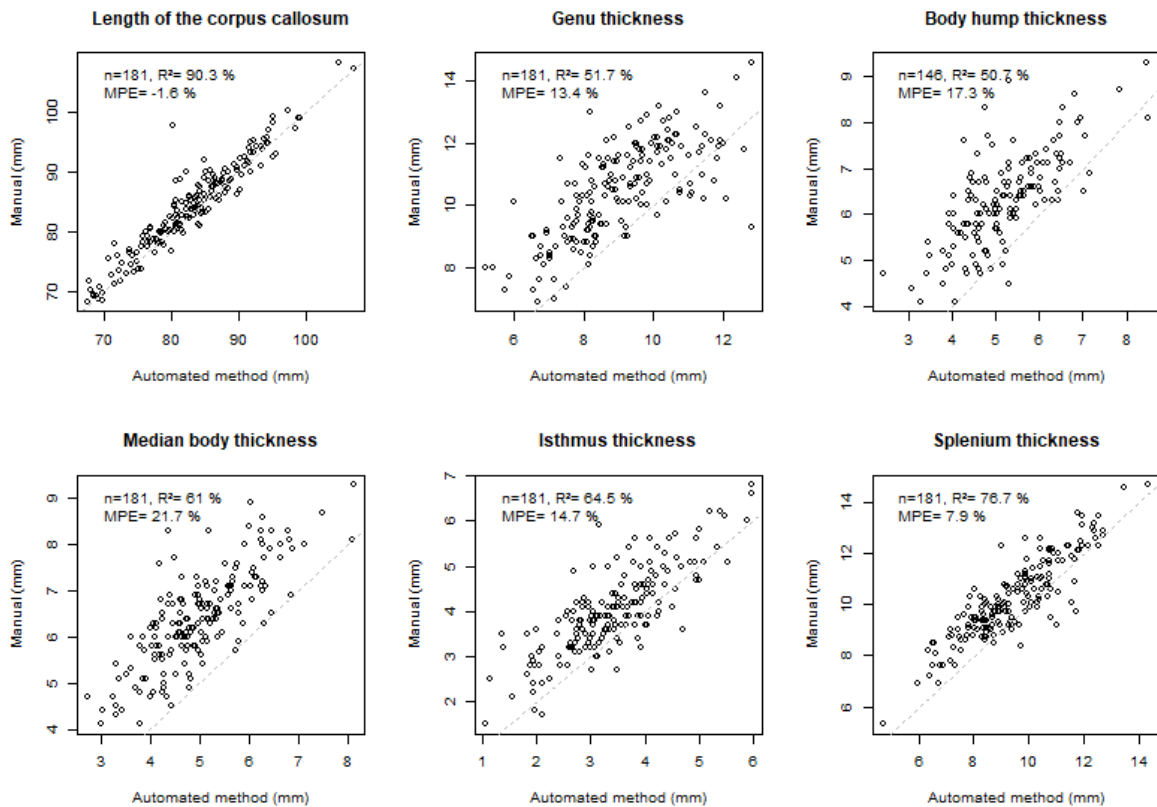
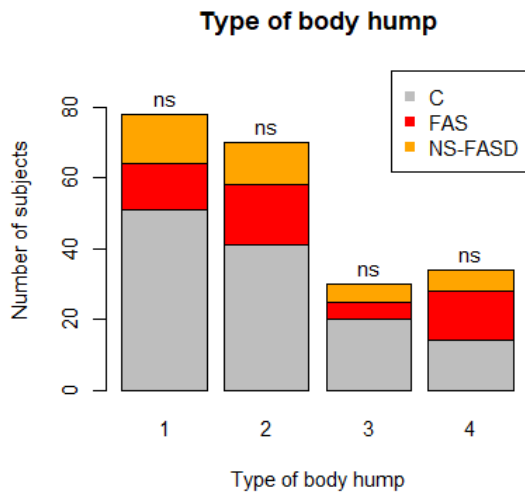


Figure 4. Comparison with manual measurements. Top left: number of subjects (n), coefficient of determination (R²), mean percentage error (MPE= mean of the difference between manual and automated measurements divided by manual measurement), correlation line 1 to 1 in grey dotted line.

3.2 | Control and FASD comparison

3.2.1 | Unifactorial comparison of thickness profiles

Comparing the thickness profiles of control and FAS subjects after rigid length normalization, we identified two significantly different sections, one around the genu and one consisting of the whole posterior half but with a peak in effect size in the anterior part of the splenium. For NS-FASD, the zone of significance was less extended, and limited to the posterior half (**Figure 5**).

3.2.2 | Unifactorial comparison of length and thickness of singular points

There was no significantly different proportion of body hump type between the FASD group and the control group. The distribution of types by groups is detailed in **Figure 3**.

A significant group effect was found for the length of the corpus callosum, the genu, the median body, the isthmus, and the

splenium thicknesses. The difference between the control group and the FAS group was significant for all parameters. The difference between the control group and the NS-FASD group was significant only for the length of the corpus callosum and the isthmus thickness ($p < 0.05$) (**Figure 6**).

3.3 | Normative analysis

3.3.1 | Growth charts

There was an excess of FASD subjects below the 10th percentile for the length of the corpus callosum, the isthmus, and only for FAS subjects for the genu and the splenium ($p < 0.05$) (**Figure 7**).

3.3.2 | Scaling charts

There was an excess of FAS subjects below the 10th percentile for the length of the corpus callosum, the isthmus, and the splenium ($p < 0.05$). NS-FASD subjects were not over-represented below the 10th percentile ($p > 0.05$) (**Figure 8**).

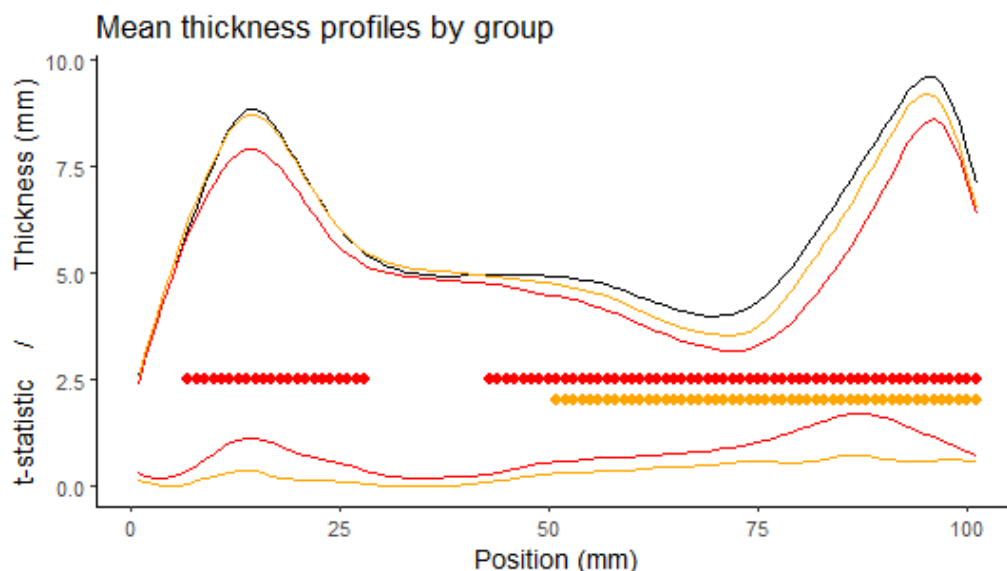


Figure 5. Comparison of the thickness profiles. First row: mean profile of the control group in black, the FAS group in red, the NS-FASD group in orange, after rigid spatial normalization. Second row: cluster of significantly different thicknesses (controls vs. FAS in red or NS-FASD in orange, p -value of cluster mass statistic < 0.05 , including adjustment for multiple comparisons). Third row: effect size (t-statistic of the linear mixed model).

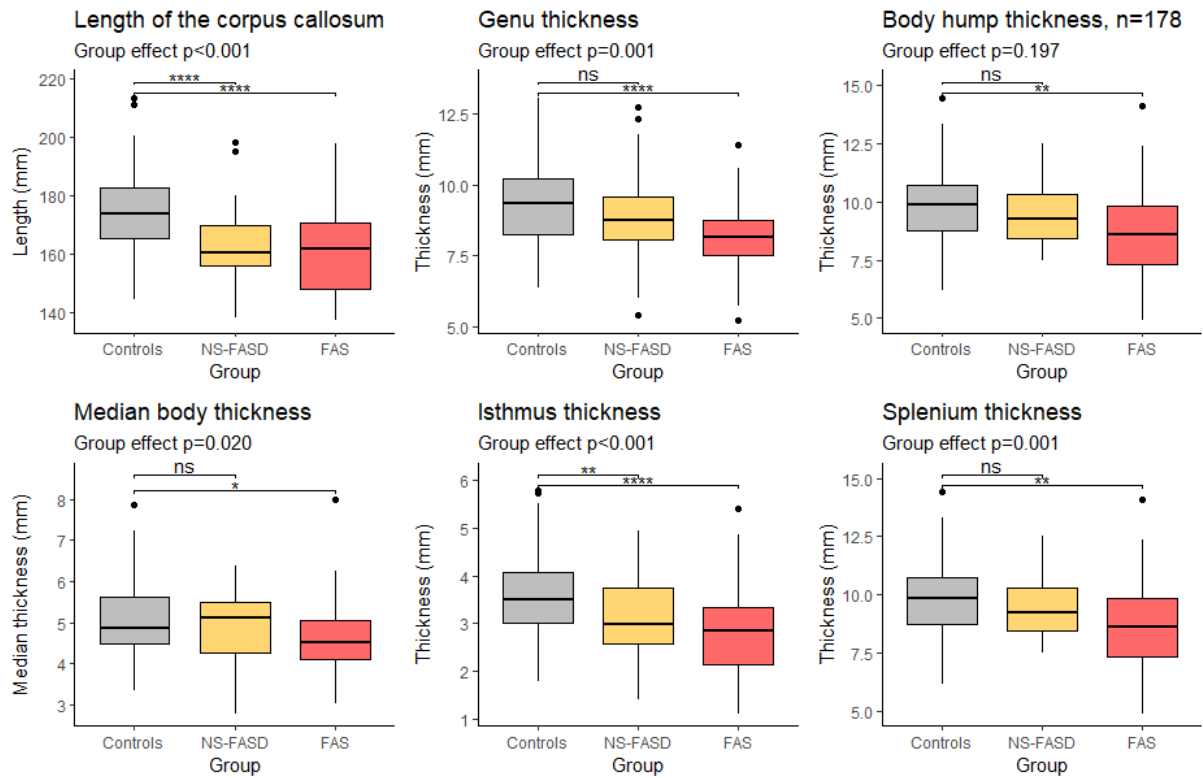


Figure 6. Comparison of length and thicknesses of singular points. Group effect (control, FAS and NS-FASD) on ANOVA. Top bracket, p-value of t-test of controls versus FAS or NS-FASD. ns: $p > 0.05$, *: $p \leq 0.05$, **: $p \leq 0.01$, ***: $p \leq 0.001$, ****: $p \leq 0.0001$. p-values were adjusted for multiple comparisons using the FDR method.

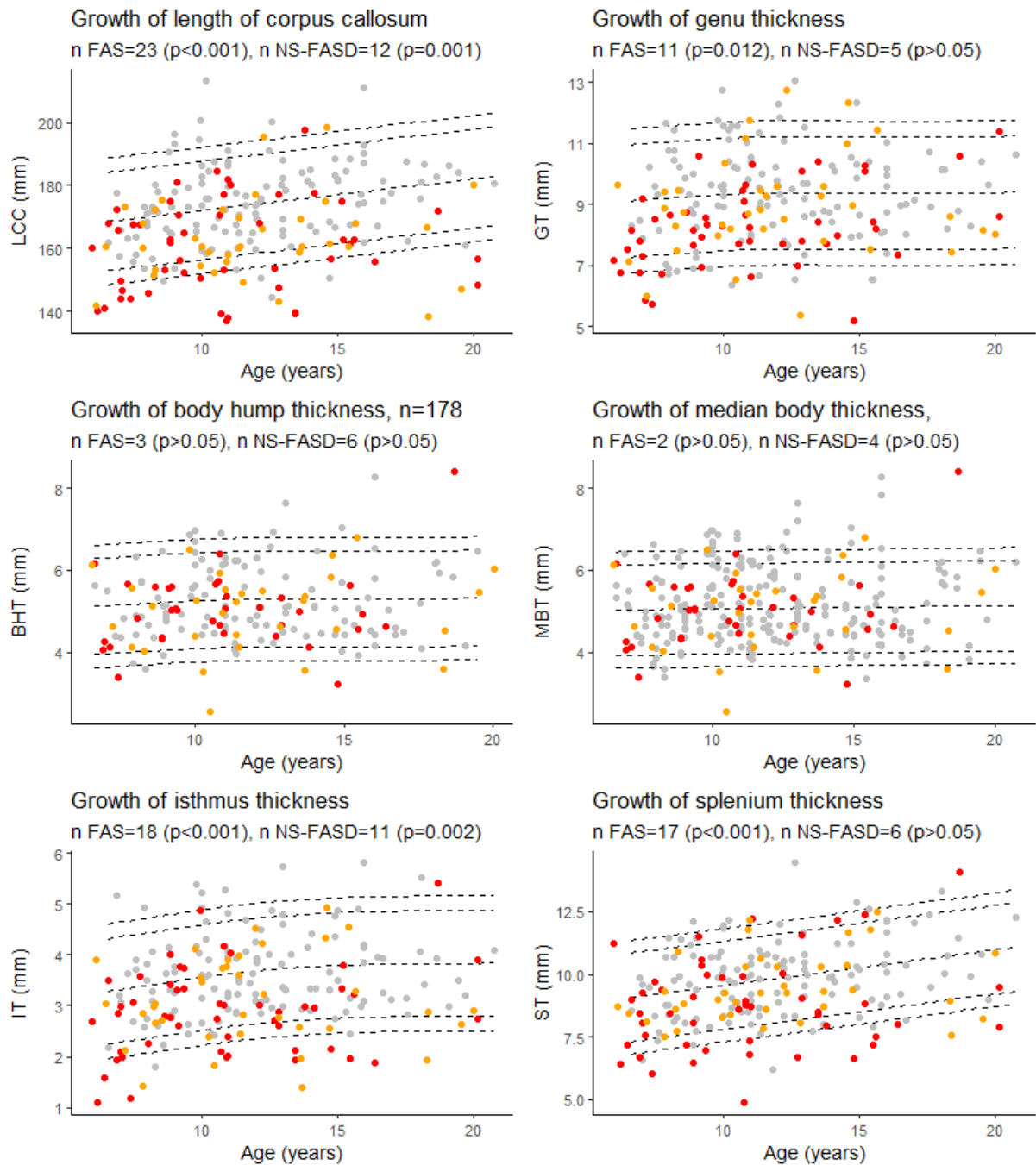


Figure 7. Growth charts for length of the corpus callosum (LCC), the genu (GT), the isthmus (IT), the body hump (BHT), the median body (MBT), and the splenium (ST) thicknesses. Number of fetal alcohol spectrum disorder subjects under the 10th percentile (p-values of binomial test, p-values were adjusted for multiple comparisons using the FDR method). Controls in grey, FAS in red, NS-FASD in orange. The 95, 90, 10 and 5th percentiles are represented in dotted lines.

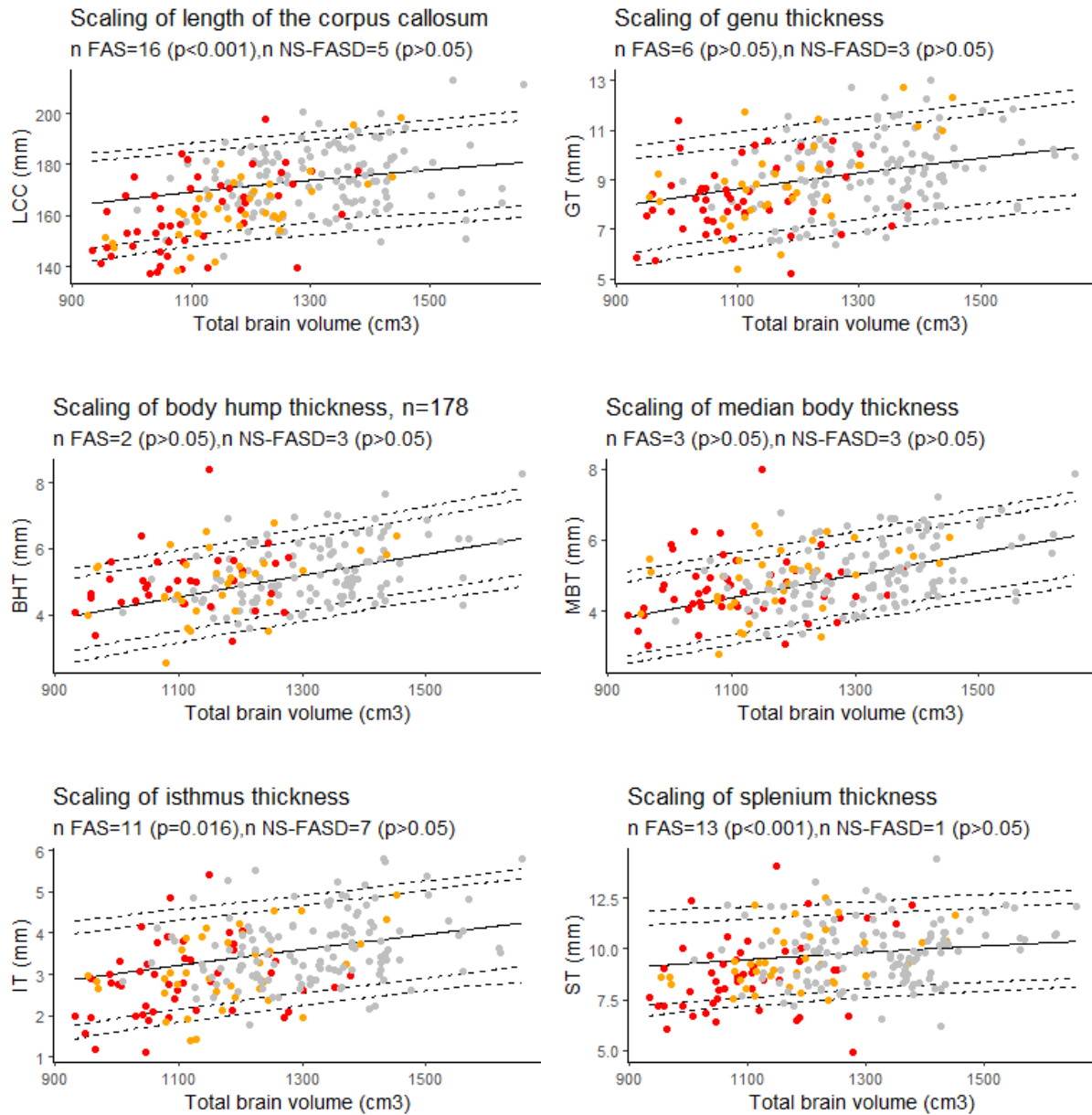


Figure 8. Scaling charts for length of the corpus callosum (LCC), the genu (GT), the isthmus (IT), the body hump (BHT), the median body (MBT), and the splenium (ST) thicknesses. Number of fetal alcohol spectrum disorder subjects under the 10th percentile (p-values of binomial test, p-values were adjusted for multiple comparisons using the FDR method.). Controls in grey, FAS in red, NS-FASD in orange. The 95, 90, 10 and 5th percentiles are represented in dotted lines.

4 | Discussion

In this study, we introduce the first fully automated, normalization-free, fast method to produce and analyze the thickness profile of the corpus callosum. We applied it to the morphometric comparison of 89 subjects with FASD to 126 typically developing controls, aged between 6 and 20 years old. We were able to show a large downsizing of the corpus callosum both in length and thickness in FAS, predominating in the posterior half and less pronounced in NS-FASD, and to establish that a recurring abnormal undersizing was observed in FAS only for the length and the isthmic and splenial thicknesses when controlling for brain size. Thus, these results with a new and convenient automated method not only replicate, but also extend our previous results with manual measurements including the same dataset, that were only able to show a recurrent isthmic anomaly (Fraize et al., 2023c).

4.1 | Confirmed and newly revealed differences between FASD and controls

4.1.1 | What can be observed on native measurements?

After rigid linear normalization and adjustment for site, native thickness profiles showed extensive but not homogeneous thinning of the corpus callosum in FASD. It was reduced in the posterior half section in both FAS and non-syndromic FASD subjects and reduced in the genu section only in FAS subjects (**Figure 5**). The rigid anteroposterior deformation coarsely aligns the thickness profiles of each subject, enabling an initial average assessment of what is visible to the radiologist in this population. It points to the posterior zone with a possible additional damage of the genu in FAS and

lower severity in NS-FASD.

Considering the native thickness of the four singular local extrema (genu, body hump, isthmus, and splenium), we observed significant differences between the FAS and the control groups for all of these extrema and between the NS-FASD and the control groups for the isthmus only (**Figure 6**). In addition to the locally conserved thickness of the body, we also showed the absence of impact of FAS on body hump morphology, since there was no significant difference in the proportion of body hump type between groups ($p < 0.05$) (**Figure 3**). Neither median or local thickness nor shape or number of body humps differed significantly between control and FASD subjects (**Figure 3 and 6**). Only one study has evoked the over-representation of “notching” among FAS subjects (Schneble et al., 2020), but it was applied in the medico-judicial context for FASD recognition and used a very qualitative assessment. We are therefore convinced that the body section between the genu and the isthmus including the body and the possible hump(s) should be considered as spared. Our results are consistent with the fact that the shape of the body section is a relevant, although not specific, marker of the FASD population and that this section is even relatively spared by global thinning.

We also showed that the overall length of the corpus callosum was reduced ($p < 0.001$) on average, with no other adjustment than site effect, in both NS-FASD and FAS (**Figure 6**). All these results are consistent with previous studies describing a smaller corpus callosum (Riley et al., 1995; Sowell et al., 2001; Astley et al., 2009; Biffen et al., 2017; Jacobson et al., 2017; Fraize et al., 2023c) and pointing out the posterior part as the most affected one (Sowell et al., 2001; Yang et al., 2012a; Fraize et al., 2023a). Even if our FASD and control groups were matched for age and sex,

there were inherent differences in brain size, both age and size having potentially nonlinear effects to be accounted for in further analyses.

4.1.2 | What remains at the individual level after independent control of major covariates?

Since birth, the shape of the corpus callosum changes as revealed by morphometric parameters (Rajapakse et al., 1996; Westerhausen et al., 2011; Herron et al., 2012). Within the increasingly promoted and clinically relevant framework of normative analyses, we proposed to take age into account on the basis of developmental growth charts derived from our typically developing control sample. We found FAS-recurrent anomalies (excess of FAS subjects below the 10th percentile) for the LCC, the genu, the isthmus, and the splenium thicknesses (**Figure 7**). This means that considering the age effect did not modify our previous description of the large downsizing of the corpus callosum both in length and thickness in FAS, predominating in the posterior half and in the genu. This minor effect of age on the measurements is consistent with asymptotic linear low (length, splenium) or null (other thicknesses) residual growth of the corpus callosum after 6 years already described in the typically developing pediatric population (Garel et al., 2011; Fraize et al., 2023c).

In the FASD population with brain growth deficiency (Archibald et al., 2001; Astley et al., 2009; Rajaprakash et al., 2014; Treit et al., 2016; Boronat et al., 2017), brain size must be properly considered when interpreting other neuroanatomical measurements. Thus, to describe the reduction of the corpus callosum measurements observed in FASD at the individual level, we added to the classical

normative analysis on growth charts (effect of age) the analysis on scaling charts (effect of size). We ensured that the scaling model fitted in the control group correctly projected to the smaller FASD range of brain sizes by using a biomathematical model that captures the gradual change in proportions along size range. This allometric scaling was modelled by a power law whose relevance and interest have been widely argued and documented (Germanaud et al., 2014; Liu et al., 2014; de Jong et al., 2017; Warling et al., 2021) and that is already used in anatomical descriptions of the corpus callosum in newborns (Lewis et al., 2022).

Hence, using allometry-sensitive scaling charts to account for brain size effect, we showed that thinning (below the 10th percentile) remained recurrently abnormal in FAS only for the isthmus and the splenium thickness (**Figure 8**). We additionally showed a significant excess of FAS subjects with undersized total LCC for their brain size (**Figure 8**). So with this analysis, we confirmed and extended the results of our previous study (Fraize et al., 2023c), by adding both brain size independent antero-posterior length and splenium thickness impairments to that of the isthmus. This involvement of the splenium is also consistent with our previous findings showing a reduction of its posterior half surface independent from hemispheric size (cortical surface) in a subsample of subjects (Fraize et al., 2023a).

These new findings may be explained by the greater number of controls (n=126 vs. 94), the more reliable estimate of brain size (total brain volume vs. surface of a reference brain area), the more elaborate model of regression and the more robust assessment of percentiles (Fraize et al., 2023c). The addition of the ComBat batch effect adjustment may also have improved sensitivity (see **sup. mat., Table S1**).

Previously, there was no significant site effect to be corrected in the manual measures (Fraize et al., 2023c). Moreover *post hoc* analyses without adjustment for batch effect showed no difference in the present results (data not shown). It could also just be that automated measurement of thickness of the splenium is more accurate and less noisy, enabling more discriminating statistical comparison.

4.1.3 | Potential neuroanatomical markers of FAS in corpus callosum

We did not find any size-independent recurrent anomalies taken one by one in our small NS-FASD subgroup. But for these subjects we have already proposed a perspective of cumulative diagnostic probability for diagnostic improvement (Fraize et al., 2023c). Arguably, that the likelihood of the causal link with alcohol exposure increases for NS-FASD subjects with one or more anomalies found to be recurrent in FAS in the final scaling analysis (LCC, IT, ST, in **Figure 8**). These results could provide an additional diagnostic argument and ease the way to more confident diagnoses in certain subjects presenting FASD without FAS.

Yet, the posterior damage of the corpus callosum and the preservation of the body is not specific to FASD, as it can be found in the general population (Glass et al., 2008) and in other neurodevelopmental disorders (Jeret et al., 1985). But we have previously argued that the whole singular profile of the corpus callosum should be associated to constitute a radiological signature which could increase diagnostic certainty, especially for subjects with a non-syndromic form. Other focal neuroanatomical anomalies such as cerebellar damage (O'Hare et al., 2005; Cardenas et al., 2014; Sullivan et al., 2020; Fraize et al., 2023b) or deep grey nuclei volume reduction (Nardelli et al., 2011;

Roussotte et al., 2012; Nakhid et al., 2022), could also be considered in a composite, multidimensional neuroanatomical score reflecting fetal alcohol-induced brain dysmorphia.

4.2 | New method for analyzing the shape of the corpus callosum

Our new method for corpus callosum shape analysis was developed to automatically detect the anterior point of the rostrum and decide on a posterior point of the splenium. Our method is advantageous over the existing ones because it does not require human intervention (Luders et al., 2006b; Adamson et al., 2011) and does not involve spatial normalization (Herron et al., 2012). In its current state, only the existence of a rostrum is considered, so that it can accommodate any posterior shape of the corpus callosum, since it is based on the maximum elongation of this two-dimensional shape. The three cases of agenesis or incomplete corpus callosum prove that this method is robust to variation of corpus callosum shape, even pathological (**Figure 2**), at least posterior ones. In these agenetic cases, we did not integrate the detection of singular points, which are not consensual and would require human supervision. For all subjects, this method produced continuous thicknesses along the entire length of the corpus callosum, and unequivocally detected singular local extrema at singular points (the genu, the hump of the body, the isthmus, and the splenium). Extracted thickness measurements were highly correlated with the gold standard manual measurements (**Figure 4**), despite a small to moderate underestimation (MPE<+15%). The manual process (the eye of the expert, but also the visualization smoothing included in the PACS viewer) and the automated one (the mask of the corpus callosum segmented on the basis of

the contrast between white, grey matter and CSF) deal with partial volume effects on the edges differently, resulting in a more skinny or even eroded profile in the second case, with logically a higher MPE for small measures than for large ones (genu, body, isthmus). Bear in mind that noise could also be induced by inaccuracy of the thinnest measurements close to the resolution of the oversampled mask (0.5 x 0.5mm). Finally, even if manual measurement is the gold standard, the automated method may be more objective, reproducible, and less sensitive to global brain shape variation.

The first step, i.e. producing the mask of the corpus callosum on the sagittal section, may seem trivial but is in fact a decisive one. In our pipeline, this step was based on robust intensity-based *Morphologist* segmentation bricks, but a quality check was systematically performed, and manual corrections were sometimes necessary. An improvement of our method could come from the use of other software able to provide the 2D voxel-based mask necessary to the rest of the process, for example *Freesurfer* or any new and specific methods (Adamson et al., 2014; Herrera et al., 2022), without modifying the subsequent steps. Ultimately, although not all steps are encapsulated and seamlessly connected, our new tool offers the advantage of having extremely short and computationally inexpensive steps. As a result, the cumulative computation time per subject to generate numerical parameters is less than 5 minutes.

On a methodological aspect, the correction of the Fiedler vector to reposition the rostrum is an example of supervised information in an unsupervised context (Lefevre et al., 2023). It may be possible in the future to add other kinds of information, of various kinds (lines), to add constraints on the Fiedler vector or more

generally on the Laplacian modes. More broadly, the developed methodological tool based on the Fiedler vector opens the way to other fields of characterization of the shape of the corpus callosum, such as the circularity, the surface per slice, or deformation per section, which could be the object of further study (Walsh et al., 2019).

For now, as far as we know, this is the only fully automated method without any human intervention and normalization step for obtaining corpus callosum thicknesses. In fact, its use could go far beyond FASD and be applied in other pathologies where the morphology of the corpus callosum needs to be described.

4.3 | Translating to daily clinical practice

In this study, we aimed to establish an analysis protocol that would ultimately be compatible with translation to the clinical practice. The ultimate goal is to switch from manual measurements, which may be imprecise and noisy if non-expert, to secure computational automated and fast measurements, which could be facilitated by a computer interface. By producing measurements that correspond to those already made in clinical settings (Garel et al., 2011; Ambrosino et al., 2022; Fraize et al., 2023c), maybe even by improving the objectivity of their anatomical positioning, the proposed tool and analysis protocol should be acceptable in clinical practice, especially since it leads to a normative analysis and therefore to categorical (normal, abnormal) information at the individual level.

Based on easy-to-use scaling charts and a proper biomathematical scaling model, we propose a method for detecting subject-level abnormalities, even with the partial overlap of brain size between patients and controls. However, the choice of reference

population and adequacy of the control group raise questions. Our study included 126 typically developing individuals matched for age and sex, with no prenatal exposure. The automated segmentation, profiling, and singular local extrema detection enable the use of large imaging databases to establish more reliable charts, potentially stratified by age and sex. Despite the need to address site effects, our results show that a population of over a hundred controls currently allows for the establishment of informative normative charts.

4.4 | Identification of a singular thickening of the body section in the general population

Our method leads to the description of a possible anatomical particularity of the corpus callosum, in FASD and more generally in healthy subjects. We identified a local thickening of the body section, either single (~70%) or double (16%) in most of the subjects (**Figure 4**). This local maximum of the thickness profile between the genu and the isthmus was automatically identified by using multi-scale-smoothed profiles inspired by scaled space implementation detecting robust maxima through a range of smoothing levels. The literature on this morphological feature in the general population is sparse (Krause et al., 2019; Simpson et al., 2020). Krause et al., reviewed MR images of the corpus callosum of over 1,600 healthy subjects and denominated concavities in the dorsal surface "undulations" and "notching". They found 50% of subjects with one notch and around 10% with two, and therefore possibly equivalent proportions of localized thickening.

To compensate for the lack of consensus on the actual existence of this hump and the absence of an exact definition for the location of the body thickness

measurement (Garel et al., 2011), we decided to add the median of the body thickness for all subjects. This corresponds to the median value of the thicknesses on the section between the genu and the isthmus. Although it was somewhat arbitrary, it correlated well with the manual measurement ($R^2 = 61\%$). In practice, and even if this is a finalist argument, the results were ultimately consistent between the two measures.

4.5 | Other limitations and future directions

One limitation of the proposed modeling for analyses is the lack of consideration of the effect of sex (Ardekani et al., 2013; Lewis et al., 2022). We made this choice on the hypothesis that the downsizing of the control sample by a factor of two to establish sex specific charts would have lowered the statistical power of our study too much and we would have increased the risk of missing results, even with a reduced residual variance due to better adequacy of the modeling. It is a questionable choice that we also made and argued for our previous study, showing that results were almost unaffected (meaning that with this population size, the two choices may probably be equivalent). Yet as mentioned previously, with larger databases being available, it will be more efficient, even with clinical applications in mind, to establish differentiated female/male referential charts. It could also very well lead to the description of differential FAS-related abnormalities and markers between males and females (Chen et al., 2011; Zhou et al., 2018; Little and Beaulieu, 2020; Treit et al., 2020).

The limitations associated to our cohort of FASD subjects are multiple: retrospective data, absence of quantitative data on the level of exposure, over-representation of FAS subjects. But we would like to confirm,

since this is not possible or recommended in all countries, that in our practice, brain imaging is systematic and that there is no predictable bias in severity or clinical representation.

5 | Conclusion

Our study is the first to propose a fully automated tool to assess the corpus callosum thickness profile along its curvilinear abscissa and analyze it through the identification of 4 singular points. We used it to describe the callosal damage in a large cohort of FASD, confirming the excessive thinning of the isthmus for brain size and revealing the global excessive shortening of the corpus callosum and thinning of the splenium for brain size to be recurrent anomalies in FAS subjects. The introduction of this tool in clinical practice is at hand and our study completes the knowledge on FASD callosal damage and reinforces the conviction that a neuroanatomical signature of FAS could be searched for in NS-FASD to improve the specificity of the diagnosis.

Acknowledgements

The authors would like to thank the volunteers, patients and families, and the French supportive association for FASD-affected families “Vivre avec le SAF.”

Funding information

This study was supported by the French National Agency for Research (ANR-19-CE17-0028-01) and the French National Institute for Public Health research (IRES-19-ADDICTIONS-08).

Conflict of interest statement

The authors have no conflicts of interest to disclose.

Data availability statement

The data that support the findings of this study are available on request from the corresponding author. The data are not publicly available due to privacy or ethical restrictions.

ORCID

Justine Fraize <https://orcid.org/0000-0001-6434-7992>

Yann Leprince <https://orcid.org/0000-0002-1846-3869>

Guillaume Auzias <https://orcid.org/0000-0002-0414-5691>

Monique Elmaleh-Bergès <https://orcid.org/0000-0001-8190-8202>

Lucie Hertz-Pannier <https://orcid.org/0000-0003-4952-7009>

Julien Lefèvre <https://orcid.org/0000-0003-3670-6112>

David Germanaud <https://orcid.org/0000-0001-5055-4624>

References

- Adamson, C., Beare, R., Walterfang, M., and Seal, M. (2014). Software Pipeline for Midsagittal Corpus Callosum Thickness Profile Processing: Automated Segmentation, Manual Editor, Thickness Profile Generator, Group-Wise Statistical Comparison and Results Display. *Neuroinform* 12, 595–614. doi: 10.1007/s12021-014-9236-3.
- Adamson, C. L., Wood, A. G., Chen, J., Barton, S., Reutens, D. C., Pantelis, C., et al. (2011). Thickness profile generation for the corpus callosum using Laplace's equation. *Hum. Brain Mapp.* 32, 2131–2140. doi: 10.1002/hbm.21174.
- Ambrosino, S., Elbendary, H., Lequin, M., Rijkkelijkhuizen, D., Banaschewski, T., Baron-Cohen, S., et al. (2022). In-depth characterization of neuroradiological findings in a large sample of individuals with autism spectrum disorder and controls. *Neuroimage Clin* 35, 103118. doi: 10.1016/j.nicl.2022.103118.
- Archibald, S. L., Fennema-Notestine, C., Gamst, A., Riley, E. P., Mattson, S. N., and Jernigan, T. L. (2001). Brain dysmorphology in individuals with severe prenatal alcohol exposure. *Developmental Medicine & Child Neurology* 43, 148–154. doi: <https://doi.org/10.1111/j.1469-8749.2001.tb00179.x>.
- Ardekani, B. A., Figarsky, K., and Sidtis, J. J. (2013). Sexual dimorphism in the human corpus callosum: an MRI study using the OASIS brain database. *Cereb Cortex* 23, 2514–2520. doi: 10.1093/cercor/bhs253.
- Astley, S. J. (2004). Diagnostic guide for fetal alcohol spectrum disorders: The 4-digit diagnostic code. *Astley SJ. Diagnostic Guide for Fetal Alcohol Spectrum Disorders: The 4-Digit Diagnostic Code. 3rd edition University of Washington Publication Services, Seattle, WA: 2004. Available from: <http://depts.washington.edu/fasdpn/pdfs/guide04.pdf>*, 123.
- Astley, S. J., Aylward, E. H., Olson, H. C., Kerns, K., Brooks, A., Coggins, T. E., et al. (2009). Magnetic resonance imaging outcomes from a comprehensive magnetic resonance study of children with fetal alcohol spectrum disorders. *Alcohol Clin Exp Res* 33, 1671–1689. doi: 10.1111/j.1530-0277.2009.01004.x.
- Autti-Rämö, I., Autti, T., Korkman, M., Kettunen, S., Salonen, O., and Valanne, L. (2002). MRI findings in children with school problems who had been exposed prenatally to alcohol. *Dev Med Child Neurol* 44, 98–106. doi: 10.1017/s0012162201001748.
- Benjamini, Y., and Hochberg, Y. (1995). Controlling the False Discovery Rate: A Practical and Powerful Approach to Multiple Testing. *Journal of the Royal Statistical Society: Series B (Methodological)* 57, 289–300. doi: 10.1111/j.2517-6161.1995.tb02031.x.
- Biffen, S. C., Warton, C. M. R., Dodge, N. C., Molteno, C. D., Jacobson, J. L., Jacobson, S. W., et al. (2020). Validity of automated FreeSurfer segmentation compared to manual tracing in detecting prenatal alcohol exposure-related

- subcortical and corpus callosal alterations in 9- to 11-year-old children. *Neuroimage Clin* 28, 102368. doi: 10.1016/j.nicl.2020.102368.
- Biffen, S. C., Warton, C. M. R., Lindinger, N. M., Randall, S. R., Lewis, C. E., Molteno, C. D., et al. (2017). Reductions in Corpus Callosum Volume Partially Mediate Effects of Prenatal Alcohol Exposure on IQ. *Front Neuroanat* 11, 132. doi: 10.3389/fnana.2017.00132.
- Bookstein, F. L., Sampson, P. D., Connor, P. D., and Streissguth, A. P. (2002). Corpus Callosum Shape and Neuropsychological Deficits in Adult Males with Heavy Fetal Alcohol Exposure. *Anat Rec* 269, 162–174. doi: 10.1002/ar.10110.
- Boronat, S., Sánchez-Montañez, A., Gómez-Barros, N., Jacas, C., Martínez-Ribot, L., Vázquez, E., et al. (2017). Correlation between morphological MRI findings and specific diagnostic categories in fetal alcohol spectrum disorders. *Eur J Med Genet* 60, 65–71. doi: 10.1016/j.ejmg.2016.09.003.
- Bouyeure, A., Germanaud, D., Bekha, D., Delattre, V., Lefèvre, J., Pinabiaux, C., et al. (2018). Three-Dimensional Probabilistic Maps of Mesial Temporal Lobe Structures in Children and Adolescents' Brains. *Front Neuroanat* 12, 98. doi: 10.3389/fnana.2018.00098.
- Cardenas, V. A., Price, M., Infante, M. A., Moore, E. M., Mattson, S. N., Riley, E. P., et al. (2014). Automated cerebellar segmentation: Validation and application to detect smaller volumes in children prenatally exposed to alcohol. *NeuroImage: Clinical* 4, 295–301. doi: 10.1016/j.nicl.2014.01.002.
- Chen, X., Coles, C. D., Lynch, M. E., and Hu, X. (2011). Understanding specific effects of prenatal alcohol exposure on brain structure in young adults. *Hum Brain Mapp* 33, 1663–1676. doi: 10.1002/hbm.21313.
- Cook, J. L., Green, C. R., Lilley, C. M., Anderson, S. M., Baldwin, M. E., Chudley, A. E., et al. (2016). Fetal alcohol spectrum disorder: A guideline for diagnosis across the lifespan. *Canadian Medical Association Journal* 188, 191–197. doi: 10.1503/cmaj.141593.
- Danielsen, V. M., Vidal-Piñeiro, D., Mowinckel, A. M., Sederevicius, D., Fjell, A. M., Walhovd, K. B., et al. (2020). Lifespan trajectories of relative corpus callosum thickness: Regional differences and cognitive relevance. *Cortex* 130, 127–141. doi: 10.1016/j.cortex.2020.05.020.
- de Jong, L. W., Vidal, J.-S., Forsberg, L. E., Zijdenbos, A. P., Haight, T., Alzheimer's Disease Neuroimaging Initiative, et al. (2017). Allometric scaling of brain regions to intracranial volume: An epidemiological MRI study. *Hum Brain Mapp* 38, 151–164. doi: 10.1002/hbm.23351.
- Dinga, R., Frazza, C. J., Bayer, J. M. M., Kia, S. M., Beckmann, C. F., and Marquand, A. F. (2021). Normative modeling of neuroimaging data using generalized additive models of location scale and shape. 2021.06.14.448106. doi: 10.1101/2021.06.14.448106.
- Dodge, N. C., Jacobson, J. L., Molteno, C. D.,

- Meintjes, E. M., Bangalore, S., Diwadkar, V., et al. (2009). Prenatal Alcohol Exposure and Interhemispheric Transfer of Tactile Information: Detroit and Cape Town Findings. *Alcoholism: Clinical and Experimental Research* 33, 1628–1637. doi: 10.1111/j.1530-0277.2009.00994.x.
- Fortin, J.-P., Cullen, N., Sheline, Y. I., Taylor, W. D., Aselcioglu, I., Cook, P. A., et al. (2018). Harmonization of cortical thickness measurements across scanners and sites. *Neuroimage* 167, 104–120. doi: 10.1016/j.neuroimage.2017.11.024 .
- Fraize, J., Convert, G., Leprince, Y., Sylvestre-Marconville, F., Kerdreux, E., Auzias, G., et al. (2023a). Mapping corpus callosum surface reduction in fetal alcohol spectrum disorders with sulci and connectivity-based parcellation. *Frontiers in Neuroscience* 17. Available at: <https://www.frontiersin.org/articles/10.3389/fnins.2023.1188367> [Accessed June 26, 2023].
- Fraize, J., Fischer, C., Elmaleh-Bergès, M., Kerdreux, E., Beggiato, A., Ntorkou, A., et al. (2023b). Enhancing fetal alcohol spectrum disorders diagnosis with a classifier based on the intracerebellar gradient of volumetric undersizing. *Hum Brain Mapp*. doi: 10.1002/hbm.26348.
- Fraize, J., Garzón, P., Ntorkou, A., Kerdreux, E., Boespflug-Tanguy, O., Beggiato, A., et al. (2023c). Combining neuroanatomical features to support diagnosis of fetal alcohol spectrum disorders. *Dev Med Child Neurol* 65, 551–562. doi: 10.1111/dmcn.15411.
- Garel, C., Cont, I., Alberti, C., Josserand, E., Moutard, M. L., and Ducou le Pointe, H. (2011). Biometry of the Corpus Callosum in Children: MR Imaging Reference Data. *AJNR Am J Neuroradiol* 32, 1436–1443. doi: 10.3174/ajnr.A2542.
- Gautam, P., Nuñez, S. C., Narr, K. L., Kan, E. C., and Sowell, E. R. (2014). Effects of prenatal alcohol exposure on the development of white matter volume and change in executive function. *NeuroImage: Clinical* 5, 19–27. doi: 10.1016/j.nicl.2014.05.010.
- Germanaud, D., Lefèvre, J., Fischer, C., Bintner, M., Curie, A., des Portes, V., et al. (2014). Simplified gyral pattern in severe developmental microcephalies? New insights from allometric modeling for spatial and spectral analysis of gyrification. *Neuroimage* 102 Pt 2, 317–331. doi: 10.1016/j.neuroimage.2014.07.057 .
- Germanaud, D., Lefèvre, J., Toro, R., Fischer, C., Dubois, J., Hertz-Pannier, L., et al. (2012). Larger is twistier: spectral analysis of gyrification (SPANGY) applied to adult brain size polymorphism. *Neuroimage* 63, 1257–1272. doi: 10.1016/j.neuroimage.2012.07.053 .
- Glass, H. C., Shaw, G. M., Ma, C., and Sherr, E. H. (2008). Agenesis of the corpus callosum in California 1983-2003: a population-based study. *Am J Med Genet A* 146A, 2495–2500. doi: 10.1002/ajmg.a.32418.
- Guenther, W. C. (1971). Unbiased

- Confidence Intervals. *The American Statistician* 25, 51–53. doi: 10.2307/2682218.
- Herrera, W., Appenzeller, S., Reis, F., Pereira, D., Bento, M., and Rittner, L. (2022). *Automated quality check of corpus callosum segmentation using deep learning*. doi: 10.1117/12.2612835.
- Herron, T. J., Kang, X., and Woods, D. L. (2012). Automated measurement of the human corpus callosum using MRI. *Front Neuroinform* 6, 25. doi: 10.3389/fninf.2012.00025.
- Hoyme, H. E., Kalberg, W. O., Elliott, A. J., Blankenship, J., Buckley, D., Marais, A.-S., et al. (2016). Updated Clinical Guidelines for Diagnosing Fetal Alcohol Spectrum Disorders. *Pediatrics* 138. doi: 10.1542/peds.2015-4256.
- Inkelis, S. M., Moore, E. M., Bischoff-Grethe, A., and Riley, E. P. (2020). Neurodevelopment in adolescents and adults with fetal alcohol spectrum disorders (FASD): A magnetic resonance region of interest analysis. *Brain Res* 1732, 146654. doi: 10.1016/j.brainres.2020.146654.
- Jacobson, S. W., Jacobson, J. L., Molteno, C. D., Warton, C. M. R., Wintermark, P., Hoyme, H. E., et al. (2017). Heavy Prenatal Alcohol Exposure is Related to Smaller Corpus Callosum in Newborn MRI Scans. *Alcohol Clin Exp Res* 41, 965–975. doi: 10.1111/acer.13363.
- Jeret, J. S., Serur, D., Wisniewski, K., and Fisch, C. (1985). Frequency of agenesis of the corpus callosum in the developmentally disabled population as determined by computerized tomography. *Pediatr Neurosci* 12, 101–103. doi: 10.1159/000120229.
- Johnson, W. E., Li, C., and Rabinovic, A. (2007). Adjusting batch effects in microarray expression data using empirical Bayes methods. *Biostatistics* 8, 118–127. doi: 10.1093/biostatistics/kxj037.
- Krause, K. L., Howard, D., Pettersson, D. R., Elstrott, S., Ross, D., Obayashi, J. T., et al. (2019). Defining the Normal Dorsal Contour of the Corpus Callosum with Time. *AJNR Am J Neuroradiol* 40, 86–91. doi: 10.3174/ajnr.A5886.
- Lee, Y. S., and Scholtes, S. (2014). Empirical prediction intervals revisited. *International Journal of Forecasting* 30, 217–234. doi: 10.1016/j.ijforecast.2013.07.018.
- Lefevre, J., Fraize, J., and Germanaud, D. (2023). Perturbation of Fiedler vector: interest for graph measures and shape analysis. in *Geometric Science of Information Lecture Notes in Computer Science*. (Cham: Springer International Publishing).
- Lewis, J. D., Acosta, H., Tuulari, J. J., Fonov, V. S., Collins, D. L., Scheinin, N. M., et al. (2022). Allometry in the corpus callosum in neonates: Sexual dimorphism. *Human Brain Mapping* 43, 4609–4619. doi: 10.1002/hbm.25977.
- Li, Z., Li, C., Fan, L., Jiang, G., Wu, J., Jiang, T., et al. (2017). Altered microstructure rather than morphology in the corpus callosum after lower limb amputation. *Scientific Reports* 7, 44780. doi:

- 10.1038/srep44780.
- Little, G., and Beaulieu, C. (2020). Multivariate models of brain volume for identification of children and adolescents with fetal alcohol spectrum disorder. *Hum Brain Mapp* 41, 1181–1194. doi: 10.1002/hbm.24867.
- Liu, D., Johnson, H. J., Long, J. D., Magnotta, V. A., and Paulsen, J. S. (2014). The power-proportion method for intracranial volume correction in volumetric imaging analysis. *Front Neurosci* 8, 356. doi: 10.3389/fnins.2014.00356.
- Luders, E., Narr, K. L., Hamilton, L. S., Phillips, O. R., Thompson, P. M., Valle, J. S., et al. (2009). Decreased callosal thickness in attention-deficit/hyperactivity disorder. *Biol Psychiatry* 65, 84–88. doi: 10.1016/j.biopsych.2008.08.027.
- Luders, E., Narr, K. L., Zaidel, E., Thompson, P. M., Jancke, L., and Toga, A. W. (2006a). Parasagittal Asymmetries of the Corpus Callosum. *Cerebral Cortex* 16, 346–354. doi: 10.1093/cercor/bhi112.
- Luders, E., Narr, K. L., Zaidel, E., Thompson, P. M., and Toga, A. W. (2006b). Gender effects on callosal thickness in scaled and unscaled space. *Neuroreport* 17, 1103–1106. doi: 10.1097/01.wnr.0000227987.77304.cc.
- Luders, E., Toga, A. W., and Thompson, P. M. (2014). Why size matters: differences in brain volume account for apparent sex differences in callosal anatomy: the sexual dimorphism of the corpus callosum. *Neuroimage* 84, 820–824. doi: 10.1016/j.neuroimage.2013.09.040
- Mangin, J.-F., Lebenberg, J., Lefranc, S., Labra, N., Auzias, G., Labit, M., et al. (2016). Spatial normalization of brain images and beyond. *Med Image Anal* 33, 127–133. doi: 10.1016/j.media.2016.06.008.
- Manjón, J. V., and Coupé, P. (2016). volBrain: An Online MRI Brain Volumetry System. *Front. Neuroinform.* 10. doi: 10.3389/fninf.2016.00030.
- Maris, E., and Oostenveld, R. (2007). Nonparametric statistical testing of EEG- and MEG-data. *Journal of Neuroscience Methods* 164, 177–190. doi: 10.1016/j.jneumeth.2007.03.024.
- Nakhid, D., McMorris, C., Sun, H., Gibbard, W. B., Tortorelli, C., and Lebel, C. (2022). Brain volume and magnetic susceptibility differences in children and adolescents with prenatal alcohol exposure. *Alcohol: Clinical and Experimental Research* 46, 1797–1807. doi: 10.1111/acer.14928.
- Nardelli, A., Lebel, C., Rasmussen, C., Andrew, G., and Beaulieu, C. (2011). Extensive Deep Gray Matter Volume Reductions in Children and Adolescents with Fetal Alcohol Spectrum Disorders: Reduced deep gray matter volume in FASD. *Alcoholism: Clinical and Experimental Research*, no-no. doi: 10.1111/j.1530-0277.2011.01476.x.
- O’Hare, E. D., Kan, E., Yoshii, J., Mattson, S. N., Riley, E. P., Thompson, P. M., et al. (2005). Mapping cerebellar

- vermal morphology and cognitive correlates in prenatal alcohol exposure. *Neuroreport* 16, 1285–1290. doi: 10.1097/01.wnr.0000176515.11723.a2.
- Rajapakse, J. C., Giedd, J. N., Rumsey, J. M., Vaituzis, A. C., Hamburger, S. D., and Rapoport, J. L. (1996). Regional MRI measurements of the corpus callosum: a methodological and developmental study. *Brain and Development* 18, 379–388. doi: 10.1016/0387-7604(96)00034-4.
- Rajaprakash, M., Chakravarty, M. M., Lerch, J. P., and Rovet, J. (2014). Cortical morphology in children with alcohol-related neurodevelopmental disorder. *Brain Behav* 4, 41–50. doi: 10.1002/brb3.191.
- Riley, E. P., Mattson, S. N., Sowell, E. R., Jernigan, T. L., Sobel, D. F., and Jones, K. L. (1995). Abnormalities of the corpus callosum in children prenatally exposed to alcohol. *Alcohol Clin Exp Res* 19, 1198–1202. doi: 10.1111/j.1530-0277.1995.tb01600.x.
- Roussotte, F. F., Sulik, K. K., Mattson, S. N., Riley, E. P., Jones, K. L., Adnams, C. M., et al. (2012). Regional brain volume reductions relate to facial dysmorphology and neurocognitive function in fetal alcohol spectrum disorders. *Hum. Brain Mapp.* 33, 920–937. doi: 10.1002/hbm.21260.
- Schneble, E., Lack, C., Zapadka, M., Pfeifer, C. M., Bardo, D. M. E., Cagley, J., et al. (2020). Increased Notching of the Corpus Callosum in Fetal Alcohol Spectrum Disorder: A Callosal Misunderstanding? *AJNR* *Am J Neuroradiol* 41, 725–728. doi: 10.3174/ajnr.A6475.
- Simpson, L. N., Schneble, E. J., Griffin, E. D., Obayashi, J. T., Setran, P. A., Ross, D. A., et al. (2020). Morphological changes of the dorsal contour of the corpus callosum during the first two years of life. *Pediatr Radiol* 50, 543–549. doi: 10.1007/s00247-019-04585-0.
- Sowell, E. R., Mattson, S. N., Thompson, P. M., Jernigan, T. L., Riley, E. P., and Toga, A. W. (2001). Mapping callosal morphology and cognitive correlates: effects of heavy prenatal alcohol exposure. *Neurology* 57, 235–244. doi: 10.1212/wnl.57.2.235.
- Sullivan, E. V., Moore, E. M., Lane, B., Pohl, K. M., Riley, E. P., and Pfefferbaum, A. (2020). Graded Cerebellar Lobular Volume Deficits in Adolescents and Young Adults with Fetal Alcohol Spectrum Disorders (FASD). *Cereb Cortex* 30, 4729–4746. doi: 10.1093/cercor/bhaa020.
- Toro, R., Chupin, M., Garnero, L., Leonard, G., Perron, M., Pike, B., et al. (2009). Brain volumes and Val66Met polymorphism of the BDNF gene: local or global effects? *Brain Struct Funct* 213, 501–509. doi: 10.1007/s00429-009-0203-y.
- Treit, S., Jeffery, D., Beaulieu, C., and Emery, D. (2020). Radiological Findings on Structural Magnetic Resonance Imaging in Fetal Alcohol Spectrum Disorders and Healthy Controls. *Alcohol Clin Exp Res* 44, 455–462. doi: 10.1111/acer.14263.
- Treit, S., Zhou, D., Chudley, A. E., Andrew,

- G., Rasmussen, C., Nikkel, S. M., et al. (2016). Relationships between Head Circumference, Brain Volume and Cognition in Children with Prenatal Alcohol Exposure. *PLoS One* 11, e0150370. doi: 10.1371/journal.pone.0150370.
- Walsh, E. I., Shaw, M. E., Oyarce, D. A. E., Fraser, M., and Cherbuin, N. (2019). Assumption-Free Assessment of Corpus Callosum Shape: Benchmarking and Application. *Concepts in Magnetic Resonance Part A* 2019, 1–10. doi: 10.1155/2019/8921901.
- Warling, A., McDermott, C. L., Liu, S., Seidlitz, J., Rodrigue, A. L., Nadig, A., et al. (2021). Regional White Matter Scaling in the Human Brain. *J. Neurosci.* 41, 7015–7028. doi: 10.1523/JNEUROSCI.1193-21.2021.
- Westerhausen, R., Luders, E., Specht, K., Ofte, S. H., Toga, A. W., Thompson, P. M., et al. (2011). Structural and functional reorganization of the corpus callosum between the age of 6 and 8 years. *Cereb Cortex* 21, 1012–1017. doi: 10.1093/cercor/bhq165.
- Wood, S. N., and Fasiolo, M. (2017). A generalized Fellner-Schall method for smoothing parameter optimization with application to Tweedie location, scale and shape models. *Biometrics* 73, 1071–1081. doi: 10.1111/biom.12666.
- Yang, Y., Phillips, O. R., Kan, E., Sulik, K. K., Mattson, S. N., Riley, E. P., et al. (2012a). Callosal thickness reductions relate to facial dysmorphology in fetal alcohol spectrum disorders. *Alcohol Clin Exp Res* 36, 798–806. doi: 10.1111/j.1530-0277.2011.01679.x.
- Yang, Y., Roussotte, F., Kan, E., Sulik, K. K., Mattson, S. N., Riley, E. P., et al. (2012b). Abnormal cortical thickness alterations in fetal alcohol spectrum disorders and their relationships with facial dysmorphology. *Cereb Cortex* 22, 1170–1179. doi: 10.1093/cercor/bhr193.
- Zhou, D., Rasmussen, C., Pei, J., Andrew, G., Reynolds, J. N., and Beaulieu, C. (2018). Preserved cortical asymmetry despite thinner cortex in children and adolescents with prenatal alcohol exposure and associated conditions. *Hum Brain Mapp* 39, 72–88. doi: 10.1002/hbm.23818.

MATÉRIELS SUPPLÉMENTAIRES

Table S1. Effect of scanner, age, and sex on raw measured parameters in the control group.

	Age effect p ^a	Sex effect p ^a	Scanner effect p ^a
Length of the corpus callosum	0.009	0.043	0.033
Genu thickness	0.659	0.186	0.022
Body hump thickness	0.659	0.015	0.021
Body median thickness	0.659	0.010	0.002
Isthmus thickness	0.058	0.001	0.001
Splenium thickness	0.001	0.036	0.450

Multivariate linear regression.

Bold type, $p < 0.05$, after FDR correction.

^a p -value from the generalized linear model including scanner, age, and sex as covariates for each parameters measured.

Figure S1. Correlation between the two proxies of brain size, the total brain volume from Volbrain and the axial reference brain area (measurement previously described in Fraize et al., 2023c. Top left, R^2 coefficient of correlation.

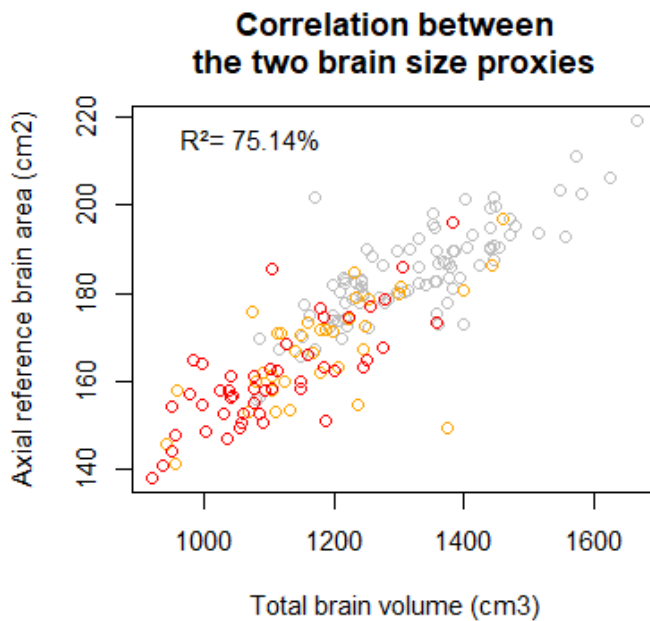
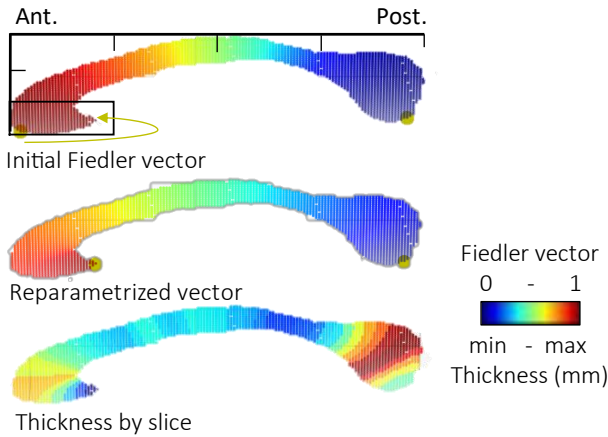


Figure S2. Algorithm for repositioning the rostrum in optimal position.

Algorithm for repositioning the rostrum in optimal position

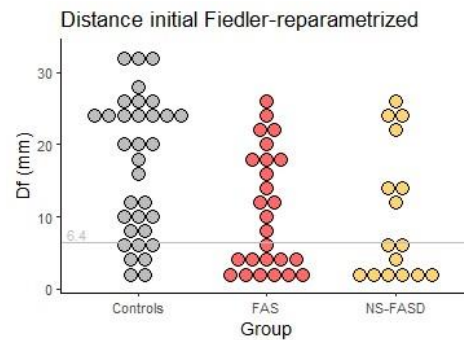
(posterior point of the lower third of the first quarter, in reference where the maximum elongation was observed)



Quantification of the distance between initial rostrum position and the reparametrized extremity (D_f , mm) and comparison by group.

	Well positioned $D_f=0$	Short repositioning $D_f < 6.4$	Large repositioning $D_f > 6.4$
Total (n=213)	138 (64.8%)	26 (12.2%)	49 (23.0%)
Controls (n=126)	93 (73.8%)	7 (5.6%)	26 (20.6%)
FASD (n=87)	45 (51.7%)	19 (21.8%)	23 (26.4%)
Comparison %control vs. FASD	p=0.002	p=0.001	p=0.410

D_f of control and FASD,
Control in grey
FASD in red
Threshold 6.4 in dotted line



COMPLÉMENTS DE DISCUSSION

RÉSULTATS CONCORDANTS

Les résultats de ces deux études nous permettent de confirmer la description du rétrécissement de l'isthme calleux indépendamment de la réduction de la taille globale du cerveau chez les sujets SAF, faite lors de la première étude radio-clinique (**chapitre 3**). Avec l'étude de parcellisation du corps calleux (**chapitre 5, partie 1**), nous avons montré que la surface de la parcelle correspondant au cortex postcentral, incluant la zone post-isthmique, est significativement sous dimensionnée chez les sujets TSAF, et qu'il en est tendanciellement de même pour la région termino-spléniale. Avec l'étude automatisée de l'épaisseur du corps calleux (**chapitre 5, partie 2**), nous avons montré que les sujets SAF dont l'épaisseur de l'isthme ou celle du splénium est trop petite pour la taille de leur cerveau étaient sur-représentés. Nous confirmons avec ces deux études que la taille de la partie antérieure du corps calleux, du rostrum au corps, bien que plus petites chez les TSAF, est préservée quand le déficit de croissance cérébrale est pris en compte. Au-delà de la cohérence interne de nos résultats, ils sont concordants avec ceux de plusieurs résultats de la littérature, sachant que celle-ci comporte des études ne retrouvant pas d'effet significatif de la maladie ou seulement en sous-groupe, des études concordantes, et aucune étude identifiant des anomalies calleuses localisées autrement (Sowell et al., 2001; Bookstein et al., 2002a; Dodge et al., 2009; Yang et al., 2012b; Gautam et al., 2014; Biffen et al., 2017; Jacobson et al., 2017). En revanche, l'étude automatisée de l'épaisseur des points singuliers du profil (**chapitre 5, partie 2**), ne nous a pas permis de déterminer si la moitié plus antérieure du splénium était également relativement préservée, comme le suggère le gradient d'atteinte de surface calleuse et l'absence d'atteinte de la parcelle correspondant au cortex pariétal. En effet, pour préciser ce point, il aurait, par exemple, fallu disposer d'un point de repère singulier homologue entre les sujets au sein de la partie antérieure du splénium, afin d'y réaliser une deuxième mesure d'épaisseur spléniale.

COHÉRENCE DES ANALYSES NORMATIVES

Tous les sujets SAF identifiés comme ayant une épaisseur de l'isthme inférieure au 10^{ème} percentile des courbes de *scaling* de l'étude du **chapitre 5 partie 2**, ont une surface post-isthmique (*i.e.* postcentrale) également trop petite en analyse multivariée prenant en compte la taille du cerveau dans l'étude de la **partie 1** (5 sujets en commun). Cinq sujets SAF sur 6 ayant une épaisseur du splénium inférieure au 10^{ème} percentile ont une surface de la parcelle termino-spléniale (*i.e.* occipitale) trop petite. Huit des 15 sujets SAF et 3 des 6 sujets TSAF-NS ayant une épaisseur isthmique anormalement petite dans l'étude radio-clinique (**chapitre 3**) ont aussi été identifiés comme anormaux avec les mesures automatiques (**chapitre 5, partie 2**). Ces correspondances sont des arguments préliminaires en faveur de la cohérence dans l'identification d'au moins certains sujets « anormaux » entre les différentes analyses normatives des trois études, mais il serait évidemment utile de réaliser une étude

systematique de la coherence intermodalite de detection des anomalies, en incluant une mesure de la taille d'effet (Z-score ou deviation au *scaling* typique comme pour le cervelet). Cette demarche avait ete debutee dans le cadre de travaux academiques, dans un sous-groupe de sujets de la meme cohorte, pour les metriques cerebelleuses (Fraize, 2021). Nous avons etudie la coherence des analyses normatives de la hauteur et du volume du vermis. Nous avons identifie et denombrer les sujets ayant un vermis trop petit en utilisant les courbes de *scaling* de hauteur et de volume. Nous avons montre que la mesure de la hauteur du vermis etait suffisamment corrlee au volume de celui-ci pour en faire un outil de depistage de l'atteinte vermienne (volume du vermis < 10^{eme} percentile) car la valeur predictive positive etait elevee (< 2% de faux positif). En revanche, le nombre important de faux negatifs (37%) montrait la limite de la mesure de hauteur unidimensionnelle.

Dans le cas du corps calleux, en realisant une etude intermodalite, nous pourrions comprendre si les differences revelent des incoherences ou bien s'il s'agit de sujets limites que l'imprecision de l'analyse normative place de part et d'autre de l'estimation du centile seuil.

A ce titre, nous avons fait le choix d'utiliser des modeles biomathematiques plus complexes et des methodes de determination des percentiles plus precises dans l'etude automatisee (**chapitre 5, partie 2**) (Wood and Fasiolo, 2017; Dinga et al., 2021) que dans l'etude radio-clinique (**chapitre 3**) a la faveur de l'augmentation de l'effectif des controles. A l'inverse, dans l'etude reposant sur la parcellisation (**chapitre 5, partie 1**), le faible effectif du sous-groupe nous a conduit a reduire notre analyse normative a l'etude des residus d'un modele multilinaire chez les controles, ce qui est une approximation affine discutable des phenomenes d'allometrie (*cf.* discussion de l'article).

Par ailleurs, il faut rappeler que nous avons fait le choix d'analyses normatives unisexes compte tenu de la taille modeste du groupe controle en considerant la balance entre la puissance statistique et la meilleure estimation du modele. Ensuite le biais potentiel lie au site a ete corrige prealablement en fonction de sa significativite en analyse multifactorielle sur les mesures natives : negligee pour l'etude manuelle des epaisseurs (**chapitre 3**), il a ete pris en compte par un pretraitement numerique dans les etudes de neuroimagerie computationnelle en particulier l'etude automatisee du profil d'epaisseur calleuse (**chapitre 5, partie 2**). Au meme titre que l'analyse du cervelet, ce procede de correction prealable est sans impact sur les conclusions, gage de leur robustesse.

OBJECTIFS COMPLÉMENTAIRES

Les deux etudes de ce chapitre, basees l'une et l'autre sur des methodologies originales permettent de tirer des informations complementaires sur l'atteinte du corps calleux dans les TSAF. A l'instar de l'etude radio-clinique, l'etude automatisee des epaisseurs calleuses, en plus d'etre descriptive du phenotypage neuroanatomique dans cette maladie, a une visee applicative directe d'identification de marqueurs pertinents pour le diagnostic clinique. L'etude des surfaces calleuses (**chapitre 5, partie 2**), bien que realisee sur un sous-echantillon, donne par

ailleurs un aperçu des liens existant entre les anomalies de l'étage cortical et celles qui affectent la structure supportant de la connectivité interhémisphérique qu'est le corps calleux. Il faut souligner que l'ensemble des données fournies par les images de diffusion dans notre série n'a pas encore été étudié et permettrait d'envisager une compréhension plus approfondie des altérations microstructurelles de la substance blanche au niveau du corps calleux (myélinisation, densité de fibres, etc.) en lien avec les anomalies identifiées de la morphologie corticale et calleuse.

CHAPITRE 6

DISCUSSION GÉNÉRALE

RÉSUMÉS DES PRINCIPAUX RÉSULTATS

Avec ces quatre études successives, nous avons montré que des anomalies neuroanatomiques récurrentes du cervelet et du corps calleux sont observées chez des sujets ayant un SAF indépendamment de la réduction de taille de leur cerveau, qu'elles constituent les éléments d'un phénotype neuroanatomique complexe distinguant ces sujets des contrôles au développement typique, et que ce phénotype pourrait être étendu à des sujets ayant une forme de TSAF non syndromique chez qui les mêmes anomalies sont parfois retrouvées. Nous avons montré que cette démarche peut avoir un impact sur le raisonnement clinique, sur la base de mesures simples et réalisables en clinique, mais aussi utilisant des outils d'imagerie computationnelle. Nous avons utilisé ces outils plus complexes pour caractériser plus finement ces atteintes calleuses et cérébelleuses tout en montrant à chaque fois que la démarche peut conduire à l'identification de caractéristiques individuelles.

En particulier, nous avons montré que le gradient antéro-inféro-postérieur d'atteinte cérébelleuse permet d'identifier un quart des sujets TSAF-NS comme ayant un phénotype de morphologie cérébelleuse identique aux sujets avec un SAF (**chapitre 4**). Nous avons aussi confirmé l'atteinte du tiers postérieur du corps calleux. Nous avons retrouvé un sur-rétrécissement isthmique par les mesures manuelles que nous avons confirmé par des mesures automatisées d'épaisseur (**chapitre 3 et 5, partie 2**). Cette méthode automatisée a permis de révéler que l'atteinte isthmique s'associait à un amincissement du splénium et un raccourcissement de la longueur du corps calleux indépendamment de la réduction de taille du cerveau. Là encore, nous avons montré que ces anomalies calleuses étaient sur-représentées dans notre population de sujets ayant un SAF et qu'une partie des sujets ayant une forme non syndromique les présentaient aussi. Dans un sous-groupe de sujets TSAF, nous avons confirmé cette atteinte postérieure en analyse surfacique sur la coupe sagittale médiane et notamment que l'atteinte spléniale est indépendante de la taille de la surface corticale qu'elle connecte, alors que l'atteinte péri-isthmique plus marquée pourrait être associée à une atteinte de l'extension corticale homologue (**chapitre 5, partie 1**).

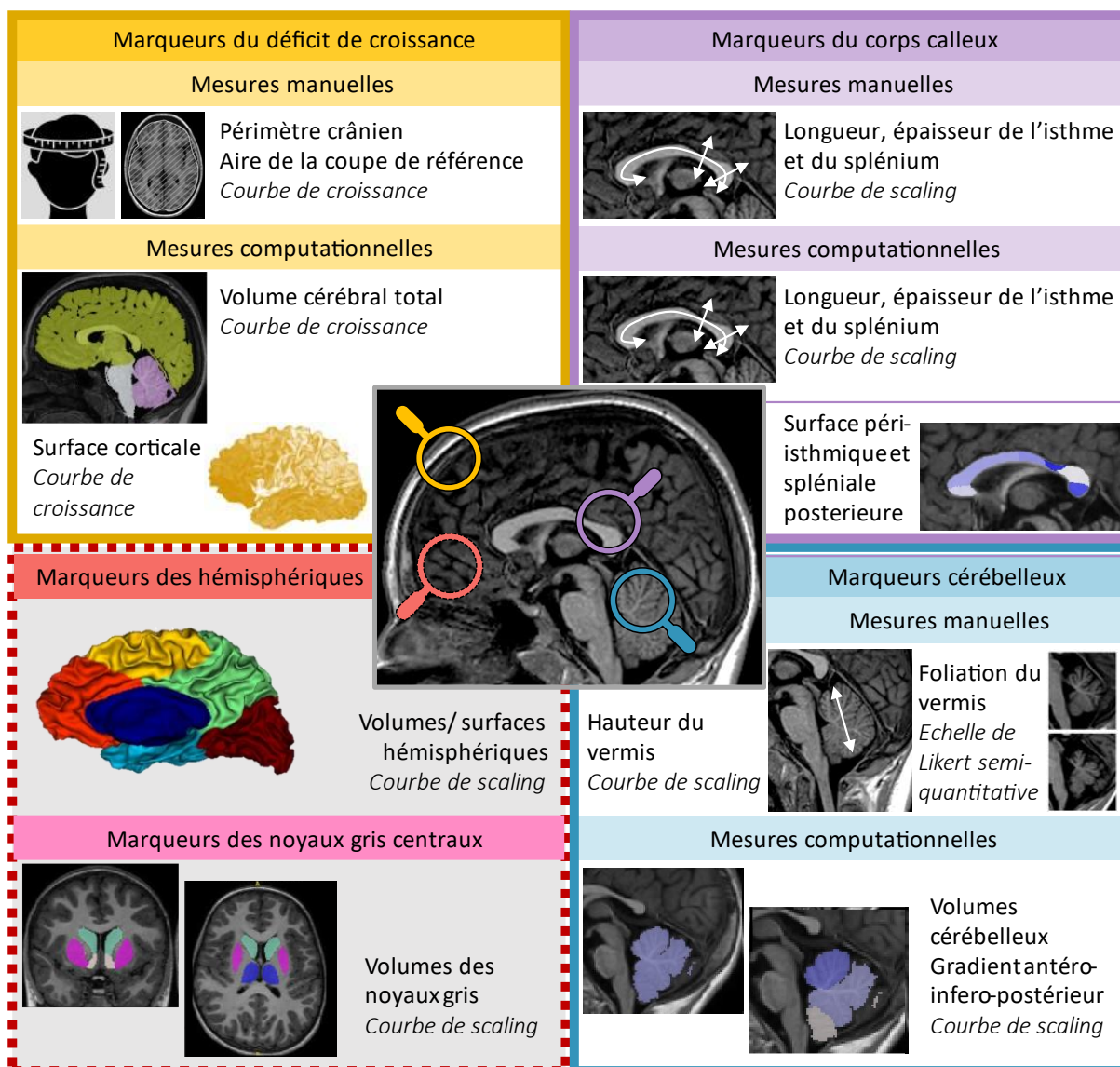


Figure 4. Synthèse des principaux résultats. Marqueurs neuroanatomiques identifiés et potentiels (grisés) chez les sujets ayant un SAF et pouvant s'étendre aux sujets ayant une forme non syndromique.

QUÊTE DE MARQUEURS NEUROANATOMIQUES DANS LES TSAF

SPECTRE D'ATTEINTE DE L'EXPOSITION PRÉNATALE À L'ALCOOL

Les TSAF sont une cause fréquente, potentiellement évitable et très certainement sous-diagnostiquée de trouble du neurodéveloppement (Germanaud and Toutain, 2017). Face à un enfant qui présente un trouble du neurodéveloppement se pose la question de l'identification d'une cause. Ce diagnostic étiologique positif peut reposer sur un ou des arguments cliniques, biologiques, génétiques, ou d'imagerie. Dans le cas des TSAF, le diagnostic de SAF est syndromique, dysmorphologique, celui des formes non syndromiques s'appuie sur des arguments anamnestiques (une exposition prénatale à l'alcool à un seuil préoccupant ou

sévère) et un faisceau d'arguments cliniques de compatibilité, mais reste probabiliste. Dans les deux cas, les explorations complémentaires (biologiques, génétiques, en imagerie) ne sont pour l'instant d'aucune utilité au diagnostic positif, exclusion faite du diagnostic fonctionnel du trouble du neurodéveloppement et du diagnostic différentiel qui n'est pas codifié. Pourtant l'alcool, en tant qu'agent causal, présente une embryo-foetotoxicité neurologique qui plaide pour la recherche d'éléments dans la morphologie cérébrale pouvant étayer ce diagnostic étiologique positif.

Le diagnostic des sujets ayant un SAF est certain, traduisant une implication causale de l'exposition prénatale à l'alcool dans le phénotype. Nous avons donc cherché à établir le phénotype anatomique cérébral de ces formes de diagnostic certain pour voir dans quelle mesure il pourrait être étendu aux formes non syndromiques. Cette démarche est basée sur la notion de *continuum* entre les sujets SAF et les sujets TSAF non syndromiques, qui concerne les caractéristiques physiques et fonctionnelles, et qui reflète aussi en partie le niveau d'exposition. Ce *continuum* concerne plusieurs aspects pouvant, chez un même individu, s'échelonner à des intensités différentes. Parmi l'ensemble des sujets TSAF qui ont donc été exposés à des niveaux d'alcool significatifs, les sujets SAF ont été exposés à des niveaux plus élevés en moyenne (May et al., 2013). L'étude de la dysmorphie faciale a également permis de montrer qu'il existe une forme de continuité entre la morphologie normale, les particularités infracliniques des sujets non syndromiques et la dysmorphie faciale typique de SAF (Suttie et al., 2013). L'étude des profils fonctionnels atteste aussi de ce *continuum*, la mesure du quotient intellectuel étant utilisée comme marqueur quantitatif de sévérité graduelle entre les SAF et les sujets TSAF-NS, avec toutes les limites d'interprétation potentielles dans ces populations aux profils hétérogènes (Sampson et al., 2000; Astley et al., 2009b; Kerdreux et al., 2023). Il s'agit de la même maladie du développement dont les caractéristiques peuvent s'exprimer à l'échelle de l'individu à des degrés variés, et qui à l'échelle du groupe, sont plus sévères chez les sujets SAF. En pratique dans nos études, nous avons retrouvé également ce *continuum* entre sujets SAF et TSAF-NS, pour tous les paramètres étudiés. Pour la valeur moyenne d'un paramètre, les tailles d'effet, le nombre de sujets anormaux, les nuages de points sur les courbes de croissance (fonction de l'âge) et de *scaling* (fonction de la taille du cerveau), les sujets TSAF-NS sont en position intermédiaire entre les SAF et les contrôles, sans qu'il existe de discontinuité entre les groupes qui sont largement chevauchants.

Il est donc justifié de rechercher une signature neuroradiologique chez les SAF pour chercher à l'étendre aux formes non syndromiques et ensuite considérer son utilité dans la démarche diagnostique. Nous avons appliqué ce raisonnement de deux manières. En premier lieu en recherchant les anomalies décrites comme récurrentes chez les SAF et indépendantes de la réduction de taille du cerveau. Nous avons procédé en utilisant les courbes de *scaling* et en dénombrant les sujets avec un SAF montrant des paramètres anormalement petits (**chapitre 3 et 5, partie 2**) pour ensuite dénombrer les sujets TSAF-NS avec ces anomalies récurrentes de SAF. Deuxièmement, nous avons construit selon la même logique un classifieur que nous

avons entraîné dans la population SAF + contrôles et testé dans celle des sujets non syndromiques (**chapitre 4**).

COMPLEXITÉ DE LA SIGNATURE

Notre objectif est de tendre vers un critère diagnostique neuroanatomique multidimensionnel prenant en compte chaque structure cérébrale atteinte, indépendamment l'une de l'autre, et précisant le type d'anomalie à considérer (nature, sévérité). Rappelons qu'à l'heure actuelle, toute anomalie structurelle peut être considérée comme « dommage cérébral », sans presque aucun impact sur la spécificité ou le degré de certitude diagnostique.

Dans l'étude du chapitre 3, nous avons synthétisé nos résultats sous la forme d'un score composite qui est une proposition préliminaire sur la base de ce concept (**résumé graphique du chapitre 3**). La **figure 4** constitue également une ébauche de ce que pourrait être ce critère et les outils pour mesurer chacun des items le composant.

Le score composite associe trois items : atteinte de la taille globale du cerveau, du corps calleux et du cervelet indépendamment du précédent. Cette idée d'une signature neuroanatomique complexe étant également applicable à l'échelle d'une même structure anatomique, ces deux derniers items intègrent plusieurs dimensions : la foliation et la taille du cervelet, la complétude du corps calleux et la réduction locale isthmique. Dans l'étude du chapitre 4, nous avons montré que l'empreinte de l'exposition prénatale à l'alcool chez les sujets SAF sur le cervelet, sous la forme d'un gradient, permet mieux de les distinguer des contrôles. L'utilisation d'un marqueur neuroanatomique multidimensionnel ici cérébelleux, lobaire et vermien a plus d'impact sur la catégorisation diagnostique. De même, au sein du corps calleux, nos résultats suggèrent que l'atteinte de sa morphologie peut se repérer en plusieurs zones, isthmique et splénium, en plus d'un raccourcissement indépendant de la réduction de taille du cerveau, permettant de décrire subtilement la morphologie calleuse avec un item lui-même composite (**chapitre 5**).

Pour dépister et caractériser ces subtilités morphologiques, des outils de mesures adaptés sont nécessaires. Ce travail de recherche de marqueurs qui pourraient être utiles au diagnostic a donc été l'occasion de développement méthodologiques dédiés.

APPROCHES MÉTHODOLOGIQUES AU SERVICE D'UNE QUESTION

CLINIQUE

Pour rechercher ces marqueurs nous avons concentré nos efforts sur deux zones cérébrales régulièrement rapportées dans la littérature comme affectées par l'alcoolisation fœtale : le cervelet et corps calleux. Des études préliminaires de notre équipe initiant l'implémentation de l'analyse de *scaling* à l'échelle de six zones cérébrales (lobes, substance grise profonde et cervelet) pointaient aussi le déficit de taille globale du cervelet (Garzón et al., 2017). Nous

avons fait le choix de mettre au point des outils de segmentation à partir de ceux déjà existants ou d'en développer de nouveaux pour répondre à l'exigence des questions soulevées. Dans la caractérisation cérébelleuse (**chapitre 4**), il nous a semblé nécessaire de décrire le cervelet, lobe par lobe, y compris le vermis. Pour cela, nous avons combiné des méthodes de segmentation déjà existantes puisqu'aucune ne fournissait à la fois une identification verticale du vermis et une segmentation horizontale lobulaire. Dans la caractérisation du corps calleux, nous souhaitons à la fois étudier les liens anatomiques entre ruban cortical et connexion calleuse, et disposer de critères de segmentation plus objectifs que les classiques découpes géométriques forcément arbitraires. Nous avons mis en place une parcellisation calleuse fondée sur la projection, par le biais du tractogramme, d'une segmentation corticale fondée sur les sillons (**chapitre 5, partie 1**). Enfin pour franchir un cap dans l'étude des épaisseurs calleuses, tant qualitatif (précision de localisation et de mesure) que quantitatif (nombre de mesures calleuses, nombre de sujets accessibles...), nous avons mis au point un outil automatisé traitant toute la longueur de façon pertinente d'un point de vue anatomique, fondé sur un premier temps d'analyse spectrale de forme (allongement) via son vecteur de Fiedler (**chapitre 5 partie 2**). Ces développements méthodologiques nous ont permis à chaque fois de répondre précisément aux besoins soulevés par une question très clinique, sans se voir imposer des paramètres par les contraintes que certains outils peuvent présenter. La contrepartie de ces outils innovants est qu'ils ne sont pas encore facilement exportables pour être mis à disposition immédiatement. Il est également plus difficile d'assurer la comparabilité intrinsèque des résultats si les méthodes pour les obtenir ne sont pas encore facilement réutilisables.

Cet effort méthodologique a aussi été fourni dans le but d'étudier le même objet anatomique selon plusieurs modalités. Ainsi, nous avons renforcé les preuves par des résultats concordants obtenus par des stratégies les plus indépendantes possibles. Le cervelet a donc été caractérisé en mesurant manuellement la hauteur du vermis, en qualifiant visuellement semi-quantitativement la foliation (**chapitre 3**), et en mesurant des volumes segmentaires obtenus par segmentation automatique (**chapitre 4**). Le corps calleux a été caractérisé en mesurant manuellement et automatiquement des épaisseurs à des points singuliers ainsi que la longueur, et en optant pour une stratégie totalement différente de segmentation à base sulcale et de mesures surfaciques.

Pour l'analyse des paramètres mesurés, nous avons fait, autant que possible, le choix d'une méthodologie singulière, largement discutée dans les différents articles, associant une modélisation sur le plan biomathématique de la variance d'intérêt à une analyse normative autorisant une interprétation catégorielle à l'échelle individuelle. En particulier nous avons ainsi introduit l'analyse normative de *scaling* pour prendre en compte l'effet de taille du cerveau, majeur dans la population des TSAF qui présente une réduction de volume cérébral bien au-delà de l'intervalle de normalité. Nous avons fait en sorte de proposer un formalisme qui s'approche le plus du raisonnement clinique et puisse faciliter l'intégration des résultats à la démarche diagnostique clinique.

Nos efforts pour développer des outils facilement utilisables en clinique, avec une méthodologie d'interprétation des paramètres morphométriques extraits à l'échelle individuelle, pourraient aussi s'avérer utiles à d'autres pathologies. En dehors du cadre de l'élaboration d'un outil diagnostique, ils pourraient permettre une description phénotypique plus détaillée des morphologies calleuses et cérébelleuses, prenant en compte la réduction de taille du cerveau dans le cas des microcéphalies quelle qu'en soit la cause.

PARTICULARITÉ DE LA SÉRIE CLINIQUE

La série clinique de notre étude est issue d'un centre unique de diagnostic expert et donc présente certaines spécificités qui pourraient limiter la reproductibilité des résultats ou même les biaiser. Tout d'abord, il s'agit d'une consultation dédiée dans un hôpital universitaire pédiatrique et d'un service surspécialisé, ce qui pourrait conduire à ce que les patients référés présentent majoritairement un tableau clinique parmi les plus sévères. Cette limite relève plus largement de la démarche rétrospective et il ne serait possible de s'en affranchir qu'en procédant à un suivi prospectif systématique d'enfants exposés (critère d'inclusion par l'exposition prénatale à l'alcool et non plus les TSAF). Plus de la moitié de la série étant composée d'enfants issus de l'adoption internationale et très majoritairement des pays de l'Est, la représentativité ethnique de la cohorte ainsi composée et donc son fond génétique pourrait être aussi à questionner. Enfin, un certain nombre d'enfants ont été adressés à cette consultation spécialisée de l'hôpital Robert-Debré par les services sociaux après des parcours de vie et dans un contexte parental singulier, marqué par une multiplicité de facteurs de risques en particulier en termes d'antécédents familiaux neurodéveloppementaux, psychopathologiques et environnementaux difficiles à démêler. Ce contexte n'est pas spécifique à notre centre et il est possible de considérer qu'il est commun aux cohortes de sujets TSAF.

Dans notre cas, la recherche de diagnostic différentiel était fondée entre autres sur des explorations génétiques systématiques en s'appuyant dès qu'il était nécessaire sur l'avis d'un généticien pédiatrique senior. Cette démarche rigoureuse fortement recommandable mais non formellement inscrite dans la plupart des recommandations internationales, est de nature à avoir limité les erreurs diagnostiques différentielles (en particulier en l'absence de TSAF) ou plus encore les situations de comorbidités étiologiques (facteurs étiologiques coïncidents), garantissant un niveau élevé de certitude diagnostique, et minimisant les sources d'hétérogénéité au sein de la série.

S'agissant du degré d'exposition prénatale à l'alcool dans notre série, sa quantification n'a pu être faite que de manière souvent grossière, voire probabiliste en considérant chez certains enfants des éléments indirects suggérant très fortement la consommation pendant la grossesse : triple association d'une adoption dans un pays à forte endémie de trouble chronique de l'usage de l'alcool (Landgren et al., 2010; Colom et al., 2021), d'un mode de vie documenté à haut risque d'abus d'alcool et d'une déchéance parentale judiciaire.

Précédemment Garzón a montré que 8% de sujets ont pu être inclus en plus, en introduisant cette catégorie au sein du critère du niveau d'exposition « non quantifié mais indirectement très probablement » et sans modification de la catégorie syndromique finale. Dans notre série, 9 % des sujets TSAF ne seraient pas inclus si ce critère n'était pas pris en compte.

En dehors du cas des sujets SAF, pour lesquels la connaissance du niveau d'exposition n'est pas cruciale pour le diagnostic, surtout si l'analyse dysmorphologique est fiable, la caractérisation de l'exposition est capitale pour le diagnostic des sujets avec une forme non syndromique (Astley, 2004). Dans le *4-Digit Diagnostic Code*, la notion de seuil minimal d'exposition n'est pas explicitée ni prévue, arguant qu'il « n'existe pas de consensus clair sur la quantité d'alcool qui peut être effectivement toxique pour chaque fœtus (Stratton et al., 1996) ». A l'inverse, les recommandations américaines révisées de l'*Institute Of Medicine* (Hoyme et al., 2016) considèrent toujours des seuils minimaux pour parler de « niveau documenté ». Ce critère de seuil minimal étant appliqué en pratique au centre expert de Robert-Debré, il l'a été dans notre série additionnellement aux critères du *4-Digit Diagnostic Code*, conduisant à l'exclusion de 9 sujets trop faiblement exposés (**Figure 1, diagramme de flux**). Ainsi, le niveau d'exposition ne pouvait être considéré comme « modéré simple » ou « léger occasionnel » pour aucun sujet avec TSAF de notre série (Germanaud and Toutain, 2017).

En pratique, dans la plupart des cas, l'enfant n'était plus sous la responsabilité de sa mère biologique pour cause de placement ou d'adoption, limitant les possibilités de recueil déclaratif direct par le médecin de consultation. En tout état de cause, ce recueil déclaratif rétrospectif est connu pour faire l'objet d'une sous-déclaration qui se majore avec le temps (May et al., 2013). Ainsi et malgré la pratique clinique d'une recherche systématique d'informations dans les dossiers médicosociaux et d'adoption ou auprès de tiers informés (père, parent, personnel des maisons d'enfants...), il était donc souvent impossible de recueillir quantitativement et précisément le niveau, la chronologie et les modalités de consommation. Il s'agit là d'une limite importante à la paramétrisation des modèles d'analyse des données neuroanatomiques, indépassable dans ce type de série clinique. Néanmoins sur la base des données disponibles dans le dossier médical, il a été possible d'établir les trois niveaux d'exposition satisfaisant aux recommandations du *4-Digit Diagnostic Code* (élevé, modéré ou non quantifié mais supérieur au seuil minimal, indéterminé).

Pour les mêmes raisons, nous n'avons pas été en mesure de répertorier systématiquement les co-intoxications possiblement associées. Les substances psychoactives ont un effet sur le développement cérébral *in utero* avec de nombreuses répercussions sur le neurodéveloppement et font souvent l'objet de co-consommation (Forray, 2016; Peterson et al., 2020). En 2013, un rapport pour la société américaine de pédiatrie, a acté dans sa revue scientifique que l'exposition prénatale à l'alcool est la plus étudiée, et que les preuves des répercussions sur la croissance fœtale, la présence d'anomalies congénitales et à long terme, sur le comportement, la cognition, le langage et la réussite académique étaient très solides,

comparativement au tabac, aux opioïdes et au tétrahydrocannabinol (Behnke et al., 2013). Donc même si des consommations s'associaient à celle de l'alcool, l'effet délétère neurodéveloppemental de celui-ci dépasserait les conséquences des autres produits, à la fois sur le plan du risque tératogène et de l'importance de la taille d'effet.

Ce questionnement sur la représentativité de l'ensemble du spectre des TSAF dans notre série revêt une importance s'agissant d'une donnée de neuroimagerie issue du soin. En effet, dans les recommandations internationales diagnostiques actuelles, la réalisation d'une imagerie cérébrale systématique n'est pas explicitement recommandée. Dans certains pays, elle peut être donc conditionnée à d'autres critères cliniques (microcéphalie, déficience intellectuelle) ou bien aux conditions de ressources de la famille, tous les systèmes de soins n'offrant pas les mêmes opportunités d'exploration diagnostique que la France. La pratique monocentrique d'une IRM cérébrale à titre systématique dans le cadre du soin et du diagnostic différentiel, bien que conforme aux pratiques françaises en la matière (trouble du neurodéveloppement précoce et sévère avec événement périnatal susceptible d'avoir engendré une lésion cérébrale, ou avec microcéphalie), constitue donc une particularité unique et précieuse de notre série par rapport à d'autres séries internationales. Il est néanmoins légitime de se questionner sur la trentaine de sujets exclus soit car n'ayant pas eu encore cet examen ou qu'il soit artefacté (**Figure 1**). Il pourrait potentiellement s'agir des patients pour lesquels la réalisation de cet examen a dû être différée car trop compliquée (agitation, refus) ou au suivi trop aléatoire (perdus de vue, refus). Cependant la réalisation de cet examen dans un centre spécialisé mettant en œuvre de nombreuses stratégies assurant un fort taux de succès permet a priori d'exclure un biais de représentativité en termes d'atteinte fonctionnelle de ces patients (anesthésie légère en cas de besoin). L'analyse quantitative des profils neuropsychologiques de la série montrant une composition en termes de sévérité compatible avec celle de la littérature nous conforte dans cette idée de l'absence de biais de sévérité en lien avec la réalisation de l'imagerie (**Tableau**).

Enfin, il faut noter que dans les études prospectives et les protocoles expérimentaux rapportés, les sujets sont souvent inclus du fait de l'exposition *in utero* à l'alcool mais sans bénéficier d'une caractérisation diagnostique complète de leur TSAF, l'atteinte fonctionnelle ou le diagnostic syndromique restant insuffisamment caractérisés sur le plan nosographique, ce qui limite parfois la représentativité et la comparabilité des populations, ou conduit à suspecter une dilution des effets observés par des patients exposés mais hors champ des TSAF (Sowell, 2002a; Lebel et al., 2012; Treit et al., 2016; Sullivan et al., 2020).

Dans notre cas, la population de TSAF est phénotypée de façon homogène, les critères de dysmorphie faciale solidement établis, les diagnostics génétiques coïncidents éliminés, l'exposition prénatale recueillie de manière fiable bien que semi-quantitativement, en intégrant un niveau minimal, et la réalisation de l'imagerie ne biaisant pas la composition finale de la série. Tous ces efforts ont convergé pour finalement limiter l'hétérogénéité de la série. En pratique, cela a pu avoir comme conséquences de diminuer le bruit dans les mesures

quantitatives (volume, longueur etc.) et potentiellement faciliter la détection d'anomalies subtiles, faute de pouvoir à ce stade augmenter la taille de l'échantillon.

QUESTION DE LA SPÉCIFICITÉ ET VALEUR PRÉDICTIVE

PREUVE DE LA SPÉCIFICITÉ

Considérer des anomalies cérébrales telles que la microcéphalie et les anomalies morphologiques du cervelet et du corps calleux comme des marqueurs potentiels d'une maladie posent la question de la spécificité qui peut leur être associée. Les affections dans lesquelles ces anomalies sont retrouvées sont très nombreuses : génétique le plus fréquemment (30-45% de causes génétiques identifiées en cas d'agénésie du corps calleux), environnementales (infections virales, autres embryo-foetotoxiques, prématurité), et métaboliques (Mehta and Hartnoll, 2001; Paul et al., 2007; Poretti et al., 2014; Santana et al., 2022; Savvidou et al., 2022).

Les résultats de plusieurs études dans les modèles animaux qui documentent l'effet de l'alcool sur le développement de l'anatomie cérébrale, cérébelleuse et calleuse (Almeida et al., 2020) convergent dans le sens d'un degré de spécificité de ces anomalies dans ce contexte. Cet argument en faveur de l'imputabilité de l'alcool ne suffit cependant pas à établir en soi la spécificité de ces marqueurs neuroanatomiques. Les arguments en faveur de la causalité de l'exposition prénatale et de ces anomalies sont discutés dans chacun des articles respectivement pour le cervelet et le corps calleux.

À partir des études d'embryo-foetopathologie humaine permettant de retracer temporellement les étapes de développement normales des structures cérébelleuses et calleuses, il a été possible de faire des hypothèses sur les mécanismes de leur dérèglement et potentiellement les périodes de vulnérabilité. Les anomalies du corps calleux peuvent résulter non seulement d'une perturbation des événements précoces de sa formation allant jusqu'à la vingtième semaine (gliogenèse, interactions glio-neuronales, modulation de la transcription de certain gène d'adhésion cellulaire, migration axonale au travers de ligne médiane), mais aussi d'une perturbation ultérieure de l'élagage neuronal (Evrard et al., 2003; Paul et al., 2007; Raybaud, 2010). Concernant le cervelet, son ébauche se forme très précocement à partir du mésencéphale, de la 7^{ème} à la 13^{ème} semaine, pour que les bourrelets lobaires apparaissent. Les hypoplasies cérébelleuses pourraient être les conséquences d'une influence néfaste de l'alcool sur une large période de vulnérabilité, allant de l'apparition de la foliation, dont la progression est antéro-postérieure à l'augmentation majeure de volume qui persiste jusqu'au dernier trimestre (Limperopoulos et al., 2005; Brossard-Racine and Limperopoulos, 2016; Gano and Barkovich, 2019). Dans notre série, les données sur les modalités d'exposition (durée, période, quantité etc.) manquent pour pouvoir les étayer à nos hypothèses.

Afin d'augmenter à la fois le pouvoir discriminant du phénotype neuroanatomique dans son ensemble et de pouvoir en attendre une meilleure spécificité, nous avons visé une approche synthétique de cette question fondée sur l'association d'anomalies neuroanatomiques. Nous avons bien conscience que la démonstration stricte de la spécificité nécessiterait d'inclure des échantillons de comparaisons transnosographiques. Nous proposons un marqueur diagnostique combiné, signature neuroanatomique ou dysmorphie cérébrale qui pourrait être porteuse de la spécificité de l'exposition prénatale à l'alcool comme peut l'être la dysmorphie faciale, elle aussi composite.

VERS DES MARQUEURS PRÉDICTIFS

La portée de ce travail est principalement diagnostique, contribuant à mieux décrire l'anatomie cérébrale et l'intégrer dans une démarche translationnelle à l'échelle individuelle. Or, l'étape suivante sera d'enrichir nos résultats en incluant la portée pronostique du phénotype quantitatif et des anomalies neuroanatomiques pour tenter de répondre aux défis de la prédiction du devenir : quel enfant est plus à risque de développer un trouble en cas d'exposition ? peut-on inférer la sévérité des troubles à partir de la morphologie cérébrale ? quels champs cognitifs ont le plus de risque d'être affectés compte tenu des anomalies neuroanatomiques observées ?

Dans le contexte d'exposition prénatale à l'alcool, des facteurs prédictifs généraux sont déjà proposés. La présence de microcéphalie apparaît comme un facteur prédictif majeur, corrélé au niveau de consommation ; viennent ensuite des facteurs tels que le caractère paroxystique des épisodes d'alcoolisation et les marqueurs de vulnérabilité maternelle liés à un trouble de l'usage de l'alcool (âge maternel, plus de trois enfants, pathologie hépatique chronique etc.) (Coles et al., 2000). Cependant, la vulnérabilité neurodéveloppementale n'a pas une expression uniquement déterministe et seulement liée aux facteurs prédictifs et dépend de nombreux facteurs psychosociaux et environnementaux.

La question de l'usage prédictif des marqueurs neuroanatomiques se pose également dans le contexte du suivi des grossesses à risque où l'imagerie anténatale tient une place de plus en plus importante. Même en considérant la microcéphalie comme un facteur prédictif postnatal qui pourrait être étendu en prénatal, la littérature est pauvre sur la recherche de marqueurs prénataux d'exposition et n'évoque pas le devenir développemental. Bookstein et al. décrivent dans une petite cohorte une réduction de taille du corps calleux à l'échographie (Bookstein et al., 2005, 2007). Une équipe autrichienne a très récemment tenté de faire l'étude morphométrique de données de 24 IRM de fœtus exposés, et a pointé des anomalies du corps calleux et de la zone périventriculaire (Stuempflen et al., 2023). La reconnaissance de marqueurs d'exposition anténataux est une question qui dépasse l'enjeu du diagnostic des TSAF mais revêt une importance particulière en considérant la fréquence potentielle des grossesses avec une exposition modérée à sévère (de Chazeron et al., 2008; Chassevent-Pajot

et al., 2011), ainsi que la corrélation de la précocité du diagnostic avec un meilleur devenir adaptatif (Alex and Feldmann, 2012).

QUESTIONNEMENTS EN SUSPENS

Comme évoqué dans l'introduction, ce travail s'inscrit dans la continuité de celui de Garzón et al. dans l'équipe. Dans un sous-groupe de SAF (n=30), l'étude avait porté sur six volumes segmentaires à l'échelle lobaire et cherché à caractériser la répartition de la réduction de taille globale du cerveau entre les lobes hémisphériques, le cervelet et une zone centrale du cerveau incluant les noyaux gris centraux (Garzón et al., 2017). Ces travaux avaient pointé une répartition spatiale hétérogène de la réduction du volume cérébral dans le SAF. Les volumes des lobes temporaux et occipitaux étaient apparus plus grands que ce qui était attendu selon l'allométrie typique des contrôles (déviation positive au *scaling* typique), et ceux des lobes frontaux et pariétaux conformes à ce qui était attendu. Cette étude princeps s'inscrivait dans une littérature relativement pauvre, faisant état d'une réduction préférentielle du cortex frontal, pariétal et temporal, successivement, sans qu'une zone spécifique et cohérente puisse être retenue (Sowell, 2002b; Sowell et al., 2008; Zhou et al., 2011; Lebel et al., 2012; Yang et al., 2012b; Marshall et al., 2022).

Par ailleurs, un certain nombre de questions restent ouvertes sur la répartition volumétrique des substances grise et blanche à l'étage sus-tentorial, certains auteurs rapportant une réduction du volume de la substance blanche (Archibald et al., 2001; Gautam et al., 2014; Fan et al., 2016), d'autres de la substance grise corticale (Zhou et al., 2011, 2018; Lebel et al., 2012; Roussotte et al., 2012; Yang et al., 2012b; Treit et al., 2013). L'analyse de l'anatomie lobaire intégrant les métriques de substance grise (surface et volume corticaux) et blanche (volume lobaire) devraient nous aider à interpréter les résultats sur les surfaces corticales (**chapitre 5, partie 1**), et à trancher sur la réalité de l'atteinte de la surface corticale postcentrale (**Figure 4, zone grisée**).

Garzón et al. avaient précédemment montré une réduction plus sévère qu'attendu du cervelet mais aussi d'un ensemble central incluant les noyaux gris centraux (« *braincore* »). La littérature fait également état d'une réduction de taille des noyaux gris centraux, notamment du noyau caudé mais sans prendre toujours en compte la taille du cerveau ou seulement de façon linéaire (Riikonen et al., 1999; Astley et al., 2009a; Nardelli et al., 2011; Roussotte et al., 2012; Treit et al., 2013; Biffen et al., 2020; Nakhid et al., 2022). L'étude morphométrique de ces structures est donc en cours de finalisation dans l'équipe en employant les méthodes d'analyse décrites (analyse de *scaling* et approche normative (**Figure 4, zone grisée**), à partir de trois segmentations de référence.

Nous avons précédemment plaidé pour l'intérêt d'un critère neuroanatomique composite associant les descriptions morphologiques de chaque zone cérébrale étudiée. Cette démarche a été préliminairement proposée dans les travaux radio-cliniques sous la forme d'un score

multidimensionnel. Nous pourrions ainsi intégrer tous les marqueurs identifiés dans un classifieur global, évaluer son efficacité et son application dans le sous-groupe des TSAF-NS, tout comme dans l'étude du chapitre 4, ainsi que le poids respectif de chacun des paramètres mesurés dans une démarche proche de celle proposée par Little et Beaulieu (Little and Beaulieu, 2020).

PERSPECTIVES ET CONCLUSION

AUTRES MARQUEURS DIAGNOSTIQUES ENVISAGEABLES

L'identification de marqueurs diagnostiques des TSAF peut également concerner d'autres cibles de la tératogénicité de l'éthanol. Les atteintes oculaires, qui commencent à être mieux décrites, pourraient être un autre champ d'exploration (Gyllencreutz et al., 2020). Une équipe suédoise a proposé et validé un critère clinique le « *FASD Eye Code* » combinant les atteintes oculaires les plus fréquemment retrouvées, qui est efficace pour discriminer les malades des contrôles (Ayoub et al., 2023). Certains proposent d'enrichir les marqueurs cliniques avec les autres caractéristiques cliniques en dehors de trois signes cardinaux de dysmorphie faciale (del Campo and Jones, 2017). S'agissant des marqueurs biologiques, la méthylation de l'ADN est un témoin des modifications épigénétiques secondaire à l'exposition prénatale à l'alcool et il a déjà été montré qu'il pouvait permettre de discriminer des sujets TSAF d'une population au développement typique ou avec un trouble du neurodéveloppement sans antécédent d'exposition prénatale à l'alcool (Lussier et al., 2018).

TRANSLATION CLINIQUE

La recherche de ces marqueurs neuroanatomiques ne se conçoit qu'en imaginant à court terme l'implémentation en pratique clinique des techniques d'analyse d'image utilisées pour les caractériser. L'accessibilité des outils d'analyse d'images est déjà une réalité dans certains centres et pour certains usages. La maturation d'une technique pour identifier un marqueur doit suivre des étapes successives (Cooper et al., 2020) après l'identification et la reconnaissance d'un besoin clinique. Il doit faire l'objet d'une preuve de concept, puis être reproduit. Les outils de mesures et d'analyses doivent ensuite être automatisés et les valeurs seuils établies pour pouvoir intégrer des critères cliniques reconnus pour qu'enfin les cliniciens l'emploient.

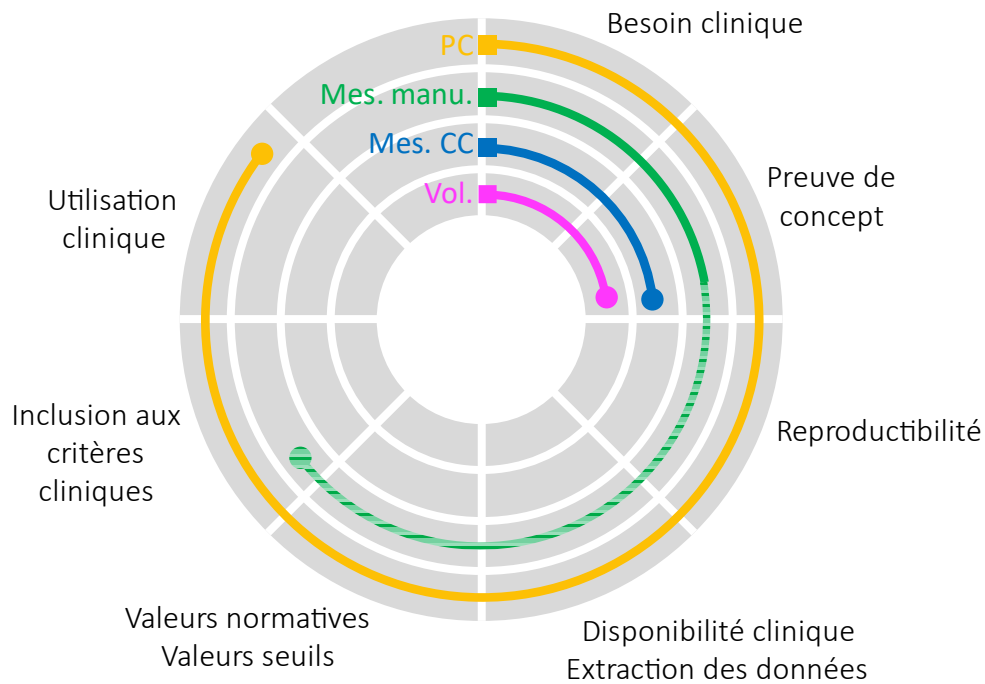


Figure 5. Maturité clinique des marqueurs neuroanatomiques dans les TSAF. Représentation schématique des étapes de développement classiques d'un marqueur, de l'identification du besoin clinique à son utilisation. Le périmètre crânien est le marqueur consensuel qui appartient d'ores et déjà dans les critères cliniques. PC : périmètre crânien. Mes. manu. : Mesures manuelles radio-cliniques (chapitre 3). Mes. CC : Mesures automatisées de la longueur et des épaisseurs du CC. Vol. : mesures volumiques automatisées, par exemple du cervelet.

La **figure 5** représente les étapes qui restent à franchir pour tendre vers l'intégration d'un critère diagnostique incluant l'anatomie cérébrale et l'apport de nos travaux dans cette optique.

CONTRIBUTIONS SCIENTIFIQUES NON INCLUSES

DANS LA THÈSE

Durant ma thèse, j'ai contribué à des recherches scientifiques en collaboration avec Eliot Kerdreux et Julien Lefèvre. Ces travaux ont donné lieu à deux publications que je résume brièvement.

QUESTIONNER L'HÉTÉROGÉNÉITÉ COGNITIVE ET LE FONCTIONNEMENT INTELLECTUEL DANS LES TROUBLES DU SPECTRE DE L'ALCOOLISATION FŒTALE À PARTIR DE L'ÉCHELLE D'INTELLIGENCE DE WECHSLER POUR LES ENFANTS

Dans ce travail, j'ai contribué à organiser et collecter la base de données. J'ai aidé à l'interprétation des résultats et à la rédaction du manuscrit.

Kerdreux, E., **Fraize, J.**, Garzón, P., Chalain, E., Etchebarren, L., Sitbon, D., Maruani, A., Boespflug-Tanguy, O., Hertz-Pannier, L., Noulhiane, M., Pinabiaux, C., & Germanaud, D. (2023). Questioning cognitive heterogeneity and intellectual functioning in fetal alcohol spectrum disorder from the Wechsler intelligence scale for children. *The Clinical Neuropsychologist*. *In review*

RÉSUMÉ

Introduction

Les troubles du spectre de l'alcoolisation fœtale (TSAF) se caractérisent par une variété de troubles cognitifs et comportementaux, les troubles du développement intellectuel et de l'attention et des fonctions exécutives étant les plus couramment rapportés. Dans les populations présentant des associations de troubles neurodéveloppementaux, le quotient d'intelligence total (QIT) peut ne pas être une mesure appropriée des capacités intellectuelles. Le QIT est rarement interprété dans la pratique clinique des TSAF, l'hétérogénéité du profil cognitif étant jugée trop importante. Nous proposons une caractérisation quantitative de cette hétérogénéité, du profil des forces et des faiblesses, et une analyse différentielle entre les capacités cognitives globales (QIT) et les capacités de raisonnement élémentaire dans un large échantillon rétrospectif monocentrique des sujets ayant un TSAF.

Matériels et méthodes

En utilisant les données cliniques et cognitives dont les échelles d'intelligence de Wechsler pour enfant (WISC) de 107 enfants ayant un TSAF, nous avons caractérisé l'hétérogénéité des sujets (variance et dispersion des scores standards/composites), recherché les forces et les

faiblesses, et spécifié le fonctionnement intellectuel en termes de QIT et de raisonnement élémentaire (indice d'aptitude générale, « plus haut score de raisonnement »), en comparaison avec des normes de standardisation et un échantillon simulé par Monte-Carlo à partir de données de normalisation.

Résultats

Les performances des enfants avec un TSAF étaient inférieures dans tous les sous-tests en moyenne, avec une faiblesse significative de la mémoire de travail et de la vitesse de traitement. Nous n'avons pas constaté d'augmentation de la variance et de la dispersion des scores, mais une discordance entre l'évaluation du fonctionnement cognitif global (28 % limite, 23 % déficitaire) et celle des capacités de raisonnement global et élémentaire (23-9 % limite, 15-14 % déficitaire).

Conclusion

Nos résultats remettent en cause la notion d'hétérogénéité du profil du WISC dans les TSAF et mettent en évidence un sur-déficit de la mémoire de travail et de la vitesse de traitement, avec des répercussions globales mais des capacités de raisonnement élémentaire le plus souvent préservées.

PERTURBATION DU VECTEUR DE FIEDLER : INTÉRÊT POUR LES MESURES DE GRAPHES ET L'ANALYSE DE FORME

Dans ce travail, j'ai contribué à soulever la question théorique, à produire des données pour l'application expérimentale ainsi qu'à optimiser les tests sur les paramétrages pour l'utilisation au corps calleux. J'ai relu le manuscrit.

Lefevre, J., Fraize, J., & Germanaud, D. (2023). Perturbation of Fiedler vector: interest for graph measures and shape analysis. *Geometric Science of Information 2023. Lecture Notes in Geometry & Biological Structures()*. In press

Pré-print accessible : <https://arxiv.org/abs/2306.04327>

RÉSUMÉ

Nous proposons d'étudier certaines propriétés du vecteur de Fiedler, le premier vecteur propre non trivial de la matrice Laplacienne d'un graphe. Il existe des résultats importants sur le vecteur de Fiedler pour identifier les coupures spectrales dans les graphes, mais ses valeurs et points extrêmes sont beaucoup moins connus. Nous proposons quelques résultats et conjectures dans cette direction. Nous apportons également deux contributions concrètes, i) en définissant une nouvelle mesure pour les graphes qui peut être interprétée en termes d'extrémalité (inverse de la centralité), ii) en appliquant une petite perturbation au vecteur de Fiedler de formes cérébrales telles que le corps calleux afin d'améliorer leur paramétrage.

COMMUNICATIONS ET PROMOTIONS

SCIENTIFIQUES

Les résultats de cette thèse ont été présentés et discutés lors de plusieurs conférences nationales et internationales, énumérées ci-dessous :

COMMUNICATIONS ORALES EN CONGRÈS

- Fraize, J., Fisher, C., Elmaleh-Bergès, M., et al. *Spectre syndromique de l'alcoolisation fœtale : étude en imagerie morphométrique de l'atteinte neuroanatomique cérébelleuse*. **30^{ème} Congrès de la Société Française de Neurologie Pédiatrique, 2020, Toulouse.**
- Fraize, J., Fisher, C., Elmaleh-Bergès, M., et al. *Cerebellar gradient of volume reduction in Fetal Alcohol Syndrome: toward a neuroanatomical marker?* **European Fetal Alcohol Spectrum Disorders Alliance, 2022.**

COMMUNICATIONS POSTER EN CONGRÈS

- Fraize, J., Garzón, P., Ntorkou, A., et al. *Combining brain size, callosal and vermian measures for Fetal Alcohol Spectrum Disorder diagnosis*. **31^{ème} Congrès de la Société Française de Neurologie Pédiatrique, 2022, Angers.**
- Convert, G., Auzias, G., Lefèvre, J., et al. *Sulci based Midsagittal Corpus Callosum Parcellation New Approach To Callosal Scaling Or Development*. **31^{ème} Congrès de la Société Française de Neurologie Pédiatrique, 2022, Angers.**
- Fraize, J., Fisher, C., Elmaleh-Bergès, M., et al. *Cerebellar gradient of volume reduction in Fetal Alcohol Syndrome: toward a neuroanatomical marker?* **28th Organization for Human Brain Mapping Annual Meeting, 2022, Glasgow.**
- Kerdreux, E., Fraize, J., Garzón, P., et al. *Psychometric profile, heterogeneity, and intellectual functioning in fetal alcohol spectrum disorder*. **14th European Pediatric Neurology Society Congress, 2022, Glasgow.**
- Convert, G., Auzias, G., Lefèvre, J., et al. *Sulci based Midsagittal Corpus Callosum Parcellation New Approach To Callosal Scaling Or Development*. **14th European Pediatric Neurology Society Congress, 2022, Glasgow.**
- Fraize, J., Garzón, P., Ntorkou, A., et al. *Combining brain size, callosal and vermian measures for Fetal Alcohol Spectrum Disorder diagnosis*. **14th European Pediatric Neurology Society Congress, 2022, Glasgow.**

- Fraize, J., Fisher, C., Elmaleh-Bergès, M., et al. *Cerebellar gradient of volume reduction in Fetal Alcohol Syndrome: toward a neuroanatomical marker?* **FENS, International Neuroscience Conference, 2022, Paris.**
- Fraize, J., Aubin, H.J., Chanal, C., et al. *TSAF-R, a multidisciplinary networking action to boost French scientific research on the consequences of prenatal alcohol exposure.* **European Fetal Alcohol Spectrum Disorders Alliance Conference, 2022, Arendal.**
- Fraize, J., Fisher, C., Elmaleh-Bergès, M., et al. *Intérêt diagnostique d'un classifieur basé sur le gradient de réduction volumique intracérébelleux dans les troubles du spectre de l'alcoolisation fœtale.* **32^{ème} Congrès de la Société Française de Neurologie Pédiatrique, 2023, Marseille.**
- Fraize, J., Aubin, H.J., Chanal, C., et al. *TSAF-R, a multidisciplinary networking action to boost French scientific research on the consequences of prenatal alcohol exposure.* **32^{ème} Congrès de la Société Française de Neurologie Pédiatrique, 2023, Marseille.**
- Fraize, J., Fisher, C., Elmaleh-Bergès, M., et al. *Intérêt diagnostique d'un classifieur basé sur le gradient de réduction volumique intracérébelleux dans les troubles du spectre de l'alcoolisation fœtale.* **Journées scientifiques de l'ED3C, 2023, Roscoff.**

ORGANISATION ET ANIMATION D'UN CONGRÈS SCIENTIFIQUE FRANÇAIS 2021 & 2022

J'ai organisé avec David Germanaud la tenue d'un congrès scientifique regroupant les équipes de recherche françaises s'intéressant aux conséquences de l'exposition prénatale à l'alcool. En 2021, le congrès a eu lieu en ligne, et en 2022 en présentiel, regroupant une cinquantaine de participants. J'ai animé un atelier scientifique et y ai présenté le travail de l'équipe. Ce congrès a permis de faire vivre le réseau TSAF-R, initiative scientifique transversale pour la recherche sur les troubles du spectre de l'alcoolisation fœtale. Nous alimentons régulièrement un [site web](#), pour animer le réseau. Le rapport d'activité de ces deux années est accessible en ligne sur le https://tsafr.files.wordpress.com/2023/05/r_final_tsaf2022.pdf.

BIBLIOGRAPHIE

- Alex, K., and Feldmann, R. (2012). Children and adolescents with fetal alcohol syndrome (FAS): better social and emotional integration after early diagnosis. *Klin Padiatr* 224, 66–71. doi: 10.1055/s-0031-1299682.
- Almeida, L., Andreu-Fernández, V., Navarro-Tapia, E., Aras-López, R., Serra-Delgado, M., Martínez, L., et al. (2020). Murine Models for the Study of Fetal Alcohol Spectrum Disorders: An Overview. *Front Pediatr* 8, 359. doi: 10.3389/fped.2020.00359.
- Amiez, C., Sallet, J., Hopkins, W. D., Meguerditchian, A., Hadj-Bouziane, F., Ben Hamed, S., et al. (2019). Sulcal organization in the medial frontal cortex provides insights into primate brain evolution. *Nat Commun* 10, 3437. doi: 10.1038/s41467-019-11347-x.
- Andersson, J. L. R., Graham, M. S., Zsoldos, E., and Sotiropoulos, S. N. (2016). Incorporating outlier detection and replacement into a non-parametric framework for movement and distortion correction of diffusion MR images. *Neuroimage* 141, 556–572. doi: 10.1016/j.neuroimage.2016.06.058.
- Andersson, J. L. R., and Sotiropoulos, S. N. (2016). An integrated approach to correction for off-resonance effects and subject movement in diffusion MR imaging. *Neuroimage* 125, 1063–1078. doi: 10.1016/j.neuroimage.2015.10.019.
- Archibald, S. L., Fennema-Notestine, C., Gamst, A., Riley, E. P., Mattson, S. N., and Jernigan, T. L. (2001). Brain dysmorphology in individuals with severe prenatal alcohol exposure. *Developmental Medicine & Child Neurology* 43, 148–154. doi: <https://doi.org/10.1111/j.1469-8749.2001.tb00179.x>.
- Astley, S. J. (2004). Diagnostic guide for fetal alcohol spectrum disorders: The 4-digit diagnostic code. *Astley SJ. Diagnostic Guide for Fetal Alcohol Spectrum Disorders: The 4-Digit Diagnostic Code. 3rd edition University of Washington Publication Services, Seattle, WA: 2004. Available from: <http://depts.washington.edu/fasdnpn/pdfs/guide04.pdf>, 123.*
- Astley, S. J. (2006). Comparison of the 4-digit diagnostic code and the Hoyme diagnostic guidelines for fetal alcohol spectrum disorders. *Pediatrics* 118, 1532–1545. doi: 10.1542/peds.2006-0577.
- Astley, S. J. (2010). Profile of the first 1,400 patients receiving diagnostic evaluations for fetal alcohol spectrum disorder at the Washington State Fetal Alcohol Syndrome Diagnostic & Prevention Network. *Can J Clin Pharmacol* 17, e132-164.
- Astley, S. J., Aylward, E. H., Olson, H. C., Kerns, K., Brooks, A., Coggins, T. E., et al. (2009a). Magnetic resonance imaging outcomes from a comprehensive magnetic resonance study of children with fetal alcohol spectrum disorders. *Alcohol Clin Exp Res* 33, 1671–1689. doi: 10.1111/j.1530-0277.2009.01004.x.

- Astley, S. J., and Clarren, S. K. (2000). Diagnosing the full spectrum of fetal alcohol-exposed individuals: introducing the 4-digit diagnostic code. *Alcohol Alcohol* 35, 400–410. doi: 10.1093/alcalc/35.4.400.
- Astley, S. J., Olson, H. C., Kerns, K., Brooks, A., Aylward, E. H., Coggins, T. E., et al. (2009b). Neuropsychological and behavioral outcomes from a comprehensive magnetic resonance study of children with fetal alcohol spectrum disorders. *Can J Clin Pharmacol* 16, e178-201.
- Astley-Hemingway, S. J., Bledsoe, J. M., Brooks, A., Davies, J. K., Jirikowic, T., Olson, E., et al. (2019). Comparison of the 4-Digit Code, Canadian 2015, Australian 2016 and Hoyme 2016 fetal alcohol spectrum disorder diagnostic guidelines. *Adv Pediatr Res* 6. doi: 10.35248/2385-4529.19.6.31.
- Autti-Rämö, I., Autti, T., Korkman, M., Kettunen, S., Salonen, O., and Valanne, L. (2002). MRI findings in children with school problems who had been exposed prenatally to alcohol. *Dev Med Child Neurol* 44, 98–106. doi: 10.1017/s0012162201001748.
- Auzias, G., Coulon, O., and Brovelli, A. (2016). MarsAtlas: A cortical parcellation atlas for functional mapping. *Hum Brain Mapp* 37, 1573–1592. doi: 10.1002/hbm.23121.
- Auzias, G., Lefèvre, J., Le Troter, A., Fischer, C., Perrot, M., Régis, J., et al. (2013). Model-driven harmonic parameterization of the cortical surface: HIP-HOP. *IEEE Trans Med Imaging* 32, 873–887. doi: 10.1109/TMI.2013.2241651.
- Ayoub, L., Aring, E., Gyllencreutz, E., Landgren, V., Svensson, L., Landgren, M., et al. (2023). Visual and ocular findings in children with fetal alcohol spectrum disorders (FASD): validating the FASD Eye Code in a clinical setting. *BMJ Open Ophthalmol* 8, e001215. doi: 10.1136/bmjophth-2022-001215.
- Bakker, R., Tiesinga, P., and Kötter, R. (2015). The Scalable Brain Atlas: Instant Web-Based Access to Public Brain Atlases and Related Content. *Neuroinformatics* 13, 353–366. doi: 10.1007/s12021-014-9258-x.
- Battle, D. E. (2013). Diagnostic and Statistical Manual of Mental Disorders (DSM). *Codas* 25, 191–192. doi: 10.1590/s2317-17822013000200017.
- Behnke, M., Smith, V. C., COMMITTEE ON SUBSTANCE ABUSE, COMMITTEE ON FETUS AND NEWBORN, Behnke, M., Smith, V. C., et al. (2013). Prenatal Substance Abuse: Short- and Long-term Effects on the Exposed Fetus. *Pediatrics* 131, e1009–e1024. doi: 10.1542/peds.2012-3931.
- Benjamini, Y., and Hochberg, Y. (1995). Controlling the False Discovery Rate: A Practical and Powerful Approach to Multiple Testing. *Journal of the Royal Statistical Society: Series B (Methodological)* 57, 289–300. doi: 10.1111/j.2517-6161.1995.tb02031.x.
- Bethlehem, R. a. I., Seidlitz, J., White, S. R., Vogel, J. W., Anderson, K. M., Adamson, C., et al. (2022). Brain charts for the human lifespan. *Nature* 604, 525–533. doi: 10.1038/s41586-022-04554-y.

- Biffen, S. C., Warton, C. M. R., Dodge, N. C., Molteno, C. D., Jacobson, J. L., Jacobson, S. W., et al. (2020). Validity of automated FreeSurfer segmentation compared to manual tracing in detecting prenatal alcohol exposure-related subcortical and corpus callosal alterations in 9- to 11-year-old children. *Neuroimage Clin* 28, 102368. doi: 10.1016/j.nicl.2020.102368.
- Biffen, S. C., Warton, C. M. R., Lindinger, N. M., Randall, S. R., Lewis, C. E., Molteno, C. D., et al. (2017). Reductions in Corpus Callosum Volume Partially Mediate Effects of Prenatal Alcohol Exposure on IQ. *Front Neuroanat* 11, 132. doi: 10.3389/fnana.2017.00132.
- Bonthius, D. J., and West, J. R. (1990). Alcohol-induced neuronal loss in developing rats: increased brain damage with binge exposure. *Alcohol Clin Exp Res* 14, 107–118. doi: 10.1111/j.1530-0277.1990.tb00455.x.
- Bookstein, F. L., Connor, P. D., Covell, K. D., Barr, H. M., Gleason, C. A., Sze, R. W., et al. (2005). Preliminary evidence that prenatal alcohol damage may be visible in averaged ultrasound images of the neonatal human corpus callosum. *Alcohol* 36, 151–160. doi: 10.1016/j.alcohol.2005.07.007.
- Bookstein, F. L., Connor, P. D., Huggins, J. E., Barr, H. M., Pimentel, K. D., and Streissguth, A. P. (2007). Many infants prenatally exposed to high levels of alcohol show one particular anomaly of the corpus callosum. *Alcohol Clin Exp Res* 31, 868–879. doi: 10.1111/j.1530-0277.2007.00367.x.
- Bookstein, F. L., Sampson, P. D., Connor, P. D., and Streissguth, A. P. (2002a). Corpus Callosum Shape and Neuropsychological Deficits in Adult Males with Heavy Fetal Alcohol Exposure. *Anat Rec* 269, 162–174. doi: 10.1002/ar.10110.
- Bookstein, F. L., Sampson, P. D., Connor, P. D., and Streissguth, A. P. (2002b). Midline corpus callosum is a neuroanatomical focus of fetal alcohol damage. *Anat Rec* 269, 162–174. doi: 10.1002/ar.10110.
- Bookstein, F. L., Streissguth, A. P., Connor, P. D., and Sampson, P. D. (2006). Damage to the human cerebellum from prenatal alcohol exposure: the anatomy of a simple biometrical explanation. *Anat Rec B New Anat* 289, 195–209. doi: 10.1002/ar.b.20114.
- Boronat, S., Sánchez-Montañez, A., Gómez-Barros, N., Jacas, C., Martínez-Ribot, L., Vázquez, E., et al. (2017). Correlation between morphological MRI findings and specific diagnostic categories in fetal alcohol spectrum disorders. *Eur J Med Genet* 60, 65–71. doi: 10.1016/j.ejmg.2016.09.003.
- Borst, G., Cachia, A., Vidal, J., Simon, G., Fischer, C., Pineau, A., et al. (2014). Folding of the anterior cingulate cortex partially explains inhibitory control during childhood: A longitudinal study. *Dev Cogn Neurosci* 9, 126–135. doi: 10.1016/j.dcn.2014.02.006.
- Bouyeure, A., Germanaud, D., Bekha, D., Delattre, V., Lefèvre, J., Pinabiaux, C., et al. (2018). Three-Dimensional Probabilistic Maps of Mesial Temporal Lobe Structures in Children and Adolescents' Brains. *Front Neuroanat* 12, 98. doi: 10.3389/fnana.2018.00098.

- Brossard-Racine, M., and Limperopoulos, C. (2016). Normal Cerebellar Development by Qualitative and Quantitative MR Imaging. *Neuroimaging Clinics of North America* 26, 331–339. doi: 10.1016/j.nic.2016.03.004.
- Cachia, A., Borst, G., Tissier, C., Fisher, C., Plaze, M., Gay, O., et al. (2016). Longitudinal stability of the folding pattern of the anterior cingulate cortex during development. *Dev Cogn Neurosci* 19, 122–127. doi: 10.1016/j.dcn.2016.02.011.
- Carass, A., Cuzzocreo, J. L., Han, S., Hernandez-Castillo, C. R., Rasser, P. E., Ganz, M., et al. (2018). Comparing fully automated state-of-the-art cerebellum parcellation from magnetic resonance images. *NeuroImage* 183, 150–172. doi: 10.1016/j.neuroimage.2018.08.003.
- Cardenas, V. A., Price, M., Infante, M. A., Moore, E. M., Mattson, S. N., Riley, E. P., et al. (2014). Automated cerebellar segmentation: Validation and application to detect smaller volumes in children prenatally exposed to alcohol. *NeuroImage: Clinical* 4, 295–301. doi: 10.1016/j.nicl.2014.01.002.
- Chao, Y.-P., Cho, K.-H., Yeh, C.-H., Chou, K.-H., Chen, J.-H., and Lin, C.-P. (2009). Probabilistic topography of human corpus callosum using cytoarchitectural parcellation and high angular resolution diffusion imaging tractography. *Hum Brain Mapp* 30, 3172–3187. doi: 10.1002/hbm.20739.
- Chassevent-Pajot, A., Guillou-Landréat, M., Grall-Bronnec, M., Wainstein, L., Philippe, H.-J., Lombraïl, P., et al. (2011). [Epidemiological study on addictive behaviours during pregnancy in a university department]. *J Gynecol Obstet Biol Reprod (Paris)* 40, 237–245. doi: 10.1016/j.jgyn.2011.01.019.
- Chen, G., Nash, T. A., Cole, K. M., Kohn, P. D., Wei, S.-M., Gregory, M. D., et al. (2021). Beyond linearity in neuroimaging: Capturing nonlinear relationships with application to longitudinal studies. *NeuroImage* 233, 117891. doi: 10.1016/j.neuroimage.2021.117891.
- Chen, X., Coles, C. D., Lynch, M. E., and Hu, X. (2011). Understanding specific effects of prenatal alcohol exposure on brain structure in young adults. *Hum Brain Mapp* 33, 1663–1676. doi: 10.1002/hbm.21313.
- Chernoff, G. F. (1977). The fetal alcohol syndrome in mice: An animal model. *Teratology* 15, 223–229. doi: 10.1002/tera.1420150303.
- Chudley, A. E. (2018). Diagnosis of fetal alcohol spectrum disorder: current practices and future considerations. *Biochem Cell Biol* 96, 231–236. doi: 10.1139/bcb-2017-0106.
- Chudley, A. E., Conry, J., Cook, J. L., Looock, C., Rosales, T., and LeBlanc, N. (2005). Fetal alcohol spectrum disorder: Canadian guidelines for diagnosis. *CMAJ* 172, S1–S21. doi: 10.1503/cmaj.1040302.

- Clarren, S. K., Chudley, A. E., Wong, L., Friesen, J., and Brant, R. (2010). Normal distribution of palpebral fissure lengths in Canadian school age children. *Can J Clin Pharmacol* 17, e67–78.
- Clarren, S. K., and Smith, D. W. (1978). The fetal alcohol syndrome. *N Engl J Med* 298, 1063–1067. doi: 10.1056/NEJM197805112981906.
- Coleman, L. G., Oguz, I., Lee, J., Styner, M., and Crews, F. T. (2012). Postnatal day 7 ethanol treatment causes persistent reductions in adult mouse brain volume and cortical neurons with sex specific effects on neurogenesis. *Alcohol* 46, 603–612. doi: 10.1016/j.alcohol.2012.01.003.
- Coles, C. D., Goldstein, F. C., Lynch, M. E., Chen, X., Kable, J. A., Johnson, K. C., et al. (2011). Memory and brain volume in adults prenatally exposed to alcohol. *Brain Cogn* 75, 67–77. doi: 10.1016/j.bandc.2010.08.013.
- Coles, C. D., Kable, J. A., Drews-Botsch, C., and Falek, A. (2000). Early identification of risk for effects of prenatal alcohol exposure. *J Stud Alcohol* 61, 607–616. doi: 10.15288/jsa.2000.61.607.
- Collège de la Haute Autorité de Santé (2013). Troubles causés par l'alcoolisation foétale : repérage. Haute Autorité de Santé Available at: https://www.has-sante.fr/upload/docs/application/pdf/2014-03/troubles_causés_par_l'alcoolisation_foetale_reperage-_rapport_delaboration.pdf.
- Colom, J., Segura-García, L., Bastons-Compta, A., Astals, M., Andreu-Fernandez, V., Barcons, N., et al. (2021). Prevalence of Fetal Alcohol Spectrum Disorders (FASD) among Children Adopted from Eastern European Countries: Russia and Ukraine. *International Journal of Environmental Research and Public Health* 18, 1388. doi: 10.3390/ijerph18041388.
- Connor, P. D., Sampson, P. D., Streissguth, A. P., Bookstein, F. L., and Barr, H. M. (2006). Effects of prenatal alcohol exposure on fine motor coordination and balance: A study of two adult samples. *Neuropsychologia* 44, 744–751. doi: 10.1016/j.neuropsychologia.2005.07.016.
- Cook, J. L., Green, C. R., Lilley, C. M., Anderson, S. M., Baldwin, M. E., Chudley, A. E., et al. (2016). Fetal alcohol spectrum disorder: A guideline for diagnosis across the lifespan. *Canadian Medical Association Journal* 188, 191–197. doi: 10.1503/cmaj.141593.
- Cooper, G., Hirsch, S., Scheel, M., Brandt, A. U., Paul, F., Finke, C., et al. (2020). Quantitative Multi-Parameter Mapping Optimized for the Clinical Routine. *Front Neurosci* 14, 611194. doi: 10.3389/fnins.2020.611194.
- Day, N. L., Leech, S. L., Richardson, G. A., Cornelius, M. D., Robles, N., and Larkby, C. (2002). Prenatal alcohol exposure predicts continued deficits in offspring size at 14 years of age. *Alcohol Clin Exp Res* 26, 1584–1591. doi: 10.1097/01.ALC.0000034036.75248.D9.

- de Chazeron, I., Llorca, P.-M., Ughetto, S., Vendittelli, F., Boussiron, D., Sapin, V., et al. (2008). Is pregnancy the time to change alcohol consumption habits in France? *Alcohol Clin Exp Res* 32, 868–873. doi: 10.1111/j.1530-0277.2008.00646.x.
- De Guio, F., Mangin, J.-F., Rivière, D., Perrot, M., Molteno, C. D., Jacobson, S. W., et al. (2014). A study of cortical morphology in children with fetal alcohol spectrum disorders: Cortical Morphology in Fetal Alcohol Spectrum Disorders. *Hum. Brain Mapp.* 35, 2285–2296. doi: 10.1002/hbm.22327.
- de Jong, L. W., Vidal, J.-S., Forsberg, L. E., Zijdenbos, A. P., Haight, T., Alzheimer's Disease Neuroimaging Initiative, et al. (2017). Allometric scaling of brain regions to intra-cranial volume: An epidemiological MRI study. *Hum Brain Mapp* 38, 151–164. doi: 10.1002/hbm.23351.
- del Campo, M., and Jones, K. L. (2017). A review of the physical features of the fetal alcohol spectrum disorders. *European Journal of Medical Genetics* 60, 55–64. doi: 10.1016/j.ejmg.2016.10.004.
- DeLong, E. R., DeLong, D. M., and Clarke-Pearson, D. L. (1988). Comparing the Areas under Two or More Correlated Receiver Operating Characteristic Curves: A Nonparametric Approach. *Biometrics* 44, 837–845. doi: 10.2307/2531595.
- Demiguel, V., Laporal, S., Quatremere, G., Barry, Y., Guseva Canu, I., Goulet, V., et al. (2021). The frequency of severe Fetal Alcohol Spectrum Disorders in the neonatal period using data from the French hospital discharge database between 2006 and 2013. *Drug Alcohol Depend* 225, 108748. doi: 10.1016/j.drugalcdep.2021.108748.
- Diedrichsen, J., Balsters, J. H., Flavell, J., Cussans, E., and Ramnani, N. (2009). A probabilistic MR atlas of the human cerebellum. *Neuroimage* 46, 39–46. doi: 10.1016/j.neuroimage.2009.01.045.
- Dinga, R., Frazza, C. J., Bayer, J. M. M., Kia, S. M., Beckmann, C. F., and Marquand, A. F. (2021). Normative modeling of neuroimaging data using generalized additive models of location scale and shape. 2021.06.14.448106. doi: 10.1101/2021.06.14.448106.
- Dodge, N. C., Jacobson, J. L., Molteno, C. D., Meintjes, E. M., Bangalore, S., Diwadkar, V., et al. (2009). Prenatal Alcohol Exposure and Interhemispheric Transfer of Tactile Information: Detroit and Cape Town Findings. *Alcoholism: Clinical and Experimental Research* 33, 1628–1637. doi: 10.1111/j.1530-0277.2009.00994.x.
- Donald, K. A., Eastman, E., Howells, F. M., Adnams, C., Riley, E. P., Woods, R. P., et al. (2015). Neuroimaging effects of prenatal alcohol exposure on the developing human brain: a magnetic resonance imaging review. *Acta Neuropsychiatr.* 27, 251–269. doi: 10.1017/neu.2015.12.
- Drakulich, S., Thiffault, A.-C., Olafson, E., Parent, O., Labbe, A., Albaugh, M. D., et al. (2021). Maturational trajectories of pericortical contrast in typical brain development. *Neuroimage* 235, 117974. doi: 10.1016/j.neuroimage.2021.117974.

- Evrard, S. G., Vega, M. D., Ramos, A. J., Tagliaferro, P., and Brusco, A. (2003). Altered neuron-glia interactions in a low, chronic prenatal ethanol exposure. *Brain Res Dev Brain Res* 147, 119–133. doi: 10.1016/j.devbrainres.2003.09.004.
- Fan, J., Jacobson, S. W., Taylor, P. A., Molteno, C. D., Dodge, N. C., Stanton, M. E., et al. (2016). White matter deficits mediate effects of prenatal alcohol exposure on cognitive development in childhood. *Hum Brain Mapp* 37, 2943–2958. doi: 10.1002/hbm.23218.
- Fan, L., Tang, Y., Sun, B., Gong, G., Chen, Z. J., Lin, X., et al. (2010). Sexual dimorphism and asymmetry in human cerebellum: An MRI-based morphometric study. *Brain Research* 1353, 60–73. doi: 10.1016/j.brainres.2010.07.031.
- Finlay, B. L., Darlington, R. B., and Nicastro, N. (2001). Developmental structure in brain evolution. *Behavioral and Brain Sciences* 24, 263–278. doi: 10.1017/S0140525X01003958.
- Forray, A. (2016). Substance use during pregnancy. *F1000Res* 5, F1000 Faculty Rev-887. doi: 10.12688/f1000research.7645.1.
- Fortin, J.-P., Cullen, N., Sheline, Y. I., Taylor, W. D., Aselcioglu, I., Cook, P. A., et al. (2018). Harmonization of cortical thickness measurements across scanners and sites. *Neuroimage* 167, 104–120. doi: 10.1016/j.neuroimage.2017.11.024.
- Fortin, J.-P., Parker, D., Tunç, B., Watanabe, T., Elliott, M. A., Ruparel, K., et al. (2017). Harmonization of multi-site diffusion tensor imaging data. *NeuroImage* 161, 149–170. doi: 10.1016/j.neuroimage.2017.08.047.
- Fraize, J. (2021). Identification et évaluation de la portée clinique de nouveaux marqueurs neuroanatomiques en imagerie dans les troubles du spectre d'alcoolisation fœtale.
- Fraize, J., Convert, G., Leprince, Y., Sylvestre-Marconville, F., Kerdreux, E., Auzias, G., et al. (2023a). Mapping corpus callosum surface reduction in fetal alcohol spectrum disorders with sulci and connectivity-based parcellation. *Front Neurosci* 17, 1188367. doi: 10.3389/fnins.2023.1188367.
- Fraize, J., Fischer, C., Elmaleh-Bergès, M., Kerdreux, E., Beggiato, A., Ntorkou, A., et al. (2023b). Enhancing fetal alcohol spectrum disorders diagnosis with a classifier based on the intracerebellar gradient of volumetric undersizing. *Hum Brain Mapp*. doi: 10.1002/hbm.26348.
- Fraize, J., Garzón, P., Ntorkou, A., Kerdreux, E., Boespflug-Tanguy, O., Beggiato, A., et al. (2023c). Combining neuroanatomical features to support diagnosis of fetal alcohol spectrum disorders. *Dev Med Child Neurol* 65, 551–562. doi: 10.1111/dmcn.15411.
- Franklin, L., Deitz, J., Jirikowic, T., and Astley, S. (2008). Children With Fetal Alcohol Spectrum Disorders: Problem Behaviors and Sensory Processing. *Am J Occup Ther* 62, 265–273. doi: 10.5014/ajot.62.3.265.

- Friedrich, P., Fraenz, C., Schlüter, C., Ocklenburg, S., Mädler, B., Güntürkün, O., et al. (2020). The Relationship Between Axon Density, Myelination, and Fractional Anisotropy in the Human Corpus Callosum. *Cerebral Cortex* 30, 2042–2056. doi: 10.1093/cercor/bhz221.
- Fryer, S. L., McGee, C. L., Matt, G. E., Riley, E. P., and Mattson, S. N. (2007). Evaluation of psychopathological conditions in children with heavy prenatal alcohol exposure. *Pediatrics* 119, e733-741. doi: 10.1542/peds.2006-1606.
- Gano, D., and Barkovich, A. J. (2019). "Chapter 9 - Cerebellar hypoplasia of prematurity: Causes and consequences," in *Handbook of Clinical Neurology Neonatal Neurology.*, eds. L. S. de Vries and H. C. Glass (Elsevier), 201–216. doi: 10.1016/B978-0-444-64029-1.00009-6.
- Garel, C., Cont, I., Alberti, C., Josserand, E., Moutard, M. L., and Ducou le Pointe, H. (2011). Biometry of the Corpus Callosum in Children: MR Imaging Reference Data. *AJNR Am J Neuroradiol* 32, 1436–1443. doi: 10.3174/ajnr.A2542.
- Garzón, P. (2017). Troubles causés par l'alcoolisation fœtale: phénotype clinique et neuroradiologique avec caractérisation de l'atteinte calleuse et cérébelleuse.
- Garzón, P., Fischer, C., Lefèvre, J., Beggiato, A., Pinabiaux, C., Sitbon, D., et al. (2017). Typical cerebellar allometry is disturbed in Fetal Alcohol Spectrum Disorders: Toward new MRI neuroanatomic markers. *European Journal of Paediatric Neurology* 21, e11. doi: 10.1016/j.ejpn.2017.04.851.
- Gautam, P., Nuñez, S. C., Narr, K. L., Kan, E. C., and Sowell, E. R. (2014). Effects of prenatal alcohol exposure on the development of white matter volume and change in executive function. *NeuroImage: Clinical* 5, 19–27. doi: 10.1016/j.nicl.2014.05.010.
- Germanaud, D., Lefèvre, J., Fischer, C., Bintner, M., Curie, A., des Portes, V., et al. (2014). Simplified gyral pattern in severe developmental microcephalies? New insights from allometric modeling for spatial and spectral analysis of gyrification. *Neuroimage* 102 Pt 2, 317–331. doi: 10.1016/j.neuroimage.2014.07.057.
- Germanaud, D., Lefèvre, J., Toro, R., Fischer, C., Dubois, J., Hertz-Pannier, L., et al. (2012). Larger is twistier: spectral analysis of gyrification (SPANGY) applied to adult brain size polymorphism. *Neuroimage* 63, 1257–1272. doi: 10.1016/j.neuroimage.2012.07.053.
- Germanaud, D., and Toutain, S. (2017). Exposition prénatale à l'alcool et troubles causés par l'alcoolisation fœtale. *Contraste* 46, 39–102.
- Ghazi Sherbaf, F., Aarabi, M. H., Hosein Yazdi, M., and Haghshomar, M. (2019). White matter microstructure in fetal alcohol spectrum disorders: A systematic review of diffusion tensor imaging studies. *Hum Brain Mapp* 40, 1017–1036. doi: 10.1002/hbm.24409.
- Giedd, J. N., and Rapoport, J. L. (2010). Structural MRI of Pediatric Brain Development: What Have We Learned and Where Are We Going? *Neuron* 67, 728–734. doi: 10.1016/j.neuron.2010.08.040.

- Glass, H. C., Shaw, G. M., Ma, C., and Sherr, E. H. (2008). Agenesis of the corpus callosum in California 1983-2003: a population-based study. *Am J Med Genet A* 146A, 2495–2500. doi: 10.1002/ajmg.a.32418.
- Gyllencreutz, E., Aring, E., Landgren, V., Svensson, L., Landgren, M., and Grönlund, M. A. (2020). Ophthalmologic Findings in Fetal Alcohol Spectrum Disorders – A Cohort Study From Childhood to Adulthood. *American Journal of Ophthalmology* 214, 14–20. doi: 10.1016/j.ajo.2019.12.016.
- Hall, J. G., Froster-Iskenius, U. G., and Allanson, J. E. (1989). *Handbook of Normal Physical Measurements*. Oxford, New York: Oxford University Press.
- Hendrickson, T. J., Mueller, B. A., Sowell, E. R., Mattson, S. N., Coles, C. D., Kable, J. A., et al. (2018). Two-year cortical trajectories are abnormal in children and adolescents with prenatal alcohol exposure. *Dev Cogn Neurosci* 30, 123–133. doi: 10.1016/j.dcn.2018.02.008.
- Hofer, S., and Frahm, J. (2006). Topography of the human corpus callosum revisited—Comprehensive fiber tractography using diffusion tensor magnetic resonance imaging. *NeuroImage* 32, 989–994. doi: 10.1016/j.neuroimage.2006.05.044.
- Hornig, H., Singh, A., Yousefi, B., Cohen, E. A., Haghghi, B., Katz, S., et al. (2022). Generalized ComBat harmonization methods for radiomic features with multi-modal distributions and multiple batch effects. *Sci Rep* 12, 4493. doi: 10.1038/s41598-022-08412-9.
- Hoyme, H. E., Hoyme, D. B., Elliott, A. J., Blankenship, J., Kalberg, W. O., Buckley, D., et al. (2015). A South African mixed race lip/philtrum guide for diagnosis of fetal alcohol spectrum disorders. *Am J Med Genet A* 167A, 752–755. doi: 10.1002/ajmg.a.37023.
- Hoyme, H. E., Kalberg, W. O., Elliott, A. J., Blankenship, J., Buckley, D., Marais, A.-S., et al. (2016). Updated Clinical Guidelines for Diagnosing Fetal Alcohol Spectrum Disorders. *Pediatrics* 138. doi: 10.1542/peds.2015-4256.
- Hoyme, H. E., May, P. A., Kalberg, W. O., Koditwakku, P., Gossage, J. P., Trujillo, P. M., et al. (2005). A practical clinical approach to diagnosis of fetal alcohol spectrum disorders: clarification of the 1996 institute of medicine criteria. *Pediatrics* 115, 39–47. doi: 10.1542/peds.2004-0259.
- Huang, H., Zhang, J., Jiang, H., Wakana, S., Poetscher, L., Miller, M. I., et al. (2005). DTI tractography based parcellation of white matter: application to the mid-sagittal morphology of corpus callosum. *Neuroimage* 26, 195–205. doi: 10.1016/j.neuroimage.2005.01.019.
- Idrus, N. M., and Napper, R. M. A. (2012). Acute and long-term Purkinje cell loss following a single ethanol binge during the early third trimester equivalent in the rat. *Alcohol Clin Exp Res* 36, 1365–1373. doi: 10.1111/j.1530-0277.2012.01743.x.

- Infante, M. A., Moore, E. M., Bischoff-Grethe, A., Migliorini, R., Mattson, S. N., and Riley, E. P. (2015). Atypical cortical gyrification in adolescents with histories of heavy prenatal alcohol exposure. *Brain Research* 1624, 446–454. doi: 10.1016/j.brainres.2015.08.002.
- Inkelis, S. M., Moore, E. M., Bischoff-Grethe, A., and Riley, E. P. (2020). Neurodevelopment in adolescents and adults with fetal alcohol spectrum disorders (FASD): A magnetic resonance region of interest analysis. *Brain Res* 1732, 146654. doi: 10.1016/j.brainres.2020.146654.
- Jacobson, S. W., Jacobson, J. L., Molteno, C. D., Warton, C. M. R., Wintermark, P., Hoyme, H. E., et al. (2017). Heavy Prenatal Alcohol Exposure is Related to Smaller Corpus Callosum in Newborn MRI Scans. *Alcohol Clin Exp Res* 41, 965–975. doi: 10.1111/acer.13363.
- Jacobson, S. W., Jacobson, J. L., Stanton, M. E., Meintjes, E. M., and Molteno, C. D. (2011). Biobehavioral markers of adverse effect in fetal alcohol spectrum disorders. *Neuropsychol Rev* 21, 148–166. doi: 10.1007/s11065-011-9169-7.
- Jandeaux, C., Kuchcinski, G., Ternynck, C., Riquet, A., Leclerc, X., Pruvo, J.-P., et al. (2019). Biometry of the Cerebellar Vermis and Brain Stem in Children: MR Imaging Reference Data from Measurements in 718 Children. *AJNR Am J Neuroradiol* 40, 1835–1841. doi: 10.3174/ajnr.A6257.
- Jenkinson, M., Bannister, P., Brady, M., and Smith, S. (2002). Improved optimization for the robust and accurate linear registration and motion correction of brain images. *Neuroimage* 17, 825–841. doi: 10.1016/s1053-8119(02)91132-8.
- Jenkinson, M., Beckmann, C. F., Behrens, T. E. J., Woolrich, M. W., and Smith, S. M. (2012). FSL. *Neuroimage* 62, 782–790. doi: 10.1016/j.neuroimage.2011.09.015.
- Jeret, J. S., Serur, D., Wisniewski, K., and Fisch, C. (1985). Frequency of agenesis of the corpus callosum in the developmentally disabled population as determined by computerized tomography. *Pediatr Neurosci* 12, 101–103. doi: 10.1159/000120229.
- Johnson, V. P., Swayze VW, I. I., Sato, Y., and Andreasen, N. C. (1996). Fetal alcohol syndrome: craniofacial and central nervous system manifestations. *Am J Med Genet* 61, 329–339. doi: 10.1002/(SICI)1096-8628(19960202)61:4<329::AID-AJMG6>3.0.CO;2-P.
- Johnson, W. E., Li, C., and Rabinovic, A. (2007). Adjusting batch effects in microarray expression data using empirical Bayes methods. *Biostatistics* 8, 118–127. doi: 10.1093/biostatistics/kxj037.
- Jones, K. L., and Smith, D. W. (1973). Recognition of the fetal alcohol syndrome in early infancy. *Lancet* 302, 999–1001. doi: 10.1016/s0140-6736(73)91092-1.
- Jones, K. L., Smith, D. W., Ulleland, C. N., and Streissguth, P. (1973). Pattern of malformation in offspring of chronic alcoholic mothers. *Lancet* 1, 1267–1271. doi: 10.1016/s0140-6736(73)91291-9.

- Kable, J. A., O'Connor, M. J., Olson, H. C., Paley, B., Mattson, S. N., Anderson, S. M., et al. (2016). Neurobehavioral Disorder Associated with Prenatal Alcohol Exposure (ND-PAE): Proposed DSM-5 Diagnosis. *Child Psychiatry Hum Dev* 47, 335–346. doi: 10.1007/s10578-015-0566-7.
- Kar, P., Reynolds, J. E., Gibbard, W. B., McMorris, C., Tortorelli, C., and Lebel, C. (2022). Trajectories of brain white matter development in young children with prenatal alcohol exposure. *Hum Brain Mapp* 43, 4145–4157. doi: 10.1002/hbm.25944.
- Kerdreux, E., Fraize, J., Garzón, P., Chalain, E., Etchebarren, L., Sitbon, D., et al. (2023). Questioning cognitive heterogeneity and intellectual functioning in fetal alcohol spectrum disorder from the Wechsler intelligence scale for children. *The Clinical Neuropsychologist*. In review.
- Kersbergen, K. J., Leroy, F., Išgum, I., Groenendaal, F., de Vries, L. S., Claessens, N. H. P., et al. (2016). Relation between clinical risk factors, early cortical changes, and neurodevelopmental outcome in preterm infants. *Neuroimage* 142, 301–310. doi: 10.1016/j.neuroimage.2016.07.010.
- Kilpatrick, L. A., Joshi, S. H., O'Neill, J., Kalender, G., Dillon, A., Best, K. M., et al. (2021). Cortical gyrification in children with attention deficit-hyperactivity disorder and prenatal alcohol exposure. *Drug Alcohol Depend* 225, 108817. doi: 10.1016/j.drugalcdep.2021.108817.
- Kodituwakku, P. W. (2009). Neurocognitive profile in children with fetal alcohol spectrum disorders. *Dev Disabil Res Revs* 15, 218–224. doi: 10.1002/ddrr.73.
- Kuczumski, R. J., Ogden, C. L., Grummer-Strawn, L. M., Flegal, K. M., Guo, S. S., Wei, R., et al. (2000). CDC growth charts: United States. *Adv Data*, 1–27.
- Kuehn, D., Aros, S., Cassorla, F., Avaria, M., Unanue, N., Henriquez, C., et al. (2012). A prospective cohort study of the prevalence of growth, facial, and central nervous system abnormalities in children with heavy prenatal alcohol exposure. *Alcohol Clin Exp Res* 36, 1811–1819. doi: 10.1111/j.1530-0277.2012.01794.x.
- Kully-Martens, K., Denys, K., Treit, S., Tamana, S., and Rasmussen, C. (2012). A review of social skills deficits in individuals with fetal alcohol spectrum disorders and prenatal alcohol exposure: profiles, mechanisms, and interventions. *Alcohol Clin Exp Res* 36, 568–576. doi: 10.1111/j.1530-0277.2011.01661.x.
- Landgren, M., Svensson, L., Strömland, K., and Andersson Grönlund, M. (2010). Prenatal alcohol exposure and neurodevelopmental disorders in children adopted from eastern Europe. *Pediatrics* 125, e1178-1185. doi: 10.1542/peds.2009-0712.
- Lange, S., Probst, C., Gmel, G., Rehm, J., Burd, L., and Popova, S. (2017). Global Prevalence of Fetal Alcohol Spectrum Disorder Among Children and Youth: A Systematic Review and Meta-analysis. *JAMA Pediatr* 171, 948–956. doi: 10.1001/jamapediatrics.2017.1919.

- Lebel, C., Mattson, S. N., Riley, E. P., Jones, K. L., Adnams, C. M., May, P. A., et al. (2012). A Longitudinal Study of the Long-Term Consequences of Drinking during Pregnancy: Heavy In Utero Alcohol Exposure Disrupts the Normal Processes of Brain Development. *Journal of Neuroscience* 32, 15243–15251. doi: 10.1523/JNEUROSCI.1161-12.2012.
- Lebel, C., Roussotte, F., and Sowell, E. R. (2011). Imaging the impact of prenatal alcohol exposure on the structure of the developing human brain. *Neuropsychol Rev* 21, 102–118. doi: 10.1007/s11065-011-9163-0.
- Lebel, C., S, C.-G., and C, B. (2010). Age-related regional variations of the corpus callosum identified by diffusion tensor tractography. *NeuroImage* 52. doi: 10.1016/j.neuroimage.2010.03.072.
- Lemoine, P., H, H., BORTEYRU, J. P., and C, M. J. (1968). *Les enfants de parents alcooliques. Anomalies observées. A propos de 127 cas.*
- Limperopoulos, C., Soul, J. S., Gauvreau, K., Huppi, P. S., Warfield, S. K., Bassan, H., et al. (2005). Late gestation cerebellar growth is rapid and impeded by premature birth. *Pediatrics* 115, 688–695. doi: 10.1542/peds.2004-1169.
- Lipinski, R. J., Godin, E. A., O’leary-Moore, S. K., Parnell, S. E., and Sulik, K. K. (2010). Genesis of teratogen-induced holoprosencephaly in mice. *Am J Med Genet C Semin Med Genet* 154C, 29–42. doi: 10.1002/ajmg.c.30239.
- Little, G., and Beaulieu, C. (2020). Multivariate models of brain volume for identification of children and adolescents with fetal alcohol spectrum disorder. *Hum Brain Mapp* 41, 1181–1194. doi: 10.1002/hbm.24867.
- Liu, D., Johnson, H. J., Long, J. D., Magnotta, V. A., and Paulsen, J. S. (2014). The power-proportion method for intracranial volume correction in volumetric imaging analysis. *Front Neurosci* 8, 356. doi: 10.3389/fnins.2014.00356.
- Luders, E., Toga, A. W., and Thompson, P. M. (2014). Why size matters: differences in brain volume account for apparent sex differences in callosal anatomy: the sexual dimorphism of the corpus callosum. *Neuroimage* 84, 820–824. doi: 10.1016/j.neuroimage.2013.09.040.
- Lussier, A. A., Morin, A. M., MacIsaac, J. L., Salmon, J., Weinberg, J., Reynolds, J. N., et al. (2018). DNA methylation as a predictor of fetal alcohol spectrum disorder. *Clin Epigenetics* 10, 5. doi: 10.1186/s13148-018-0439-6.
- Mamelle, N., Cochet, V., and Claris, O. (2001). Definition of Fetal Growth Restriction According to Constitutional Growth Potential. *Neonatology* 80, 277–285. doi: 10.1159/000047157.
- Manjón, J. V., Romero, J. E., Vivo-Hernando, R., Rubio, G., Aparici, F., Iglesia-Vaya, M. de la, et al. (2022). vol2Brain: A New Online Pipeline for Whole Brain MRI Analysis. *Frontiers in Neuroinformatics* 16. doi: 10.3389/fninf.2022.862805.

- Mankiw, C., Park, M. T. M., Reardon, P. K., Fish, A. M., Clasen, L. S., Greenstein, D., et al. (2017). Allometric Analysis Detects Brain Size-Independent Effects of Sex and Sex Chromosome Complement on Human Cerebellar Organization. *J Neurosci* 37, 5221–5231. doi: 10.1523/JNEUROSCI.2158-16.2017.
- Mantha, K., Kleiber, M., and Singh, S. (2013). Neurodevelopmental Timing of Ethanol Exposure May Contribute to Observed Heterogeneity of Behavioral Deficits in a Mouse Model of Fetal Alcohol Spectrum Disorder (FASD). *Journal of Behavioral and Brain Science* 3, 85–99. doi: 10.4236/jbbs.2013.31009.
- Marcussen, B. L., Goodlett, C. R., Mahoney, J. C., and West, J. R. (1994). Developing rat Purkinje cells are more vulnerable to alcohol-induced depletion during differentiation than during neurogenesis. *Alcohol* 11, 147–156. doi: 10.1016/0741-8329(94)90056-6.
- Marquand, A. F., Rezek, I., Buitelaar, J., and Beckmann, C. F. (2016a). Understanding Heterogeneity in Clinical Cohorts Using Normative Models: Beyond Case-Control Studies. *Biol Psychiatry* 80, 552–561. doi: 10.1016/j.biopsych.2015.12.023.
- Marquand, A. F., Wolfers, T., Mennes, M., Buitelaar, J., and Beckmann, C. F. (2016b). Beyond Lumping and Splitting: A Review of Computational Approaches for Stratifying Psychiatric Disorders. *Biol Psychiatry Cogn Neurosci Neuroimaging* 1, 433–447. doi: 10.1016/j.bpsc.2016.04.002.
- Marshall, A. T., Bodison, S. C., Uban, K. A., Adise, S., Jonker, D., Charles, W., et al. (2022). The impact of prenatal alcohol and/or tobacco exposure on brain structure in a large sample of children from a South African birth cohort. *Alcohol Clin Exp Res* 46, 1980–1992. doi: 10.1111/acer.14945.
- Mattson, S. N., Crocker, N., and Nguyen, T. T. (2011). Fetal alcohol spectrum disorders: neuropsychological and behavioral features. *Neuropsychol Rev* 21, 81–101. doi: 10.1007/s11065-011-9167-9.
- May, P. A., Blankenship, J., Marais, A.-S., Gossage, J. P., Kalberg, W. O., Joubert, B., et al. (2013). Maternal alcohol consumption producing fetal alcohol spectrum disorders (FASD): Quantity, frequency, and timing of drinking. *Drug and Alcohol Dependence* 133, 502–512. doi: 10.1016/j.drugalcdep.2013.07.013.
- Mehta, N. M., and Hartnoll, G. (2001). Congenital CMV with callosal lipoma and agenesis. *Pediatr Neurol* 24, 222–224. doi: 10.1016/s0887-8994(00)00256-3.
- Milbocker, K. A., LeBlanc, G. L., Brengel, E. K., Hekmatyar, K. S., Kulkarni, P., Ferris, C. F., et al. (2022). Reduced and delayed myelination and volume of corpus callosum in an animal model of Fetal Alcohol Spectrum Disorders partially benefit from voluntary exercise. *Sci Rep* 12, 10653. doi: 10.1038/s41598-022-14752-3.
- Moore, E. M., and Xia, Y. (2021). Neurodevelopmental Trajectories Following Prenatal Alcohol Exposure. *Front Hum Neurosci* 15, 695855. doi: 10.3389/fnhum.2021.695855.

- Moreland, N., La Grange, L., and Montoya, R. (2002). Impact of in utero exposure to EtOH on corpus callosum development and paw preference in rats: protective effects of silymarin. *BMC Complement Altern Med* 2, 10. doi: 10.1186/1472-6882-2-10.
- Mosteller, F. (1968). Data analysis, including statistics. *Handbook of social psychology*.
- Nakhid, D., McMorris, C., Sun, H., Gibbard, W. B., Tortorelli, C., and Lebel, C. (2022). Brain volume and magnetic susceptibility differences in children and adolescents with prenatal alcohol exposure. *Alcohol: Clinical and Experimental Research* 46, 1797–1807. doi: 10.1111/acer.14928.
- Nardelli, A., Lebel, C., Rasmussen, C., Andrew, G., and Beaulieu, C. (2011). Extensive Deep Gray Matter Volume Reductions in Children and Adolescents with Fetal Alcohol Spectrum Disorders: Reduced deep gray matter volume in FASD. *Alcoholism: Clinical and Experimental Research*, no-no. doi: 10.1111/j.1530-0277.2011.01476.x.
- Nguyen, V. T., Chong, S., Tieng, Q. M., Mardon, K., Galloway, G. J., and Kurniawan, N. D. (2017). Radiological studies of fetal alcohol spectrum disorders in humans and animal models: An updated comprehensive review. *Magnetic Resonance Imaging* 43, 10–26. doi: 10.1016/j.mri.2017.06.012.
- Nirgudkar, P., Taylor, D. H., Yanagawa, Y., and Valenzuela, C. F. (2016). Ethanol Exposure during Development Reduces GABAergic/Glycinergic Neuron Numbers and Lobule Volumes in the Mouse Cerebellar Vermis. *Neurosci Lett* 632, 86–91. doi: 10.1016/j.neulet.2016.08.039.
- O’Hare, E. D., Kan, E., Yoshii, J., Mattson, S. N., Riley, E. P., Thompson, P. M., et al. (2005). Mapping cerebellar vermal morphology and cognitive correlates in prenatal alcohol exposure. *Neuroreport* 16, 1285–1290. doi: 10.1097/01.wnr.0000176515.11723.a2.
- O’Leary-Moore, S. K., Parnell, S. E., Lipinski, R. J., and Sulik, K. K. (2011). Magnetic resonance-based imaging in animal models of fetal alcohol spectrum disorder. *Neuropsychol Rev* 21, 167–185. doi: 10.1007/s11065-011-9164-z.
- Pandya, D. N., Karol, E. A., and Heilbronn, D. (1971). The topographical distribution of interhemispheric projections in the corpus callosum of the rhesus monkey. *Brain Res* 32, 31–43. doi: 10.1016/0006-8993(71)90153-3.
- Park, H.-J., Kim, J. J., Lee, S.-K., Seok, J. H., Chun, J., Kim, D. I., et al. (2008). Corpus callosal connection mapping using cortical gray matter parcellation and DT-MRI. *Hum Brain Mapp* 29, 503–516. doi: 10.1002/hbm.20314.
- Parnell, S. E., Holloway, H. E., Baker, L. K., Styner, M. A., and Sulik, K. K. (2014). Dymorphogenic Effects of First Trimester-Equivalent Ethanol Exposure in Mice: A Magnetic Resonance Microscopy-Based Study. *Alcohol Clin Exp Res* 38, 2008–2014. doi: 10.1111/acer.12464.

- Patten, A. R., Fontaine, C. J., and Christie, B. R. (2014). A Comparison of the Different Animal Models of Fetal Alcohol Spectrum Disorders and Their Use in Studying Complex Behaviors. *Front Pediatr* 2, 93. doi: 10.3389/fped.2014.00093.
- Paul, L. K., Brown, W. S., Adolphs, R., Tyszka, J. M., Richards, L. J., Mukherjee, P., et al. (2007). Agenesis of the corpus callosum: genetic, developmental and functional aspects of connectivity. *Nat Rev Neurosci* 8, 287–299. doi: 10.1038/nrn2107.
- Perrot, M., Rivière, D., and Mangin, J.-F. (2011). Cortical sulci recognition and spatial normalization. *Med Image Anal* 15, 529–550. doi: 10.1016/j.media.2011.02.008.
- Peterson, B. S., Rosen, T., Dingman, S., Toth, Z. R., Sawardekar, S., Hao, X., et al. (2020). Associations of Maternal Prenatal Drug Abuse With Measures of Newborn Brain Structure, Tissue Organization, and Metabolite Concentrations. *JAMA Pediatr* 174, 831–842. doi: 10.1001/jamapediatrics.2020.1622.
- Popova, S., Lange, S., Probst, C., Gmel, G., and Rehm, J. (2017). Estimation of national, regional, and global prevalence of alcohol use during pregnancy and fetal alcohol syndrome: a systematic review and meta-analysis. *The Lancet Global Health* 5, e290–e299. doi: 10.1016/S2214-109X(17)30021-9.
- Poretti, A., Boltshauser, E., and Doherty, D. (2014). Cerebellar hypoplasia: Differential diagnosis and diagnostic approach. *American Journal of Medical Genetics Part C: Seminars in Medical Genetics* 166, 211–226. doi: 10.1002/ajmg.c.31398.
- Rajapakse, J. C., Giedd, J. N., Rumsey, J. M., Vaituzis, A. C., Hamburger, S. D., and Rapoport, J. L. (1996). Regional MRI measurements of the corpus callosum: a methodological and developmental study. *Brain and Development* 18, 379–388. doi: 10.1016/0387-7604(96)00034-4.
- Rajaprakash, M., Chakravarty, M. M., Lerch, J. P., and Rovet, J. (2014). Cortical morphology in children with alcohol-related neurodevelopmental disorder. *Brain Behav* 4, 41–50. doi: 10.1002/brb3.191.
- Raybaud, C. (2010). The corpus callosum, the other great forebrain commissures, and the septum pellucidum: anatomy, development, and malformation. *Neuroradiology* 52, 447–477. doi: 10.1007/s00234-010-0696-3.
- Reardon, P. K., Clasen, L., Giedd, J. N., Blumenthal, J., Lerch, J. P., Chakravarty, M. M., et al. (2016). An Allometric Analysis of Sex and Sex Chromosome Dosage Effects on Subcortical Anatomy in Humans. *J Neurosci* 36, 2438–2448. doi: 10.1523/JNEUROSCI.3195-15.2016.
- Reardon, P. K., Seidlitz, J., Vandekar, S., Liu, S., Patel, R., Park, M. T. M., et al. (2018). Normative brain size variation and brain shape diversity in humans. *Science* 360, 1222–1227. doi: 10.1126/science.aar2578.

- Riikonen, R., Salonen, I., Partanen, K., and Verho, S. (1999). Brain perfusion SPECT and MRI in foetal alcohol syndrome. *Dev Med Child Neurol* 41, 652–659. doi: 10.1017/s0012162299001358.
- Riley, E. P., Mattson, S. N., Sowell, E. R., Jernigan, T. L., Sobel, D. F., and Jones, K. L. (1995). Abnormalities of the corpus callosum in children prenatally exposed to alcohol. *Alcohol Clin Exp Res* 19, 1198–1202. doi: 10.1111/j.1530-0277.1995.tb01600.x.
- Rivière, D., Geffroy, D., Denghien, I., Souedet, N., and Cointepas, Y. (2009). BrainVISA: an extensible software environment for sharing multimodal neuroimaging data and processing tools. *Neuroimage* 47. doi: 10.1016/S1053-8119(09)71720-3.
- Rockhold, M. N., Krueger, A. M., de Water, E., Lindgren, C. W., Sandness, K. E., Eckerle, J. K., et al. (2020). Executive and Social Functioning Across Development in Children and Adolescents with Prenatal Alcohol Exposure. *Alcohol Clin Exp Res*. doi: 10.1111/acer.14538.
- Roebuck, T. M., Mattson, S. N., and Riley, E. P. (1998). A review of the neuroanatomical findings in children with fetal alcohol syndrome or prenatal exposure to alcohol. *Alcohol Clin Exp Res* 22, 339–344. doi: 10.1111/j.1530-0277.1998.tb03658.x.
- Rollins, J., Collins, J. S., and Holden, K. (2010). United States head circumference growth reference charts: birth to 21 years. *The Journal of pediatrics*. doi: 10.1016/j.jpeds.2010.01.009.
- Romero, J. E., Coupé, P., Giraud, R., Ta, V.-T., Fonov, V., Park, M. T. M., et al. (2017). CERES: A new cerebellum lobule segmentation method. *Neuroimage* 147, 916–924. doi: 10.1016/j.neuroimage.2016.11.003.
- Rosett, H. L. (1980). A clinical perspective of the Fetal Alcohol Syndrome. *Alcohol Clin Exp Res* 4, 119–122. doi: 10.1111/j.1530-0277.1980.tb05626.x.
- Roussotte, F. F., Sulik, K. K., Mattson, S. N., Riley, E. P., Jones, K. L., Adnams, C. M., et al. (2012). Regional brain volume reductions relate to facial dysmorphology and neurocognitive function in fetal alcohol spectrum disorders. *Hum. Brain Mapp.* 33, 920–937. doi: 10.1002/hbm.21260.
- Rutherford, S., Barkema, P., Tso, I. F., Sripada, C., Beckmann, C. F., Ruhe, H. G., et al. (2023). Evidence for embracing normative modeling. *Elife* 12, e85082. doi: 10.7554/eLife.85082.
- Sampson, P. D., Streissguth, A. P., Bookstein, F. L., and Barr, H. M. (2000). On categorizations in analyses of alcohol teratogenesis. *Environ Health Perspect* 108 Suppl 3, 421–428. doi: 10.1289/ehp.00108s3421.
- Santana, E. F. M., Casati, M. F. M., Geraldo, M. de S. P., Werner, H., and Araujo Júnior, E. (2022). Intrauterine Zika virus infection: review of the current findings with emphasis in the prenatal and postnatal brain imaging diagnostic methods. *J Matern Fetal Neonatal Med* 35, 6062–6068. doi: 10.1080/14767058.2021.1904874.

- Savvidou, A., Ivarsson, L., Naess, K., Eklund, E. A., Lundgren, J., Dahlin, M., et al. (2022). Novel imaging findings in pyruvate dehydrogenase complex (PDHc) deficiency—Results from a nationwide population-based study. *Journal of Inherited Metabolic Disease* 45, 248–263. doi: 10.1002/jimd.12463.
- Sawant, O. B., Lunde, E. R., Washburn, S. E., Chen, W.-J. A., Goodlett, C. R., and Cudd, T. A. (2013). Different patterns of regional Purkinje cell loss in the cerebellar vermis as a function of the timing of prenatal ethanol exposure in an ovine model. *Neurotoxicol Teratol* 35, 7–13. doi: 10.1016/j.ntt.2012.11.001.
- Schmahmann (1998). The cerebellar cognitive affective syndrome - PubMed. Available at: <https://pubmed.ncbi.nlm.nih.gov/9577385/> [Accessed December 17, 2020].
- Schmahmann, J. D. (2010). The Role of the Cerebellum in Cognition and Emotion: Personal Reflections Since 1982 on the Dysmetria of Thought Hypothesis, and Its Historical Evolution from Theory to Therapy. *Neuropsychol Rev* 20, 236–260. doi: 10.1007/s11065-010-9142-x.
- Schmahmann, J. D., Doyon, J., McDonald, D., Holmes, C., Lavoie, K., Hurwitz, A. S., et al. (1999). Three-dimensional MRI atlas of the human cerebellum in proportional stereotaxic space. *Neuroimage* 10, 233–260. doi: 10.1006/nimg.1999.0459.
- Schmahmann, J. D., Guell, X., Stoodley, C. J., and Halko, M. A. (2019). The Theory and Neuroscience of Cerebellar Cognition. *Annu Rev Neurosci* 42, 337–364. doi: 10.1146/annurev-neuro-070918-050258.
- Smith, R. E., Tournier, J.-D., Calamante, F., and Connelly, A. (2012). Anatomically-constrained tractography: improved diffusion MRI streamlines tractography through effective use of anatomical information. *Neuroimage* 62, 1924–1938. doi: 10.1016/j.neuroimage.2012.06.005.
- Smith, R. E., Tournier, J.-D., Calamante, F., and Connelly, A. (2015). SIFT2: Enabling dense quantitative assessment of brain white matter connectivity using streamlines tractography. *Neuroimage* 119, 338–351. doi: 10.1016/j.neuroimage.2015.06.092.
- Sokol, R. J., and Clarren, S. K. (1989). Guidelines for Use of Terminology Describing the Impact of Prenatal Alcohol on the Offspring. *Alcohol: Clinical and Experimental Research* 13, 597–598. doi: 10.1111/j.1530-0277.1989.tb00384.x.
- Sowell, E. (2002a). Mapping Cortical Gray Matter Asymmetry Patterns in Adolescents with Heavy Prenatal Alcohol Exposure. *NeuroImage* 17, 1807–1819. doi: 10.1006/nimg.2002.1328.
- Sowell, E. R. (2002b). Regional Brain Shape Abnormalities Persist into Adolescence after Heavy Prenatal Alcohol Exposure. *Cerebral Cortex* 12, 856–865. doi: 10.1093/cercor/12.8.856.
- Sowell, E. R., Jernigan, T. L., Mattson, S. N., Riley, E. P., Sobel, D. F., and Jones, K. L. (1996). Abnormal development of the cerebellar vermis in children prenatally exposed to

- alcohol: size reduction in lobules I-V. *Alcohol Clin Exp Res* 20, 31–34. doi: 10.1111/j.1530-0277.1996.tb01039.x.
- Sowell, E. R., Mattson, S. N., Kan, E., Thompson, P. M., Riley, E. P., and Toga, A. W. (2008). Abnormal cortical thickness and brain-behavior correlation patterns in individuals with heavy prenatal alcohol exposure. *Cereb Cortex* 18, 136–144. doi: 10.1093/cercor/bhm039.
- Sowell, E. R., Mattson, S. N., Thompson, P. M., Jernigan, T. L., Riley, E. P., and Toga, A. W. (2001). Mapping callosal morphology and cognitive correlates: effects of heavy prenatal alcohol exposure. *Neurology* 57, 235–244. doi: 10.1212/wnl.57.2.235.
- Stoodley, C. J., and Schmahmann, J. D. (2009). Functional topography in the human cerebellum: a meta-analysis of neuroimaging studies. *Neuroimage* 44, 489–501. doi: 10.1016/j.neuroimage.2008.08.039.
- Stratton, K. R., Howe, C. J., and Battaglia, F. C. (1996). *Fetal Alcohol Syndrome: Diagnosis, Epidemiology, Prevention, and Treatment*. National Academies Press.
- Streissguth, A. P. (1978). FETAL ALCOHOL SYNDROME: AN EPIDEMIOLOGIC PERSPECTIVE. *American Journal of Epidemiology* 107, 467–478. doi: 10.1093/oxfordjournals.aje.a112566.
- Streissguth, A. P., Randels, S. P., and Smith, D. F. (1991). A test-retest study of intelligence in patients with fetal alcohol syndrome: implications for care. *J Am Acad Child Adolesc Psychiatry* 30, 584–587. doi: 10.1097/00004583-199107000-00009.
- Stuempflen, M., Schwartz, E., Diogo, M. C., Glatter, S., Pfeiler, B., Kienast, P., et al. (2023). Fetal MRI based brain atlas analysis detects initial in utero effects of prenatal alcohol exposure. *Cereb Cortex* 33, 6852–6861. doi: 10.1093/cercor/bhad005.
- Styner, M. A., Oguz, I., Smith, R. G., Cascio, C., and Jomier, M. (2005). Corpus callosum subdivision based on a probabilistic model of inter-hemispheric connectivity. *Med Image Comput Comput Assist Interv* 8, 765–772. doi: 10.1007/11566489_94.
- Subramoney, S., Joshi, S. H., Wedderburn, C. J., Lee, D., Roos, A., Woods, R. P., et al. (2022). The impact of prenatal alcohol exposure on gray matter volume and cortical surface area of 2 to 3-year-old children in a South African birth cohort. *Alcohol Clin Exp Res* 46, 1233–1247. doi: 10.1111/acer.14873.
- Sulik, K. K., Johnston, M. C., and Webb, M. A. (1981). Fetal alcohol syndrome: embryogenesis in a mouse model. *Science* 214, 936–938. doi: 10.1126/science.6795717.
- Sullivan, E. V., Moore, E. M., Lane, B., Pohl, K. M., Riley, E. P., and Pfefferbaum, A. (2020). Graded Cerebellar Lobular Volume Deficits in Adolescents and Young Adults with Fetal Alcohol Spectrum Disorders (FASD). *Cereb Cortex* 30, 4729–4746. doi: 10.1093/cercor/bhaa020.

- Sullivan, E. V., Zahr, N. M., Saranathan, M., Pohl, K. M., and Pfefferbaum, A. (2019). Convergence of three parcellation approaches demonstrating cerebellar lobule volume deficits in Alcohol Use Disorder. *NeuroImage: Clinical* 24, 101974. doi: 10.1016/j.nicl.2019.101974.
- Suttie, M., Foroud, T., Wetherill, L., Jacobson, J. L., Molteno, C. D., Meintjes, E. M., et al. (2013). Facial Dysmorphism Across the Fetal Alcohol Spectrum. *Pediatrics* 131, e779–e788. doi: 10.1542/peds.2012-1371.
- Swayze, V. W., Johnson, V. P., Hanson, J. W., Piven, J., Sato, Y., Giedd, J. N., et al. (1997). Magnetic resonance imaging of brain anomalies in fetal alcohol syndrome. *Pediatrics* 99, 232–240. doi: 10.1542/peds.99.2.232.
- Takao, H., Hayashi, N., and Ohtomo, K. (2011). Effect of scanner in longitudinal studies of brain volume changes. *J Magn Reson Imaging* 34, 438–444. doi: 10.1002/jmri.22636.
- Thomas, S. E., Kelly, S. J., Mattson, S. N., and Riley, E. P. (1998). Comparison of social abilities of children with fetal alcohol syndrome to those of children with similar IQ scores and normal controls. *Alcohol Clin Exp Res* 22, 528–533.
- Thorne, J. C. (2017). Accentuate the Negative: Grammatical Errors During Narrative Production as a Clinical Marker of Central Nervous System Abnormality in School-Aged Children With Fetal Alcohol Spectrum Disorders. *J Speech Lang Hear Res* 60, 3523–3537. doi: 10.1044/2017_JSLHR-L-17-0128.
- Toro, R., Chupin, M., Garnero, L., Leonard, G., Perron, M., Pike, B., et al. (2009). Brain volumes and Val66Met polymorphism of the BDNF gene: local or global effects? *Brain Struct Funct* 213, 501–509. doi: 10.1007/s00429-009-0203-y.
- Tournier, J.-D., Calamante, F., and Connelly, A. (2007). Robust determination of the fibre orientation distribution in diffusion MRI: non-negativity constrained super-resolved spherical deconvolution. *Neuroimage* 35, 1459–1472. doi: 10.1016/j.neuroimage.2007.02.016.
- Tournier, J.-D., Calamante, F., and Connelly, A. (2010). Improved probabilistic streamlines tractography by 2nd order integration over fibre orientation distributions. *Proc. Intl. Soc. Mag. Reson. Med. (ISMRM)* 18.
- Tournier, J.-D., Smith, R., Raffelt, D., Tabbara, R., Dhollander, T., Pietsch, M., et al. (2019). MRtrix3: A fast, flexible and open software framework for medical image processing and visualisation. *Neuroimage* 202, 116137. doi: 10.1016/j.neuroimage.2019.116137.
- Treit, S., Chen, Z., Zhou, D., Baugh, L., Rasmussen, C., Andrew, G., et al. (2017). Sexual dimorphism of volume reduction but not cognitive deficit in fetal alcohol spectrum disorders: A combined diffusion tensor imaging, cortical thickness and brain volume study. *Neuroimage Clin* 15, 284–297. doi: 10.1016/j.nicl.2017.05.006.

- Treit, S., Jeffery, D., Beaulieu, C., and Emery, D. (2020). Radiological Findings on Structural Magnetic Resonance Imaging in Fetal Alcohol Spectrum Disorders and Healthy Controls. *Alcohol Clin Exp Res* 44, 455–462. doi: 10.1111/acer.14263.
- Treit, S., Lebel, C., Baugh, L., Rasmussen, C., Andrew, G., and Beaulieu, C. (2013). Longitudinal MRI Reveals Altered Trajectory of Brain Development during Childhood and Adolescence in Fetal Alcohol Spectrum Disorders. *J Neurosci* 33, 10098–10109. doi: 10.1523/JNEUROSCI.5004-12.2013.
- Treit, S., Zhou, D., Chudley, A. E., Andrew, G., Rasmussen, C., Nikkel, S. M., et al. (2016). Relationships between Head Circumference, Brain Volume and Cognition in Children with Prenatal Alcohol Exposure. *PLoS One* 11, e0150370. doi: 10.1371/journal.pone.0150370.
- Treit, S., Zhou, D., Lebel, C., Rasmussen, C., Andrew, G., and Beaulieu, C. (2014). Longitudinal MRI reveals impaired cortical thinning in children and adolescents prenatally exposed to alcohol. *Hum Brain Mapp* 35, 4892–4903. doi: 10.1002/hbm.22520.
- Vaurio, L., Riley, E. P., and Mattson, S. N. (2011). Neuropsychological comparison of children with heavy prenatal alcohol exposure and an IQ-matched comparison group. *J Int Neuropsychol Soc* 17, 463–473. doi: 10.1017/S1355617711000063.
- Wang, X., Cuzon Carlson, V. C., Studholme, C., Newman, N., Ford, M. M., Grant, K. A., et al. (2020). In utero MRI identifies consequences of early-gestation alcohol drinking on fetal brain development in rhesus macaques. *Proc Natl Acad Sci U S A* 117, 10035–10044. doi: 10.1073/pnas.1919048117.
- Warling, A., McDermott, C. L., Liu, S., Seidlitz, J., Rodrigue, A. L., Nadig, A., et al. (2021). Regional White Matter Scaling in the Human Brain. *J. Neurosci.* 41, 7015–7028. doi: 10.1523/JNEUROSCI.1193-21.2021.
- White, T., Su, S., Schmidt, M., Kao, C.-Y., and Sapiro, G. (2010). The development of gyrification in childhood and adolescence. *Brain Cogn* 72, 36–45. doi: 10.1016/j.bandc.2009.10.009.
- Willford, J., Day, R., Aizenstein, H., and Day, N. (2010). Caudate asymmetry: a neurobiological marker of moderate prenatal alcohol exposure in young adults. *Neurotoxicol Teratol* 32, 589–594. doi: 10.1016/j.ntt.2010.06.012.
- Williams, C. M., Peyre, H., Toro, R., Beggiato, A., and Ramus, F. (2020). Adjusting for allometric scaling in ABIDE I challenges subcortical volume differences in autism spectrum disorder. *Human Brain Mapping* 41, 4610. doi: 10.1002/hbm.25145.
- Willoughby, K. A., Sheard, E. D., Nash, K., and Rovet, J. (2008). Effects of prenatal alcohol exposure on hippocampal volume, verbal learning, and verbal and spatial recall in late childhood. *J Int Neuropsychol Soc* 14, 1022–1033. doi: 10.1017/S1355617708081368.

- Witelson, S. F. (1989). Hand and sex differences in the isthmus and genu of the human corpus callosum. A postmortem morphological study. *Brain* 112 (Pt 3), 799–835. doi: 10.1093/brain/112.3.799.
- Wood, S. N., and Fasiolo, M. (2017). A generalized Fellner-Schall method for smoothing parameter optimization with application to Tweedie location, scale and shape models. *Biometrics* 73, 1071–1081. doi: 10.1111/biom.12666.
- Wyper, K. R., and Rasmussen, C. R. (2011). Language impairments in children with fetal alcohol spectrum disorders. *J Popul Ther Clin Pharmacol* 18, e364-376.
- Yang, Y., Phillips, O. R., Kan, E., Sulik, K. K., Mattson, S. N., Riley, E. P., et al. (2012a). Callosal thickness reductions relate to facial dysmorphology in fetal alcohol spectrum disorders. *Alcohol Clin Exp Res* 36, 798–806. doi: 10.1111/j.1530-0277.2011.01679.x.
- Yang, Y., Roussotte, F., Kan, E., Sulik, K. K., Mattson, S. N., Riley, E. P., et al. (2012b). Abnormal cortical thickness alterations in fetal alcohol spectrum disorders and their relationships with facial dysmorphology. *Cereb Cortex* 22, 1170–1179. doi: 10.1093/cercor/bhr193.
- Zhang, C. R., Kurniawan, N. D., Yamada, L., Fleming, W., Kaminen-Ahola, N., Ahola, A., et al. (2019). Early gestational ethanol exposure in mice: Effects on brain structure, energy metabolism and adiposity in adult offspring. *Alcohol* 75, 1–10. doi: 10.1016/j.alcohol.2018.04.008.
- Zhang, Y., Brady, M., and Smith, S. (2001). Segmentation of brain MR images through a hidden Markov random field model and the expectation-maximization algorithm. *IEEE Trans Med Imaging* 20, 45–57. doi: 10.1109/42.906424.
- Zhou, D., Lebel, C., Lepage, C., Rasmussen, C., Evans, A., Wyper, K., et al. (2011). Developmental cortical thinning in fetal alcohol spectrum disorders. *NeuroImage* 58, 16–25. doi: 10.1016/j.neuroimage.2011.06.026.
- Zhou, D., Rasmussen, C., Pei, J., Andrew, G., Reynolds, J. N., and Beaulieu, C. (2018). Preserved cortical asymmetry despite thinner cortex in children and adolescents with prenatal alcohol exposure and associated conditions. *Hum Brain Mapp* 39, 72–88. doi: 10.1002/hbm.23818.

OUTIL D'INTERPRÉTATION DES MESURES RADIOLOGIQUES UTILISABLE EN CLINIQUE

